Analysis of Poxvirus Host Cell Entry by Electron Microscopy

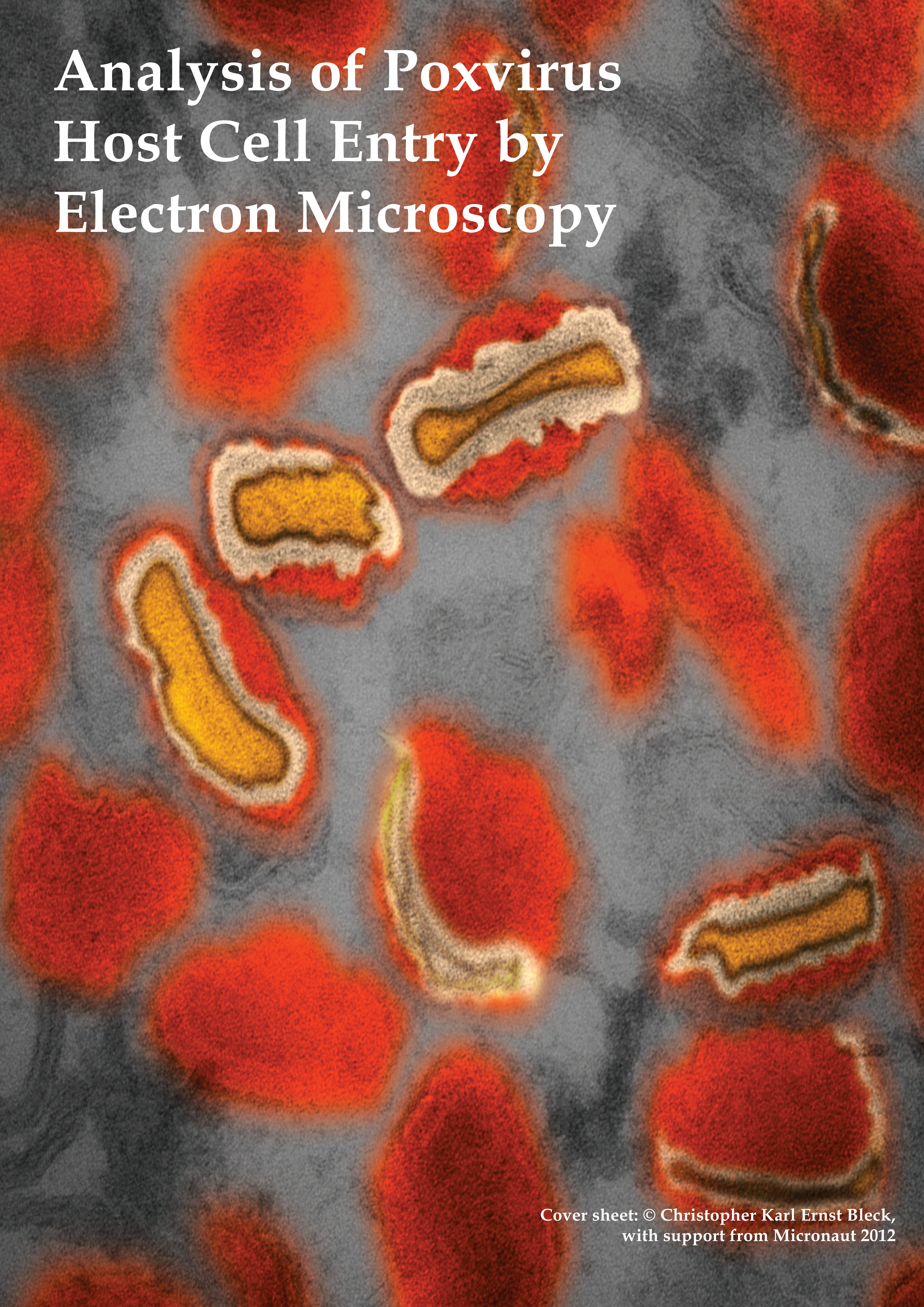

Cover sheet: © Christopher Karl Ernst Bleck,
with support from Micronaut 2012

ANALYSIS OF POXVIRUS HOST CELL ENTRY BY ELECTRON MICROSCOPY

Inauguraldissertation

zur
Erlangung der Würde eines Doktors der Philosophie
vorgelegt der
Philosophisch-Naturwissenschaftlichen Fakultät
der Universität Basel

von

CHRISTOPHER KARL ERNST BLECK

Diplom Biologe, Ruprechts-Karl Universität Heidelberg
geboren am 17. Juni 1976
aus Heidelberg, Deutschland

Basel, Schweiz 2013

Namensnennung-Keine kommerzielle Nutzung-Keine Bearbeitung 2.5 Schweiz

---

Sie dürfen:

das Werk vervielfältigen, verbreiten und öffentlich zugänglich machen

Zu den folgenden Bedingungen:

Namensnennung. Sie müssen den Namen des Autors/Rechteinhabers in der von ihm festgelegten Weise nennen (wodurch aber nicht der Eindruck entstehen darf, Sie oder die Nutzung des Werkes durch Sie würden entlohnt).

Keine kommerzielle Nutzung. Dieses Werk darf nicht für kommerzielle Zwecke verwendet werden.

Keine Bearbeitung. Dieses Werk darf nicht bearbeitet oder in anderer Weise verändert werden.

- Im Falle einer Verbreitung müssen Sie anderen die Lizenzbedingungen, unter welche dieses Werk fällt, mitteilen. Am Einfachsten ist es, einen Link auf diese Seite einzubinden.

- Jede der vorgenannten Bedingungen kann aufgehoben werden, sofern Sie die Einwilligung des Rechteinhabers dazu erhalten.
- Diese Lizenz lässt die Urheberpersönlichkeitsrechte unberührt.

Die gesetzlichen Schranken des Urheberrechts bleiben hiervon unberührt.

Die Commons Deed ist eine Zusammenfassung des Lizenzvertrags in allgemeinverständlicher Sprache: http://creativecommons.org/licenses/by-nc-nd/2.5/ch/legalcode.de

Haftungsausschluss:
Die Commons Deed ist kein Lizenzvertrag. Sie ist lediglich ein Referenztext, der den zugrundeliegenden Lizenzvertrag übersichtlich und in allgemeinverständlicher Sprache wiedergibt. Die Deed selbst entfaltet keine juristische Wirkung und erscheint im eigentlichen Lizenzvertrag nicht. Creative Commons ist keine Rechtsanwaltsgesellschaft und leistet keine Rechtsberatung. Die Weitergabe und Verlinkung des Commons Deeds führt zu keinem Mandatsverhältnis.

Quelle: http://creativecommons.org/licenses/by-nc-nd/2.5/ch/ Datum: 3.4.2009

Genehmigt von der Philosophisch-Naturwissenschaftlichen Fakultät auf

Antrag von

Prof. Dr. H. Stahlberg, Prof. Dr. C. Dehio & Dr. J. Mercer

Basel, den 16. Oktober 2012

Prof. Dr. Jörg Schibler

Dekan der Philosophisch-
Naturwissenschaftlichen Fakultät

I dedicate this thesis to
my lovely wife and son,
who offered me unconditional love and support
throughout the course of this thesis.

Summary

Vaccinia virus (VACV) is the prototypic poxvirus and is complex in both composition and life cycle. In contrast to most viruses, poxviruses produce two types of infectious particles with different roles in virus dissemination: Mature virions (MVs) mediate host-to-host transmission, whereas extracellular virions (EVs) accomplish virus dissemination in an infected organism. While MVs are enveloped by a single lipid membrane, EVs exhibit an unusual composition – they consist of an MV-like particle that is wrapped with a second membrane.

Like all viruses, poxviruses depend on the host cell machinery to reach their final site of replication in the cytosol. Host cell entry of MVs is known to involve macropinocytosis and fusion of viral membranes with cellular membranes of endocytic compartments. Due to their topology, EVs require an unusual entry strategy and the outermost membrane is thought to be lost by non-fusogenic disruption, whereas the inner membrane is removed by fusion. Hence, EV and MV entry both result in the release of viral cores containing the DNA genome into the host cell cytosol.

One aim of this thesis was to understand the cellular entry process of VACV EVs, chapter 2 (see page 27), and MVs, chapter 4 (see page 87), in detail. In the case of EVs, we wanted to investigate whether this process involves endocytosis, where and how the EV membrane is lost, and which cellular factors and processes were exploited in the course of this process. Furthermore, we intended to study the processes that occur after release of viral cores into the cytosol and allow early gene expression.

The results of our investigations on the cellular entry mechanism of VACV EVs are presented in chapter 2 (see page 27). EV entry into HeLa cells was studied using fluorescence microscopy and electron microscopy in combination with flow cytometry. We show that complete EVs are internalized by macropinocytosis and that this step is actively triggered by EVs. Acidification of macropinosomes induces disruption of EV membranes and this exposes the underlying MV-like particle. The latter presumably fuses with cellular membranes and releases the viral core into the host cell cytosol.

A further issue of this thesis was to support a high-throughput RNAi silencing screen, which identifies host cell factors required during vaccinia virus infection, with electron microscopy analysis. Validation and analysis of clustered hits revealed previously unknown processes during virus entry including a new mechanism for genome uncoating and was confirmed by EM. Viral core proteins were found to be ubiquitinated already during virus assembly. After entering the cytosol of an uninfected cell, the viral DNA was released from the core through the activity of the cell's proteasomes. Next, a Cullin3-based ubiquitin ligase-mediated round of ubiquitination and proteasome action was needed to initiate viral DNA replication.

Our efforts to clarify the mechanisms underlying core activation after fusion are presented in chapter 4 (see page 87) and the main research aspect of this thesis. Morphological changes in viral structures were observed by conventional and cryo-electron microscopy to occur immediately after viral fusion and may involve the reduction of disulfide bonds in proteins that comprise the viral core wall. Lateral bodies, proteinaceous structures that are packaged into VACV MVs and EVs in addition to the cores, dissociate from viral cores upon fusion. Both processes, core activation and dissociation of lateral bodies, require cellular factors or components. They cannot be recapitulated by removal of membranes and reduction *in vitro*.

We identified F18 as a major structural protein of the lateral bodies, which are left back at the membrane after fusion. We found that the decomposition of lateral bodies by the host cell proteasome releases at least one immediate effector protein into the host cell, the dual specific viral phosphatase VH1. Furthermore, we identified a number of disulfide-bonded core proteins and found that some of them are reduced during activation. This possibly contributes to subtle changes that finally allow early gene transcription in the core.

We thus have compelling reasons to propose a new viral delivery mechanism for immediate effector proteins that is very likely used to release additional, so far unknown, effector proteins.

Contents

Chapter 1

Introduction

1.1 Vaccinia Virus

1.1.1 The poxvirus family

Poxviruses are large cytoplasmic DNA viruses that replicate entirely in the host cell cytoplasm and co-evolved with animals from insects (entomopoxviruses) to vertebrates (chordopoxviruses). They encode 130-328 genes, among which 66 are shared by all poxviruses and 119 are found in all chordopoxviruses. Poxviruses share a set of 41 genes with other nucleo-cytoplasmic

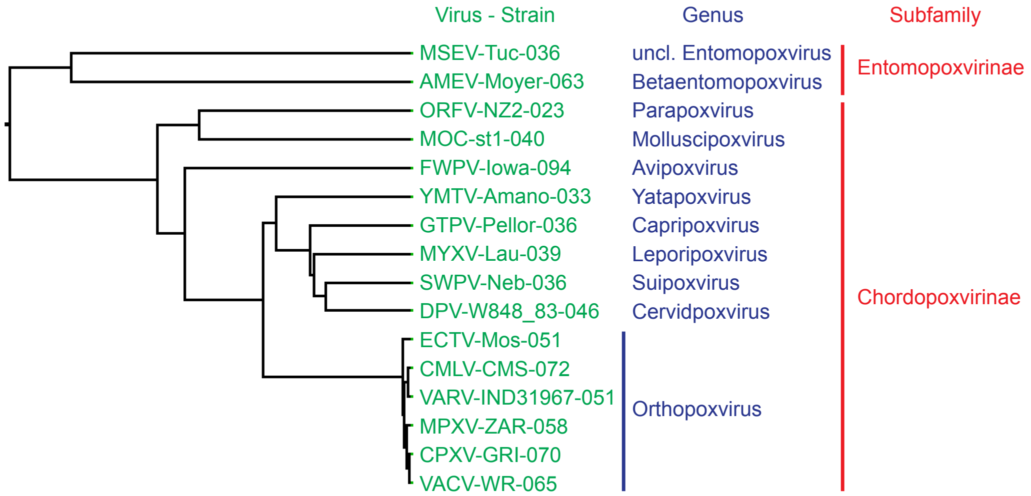

Figure 1.1 Poxvirus phylogeny based on the DNA polymerase sequence. Complete linkage tree based on ClustalW alignment created with Viral Orthologous Clusters [248]. uncl. = unclassified.

large DNA viruses and a common origin has been suggested [109]. Among the nine distinguished chordopoxvirus genera (see Figure 1.1), orthopoxviruses are the best studied and contain *vaccinia virus* (VACV), the prototype poxvirus, *variola virus* (VARV), the etiologic agent of smallpox, and *monkeypox virus* (MPXV), which induces morbidity similar to smallpox in humans. Besides that, only *molluscum contagiosum virus* (MOCV), a molluscipoxvirus, is considered a human pathogen and causes benign skin lesions. Many other poxviruses, however, can elicit zoonotic infections in humans [241, 131].

Poxvirus infection in host organisms can occur through the airway (VARV), skin lesions (MOCV), or ingestion (entomopoxviruses) [53, 155]. Infection may be restricted locally, often in the skin (MOCV, VACV after intradermal inoculation) or spread systemically (VARV). Systemic infections may, as in the case of VARV, involve multiple rounds of virus spread at the site of entry, in secondary lymphoid organs and in the skin. During virus spread, diverse cell types such as epithelial cells, fibroblasts, and cells of the hematopoietic lineage are infected. Thus poxviruses possess a relatively broad cellular tropism within a host species. Poxvirus infection in non-permissive cells is in most cases blocked at post entry steps [145].

1.1.2 Vaccinia virus

VACV was successfully used as a live vaccine against smallpox and most of our current knowledge on the molecular biology of poxvirus infections has been learned through the study of this virus. However, its origin and natural host remains obscure [163]. Confusion is in part caused by the use of the term *cowpox virus* (CPXV) to describe a variety of divergent orthopoxviruses infecting cattle. In fact, different CPXV isolates were found to be more distantly related than other accepted orthopoxvirus species and may comprise up to five different orthopoxvirus species [28]. While CPXV from the British Isles was presumably used as a live vaccine against smallpox in initial vaccination attempts, VACV was recently found to be closely related to CPXV isolates found in continental Europe, which are only distantly related to CPXV from the British Isles [28]. VACV strains preserved as freeze-dried vaccines were ultimatively used in the worldwide WHO vaccination campaign that lead to the eradication of smallpox in 1979. VACV-related viruses are currently circulating in cattle in Brazil as well as buffaloes in India; both may be derived from vaccine strains [130, 271]. The two most commonly used VACV laboratory strains, Western Reserve (WR) and International Health Department strain J (IHD-J), are both neurotropic in mice as a result of multiple intra-cerebral mouse passages of VACV vaccine strains [266, 105, 70].

1.1.3 Replication and assembly of infectious particles

The 195 kbp dsDNA genome of VACV encodes for around 200 proteins, which are expressed in a hierarchical and temporally controlled fashion. This is coordinated by early, intermediate, and late transcription factors that recognise specific promoter elements upstream of the coding sequences [163]. Early transcription factors and the viral RNA polymerase complex are packaged into the cores of infectious particles and early viral genes are immediately transcribed and expressed following release of viral cores into the host cell cytoplasm (see chapter 1.1.6). Early genes encode host modulatory factors as well as viral enzymes that set the stage for core uncoating and DNA replication [274]. In addition, intermediate transcription factors are produced that allow the next set of viral genes to be transcribed and translated. After uncoating, the DNA genome is replicated by viral enzymes in distinct cytoplasmic replication sites [119, 141]. The two strands of poxvirus dsDNA genomes are connected by terminal loops and their replication involves the formation of DNA concatamers. Replicated DNA genomes are the template for the transcription of viral intermediate genes encoding proteins for DNA packaging and organisation, structural proteins of the viral core, and late transcription factors [276]. Late transcription then drives the expression of additional structural components needed for the formation of viral particles. Included are early transcription factors and the RNA polymerase complexes that are packaged into newly formed progeny virus [276].

Members of the poxvirus family are unique in that they produce two types of progeny virus: mature virions (MVs) and extracellular virions (EVs) [163]. When intact, both viral particles do not share common viral surface epitopes, although they share the same viral core and genome.

1.1.3.1 Mature Virions

MVs are the less complex infectious virus form produced by VACV-infected cells. They contain a viral core with the DNA genome and two proteinaceous lateral bodies, which are surrounded by one lipid bilayer containing at least 25 viral proteins [163]. MV membrane proteins are highly cross-linked by disulfide bonds and the combined treatment with detergents and reducing agents is required to solubilize them [65]. MV assembly starts with the accumulation of electron dense viral material and the occurrence of crescents – curved single lipid bilayer sheets, which are supported by scaffold proteins (see Figure 1.3 and 1.4) [163]. Crescent membranes may be derived from membranes of the endoplasmic reticulum and it was speculated that they are generated *de novo* or by rupture of cytosolic vesicles [46, 89, 41]. The

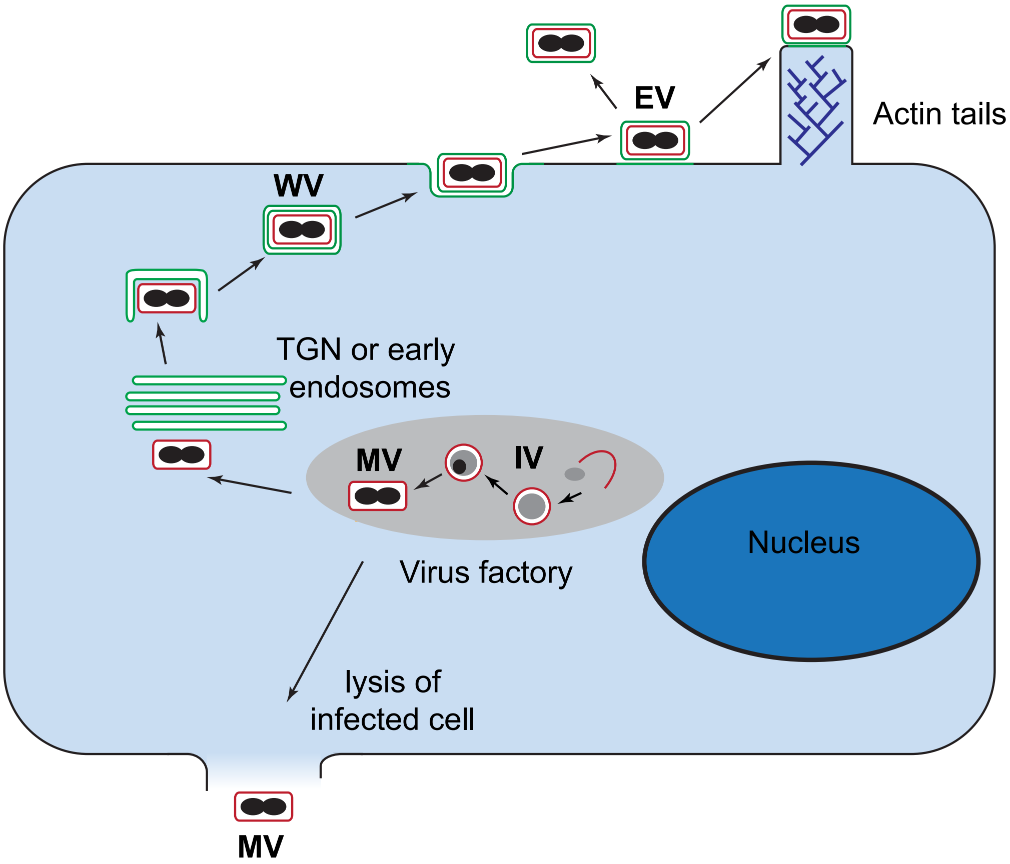

Figure 1.2 Vaccinia virus replication cycle. IV = immature virion, EV = extracellular virion, MV = mature virion, WV = wrapped virion, TGN = trans-golgi network.

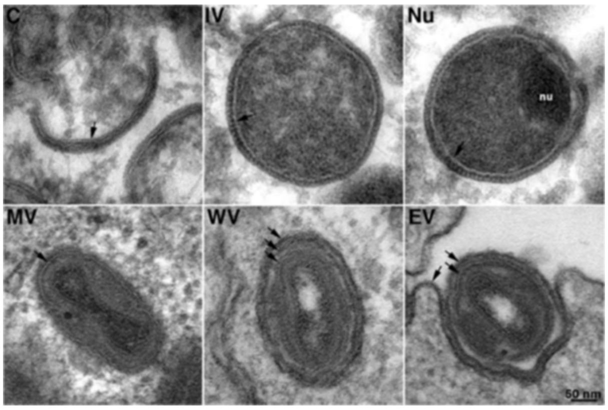

Figure 1.3 Vaccinia virus particles. C = crescent, IV = immature virion, Nu = immature virion with nucleoid, MV = mature virion, WV = wrapped virion, EV = extracellular virion. Illustration from [163].

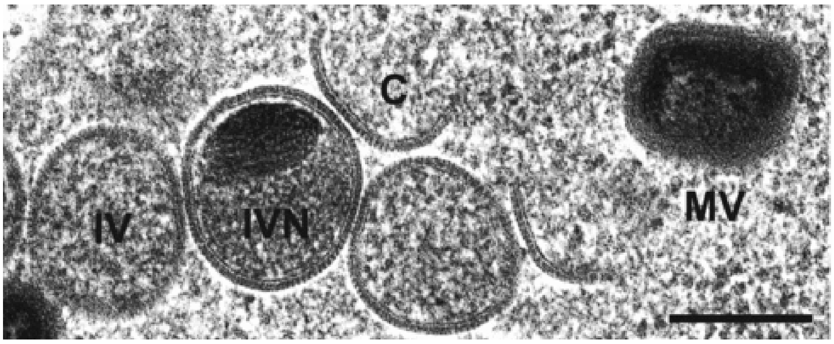

Figure 1.4 Vaccinia virus MV morphogenesis. C = crescent, IV = immature virion, IVN = immature virion with nucleoid, MV = mature virion. Reproduced with permission, from Chichon *et al.*, 2009, Biology of the Cell, 101 (7), 401–414 [38]. © the Biochemical Society.

first virus intermediates with a closed viral membrane are immature virions (IVs). They contain viral core proteins and a single membrane, which is coated by the scaffolding protein D13 on the outside [46]. D13, interestingly, is a structural homologue of capsid proteins found in all large icosahedral dsDNA viruses [103, 11]. When the condensed viral DNA is visible in electron micrographs, IVs are called immature virions with nucleoid (IVN) [163]. It was speculated that viral DNA may not be visible in IVs due to the position of the cross section or due to the un-condensed state of the DNA [46, 41]. In this case, DNA would be packaged during IV formation, whereas DNA acquisition after IV membrane closure would require DNA transport across membranes.

A complex maturation process transforms IVs into MVs and this morphogenesis leads to the formation of distinct viral cores and lateral bodies within the viral envelope (see Figure 1.3 and 1.4) [46]. Maturation involves proteolytic cleavage of core and membrane proteins by the VACV cysteine protease I7. Cleavage of the membrane protein A17 results in loss of the D13 and the respective protein coat that surrounds IVs. The viral metalloprotease G1 is also required for final steps in morphogenesis, but its substrates are currently unknown [46]. Maturation also includes the formation of disulfide bonds in MV membrane proteins as well as several core proteins [46, 216, 135]. Oxidation of membrane proteins within the reducing host cell cytosol is catalysed by a cascade of viral enzymes. Electrons of the respective substrates are transferred to the viral oxidoreductases G4, which again reduces a dimer of the sulphydryl oxidase E10 and A2.5. Possibly using the cofactor FAD, electrons are ultimatively transferred to O_2 (see Figure 1.5) [216]. That disulfide bonds in VACV proteins are stable in the reducing host cell cytosol demands that the involved residues are not solvent-accessible or secluded from the cytosol by compartmentalisation, since the cytosol remains reducing in the course of the infection [135]. The catalytic mechanism of disulfide bond formation in core proteins has not yet been studied in detail. Finally, MV maturation involves the acquisition of additional MV membrane proteins, e.g. A27 and L1. While all mentioned steps are a prerequisite for successful MV formation, their exact order is not known [46].

MVs accumulate in the host cell cytosol and eventually leave the cell upon lysis. They are the more abundantly produced infectious form and are, due to their stability, thought to mediate host-to-host transmission of poxvirus infection [222].

In entomopoxviruses, avipoxviruses and some orthopoxviruses, MVs can be clustered into cytosolic proteinaceous A-type inclusions (ATIs). ATIs are released by host cell lysis and may protect virus particles in the harsh extracellular environment [163]. Formation of ATIs requires the viral ATI protein and incorporation of MVs into ATIs is dependent on A26, which links A27 on the MV membrane to ATI proteins [95]. VACV and VARV only encode a truncated form of the ATI protein, A25, and consequently do not form ATIs [5, 163].

1.1.3.2 Extracellular Virions

EVs are composed of an MV-like particle that is surrounded by an additional membrane that includes unique EV proteins. EVs and MVs contain the same viral core and the inner membrane of an EV is similar, but not identical, to the MV membrane. The outermost membrane contains cellular proteins and at least 6 unique EV membrane proteins: A33, A34, A56, B5, F13, and K2 [175, 223, 221].

To form EVs, a distinct subset of MV-like particles is wrapped with two additional membranes that are derived from the trans-golgi network (TGN), early endosomes, or a hybrid compartment. This process results in wrapped virions (WVs), intermediates which are surrounded by three membranes. The outer membrane of WVs contains EV membrane proteins and three viral proteins only found in WVs: A36, F12, and E2 [223, 61]. The outermost WV membranes fuse with the plasma membrane to release EV particles by

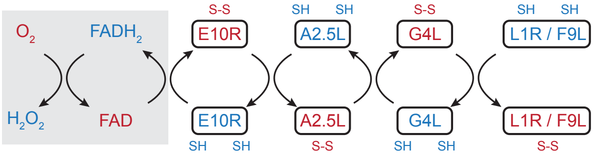

Figure 1.5 Vaccinia virus disulfide bond formation pathway. Illustration adapted from [216].

exocytosis.

Purified EVs do not contain A25 (truncated N-terminus of ATI protein) and A26, two proteins tethered to the MV membrane via A27. It is therefore likely that the MV-like particles that are wrapped to form EVs are distinct from the majority of MVs [246, 94]. In accordance with this, peak EV production precedes peak MV production [246]. A27 on the MV-like membrane is required for microtubule-dependent transport of virus particles to the site of wrapping, the microtubule organising centre [198]. It is tempting to speculate that the accessibility of A27 – in MVs bound to A25/A26 – is critical for EV formation. Wrapping itself is dependent on A27 as well as F13, B5, F12, and E2 in what become the outer two WV membranes [223, 60]. WVs are transported to the plasma membrane along microtubule and this requires kinesin-1 and A36 [192, 61]. F12 has been implicated in this process as well [158]. WVs undergo actin-dependent movement in the cell cortex and this requires F11-mediated inhibition of RhoA-mDia signalling [9].

Once released by exocytosis, the majority of EVs remains cell-associated and only few EVs are released into the surrounding liquid. The amount of released EVs is virus strain and cell-type specific. A point mutation in the EV protein A34 of VACV strain IHD-J that is not found in VACV strain WR or VARV leads to the enhanced release of EVs [187, 176]. In addition, infected cells of the rabbit epithelial cell line RK13 released more EVs into the medium than HeLa cells [176]. Cell-associated EVs can induce the formation of actin tails, which project viral particles away from the producer cell towards adjacent cells [223].

Fusion of the outermost WV membrane deposits viral proteins below cell-associated EVs. One of them, A36, can be phosphorylated by Src kinases and recruits a signalling complex containing of Grb2, Nck, WIP, and N-WASP [74, 157, 205, 259]. Locally restricted activation of Arp2/3 complexes induces actin polymerisation below EVs, resulting in protruding actin tails with EVs at their tip. This process can also be induced by super-infecting EVs that attach to VACV-infected cells expressing the viral proteins A33 and A36 [59].

EVs are the less abundant infectious form, but are crucial for virus spread within an infected organism [177]. EVs on the tip of actin tails are though to mediate virus spread within a tissue and efficient plaque formation in monolayers of tissue culture cell lines [223]. Free EVs are responsible for tissue-to-tissue spread within an infected organism and mediate infection of more distant cells in monolayers of tissue culture cells. In the latter case, this results in the formation of satellite plaques appearing as “comet tails”of plaques [223, 222]. In line with their role in virus spread through body fluids, EVs incorporate host cell complement control proteins and are more difficult to neutralise by antibodies than MVs [252, 129].

1.1.4 Host cell entry of MVs

Viruses are obligate intracellular pathogens and have to deliver their genome and accessory proteins to their final site of replication in the host cell. Viral entry involves virus binding to surface receptors on the host cell and either direct penetration of the plasma membrane, or virus-induced endocytosis followed by membrane penetration from endocytic organelles. Membrane penetration may include fusion of viral and cellular membranes, or non-fusogenic mechanisms such as pore formation, injection, translocation, or physical disruption of cellular membranes [143].

VACV MVs and EVs share no common viral or cellular surface proteins and their membranes are of different cellular origin. Thus, both infectious forms of VACV have to be able to gain access to the host cell cytoplasm independently. While MVs are surrounded by a single lipid bilayer and can penetrate cellular membranes by a simple fusion event, EVs contain two membranes and have a more complex entry strategy that involves non-fusogenic disruption of one and fusion of the other membrane [162]. Since MVs and EVs contain the same viral core and genome, both entry pathways converge when the viral core is released into the host cell cytosol, where uncoating (see section 1.1.6 on page 16) and viral replication (see section 1.1.3 on page 3) occurs.

1.1.4.1 Binding

The first step in virus entry is the attachment of the viral particle to the cell surface. Cellular factors in the plasma membrane contribute to both enrichment of viruses on cells (attachment factors) and promotion of subsequent entry steps such as activation of fusion proteins, signalling, or endocytosis [143].

Binding of VACV MVs was analysed in multiple studies and it has become evident that MVs employ several and partly redundant binding modes. This explains why poxviruses can infect many different cell types in an infected animal and why pure MVs are able to bind to all cell lines tested. Glycosaminoglycans (GAGs) at the cell surface can be hijacked as attachment factors by MVs. Binding to heparan sulphate was proposed to be mediated by the MV membrane proteins A27 [44, 96] and H3 [133], and binding to chondroitin sulphate conferred by D8 [97]. The dependence on GAGs for binding and infection, however, varies with cell type, virus strain, and experimental conditions [16, 29, 261]. There is evidence for GAG-independent cell binding mediated by the MV membrane protein L1 [73] and the MV membrane-associated protein A26 mediates binding to the extracellular matrix glycoprotein laminin [39]. A monoclonal antibody with an unknown cellular epitope has been shown to inhibit MV binding and infection, although it may prevent virus binding sterically [40, 250]. The finding that MVs move along filopodia towards the cell body suggests that at least one of the attachment factors can undergo retrograde flow along the actin cytoskeleton [148, 99]. MVs have also been reported to bind to liposomes directly, suggesting GAG- and protein-independent binding mechanisms exist [182, 173].

Although details of the host cell attachment factors exploited by MVs remain to be determined, it is evident that several redundant attachment modes have evolved to secure binding to a broad range of host cells.

1.1.4.2 Phagocytosis

Phagocytosis is a specific form of endocytosis involving the vesicular internalisation of solid particles, such as bacteria or dead tissue cells and therefore distinct from other forms of endocytosis such as pinocytosis, the vesicular internalisation of liquids.

Phagocytosis is the cellular process of engulfing solid particles by the cell membrane to form an internal phagosome. The phagosome fuses sequentially with the different organelles of the endocytic pathway. First early endosomes, then late endosomes and finally lysosomes. The latter two organelles, that are often together termed as “lysosomes”allow the delivery of hydrolases and the protein ATPase to the phagosome, thereby providing a low pH hydrolytic environment in this organelle. The contents are subsequently degraded and either released extracellularly via exocytosis, or remain intra-cellularly to undergo further processing. This process is commonly named “phagosome maturation”.

It is mainly carried out by specialised cells that are “professional”phagocytes. In mammals there are three classes of white blood cells that act as professional phagocytes: macrophages, neutrophils and dendritic cells [72]. These three types of cells develop from a common precursor cell, and they defend us against infection by ingesting invading microorganisms. Macrophages also play an important part in scavenging senescent and damaged cells and cellular debris. Phagocytosis is considered a centrepiece in mechanisms of innate immunity.

Whereas the endocytic vesicles involved in pinocytosis (receptor mediated endocytosis) are small (50-100 nm), phagosomes have diameters that are determined by the size of the ingested particle, and they can be almost as large as the phagocytic cell itself. The phagosomes fuse with lysosomes, and the ingested material is degraded; indigestible substances will remain in lysosomes, forming residual bodies.

In order to be phagocytosed, particles must first bind to the surface of the phagocyte. Not all particles that bind are ingested, however. Phagocytes have a variety of specialised surface receptors that are functionally linked to the phagocytic machinery of the cell. Unlike pinocytosis, which is a constitutive process that occurs continuously, phagocytosis is a triggered process that requires activated receptors transmitting signals to the cell interior to initiate the response. The best characterised triggers are antibodies, which protect us by binding to the surface of infectious micro-organisms to form a coat in which the tail region of each antibody molecule (called the Fc region) is exposed on the exterior. This antibody coat is then recognised by specific Fc receptors on the surface of macrophages and neutrophils. The binding of antibody-coated particles to these receptors induces the phagocytic cell to extend pseudopods that engulf the particle and fuse at their tips to form a phagosome [72].

Several other classes of receptors that promote phagocytosis have been characterised – such as those that recognise complement (a class of molecules that circulate in the blood and collaborate with antibodies in targeting undesirable cells for destruction) and those that directly recognise sugars such as mannose that present oligo-saccharides on the surface of many microorganisms.

1.1.4.3 Endocytosis

In eukaryote cells, the routes that lead inward towards the lysosomes from the cell surface start with the process of endocytosis, by which cells take up fluid, specific ligands such as hormones, macromolecules, particulate substances, and, in specialised cases, even other cells [81, 180].

Material to be ingested is progressively enclosed by a small portion of the plasma membrane, which first invaginates and then pinches off to form an intracellular vesicle containing the ingested substance or particle. Two main types of endocytosis are distinguished on the basis of the size of the endocytic vesicles formed: pinocytosis (most prominently clathrin-coated vesicles) [52, 180], which involves the ingestion of fluid and solutes via small vesicles (50-150 nm in diameter), and phagocytosis, which involves the ingestion of large particles, such as microorganisms or cell debris, via large vesicles called phagosomes, generally >250 nm in diameter. A related mechanism that allows cells to take large amounts of volume in relatively large vesicles is macropinocytosis [120, 149].

Although most eukaryotic cells are continually ingesting fluid and solutes by pinocytosis, large particles are ingested mainly by specialised phagocytic cells.

Fusion of enveloped viruses with cellular membranes can occur at the plasma membrane or after endocytic uptake of viral particles. While fusion at the plasma membrane seems to be less demanding on the cellular machinery needed, fusion after endocytic uptake has several striking advantages: (i) Cellular transport mechanisms ferry the virus particle to the point of fusion, the cortical actin cytoskeleton barrier is thus avoided. (ii) No traces that could be recognised by the immune system are left behind in the plasma membrane. (iii) Active conformations of the fusion proteins, often sensitive to neutralising antibodies, are not accessible to the immune system [143, 218].

Conflicting results on MV entry had previously been obtained and both fusion at the plasma membrane and endocytic internalisation of MVs was visualised by electron microscopy [51, 34, 239]. However, the application of large numbers of viral particles for electron microscopy experiments may have led to the observation of less important or even artificial entry pathways at the plasma membrane and in most cases defied thorough quantification. Recent studies using internalisation assays and inhibitors of distinct endocytic processes confirmed that the main entry route of VACV MVs in HeLa and several other cell types is endocytosis [239, 148, 99, 152, 199]. In the case of strain WR, artificial fusion with plasma membranes induced by brief acidification allowed infection in the presence of endocytosis inhibitors, indicating that these only blocked endocytosis and no other aspects of viral replication [148].

To be internalised, MVs exploit macropinocytosis (see Section 1.2.3 on page 21). This form of endocytosis is signalling-induced and involves dramatic actin rearrangements to engulf large amounts of bulk fluid. Cargo is therefore taken up in a receptor-independent fashion. MV-induced macropinocytosis is dependent on phosphatidylserine (PS) in the MV membrane and requires epidermal growth factor receptor (EGFR) signalling [148, 152]. In intact cells, PS is confined to the inner leaflet of the plasma membrane and its exposure on apoptotic bodies marks them for endocytic uptake [249]. MVs resemble apoptotic bodies in this aspect and since the latter can be cleared from tissue by macropinocytosis, it was postulated that VACV MVs employ apoptotic mimicry [91, 148]. Despite the discovery of several PS receptors, the receptor used by MVs remains elusive and so does the question whether the hypothetical receptor binds phosphatidylglycerol or the D-stereoisomer of PS, two lipids not found in the MV membrane, which can functionally substitute the naturally occurring PS [126]. Uptake of apoptotic bodies elicits anti-inflammatory signals in the cells [69]; it is intriguing to speculate that VACV infection could benefit from such modifications of the host immune system.

Macropinocytosis is initiated by the formation of dynamic membrane pro-

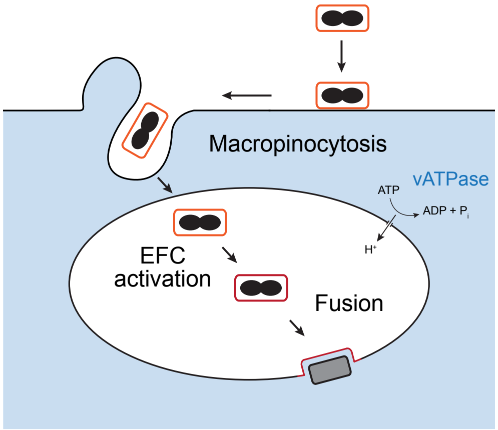

Figure 1.6 Summary of VACV MV entry. VACV MVs bind to host cells and trigger macropinocytosis through phosphatidylserin (PS)-dependent signalling processes. Internalisation is followed by acidification of macropinosomes, activation of EFCs, fusion, and release of cores into the host cell cytosol.

trusions that may appear as lamellipodia, circular ruffles, or blebs. Macropinocytosis induced by MVs of strain WR, in fact, helped to define the latter type of membrane protrusions. Whether the massive induction of filopodia caused by MVs of strain IHD-J is involved in macropinosome formation is currently unclear [148]. A fraction of the signalling-triggered membrane protrusions folds back to form macropinosomes of irregular size and shape, which internalise bulk fluid and virus particles. Important cellular factors involved in this process include cholesterol, Na^+/H^+ exchangers, tyrosine kinases, protein kinase C (PKC), members of the Rho GTPase family, p21-activated kinase 1 (PAK1), and myosins [136, 148, 99, 152]. They all act in concert to mediate the required actin rearrangements as well as subsequent steps of macropinosome formation. An additional cellular factor, VPEF/FAM21, is required for MV infection. Unlike previously suggested, it is a cytosolic protein and has recently been shown to be involved in Arp2/3-dependent vesicle scission [99, 78]. Macropinocytotic uptake into HeLa cells induced by MVs of the two VACV strains WR and IHD-J exhibited slight differences in the involved signalling cascades [151]. This suggests that different types of macropinocytosis exist and can be induced by subtly different triggers. Macropinocytic uptake of MVs was confirmed in several cell types, including monocyte-derived dendritic cells (MDDCs) [199]. Macropinocytosis, however, does not need to be triggered in MDDCs and is constantly active to monitor the environment as part of the immuno surveillance function of these cells [169]. Contrary to that, MV entry into CHO cells is most likely independent of macropinocytosis [151].

1.1.4.4 Fusion

Enveloped animal viruses undergo fusion events with cellular membranes to deposit the viral core or capsid into the host cell cytosol. The process is catalysed by viral fusion proteins in the virus envelope [143].

In the case of poxvirus MVs, the fusion activity is found in the single MV membrane and fusion is thought to be mediated or catalysed by a large macromolecular assembly of viral proteins, the entry/fusion complex (EFC) [213]. The EFC consists of stoichiometric amounts of the trans-membrane proteins A16, A21, A28, G3, G9, H2, J5, and L5. Associated with this are three further viral membrane proteins: F9, L1, and O3 [202, 22, 18]. All mentioned viral membrane proteins except for J5, which has not yet been tested, are required for efficient fusion of VACV MVs [171, 214, 215, 172, 213, 110, 213, 238]. A twelfth MV membrane protein, I2, is also required for fusion, although interaction with the other components has not yet been shown [168]. I2 and O3 are conserved in all chordopoxviruses, whereas all other factors are found in all sequenced poxvirus genomes, suggesting that a common fusion mechanism is used by all poxviruses [109]. The architecture of the EFC and the molecular details of the fusion reaction remain elusive. However, binary complexes between A28 and H2, A16 and G9, as well as G3 and L5 have been observed [166, 258, 267].

Two protein complexes have been shown to negatively regulate the EFC. A56-K2 dimers are localised to the plasma membrane of infected cells and to EV membranes [244]. They prevent super-infection of infected cells with MVs and are thought to prevent back-fusion of disrupted EVs with the plasma membrane of producer cells [245, 257]. In accordance with this function, VACV strains lacking A56 or K2 form extensive syncytia at neutral pH [105, 243]. This is mediated by progeny EVs at the plasma membrane, a fraction of which contains disrupted EV membranes. Exposed EFCs in the underlying MV membrane consecutively mediate virus-cell and cell-cell fusion (fusion from within).

Dimers of A25 and A26, which are tethered to the MV membrane through A27 and the trans-membrane protein A17, are thought to inhibit premature EFC-mediated fusion at neutral pH [35, 94]. Fusion of WR MVs containing A25/A26 with cellular membranes requires passage through acidified endocytic vesicles, whereas VACV strains lacking either of the two components do not need to traffic through low pH compartments and cause syncytia at neutral pH. While some laboratory VACV strains, such as MVA and IHD-W, naturally lack full length A25 or A26, VARV encodes A25 and A26 proteins at similar lengths as VACV WR [246, 35]. Fusion of VACV WR MVs with the plasma membrane and syncytia formation can be induced by acidification of bound virus particles (pH optimum 4.5-5.0), suggesting that such a treatment overcomes inhibition of fusion by A25/A26 [239]. However, treatment of MVs with low pH or proteases before binding accelerates infection, but does not override the need to passage through acidic compartments for successful infection [237]. This suggests that two steps in MV entry are dependent on low pH, which can both take place when bound MVs are treated with acidic solutions. Of note, A27, one of the proteins required to tether A25/A26 to the MV membrane, is lost when MV infection is accelerated by papain treatment [237].

MVs of several VACV strains do not need endocytic acidification for infection and their fusion with the plasma membrane cannot be induced by low pH [16, 261, 152]. Of note, MVs of VACV strain IHD-J are independent of low pH, but still enter cells through a macropinocytic mechanism [152]. The entry pathways of other pH-independent VACV strains have not been characterised in detail.

1.1.5 Host cell entry of EVs

Studies on EV entry have been hampered by the intrinsic instability of the outer EV membrane: not all released EVs contain an intact outer membrane and intact EV membranes are efficiently disrupted during freeze-thawing and EV purification strategies using different gradient material [107, 252]. To investigate genuine EV entry, intact EVs have to be discriminated from EVs with disrupted outer membranes as well as contaminating MVs. For infection experiments, MV-neutralising antibodies can be employed to block infection by MVs and EVs with disrupted outer membranes [107, 252]. Microscopic studies can only discriminate MVs from intact or disrupted EVs by visualising proteins in the EV membrane [250].

1.1.5.1 Binding

VACV MVs and EVs do not share any common epitopes and have been shown to use different attachment factors [250]. However, no cellular attachment factors for free EVs have been found so far. The serum protein Gas6 was shown to link phosphatidylserine in lentivirus membranes to the TAM receptor tyrosine kinase Axl on cells [159]. That Gas6 incubation boosts EV infection led to the speculation that similar mechanisms may be exploited by this virus form. Artificially disrupted EVs did not bind to naive T cells. However, the same virus particles bound to T cells after activation and transport of newly synthesised cellular receptors to the plasma membrane [32]. It is, however, unclear if factors in the EV or in the MV membrane mediated attachment.

1.1.5.2 Endocytosis or entry at the plasma membrane?

The presence of two membranes imposes unique requirements on EV entry because fusion of both membranes with cellular membranes would release the viral core into a compartment equivalent to the outside of the cell. It is therefore assumed, that the outer membrane is lost in a non-fusogenic process and that the inner membrane, containing the MV fusion machinery, undergoes fusion with cellular membranes. This is supported by the following observations: (1) EV entry depends on the EFC in the inner membrane, which is similar to MV membranes [214, 215]. (2) The outer EV membrane can be artificially disrupted by treatment with low pH and anionic polysaccharides *in vitro* [107, 252, 128]. (3) Electron micrographs show MV-like particles fusing with the plasma membrane in proximity of shed EV membranes [128].

Intact EVs were initially proposed to enter cells by endocytosis followed by acid-induced disruption of the EV membrane. This model of EV entry was based on the observations that (1) EV infection could take place in the presence of antibodies targeting proteins in the MV/MV-like membrane, (2) lysosomotropic agents inhibited EV infection, and (3) low pH triggered EV membrane disruption *in vitro* [107, 252]. A more recent study, however, concluded that EV membranes are disrupted upon contact with GAGs at the cell surface and that the released MV-like particle subsequently fuses with the plasma membrane. This model is supported by the finding that (1) the postulated events could be visualised by electron microscopy on cells producing GAGs, but not on cells deficient in GAG synthesis, and (2) EV membranes were disrupted by soluble anionic polysaccharides [128].

Entry of EV particles pushed to adjacent cells by actin tails has not been studied in detail. However, cell-associated and free EVs have the same composition and may follow similar entry routes.

1.1.5.3 EV disruption and fusion

Both proposed models for EV entry concur in that loss of the EV membrane occurs by non-fusogenic disruption [107, 252, 128]. The mechanism of EV membrane disruption *in vivo* or after low pH- or GAG-exposure *in vitro* is unclear. GAG-mediated EV disruption depends on the EV proteins B5 and A34, although A34 may only be required to recruit sufficient amounts of B5 to the EV membrane [128, 193]. Acidic residues in the membrane-proximal stalk region of B5 have been proposed to be required for GAG-induced membrane disruption [193]. Since EFCs in the inner MV-like membrane are crucial for EV infection [214, 215], it is assumed that the exposed MV-like particles subsequently undergo fusion with cellular membranes to release the viral core into the cytosol.

1.1.6 Core disassembly

Proteinaceous cores or capsids protect viral genomes and need to be uncoated to release the viral DNA or RNA. Often, viral capsids are in an intrinsically meta-stable state and disassembly is energetically favourable under certain conditions. Meta-stability may either be generated by structural rearrangements that occur during capsid maturation, or be induced by triggers in the host cell [79]. Uncoating induced by the latter mechanism may allow intracellular transport of viral cores or capsids within the host cell before disassembly begins.

Both MV and EV entry result in the release of viral cores into the host cell cytosol by fusion of viral and cellular membranes. Released cores undergo at least two distinct disassembly steps, activation and uncoating, that ultimately release the viral dsDNA genome from the core structure. This allows for DNA replication and production of progeny virus.

1.1.6.1 Activation

During or shortly after fusion, VACV cores undergo morphological changes that can be visualised by electron microscopy [51]. While viral cores in MVs or EVs possess biconcave cores as well as two lateral bodies, released cores are oval and lateral bodies are not visible. The nature of the morphological changes is currently unknown. However, treatment of virons with DTT *in vitro* led to similar morphological changes and the disulfide-bonded core proteins L4 and 4a were shown to be reduced in the course of infection, suggesting that reduction of core disulfide bonds may play a role in this process [135]. In addition, protein F18 found in cores of MVs and EVs has been shown to be absent from released viral cores [178].

VACV cores contain complexes of the viral RNA polymerase and early transcription factors pre-assembled on early promoters of the viral DNA. Early gene transcription and mRNA export from viral cores starts immediately after core release [272]. Early transcription can be artificially induced by treating MVs with mild detergents and reducing agents in the presence of NTPs [219]. The set of viral proteins required for early transcription from artificial templates *in vitro* has been defined. However, in the context of the viral core, transcription has additional requirements. MVs lacking L3, VP8, or H1, or MVs containing temperature sensitive (ts) mutants of E6 or E8 are unable to undergo efficient artificial core transcription [190, 265, 134, 21, 118]. However, none of these proteins bear a catalytic activity known to be required for transcription. Lysates of MVs lacking L3 or VP8, and lysates of MVs incorporating mutant E8 contain all required catalytic activities to transcribe early genes from artificial DNA templates. A relationship between morphological changes and the onset of transcription is conceivable, but has not been formally shown.

Released viral cores accumulate in the perinuclear region of the host cell and this localisation has been attributed to microtubule-dependent transport mechanisms or VACV-induced cell contractions [30, 212]. Early viral mRNAs have been reported to move along microtubule as well, and accumulate in distinct sites of early gene translation [142].

1.1.6.2 Uncoating

In a second core disassembly step, viral DNA has to be released from the proteinaceous core to allow DNA replication as well as intermediate and late gene expression.

Viral DNA in intact cores is insensitive to DNase treatment and uncoating was defined as the step that renders DNA sensitive to DNase [113, 114]. VACV DNA next to remnants of opened or empty viral cores has been observed in electron micrographs and this mode of DNA release suggests that the viral core structure does not need to be completely disassembled for DNA release [51, 178]. The viral core and DNA-binding protein VP8 was shown to remain associated with released viral DNA [178].

Uncoating of viral cores requires the expression of early viral genes. Thus, viral cores accumulate when transcription or translation is inhibited [112]. A viral uncoating factor has been partly purified and characterised using an *in vitro* uncoating assay [179]. However, the protein itself was not identified. The activity was found to be sensitive to protease inhibitors, but no early expressed viral protease has so far been identified or predicted.

1.2 Endocytosis

1.2.1 Overview of endocytic processes

The term endocytosis summarises different cellular transport pathways that result in the internalisation of cargo from the extracellular space or the plasma membrane into vesicles that fission into the cytosol [62, 152, 101]. Transported cargo is found in both the formed vesicle and the membrane

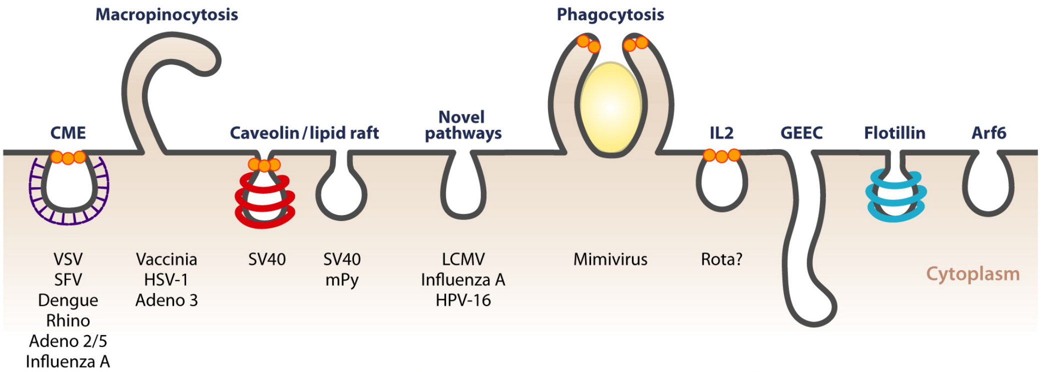

Figure 1.7 Endocytic mechanisms. Overview of described endocytic mechanisms with examples of viruses that exploit them. Abbreviations: Adeno 2/5, adenovirus 2/5; Adeno 3, adenovirus 3; CME, clathrin-mediated endocytosis; HPV-16, human papillomavirus 16; HSV-1, herpes simplex virus 1; LCMV, lymphocytic choriomeningitis virus; mPy, mouse polyomavirus; SFV, Semliki Forest virus; SV40, simian virus 40; VSV, vesicular stomatis virus. Illustration from [152]. Annual review of biochemistry Copyright 2010 by ANNUAL REVIEWS, INC.. Reproduced with permission of ANNUAL REVIEWS, INC. in the format Dissertation via Copyright Clearance Center (Order Detail ID: 57761303).

that surrounds it, and includes nutrients and their carriers, receptor-ligand complexes, fluid and solutes, lipids, membrane proteins, extracellular-matrix components, cell-debris, bacteria, viruses, and toxins [101]. Endocytosis controls protein and lipid composition of the plasma membrane and the extracellular space, and defines the availability of cargo molecules within the cell. It is involved in numerous cellular processes such as nutrient uptake, signalling, pathogen entry, cell adhesion and migration, cell growth and differentiation, and drug delivery [62].

Different mechanisms to form primary endocytic vesicles have evolved and they are classified mainly by the required cellular components, or the cargo (see Figure 1.7 and paragraph 1.2.2). Many types of endocytosis are exploited by viruses to gain access to the dynamic endosomal network, in which they transiently reside to be ferried to the site of membrane penetration. Using endocytosis has a number of advantages for the virus (summarised in paragraph 1.1.4.3). As defined and traceable cargo whose successful uptake leads to infection and can easily be quantified, viruses have proven invaluable tools to study endocytosis.

Endocytosis feeds cargo into early endosomes (EE) or equivalent compartments. Most knowledge on the subsequent processes has been gained through the study of clathrin-mediated endocytosis (CME), but trafficking of primary endocytic vesicles generated by other mechanisms is poorly stud-

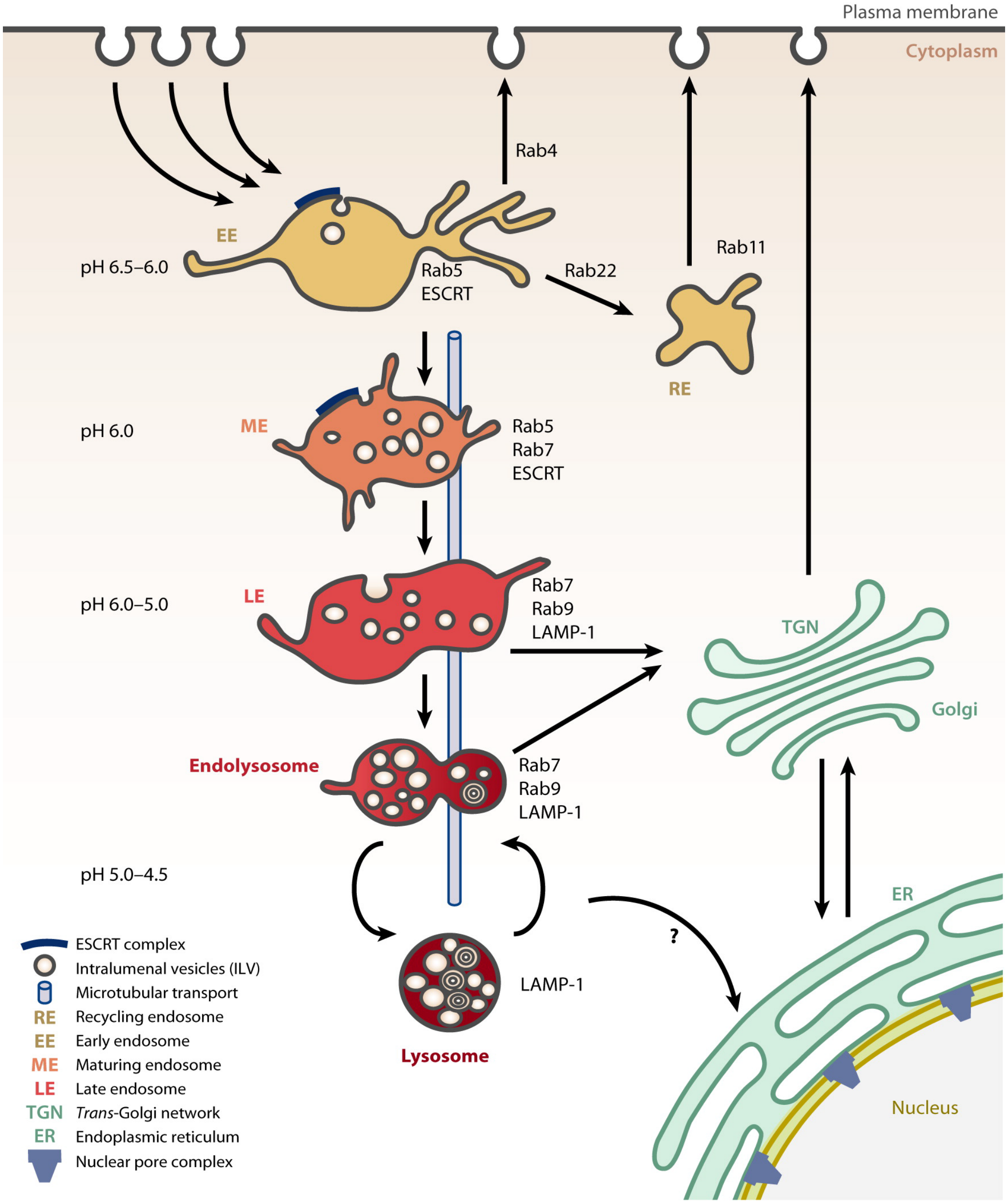

Figure 1.8 Overview of classical endosomal system. Illustration from [150]. Annual review of biochemistry Copyright 2010 by ANNUAL REVIEWS, INC.. Reproduced with permission of ANNUAL REVIEWS, INC. in the format Dissertation via Copyright Clearance Center (Order Detail ID: 57761308).

ied. Many of them, however, are assumed to merge with classical EE and thus exhibit intracellular trafficking similar to cargo of CME (see Figure 1.8) [152]. The bulk of the endocytosed material is shuttled back to the plasma membrane directly or via recycling endosomes, mostly from tubular domains of EE. A fraction of the cargo is destined to enter the degradative arm of the endosomal system via maturing endosomes, late endosomes (LE), endolysosomes, and lysosomes. The content of these organelles undergoes a number of changes. The lumenal pH becomes more and more acidic and at the same time concentrations of other ions change, hydrolases accumulate, and a fraction of the endosomal membrane and their protein content is internalised as intralumenal vesicles. Together, intralumenal conditions allow for the degradation of soluble and membrane-resident molecules by acid-activated hydrolases. These and other processes involving trafficking, fusion, and fission of endosomal vesicles are regulated by cytosolic proteins that are transiently associated with endocytic vesicles. Key regulators define the identity of the endocytic compartments and recruit effector proteins that modify it. Among them are members of the Rab family of small GTPases. Whereas Rab5 recruits effector proteins to EEs, similar roles are performed by Rab7 in LEs, while both are present in maturing endosomes. A platform for the recruitment of cellular effectors is also the lipid membrane of the respective vesicles itself. In particular phosphoinositides are modified by kinases and phosphatases to form docking sites for various proteins. While phosphatidylinositol 3-phosphate is mainly found in EEs, phosphatidylinositol 3,5-bisphosphate is predominantly found in LEs [101].

Endocytosis is regulated at the level of cargo internalisation and a complex network of regulator and effector proteins subsequently directs trafficking and maturation of endosomes. The versatile endosomal system allows the cell to fine-tune the plasma membrane composition and cellular uptake according to the cell's need.

1.2.2 Mechanisms of endocytosis

Primary endocytic vesicles are produced by a number of different mechanisms (see Figure 1.7), which all involve the formation membrane invaginations and division of vesicles from the plasma membrane. They differ in the cellular components that regulate their induction, induce membrane curvature, decorate invaginations and vesicles in the form of coats, and catalyse their fission.

The best understood and presumably most prevalent form of endocytosis is clathrin-mediated endocytosis (CME). In CME, primary vesicles are derived from clathrin coated-pits that contain macromolecular assemblies of receptor proteins, adaptor complexes and clathrin coat structures. Those pits are either assembled *de novo* around receptor-bound cargo or are present in the plasma membrane in a preformed state. Scission of clathrin-coated vesicles requires the GTPase dynamin-2 and the clathrin coat is rapidly disassembled after vesicle formation.

Clathrin-independent endocytic mechanisms often involve more complex signalling events and may require lipid rafts and cholesterol. Both caveolin and flotillin can form proteinaceous coats around invaginations at the plasma membrane or vesicles, although their role in endocytosis is a matter of intense debate [62, 152]. A number of mechanisms have been described that lead to the scission of small uncoated primary endocytic vesicles. The pathways are defined by the combination of required cellular factors and include lipid-raft mediated endocytosis, the IL-2 pathway, the CLIC/GEEC pathway, the Arf6 pathway, as well as other uncategorised entry pathways involved in the entry of lymphocytic choriomeningitis virus (LCMV) and human papillomavirus 16. Membrane curvature is induced by different proteins or the modified lipid composition. Scission may in these processes be catalysed by dynamin-2 or other, so far unidentified proteins.

Two types of endocytosis, macropinocytosis and phagocytosis, are distinct from other endocytic pathways in that they allow the internalisation of large volumes of fluid or large particles, respectively. Macropinocytosis is introduced in more detail in the next paragraph. Phagocytosis describes a number of related processes that allow the engulfment of large particles during which receptor interactions with the cargo guide the formation of primary vesicles that tightly wrap around the internalised particle. Cells of the immune system like macrophages, dendritic cells, and neutrophiles internalise pathogens by phagocytosis. Apoptotic bodies may in addition be phagocytosed by fibroblasts, epithelial cells, or endothelial cells. Phagocytosis shares the need for complex signalling events and dramatic cytoskeleton rearrangements with macropinocytosis [72].

1.2.3 Macropinocytosis

In contrast to other endocytic processes for the internalisation of soluble cargo, macropinocytosis results in the uptake of large quantities of bulk fluid into primary vesicles of heterogeneous sise termed macropinosomes. Few cells of the immune system, such as dendritic cells, constitutively sample their environment by macropinocytosis [169, 170, 197]. In most other cell types, macropinocytosis is a growth factor-induced process that is triggered by stimulation of the respective receptor tyrosine kinases (RTKs). The activated RTKs are thus removed from the plasma membrane, preventing further signalling. Macropinocytosis is also induced and exploited by several

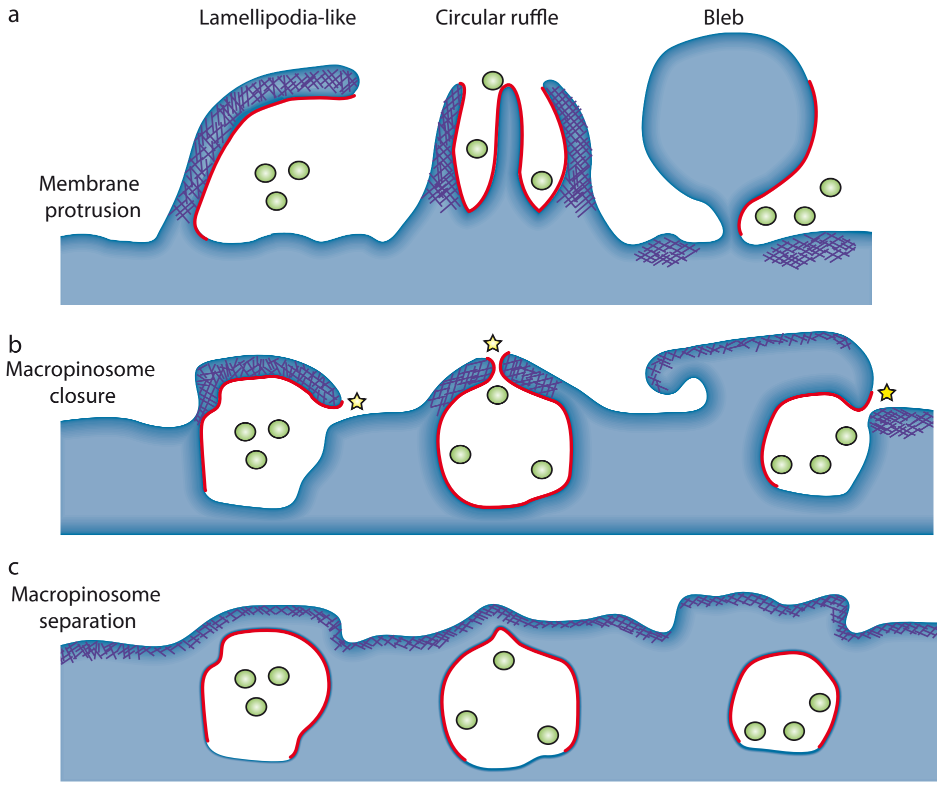

Figure 1.9 Macropinosome formation. Overview of different steps of macropinocytosis, which involves membrane protrusions in the form of lamellipodia, circular ruffles, or blebs (a), macropinosome closure (b), and fission of macropinosomes (c). Yellow stars highlight sites of vesicle closure. Reprinted by permission from Macmillan Publishers Ltd: NATURE CELL BIOLOGY [149], copyright 2009.

viruses, such as VACV MVs, adenovirus 3, adenovirus 35, echovirus 1, coxsackievirus B, herpes simplex virus 1, human immunodeficiency virus, and ebola virus, as well as bacteria, e.g. legionella, salmonella, shigella, and mycobacteria [120, 149, 6, 115, 165, 196, 55].

Induction of macropinocytosis is initiated by ligand-induced RTK activation or virus-induced receptor clustering, both of which may be accompanied by signal amplification and transmission by small GTPases of the Ras superfamily. For many pathogens exploiting macropinocytosis, the initial trigger for macropinocytosis has not yet been identified. Complex downstream signalling events subsequently mediate the formation of large plasma membrane protrusions that may have the form of lamellipodia, circular ruffles, or blebs (see Figure 1.9). Some of these may fold back and, through a membrane fusion step, internalise the incorporated fluid and, if present, virus particles [120, 149].

While the involvement of several kinases and small GTPases has been implicated in macropinocytosis upon various stimuli and in different cells, not all of them have been confirmed to be required in all cases. It is clear, however, that macropinocytosis depends on dramatic rearrangements of the actin cytoskeleton and a key regulator of these processes seems to be the small GTPase Rac1, or – in some cases – Cdc42. High metabolic activity below the plasma membrane causes local acidification, which needs to be neutralised by the sodium proton exchanger NHE1 to allow for efficient signalling of Rac1 and other small GTPases [122]. Activity of p21-activated kinase 1 (PAK1) downstream of Rac1 is critical for all stages of macropinocytosis. At the same time, cellular membranes are modified by posphoinositide 3-kinases (PI3K) to create docking sites for other signalling and effector proteins. Closure of macropinosomes seems to require myosin motors and either the activity of CtBP1/BARS, which is activated by PAK1, or dynamin 2. In addition, protein kinase C (PKC) is required for macropinocytosis, although the exact role of PKC signalling has not yet been defined [149].

The availability of small compound inhibitors allows the inhibition of various cellular process involved in macropinocytosis. Many growth factor receptors are targets of anti-cancer drugs and e.g. activation of the epithelial growth factor receptor (EGFR) is sensitive to Iressa [270]. Na^+/H^+ exchangers are inhibited by amiloride and amiloride derivatives like ethylisopropyl amiloride (EIPA) [255]. Rac1 and other small GTPases can be inhibited by peptide inhibitors [76] or over-expression of dominant negative mutants, while PAK1 activity is blocked by IPA-3 [56] or over-expression of the PAK1 autoinhibitory domain. Cytochalasin D prevents actin polymerization [47], and jasplakinolide is an efficient activator of actin polymerisation and stabilises the polymers [23]. Activity of myosin II motors can be inhibited with blebbistatin [229], while smooth muscle myosin light chain kinase (smMLCK), which is required for myosin activity, is blocked by ML-7 and similar compounds [139]. PI(3)K and PKC are e.g. blocked by wortmannin [186] and calphostin C [121], respectively. Most cellular factors required for macropinocytosis are involved in multiple cellular processes. Thus, only the requirement of the combination of the mentioned factors in addition to morphological and functional evidence, e.g. membrane protrusions and fluid phase uptake, define a process as macropinocytosis.

Once formed, macropinosomes can undergo homotypic fusion and maturation steps that are poorly defined and may depend on the trigger and the cell type. A large fraction of fluid and membranes needs to be recycled back to the plasma membrane and this may involve the formation of tubular domains and sorting nexin family members. Other cargo, in particular when internalized for immuno-surveillance or receptor down regulation, enters the degradative pathway and is finally degraded in lysosomes. Maturation of macropinosomes includes the modification of phosphoinositides in the outer leaflet of vesicles membranes, acquisition of Rab GTPases and their effectors, and acidification [120, 149]. To what extent macropinosomes cross-talk to the classical endosomal system with EEs and LEs, however, remains unclear.

A part of this introduction has been printed or published in [209] and [211].

1.3 Aim and structure of the thesis

1.3.1 EV entry

The membrane topology of poxvirus EVs demands a unique entry process. It is common belief in the field that EVs lose their outer membrane by a nonfusogenic process and that the EFC in the then exposed inner membrane catalyses or regulates fusion with cellular membranes. However, the location of EV membrane disruption and whether it involves endocytosis was controversial (see Figure 1.1.5.2). This thesis aimed at clarifying the entry route of VACV EVs with a focus on cellular processes hijacked by EVs to accomplish host cell entry. In a follow up project, insights into the activation of viral cores released into the host cell cytosol were supposed to be gained.

The experimental approach taken for this study has to be chosen in a way that all possible entry routes can be distinguished. When the membrane topology of EVs is taken into account, three different entry pathways are conceivable (illustrated in Figure 1.10): EVs may lose their outer membrane upon contact with the plasma membrane (possibilities A and B) or after endocytic uptake of intact EVs (C). Loss of the EV membrane at the plasma membrane may be followed by (A) endocytic internalisation of released MV-like particles and fusion with limiting membranes of endocytic vesicles, or (B) direct fusion of the released particles with the plasma membrane. Internalisation of intact EVs (C) would be followed by loss of the EV membrane in endocytic vesicles and subsequent fusion of the released MV-like particle with cellular membranes.

The study of EV entry has been published in The EMBO Journal (2011), issue 30, pages 3647 - 3661.

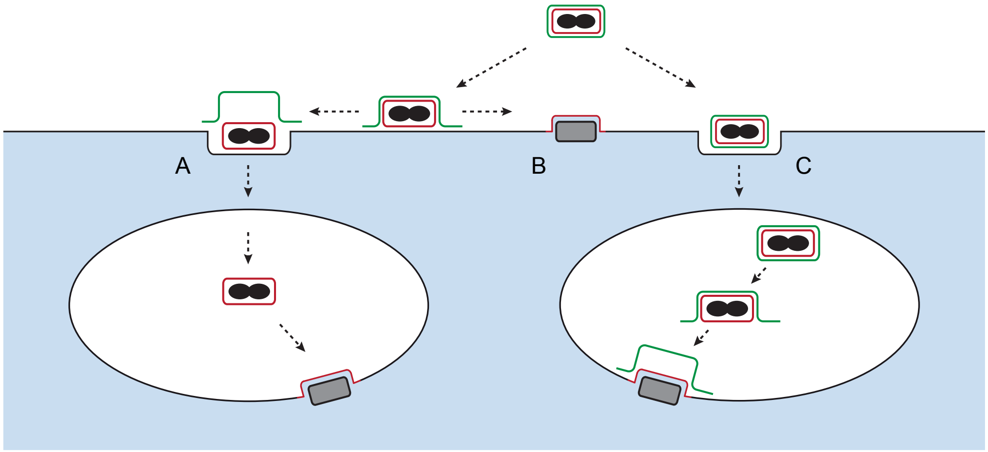

Figure 1.10 Possible entry routes of EVs [211].

1.3.2 RNAi screen for host factors required for in VACV infection

RNAi screening in VACV infection was a small side project. A high-throughput RNAi silencing screen was used to identify host cell factors required during vaccinia virus infection (see page 61). We validated and analysed the clustered hits which revealed an previously unknown processes during virus entry including a new mechanism for genome uncoating. For clarification, we investigated the morphology of stabilised cytoplasmic cores after entry using electron microscopy, which was my contribution to this study.

The results of this section has been published in CellReports (2012), issue 1-12, doi:10.1016/j.celrep.2012.09.003.

1.3.3 VACV LBs deliver effector proteins

Furthermore, little is known about the exact timing or core activation, whether cellular and viral factors are required for this process, or whether the molecular changes are intrinsically laid down in the matured viral core. Indeed, not even the molecular components of the lateral bodies and the exact architecture of the core wall have been elucidated to date. In this study, we used fluorescence and electron microscopy in combination with biochemical approaches to visualise viral core activation and elucidate some of the molecular details. Data of VACV core activation is presented in chapter 4 (see page 87) and will be submitted to a peer-reviewed journal.

Florian I. Schmidt and I have contributed equally to this studies.

Chapter 2

VACV EVs enter cells by macropinocytosis and acid-activated membrane rupture

The results of this section have been published in:

The EMBO Journal (2011), ***30****, 3647–3661 (doi:10.1038/emboj.2011.245)*

Vaccinia Extracellular Virions Enter Cells by Macropinocytosis and Acid-activated Membrane Rupture

Florian Ingo Schmidt[1], Christopher Karl Ernst Bleck[2], Ari Helenius[1], and Jason Mercer[1*]

[1] Institute of Biochemistry, ETH Zurich, 8093 Zurich, Switzerland

[2] Center for Cellular Imaging and NanoAnalytics (C-CINA), Biozentrum, University of Basel, 4058 Basel, Switzerland

[*] Corresponding author: jason.mercer@bc.biol.ethz.ch

Experiments shown in Figure 2.3 and 2.4 were performed by Christopher K. E. Bleck.

2.1 Abstract

Vaccinia virus (VACV), the model poxvirus, produces two types of infectious particles: mature virions (MVs) and extracellular virions (EVs). EV particles possess two membranes and therefore require an unusual cellular entry

mechanism. By a combination of fluorescence and electron microscopy as well as flow cytometry, we investigated the cellular processes that EVs require to infect HeLa cells. We found that EV particles were endocytosed, and that internalization and infection depended on actin rearrangements, activity of Na^+/H^+ exchangers, and signalling events typical for the macropinocytic mechanism of endocytosis. To promote their internalization, EVs were capable of actively triggering macropinocytosis. EV infection also required vacuolar acidification, and acid exposure in endocytic vacuoles was needed to disrupt the outer EV membrane. Once exposed, the underlying MV-like particle presumably fused its single membrane with the limiting vacuolar membrane. Release of the viral core into the host cell cytosol allowed for productive infection.

2.2 Introduction

To successfully replicate, viruses have to deliver their genome and accessory proteins into the cytosol or nucleus of a host cell. This implies that virus particles or their packaged genome must cross the plasma membrane (PM) or the limiting membrane of endocytic vacuoles. In the case of animal viruses that have a lipid bilayer envelope, the critical step of membrane penetration involves fusion of the viral membrane with a cellular membrane. The packaged genome is thus released into the cytosol [143].

Vaccinia virus (VACV) is the prototypic poxvirus and is closely related to variola virus, the causative agent of smallpox [53]. Poxviruses are enveloped DNA viruses that use a fusion mechanism to enter cells [213]. They are unusual because they exist in two different, infectious forms [163]. In addition to single membrane containing particles (mature virions, MVs) [50, 92], particles are produced that contain two concentric membranes (extracellular virions, EVs) [223]. MVs are released after lysis of infected cells and mediate host-to-host transmission [163, 222]. EVs leave the cell by exocytosis and are required for virus spread within a tissue or from tissue to tissue [177]. An EV particle consists of an MV-like particle surrounded by an additional membrane containing cellular proteins and at least six viral proteins unique to the EV [175, 176, 223]. With two membranes, a conventional mechanism of entry is not possible. Loss of the outer membrane by fusion would release a particle into the cytosol that is still covered by the inner membrane. Such a particle is unlikely to cause productive infection.

Recent studies have shown that the majority of MVs enter cells by endocytosis and penetration occurs by membrane fusion in intracellular vacuoles [239, 237]. The entry process involves macropinocytic internalization induced by phosphatidylserine (PS) exposed on the MV membrane [280, 106, 148, 99, 150].

Available information on EV entry suggests that the outer of the two membranes is simply lost or ruptured revealing the underlying MV-like membrane, which then undergoes fusion with the plasma membrane or the limiting membrane of a vacuole [162]. The core could thus be delivered into the cytosol without a membrane. The model proposing rupture of the outer membrane of the EV is based on the following observations: (1) The entry/fusion complex (EFC) present in the inner of the two membranes is essential for EV infection [214, 215]. (2) The outer membrane of the EV is fragile and sensitive to *in vitro* treatment with reduced pH and anionic polysaccharides [107, 251, 128]. EV disruption with anionic polysaccharides has been shown to depend on two EV specific proteins, A34 and B5 [128, 193]. (3) Electron micrographs of cell surface bound EVs show the presence of ruptured EV membranes covering MV-like particles [128].

However, it has been observed that antibodies directed against MV-membrane proteins that neutralize MV infection, fail to neutralize infection by EVs [107, 251]. This suggests that upon rupture of the outer EV membrane, the underlying MV-like particle is inaccessible to antibodies. One explanation could be that EV rupture takes place at the PM and the disrupted outer membrane covers the PM-bound MV-like particle. Another possibility is that rupture occurs only after endocytic internalization of the intact EV particle. Several studies have addressed the EV entry process using epithelial cell lines and human monocyte-derived dendritic cells (DCs) with conflicting results [107, 251, 136, 128, 193, 199].

In this study, we used flow cytometry-based assays and microscopy in combination with different perturbants of cellular proteins and functions to analyse EV infection of HeLa cells. We found that VACV EVs induced their own endocytic uptake by macropinocytosis. Acidification of endocytic compartments was needed to trigger disruption of EV membranes, presumably followed by fusion of the underlying virus particles with limiting membranes of endocytic organelles. This would release virus cores into the cytosol and allow productive infection.

2.3 Results

2.3.1 Quality of EV particles

In our study, we used EVs released into the medium as free particles by infected cells. They correspond to the population of VACV particles responsible for long-range spread in the infected organism [177]. The outer membrane of EVs is fragile and easily disrupted during purification [107, 253] (our unpublished results). We therefore used freshly produced EVs of VACV strains WR and IHD-J in clarified supernatants of infected RK13 cells without further purification.

To quantify the fraction of intact EVs, we used the monoclonal antibody (MAb) 7D11, which binds to the L1 protein in the MV membrane, and selectively neutralizes MVs and broken EVs (Figure 2.1 A) [269]. Using plaque assays, we determined that MVs of VACV strains WR and IHD-J were neutralized by 5 µg/mL 7D11. Depending on the preparation, 10–40 % of WR and IHD-J infectivity in the supernatant was insensitive to 7D11 and therefore represented infectivity caused by intact EVs. In contrast, WR Δ A34R, a deletion mutant of the EV membrane protein A34 known to contain stabilized EV membranes [128, 102], was ∼ 90 % insensitive to 7D11.

To confirm the presence of intact EVs in the supernatant, we analysed VACV particles released from RK13 cells by confocal microscopy. To discriminate between MVs and EVs, we used a recombinant IHD-J strain expressing two different fluorescent fusion proteins: mCherry was fused to the core protein A5 and GFP to the EV-specific outer membrane protein F13. Both MVs and EVs therefore contained a red fluorescent core and could be visualized as discrete spots. The majority of particles in the supernatant of infected RK13 cells (83 %) was also positive for the outer EV membrane (green fluorescent). Some green fluorescent particles without a red fluorescent core were observed, likely representing EV membranes that had lost the core (15 spots per 100 virus cores, data not shown).

To determine the fraction of intact EVs, cell supernatants containing recombinant IHD-J viruses were pre-incubated with 7D11, applied to a cover slip, and stained with a fluorescently labelled secondary antibody. MVs and broken EVs with exposed L1 were expected to be stained whereas intact EVs were not. Figure 2.1 C shows a field with MVs (mCherry and 7D11 staining; open arrowhead), disrupted EVs (mCherry, GFP, and 7D11 staining; closed arrowhead), and intact EVs (mCherry and GFP, arrow). Analysis of more than 600 virus particles in three independent experiments showed that 17 % of the viruses were MVs, 69 % were disrupted EVs, and 14 % were intact EVs (Figure 2.1 B). This amount of intact EVs corresponded to the fraction of 7D11-insensitive EVs determined by plaque assay for the same supernatants (data not shown).

After analysing EV particles for both infectivity and integrity, we concluded that MAb 7D11 could be used to discriminate between intact and broken EVs. It was evident that the majority of IHD-J and WR EVs released into the supernatant did not possess an intact second membrane. In

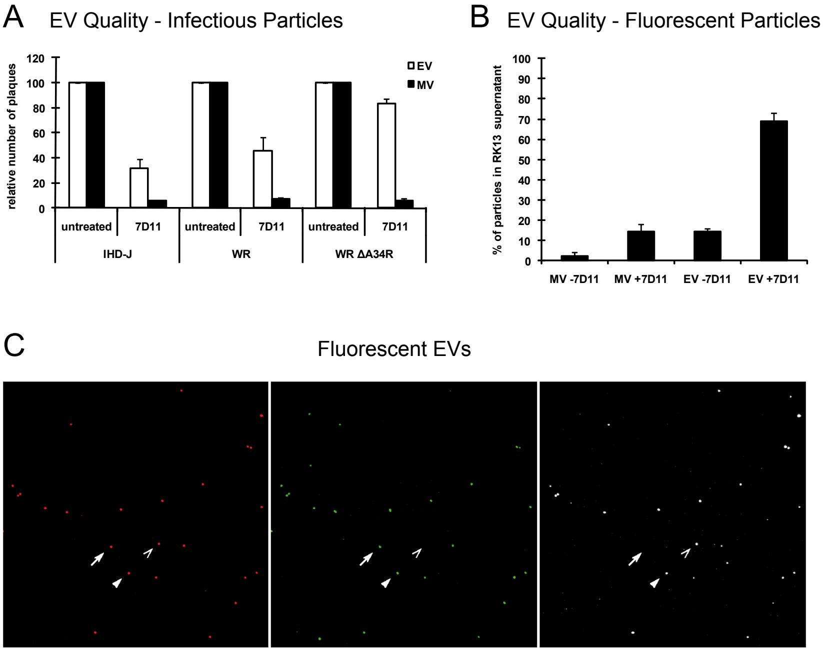

Core
(mCherry-A5)

EV membrane
(F13-GFP)

accessible MV membrane
(7D11, unpermeabilized)

Figure 2.1 Quality of EV particles. (A) Clarified supernatants of RK13 cells infected with VACV IHD-J, WR, or WR Δ A34R were titrated on BSC-40 cells after incubation with or without Mab 7D11. As a control, purified MVs of the same strains were subjected to the same treatment and titration. Plaque numbers were normalized to untreated virus samples. Results represent the average of three independent experiments (mean ± SEM). (B) Clarified supernatants of RK13 cells infected with IHD-J mCherry-A5 F13-GFP were incubated with 7D11, bound to cover slips, and fixed. 7D11 was visualized with Alexa fluor (AF) 647 goat anti-mouse and images recorded by confocal microscopy. Virus particles were detected by their fluorescent core and assigned to the following categories: MV -7D11 (mCherry), MV +7D11 (mCherry and 7D11 staining), EV -7D11 (mCherry, GFP), or EV +7D11 (mCherry, GFP, and 7D11 staining). Average values of three independent experiments are shown ± SEM. (C) Representative images from B. Examples of a neutralized MV (MV +7D11, open arrowhead), an intact EV (EV -7D11, arrow), and a disrupted EV (EV +7D11, closed arrowhead) are highlighted.

most instances – judging by the presence of F13-GFP – the disrupted EV membrane remained associated with the virus particle. Disruption of the outer membrane did not interfere with the infectivity of EVs.

2.3.2 EV particles are endocytosed

For productive infection, both EV membranes must be removed during the entry process. While it has been suggested that removal of the outer membrane of EVs happens already on the PM [128], it is conceivable that the EV particles are endocytosed first with loss of the outer EV membrane taking place in endocytic compartments.

To test whether EVs can be internalized with their outer membrane still in place, we used recombinant IHD-J EVs containing F13-GFP to infect HeLa cells for 30 min at 37 °C. Samples were stained for the EV membrane protein B5 under non-permeabilizing conditions to distinguish between external and intracellular EVs (Figure 2.2 B). A fraction of EV particles (green spots; white arrows, inset) was inaccessible to antibody staining, indicating they were internalized. To control for changes in the B5 epitope or inappropriate staining, the same procedure was performed either with cells in which the virus had not been allowed to internalize (bound EVs, Figure 2.2 A) or with cells permeabilized with saponin after fixation (Figure 2.2 C). In both conditions, all EV particles were stained for B5.

To assure that intact EV particles, and not only dissociated EV membranes without cores were internalized, HeLa cells were infected with IHD-J mCherry-A5 F13-GFP EVs and subjected to B5 staining under non-permeabilizing conditions (Figure 2.2 D). That a sub-population of the dual-coloured EVs was not stained (white arrows, inset) indicated that EV particles were internalized with the outer membrane. Virus cores or MVs without an EV membrane (closed arrowhead) and internalized EV membranes without a core (open arrowhead) were also observed. These may represent intermediates of the EV entry process or may have been internalized from the inoculum.

To confirm these findings, HeLa cells incubated with IHD-J F13-GFP EVs for 30 min were analysed by electron microscopy for the presence of internalized particles with EV membranes. Ultra-thin sections of cells were subjected to negative staining to visualize the EV membrane. Immunogold labelling directed against GFP was used to detect the F13-GFP fusion protein in the EV membrane (Figure 2.3 and 2.4). Gold-labelled EV particles were found both at the PM, often next to membrane protrusions (Figures 2.3 A and 2.4 A and B), and in intracellular vesicles (Figures 2.3 A and B and 2.4 A-F). In some particles, two membranes could be clearly distinguished

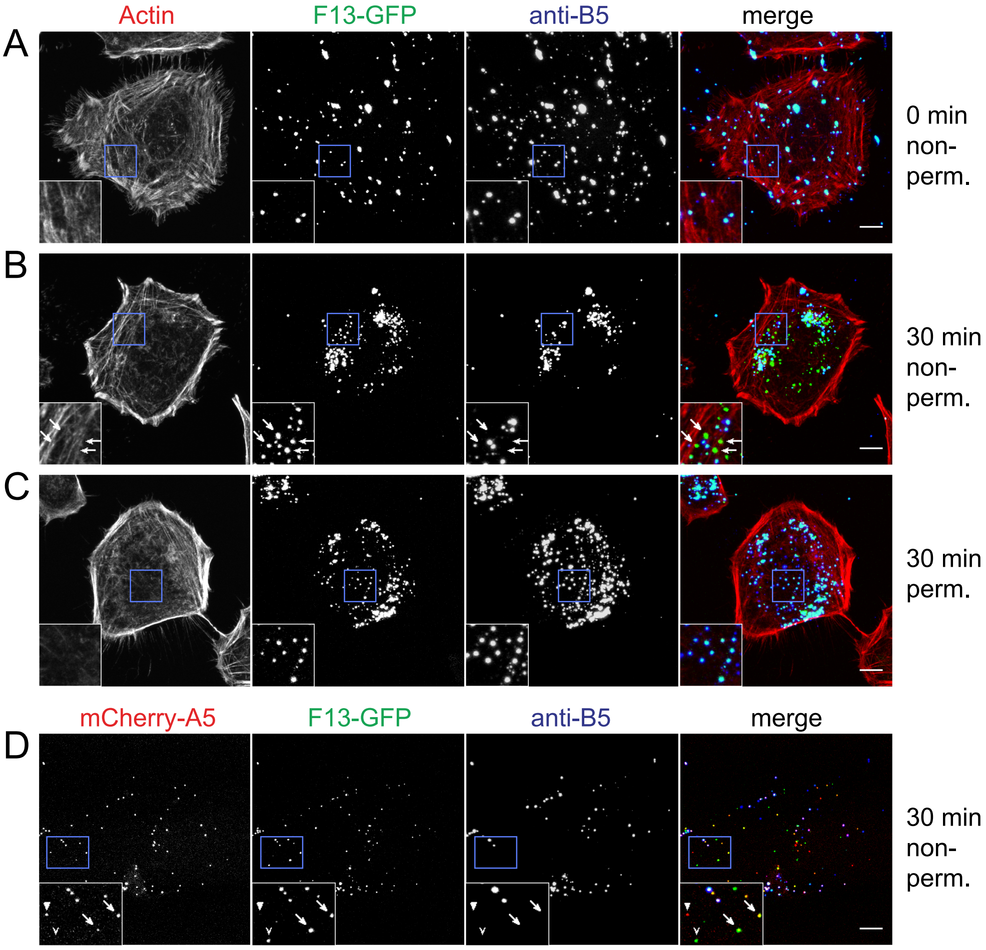

Figure 2.2 EV internalization by fluorescence microscopy. IHD-J F13-GFP EVs (A–C) or IHD-J mCherry-A5 F13-GFP EVs (D) were bound to HeLa cells on ice for 1 h (MOI 15). EV particles were stained with VMC-20 (anti-B5) directly (A) or after incubation at 37 °C for 30 min (B–D). VMC-20 staining was either performed under non-permeabilizing (non-perm.) conditions to visualize bound virions (A, B, and D) or under permeabilizing (perm.) conditions to visualize bound and internalized virions (C). Images were recorded by confocal microscopy and representative maximum projections of Z-stacks are shown. Arrows in the inset of B highlight F13-GFP-containing EV membranes not accessible to VMC-20 staining. In the inset of (D), EV particles (arrows) and an EV membrane without a core (open arrowhead), all not accessible to VMC-20 staining, as well as a virus core or MV without an EV membrane (closed arrowhead), are highlighted. Scale bars = 10 µm.

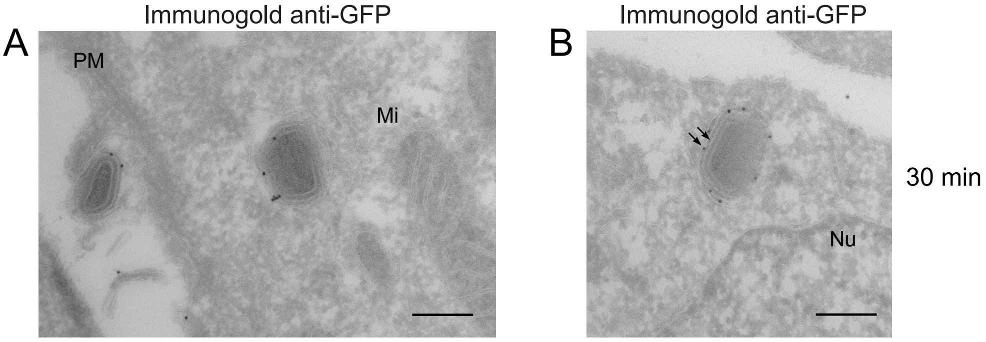

Figure 2.3 EV internalization by electron microscopy. IHD-J F13-GFP EVs were bound to HeLa cells on ice for 1 h (MOI 300). Cells were incubated at 37 °C for 30 min, fixed, and subjected to cryo-sectioning and immuno labelling with anti-GFP and protein A-gold. Images were recorded by transmission electron microscopy and representative pictures are shown. Arrows in (F) highlight MV and EV membranes. Mi: mitochondrion; Nu: nucleus. Scale bars = 200 nm.

(arrows in Figures 2.3 B and 2.4 D) confirming that full EV particles were endocytosed. In a few particles (Figure 2.4 F), the EV membrane was partly disrupted. EV membranes devoid of cores were also observed bound to the PM. They may have originated from free membranes in the inoculum, or from particles disrupted at the PM.

Internalization of EVs was confirmed using flow cytometry. IHD-J F13-GFP EVs were bound to HeLa cells on ice and incubated either on ice or at 37 °C for a further 30 min. Bound virus particles were removed by trypsin digestion and the cells subjected to flow cytometry to determine the cell-associated fluorescence from internalized particles (Figure 2.5 A and B). The low temperature control showed that bound EVs could be almost completely removed by trypsin, whereas cells incubated at 37 °C were green fluorescent, confirming the presence of internalized IHD-J F13-GFP EVs. When cells were detached with EDTA, fluorescence of both bound and internalized EVs could be measured (Figure 2.5 A and C). Fluorescence intensities with and without incubation at 37 °C were comparable, confirming that GFP fluorescence and virus binding was not affected by incubation at 37 °C.

These experiments showed that cell-bound EVs were rapidly internalized by endocytosis. Although disrupted EVs were not distinguished from intact EVs in these experiments, we could show by fluorescence microscopy, electron microscopy, and flow cytometry that the outer membrane of EVs was not lost prior to internalization.

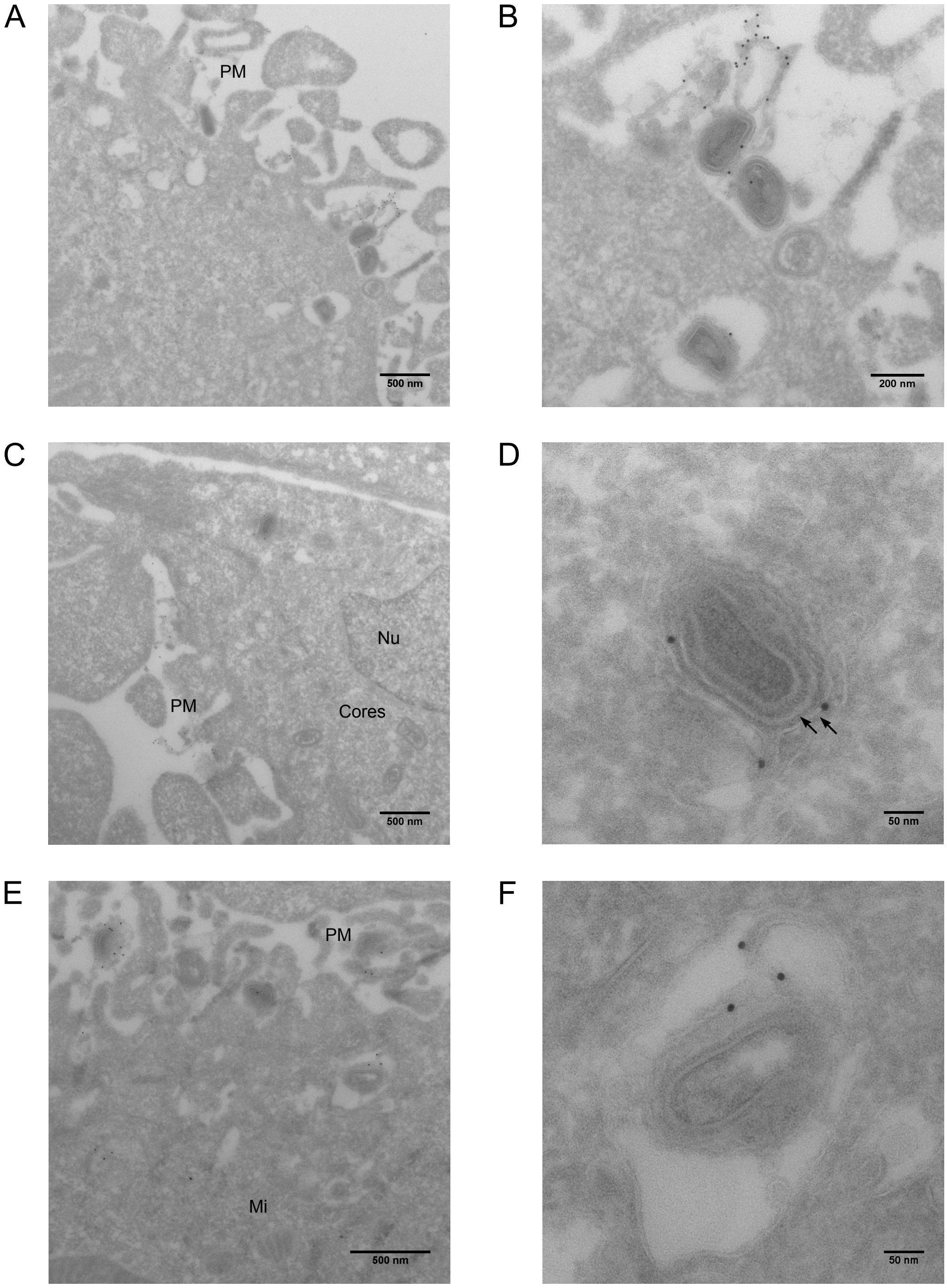

Figure 2.4 EV internalization by electron microscopy. Internalization of IHD-J F13-GFP EVs by HeLa cells was analysed by transmission electron microscopy and immunogold labelling of GFP as described in Figure 2.3. Panels B, D, and F represent magnified views of virus particles in panels A, C, and E, respectively. Arrows in D highlight the two viral membranes of internalized EVs.

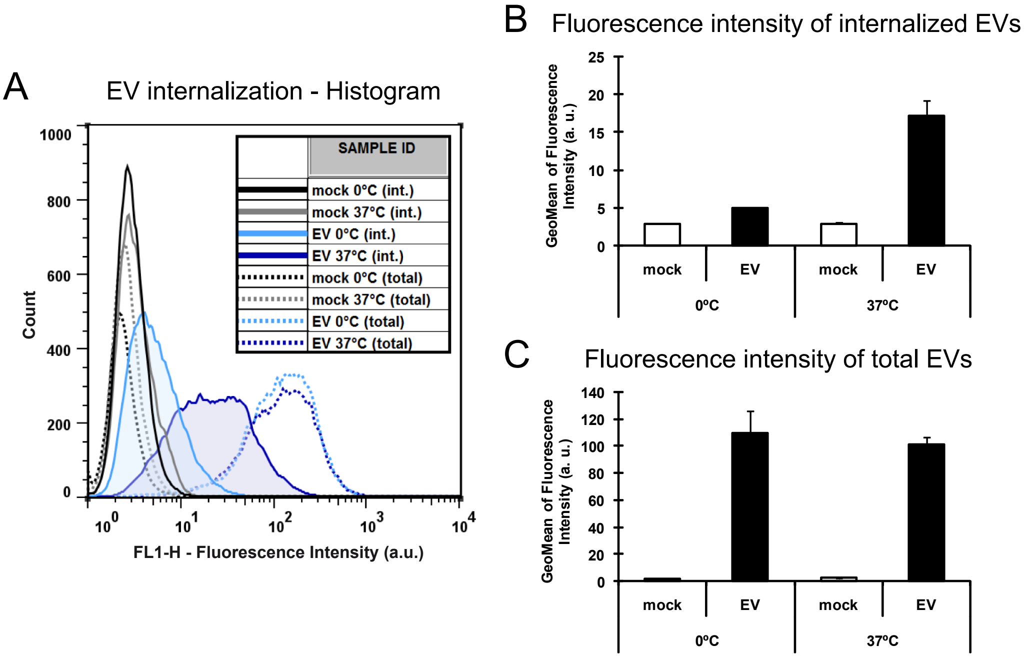

Figure 2.5 IHD-J F13-GFP EVs (MOI 175) were bound to HeLa cells on ice for 1 h and cells incubated at 0 or 37 °C for 30 min. To detect internalized EVs (int.), bound virions were removed and cells detached with trypsin; to measure total cell-associated virions (total), cells were detached with EDTA. Cells were fixed, and green fluorescence quantified by flow cytometry. Representative histograms of untreated samples are shown in (A); green fluorescence intensity from three independent experiments was quantified and the average of measured geometric means of internalized (B) and total (C) EVs is displayed ± SEM.

2.3.3 EVs are internalized by macropinocytosis

To analyse the endocytic mechanism responsible for EV internalization, and to test whether endocytosis was required for infection by intact EVs, we infected HeLa cells in the presence of a spectrum of small compound inhibitors known to affect endocytic processes. GFP-expressing viruses and flow cytometry were used to quantify infection by VACV EVs of the strains IHD-J and WR (Figure 2.6 A and C).

To assure that infection by intact EVs was specifically analysed, we pretreated EV-containing supernatants with Mab 7D11 for all infection experiments. Since cells infected with VACV WR released less EVs into the medium than cells infected with strain IHD-J, WR EV supernatants were concentrated by sedimentation prior to MV neutralization. This did not significantly reduce the fraction of intact EVs (data not shown). In all cases, MVs were used as controls. IHD-J and WR MVs have been found to in-

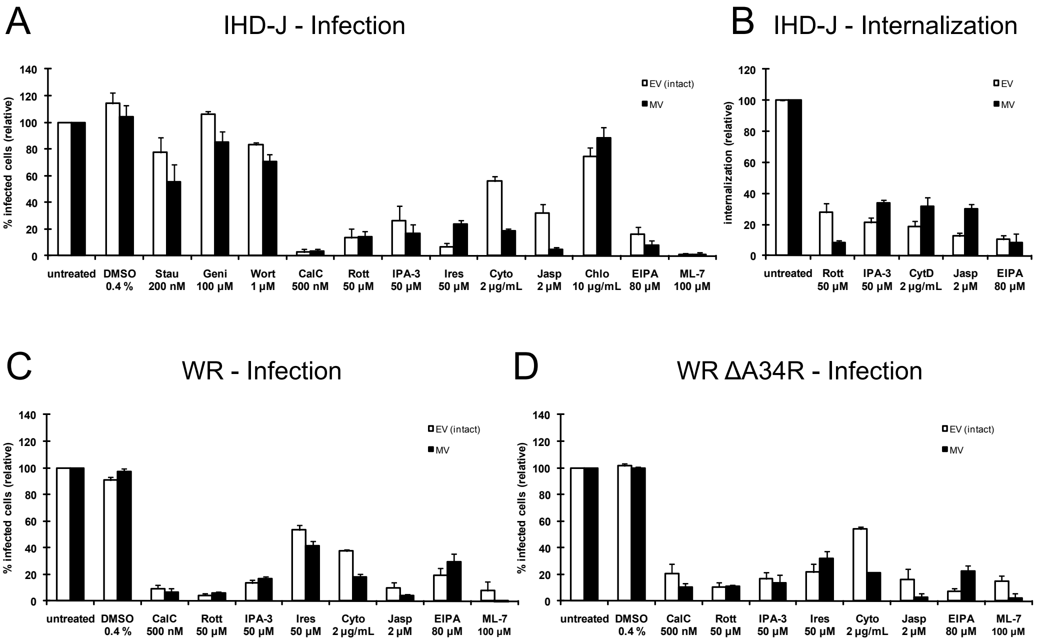

Figure 2.6 HeLa cells were left untreated or treated with DMSO (highest used concentration), staurosporine (Stau), genistein (Geni), wortmannin (Wort), calphostin C (CalC), rottlerin (Rott), IPA-3, Iressa (Ires), chlorpromazine (Chlo), ML-7 (all 30 min), cytochalasin D (Cyto), jasplakinolide (Jasp), or EIPA (all 15 min). MVs or EVs of IHD-J GFP (A), WR GFP (C), or WR Δ A34R GFP (D) were pre-incubated in the presence of drugs and in the case of EVs with 7D11 (MOI 2). Cells were infected and green fluorescent cells quantified 4 h p.i. by flow cytometry. Infection levels were normalized to untreated samples. (B) EV (IHD-J F13-GFP) and MV (IHD-J EGFP-A5) internalization in the presence of various drugs was quantified as described in Figure 2.5. The geometric mean of green fluorescence intensity of 0 °C samples was subtracted from 37 °C samples and internalization normalized to untreated samples. All experiments were performed three times independently, mean values ± SEM are shown.

duce macropinocytosis in host cells, and to utilize this pathway as a route of productive infection [148].

Inhibition of clathrin-mediated endocytosis by chlorpromazine affected neither IHD-J EV nor MV infection (Figure 2.6 A). Infection with EVs and MVs was only moderately affected by the general protein kinase inhibitor staurosporine, and it was not influenced by the tyrosine-kinase inhibitor genistein or the posphoinositide 3-kinase inhibitor wortmannin. In contrast, infection with both EVs and MVs was dramatically blocked by Iressa, an inhibitor of the epidermal growth factor receptor (EGFR); by the protein kinase C (PKC) inhibitor calphostin C (CalC); by IPA-3, an inhibitor of p21-activated kinase 1 (PAK1); and by the smooth muscle myosin light chain kinase (smMLCK) inhibitor ML-7. Rottlerin, originally described to specifically inhibit PKCδ [85], but later found to have multiple effects [54, 227, 234], nearly abolished infection. Perturbation of actin dynamics with cytochalasin D (Cyto) and jasplakinolide (Jasp) strongly reduced EV infection; the block of infection was, however, even more pronounced for MVs. An inhibitor of Na^+/H^+ antiporters, EIPA, also efficiently prevented infection with both EVs and MVs. The requirement of PAK1, smMLCK, PKC activity, actin dynamics, and sodium-proton exchangers strongly suggested an endocytic process categorized as macropinocytosis [149].

To determine if the inhibitors of infection blocked macropinocytic uptake of EVs, we quantified internalization of IHD-J EVs and MVs using flow cytometry (Figure 2.6 B). For EV internalization experiments, IHD-J EVs containing F13-GFP were used without neutralization as 7D11 treatment did not affect endocytic uptake of neutralized, disrupted EVs (data not shown). For MV internalization experiments, MV particles incorporating EGFP-A5 in the core were employed (Figure 2.7). Bound MVs, in contrast to EVs, were only partially removed by trypsin digestion (sample MV 0 °C (int.)). Signal intensity of cells incubated at 37 °C was significantly higher than that of cells kept at 0 °C allowing for quantification after background subtraction. Rottlerin, IPA-3, Cyto, Jasp, and EIPA efficiently blocked internalization of both EVs and MVs, confirming that the observed effects on infection occurred due to impaired endocytic uptake.

The inhibitors that blocked IHD-J EV infection were then tested against WR EVs (Figure 2.6 C). Inhibition of EGFR, PAK1, smMLCK, PKC, actin dynamics, and Na^+/H^+ antiport caused a strong reduction of WR EV infection. These results indicated that EVs of both IHD-J and WR strains exploited macropinocytosis for infection.

Throughout these infection experiments, neutralized MVs and neutralized disrupted EVs were present in the inocula. Thus, it was conceivable that these particles – although neutralized by antibody binding – stimulated macropinocytosis resulting in the co-internalization of intact EVs. To test whether MVs stimulated the internalization of EVs, we performed infection assays with a GFP-expressing version of the mutant virus WR Δ A34R, a virus that produces $\sim$90 % intact EVs (Figure 2.6 D). EV infection was reduced by the same panel of drugs as infection by EVs of wild-type IHD-J and WR. It was sensitive to Iressa, CalC, rottlerin, ML-7, IPA-3, actin perturbants, and EIPA, indicating that EV uptake by macropinocytosis was not influenced by the presence of neutralized, disrupted EVs or neutralized MVs. Along the same lines, we tested if the addition of excess amounts of neutralized MVs would boost infection by WR Δ A34R EVs (Figure 2.8). Even when a 25-fold excess of neutralized MVs was used, no boost in EV infection was observed. These results indicated that VACV EVs of IHD-J and WR

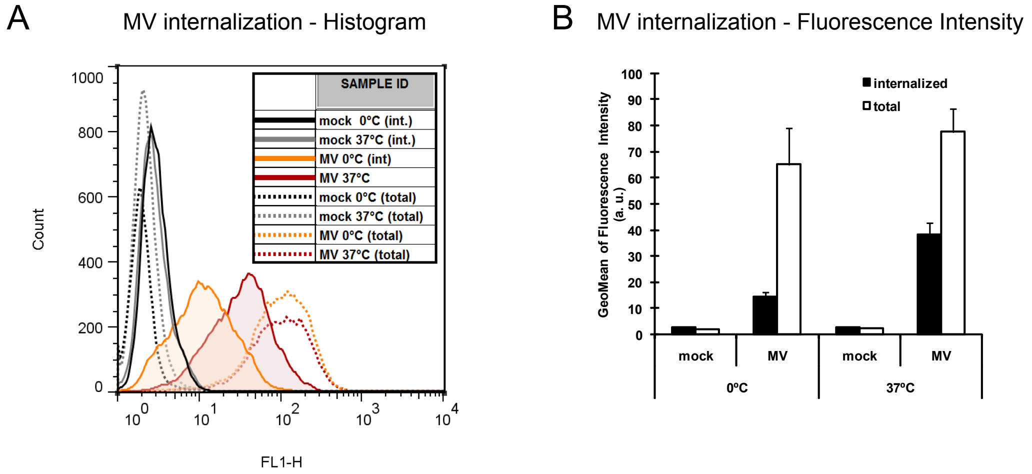

Figure 2.7 MV internalization by flow cytometry. IHD-J EGFP-A5 MVs (MOI 75) were bound to HeLa cells on ice for 1 h and cells subsequently incubated at 0 or 37 °C for 30 min. To detect internalized MVs, bound virions were removed and cells detached with trypsin (int.); to quantify total cell-associated virions, cells were detached with EDTA (total). Cells were fixed, and green fluorescence quantified by flow cytometry. Representative histograms of untreated samples are shown in (A); green fluorescence intensity from three independent experiments was quantified and the average of measured geometric means of internalized (B) and total (C) MVs is displayed ± SEM.

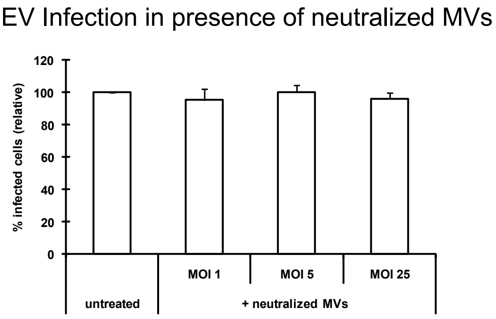

Figure 2.8 WR Δ A34R GFP EVs were incubated with 7D11 for 1 h at 37 °C (MOI 2). EVs and increasing amounts of neutralized MVs of the same strain were added to HeLa cells and incubated at 37 °C for 30 min. Cells were washed, incubated in full medium, and harvested 4 h p.i.; infection was quantified as in Figure 2.6. Experiments were performed three times independently and normalized to untreated samples, mean ± SEM is shown.

strains are capable of triggering macropinocytosis resulting in internalization and productive infection of host cells.

2.3.4 EV particles induce macropinocytosis

Macropinocytosis can be distinguished from other types of endocytosis by a dramatic rearrangement of the actin cytoskeleton and by enhanced cellular fluid-phase uptake [149]. To investigate cellular phenotypes of macropinocytosis, WR Δ A34R was used. The integrity of the EV membrane on WR Δ A34R EV particles allowed us to distinguish between EV- and MV-induced changes. If EVs use macropinocytosis for their internalization, increased uptake of fluid phase markers would be expected. To test this, uptake of 10 kDa dextran-Alexa fluor (AF) 488 into serum-starved HeLa cells after stimulation with EVs and MVs was quantified by flow cytometry (Figure 2.9 A). Indeed, uptake of dextran during a 10 min pulse was increased by 42 and 51 %, respectively. In addition, we observed IHD-J F13-GFP EVs colocalizing with 10 kDa dextran AF 594 in large intracellular vesicles (Figure 2.10), suggesting EV particles are internalized into macropinosomes.

Uptake of fluid by macropinocytosis requires the formation of dynamic membrane protrusions. These protrusions occur as lamellipodia, circular ruffles, or blebs. Functionally, they all lead to the formation of macropinosomes of irregular size and shape [149].

To determine if EVs induce the formation of membrane protrusions, HeLa cells were treated with EVs of WR Δ A34R EGFP-A5. MVs known to induce blebbing [148] were used as a control. Virus particles were bound to HeLa cells and incubated at 37 °C for 40 min. Cells were fixed and analysed by differential interference contrast (DIC) and wide-field fluorescence microscopy (Figure 2.9 B and C). A low level of membrane blebbing was observed in mock-treated cells (3 %), whereas 20–70 % of all cells treated with different amounts of EVs or MVs exhibited extensive, systemic bleb formation.

The finding that WR Δ A34R EVs triggered both fluid-phase uptake and extensive blebbing confirmed the capacity of EVs to induce macropinocytosis at a level similar to that seen for MVs.

Uptake of MVs by macropinocytosis has been shown to be triggered by PS, a phospholipid enriched in the MV membrane. When PS in the MV membrane is masked by the PS-binding protein annexin V (ANX5), MV infection is almost completely blocked [148]. If EVs induce macropinocytosis through a similar mechanism, EV infection would be expected to be blocked by ANX5 as well. To test this, EVs and MVs of WR Δ A34R GFP were pretreated with ANX5 and used for infection experiments (Figure 2.11). While MV infectivity was reduced to 38 % by ANX5, EV infection was not affected. This suggested that VACV EVs induce macropinocytosis through a different trigger than MVs.

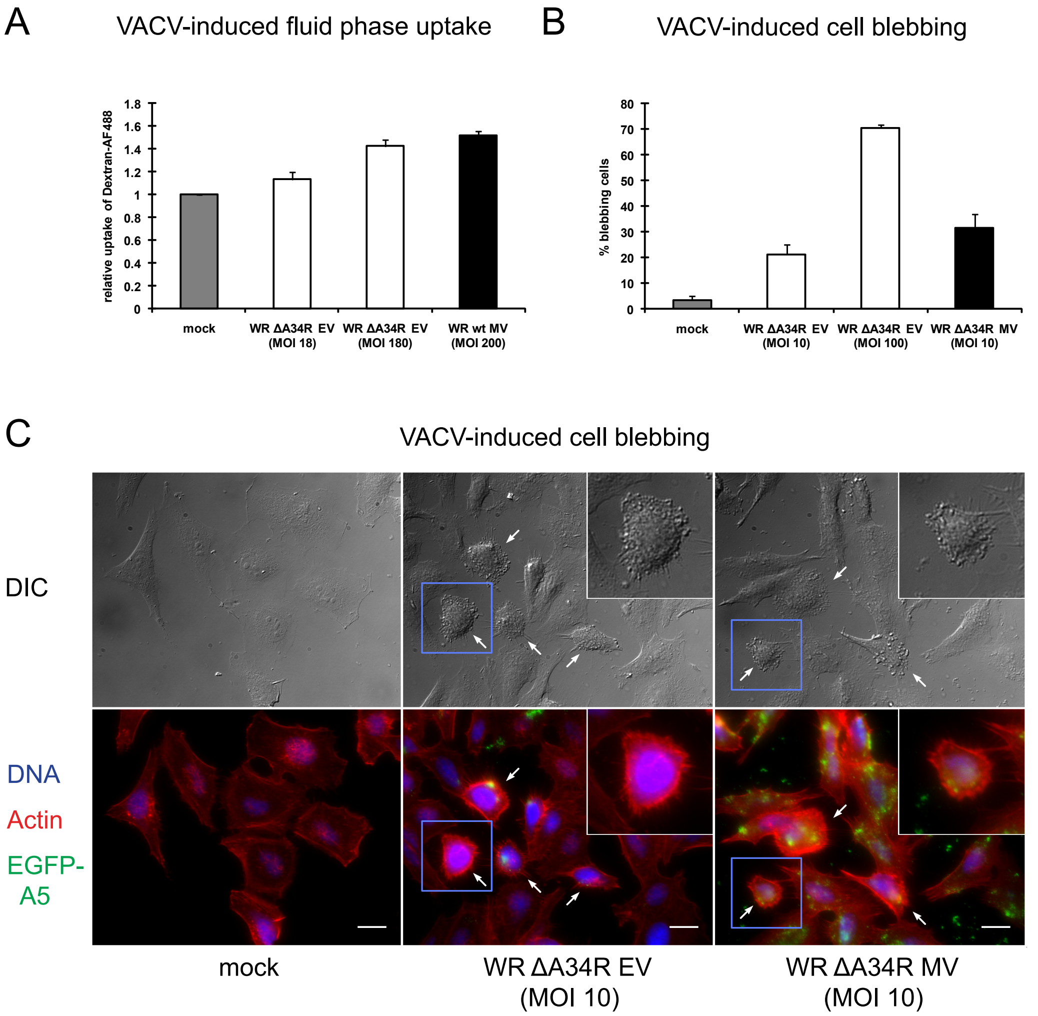

Figure 2.9 EVs and cellular phenotypes of macropinocytosis. (A) WR Δ A34R EVs and WR wt MVs were bound to serum-starved HeLa cells on ice for 1.5 h and pulsed for 10 min at 37 °C with 10 kDa dextran AF 488. Cells were washed, harvested, fixed, and geometric means of green fluorescence quantified by flow cytometry. Dextran uptake was normalized to uptake by unstimulated cells and mean values ± SEM of three independent experiments are shown. (B)–(C) WR Δ A34R EGFP-A5 MVs or concentrated EVs were bound to HeLa cells at RT. Cells were incubated at 37 °C for 40 min, fixed, stained, and analysed by DIC and wide-field fluorescence microscopy. The number of total and blebbing cells from three independent experiments (∼250 cells per condition and experiment) was counted and mean ± SEM is shown (B). Representative images are shown in (C). Scale bars = 20 µm.

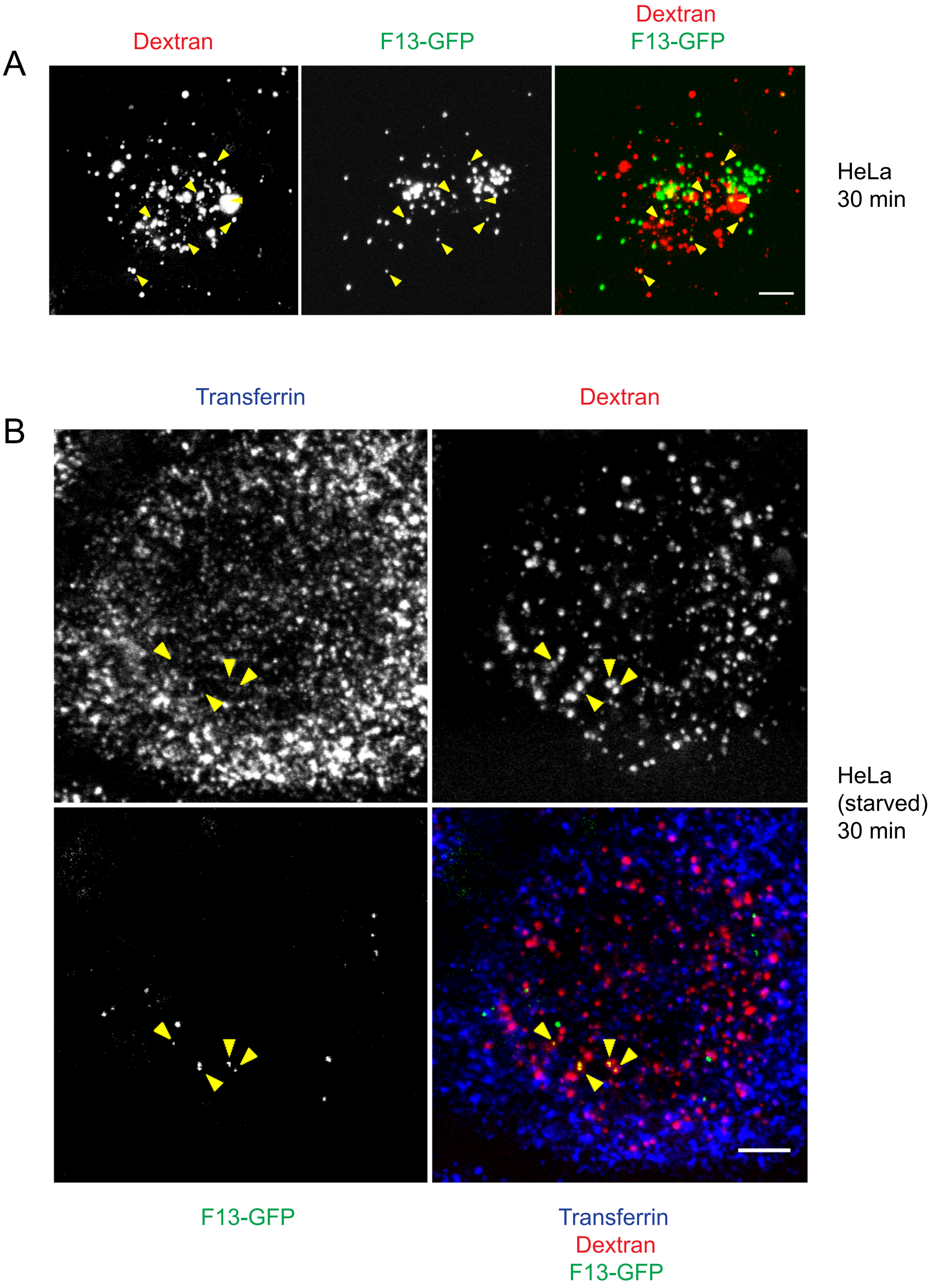

Figure 2.10 EVs in dextran-containing macropinosomes. HeLa cells were preincubated with full (A) or serum-free medium (B) for 4 h. IHD-J F13-GFP EVs in 0.2 % BSA/RPMI were bound to cells on ice for 1 h (MOI 25) and incubated for 30 min at 37 °C in presence of 0.5 mg/mL 10 kDa dextran AF 594 (A), or dextran and 25 µg/mL transferrin AF 647 (B). Images were recorded by confocal microscopy and representative maximum projections of Z-stacks are shown. Arrowheads highlight EV particles in dextran-containing vesicles. Scale bars = 5 µm.

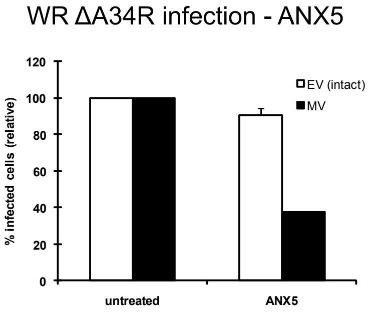

Figure 2.11 EVs and cellular phenotypes of macropinocytosis. Exposed PS of concentrated EVs or MVs of WR Δ A34R GFP (MOI 4) was masked with ANX5. Subsequently, virions were incubated at 37 °C for 1 h (in case of EVs in the presence of 7D11) and used for infection experiments as described in Figure 2.6. Experiments were performed three times independently, mean values ±SEM are shown.

2.3.5 EV infection requires acidification of endocytic vacuoles

Macropinocytosis leads to the uptake of fluid and particles into endocytic vacuoles that subsequently undergo acidification [149]. To determine if low pH was needed for EV infection, we blocked acidification of endocytic organelles in HeLa cells using the vATPase inhibitor bafilomycin A1 (BafA) and the carboxylic ionophore monensin A (MonA) (Figure 2.12 A-F). At concentrations that did not significantly affect infection by MVs, both compounds reduced EV infection in a dose-dependent manner. IHD-J and WR Δ A34R EV infection was reduced by 80 % at the highest concentrations. WR EV infection was only reduced by up to 65 %. Infection with IHD-J EVs was also blocked by BafA in several other cell lines including A549N, BSC-40, RK13, and Vero (data not shown).

Thus, acidification of endocytic vesicles was required for efficient infection by intact EVs, whereas MVs were less sensitive to the perturbants of vacuolar acidification at the concentrations used.

2.3.6 Acidification has a role in EV membrane disruption

To determine which step(s) in the entry process required low pH, we quantified endocytic internalization of IHD-J EVs and MVs in the presence of BafA and MonA (Figure 2.13 A). Internalization into EIPA-treated cells was used as a control. BafA did not affect EV or MV internalization. MonA reduced internalization moderately, and EIPA strongly. This suggested that the effect of BafA on infection occurred after EV internalization.

To determine if the BafA-sensitive intracellular step of EV entry involved disruption of the outer membrane of EVs in endocytic compartments, we first tested whether EV membranes could be disrupted by low pH treatment *in vitro* as previously reported [252]. When supernatants containing IHD-J and

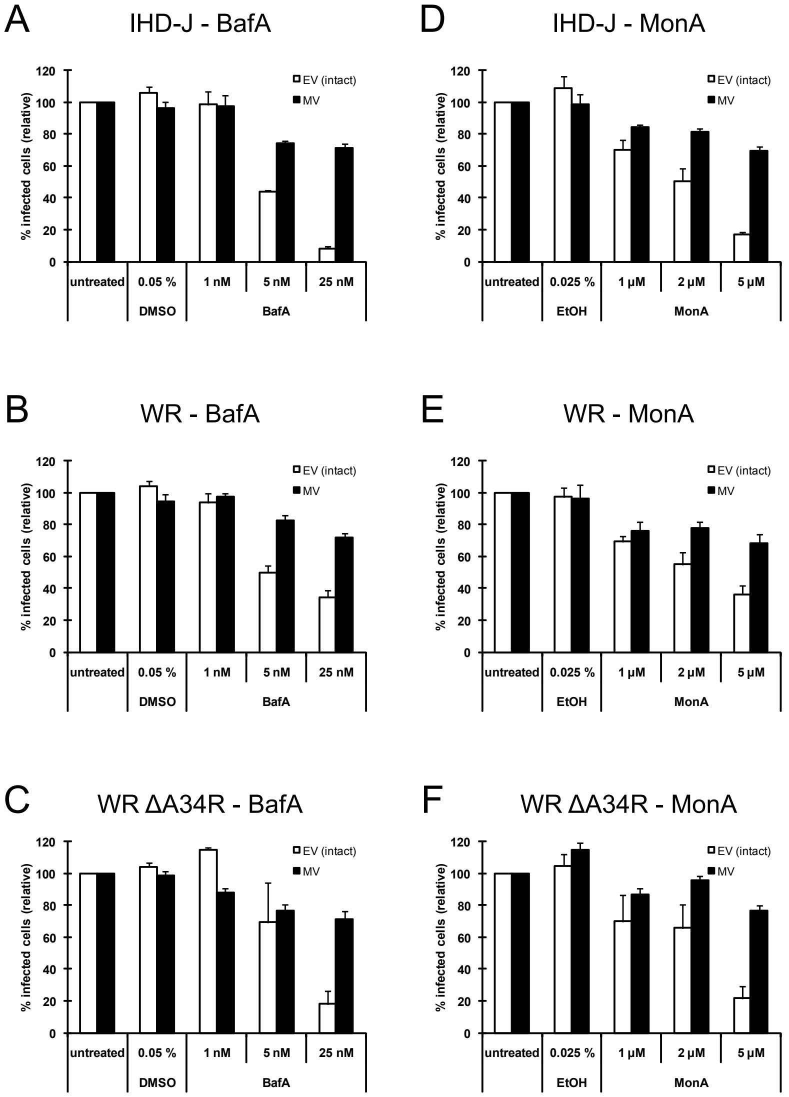

Figure 2.12 Experimental setup as in Figure 2.6; HeLa cells were pretreated with BafA (A–C) or MonA (D–F) for 1 h; controls with solvents at the highest used concentrations were included. Infection with IHD-J GFP (A, D), WR GFP (B, E), or WR Δ A34R GFP (C, F) in the presence of drugs was quantified by flow cytometry; mean ± SEM of three independent, normalized experiments are shown.

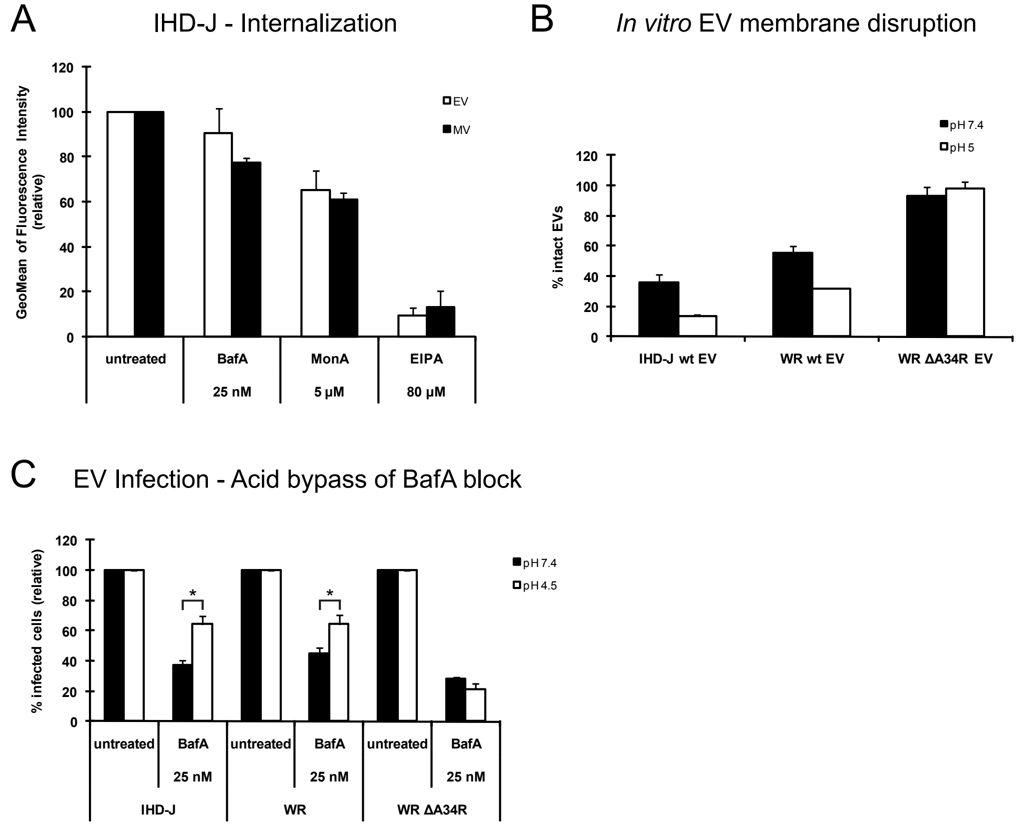

Figure 2.13 (A) EV (IHD-J F13-GFP) and MV (IHD-J EGFP-A5) internalization in the presence of BafA, MonA, and EIPA was quantified as described in Figure 2.6 B. (B) IHD-J, WR, and WR Δ A34R EVs were incubated at pH 5.0 or pH 7.4 and 37 °C for 5 min. EVs were titrated with or without 7D11 at pH 7.4 as described in Figure 2.1 A. The percentage of intact EVs was calculated by normalizing plaque numbers after 7D11 neutralization to plaque numbers in untreated samples; mean values ± SEM of three independent experiments are presented. (C) HeLa cells were left untreated or treated with BafA for 1 h. EVs of IHD-J GFP, WR GFP, or WR Δ A34R GFP were preincubated in the presence of drugs and 7D11 for 1 h at 37 °C (MOI 2). Virus particles were bound to cells on ice. Cells were shifted to 37 °C in pH 7.4 or pH 4.5 medium for 5 min and then incubated in full medium with drugs for 4 h. Infected cells were quantified by flow cytometry. The percentage of infected cells was normalized to the untreated samples. All experiments were performed three times independently, mean values ± SEM are shown, asterisks mark significant differences (P ⟨ 0.05).

WR EVs were incubated with pH 5 buffer at 37 °C for 5 min, the fraction of 7D11-resistant intact EVs dropped by 62 % and 42 %, respectively (Figure 2.13 B). The fraction of intact WR Δ A34R EVs was not significantly altered, suggesting that EV membranes of this mutant cannot be disrupted by low pH *in vitro*. When fluorescent EV particles of strain IHD-J mCherry-A5 F13-GFP were subjected to the same treatment and bound to cover slips, however, no significant loss of F13-GFP fluorescence was detected (data not shown), suggesting that disrupted EV membranes remained associated with the underlying virus particle.

The observed increase in 7D11 sensitivity upon low pH treatment suggested that the BafA-sensitive step of EV entry may involve rupture of the EV membrane within acidified endocytic compartments. If this were the case, infection in the presence of BafA might be rescued if EV membranes were artificially disrupted before internalization. To test this, 7D11-treated EVs were bound to HeLa cells in the cold and cells treated for 5 min at 37 °C with pH 7.4 or pH 4.5 medium. Infection was quantified 4 h post treatment (Figure 2.13 C).

After neutral or low pH treatment, infection of untreated cells with EVs of strains IHD-J (32 % and 31 %), and WR (20 % and 20 %) was similar (absolute data not shown). In BafA-treated cells, however, IHD-J and WR infection was increased by 72 and 43 % in cells exposed to low pH when compared to controls. That acid-induced disruption of EV membranes partly rescued infection in cells with impaired macropinosomal acidification suggested that EV membrane disruption was indeed the step in EV entry that was inhibited by BafA. Infection with WR Δ A34R EVs in the presence of BafA was not increased after low pH treatment. This was consistent with the finding that low pH did not trigger disruption of the EV membrane of this strain *in vitro*.

If EV membrane disruption required acidification of endocytic vesicles, intact EV particles would be expected to accumulate in those compartments when acidification is inhibited by BafA. To test this, we infected HeLa cells with IHD-J mCherry-A5 F13-GFP EVs for 3 hours in the absence or presence of BafA. Disrupted EVs were not neutralized with 7D11 in this experiment as they would accumulate in macropinosomes making them indistinguishable from accumulated intact EVs. To prevent early gene expression, which hampers microscopic analysis due to transient cell rounding, microscopy experiments were performed in the presence of actinomycin D (ActD) (typical cells shown in Figure 2.14 A and B). Significantly more EVs were observed in cells infected in the presence of BafA (arrows B, inset) than in cells with unperturbed acidification. EV membranes without viral cores were also detected (filled arrowhead, inset). These may be the remnants of disrupted

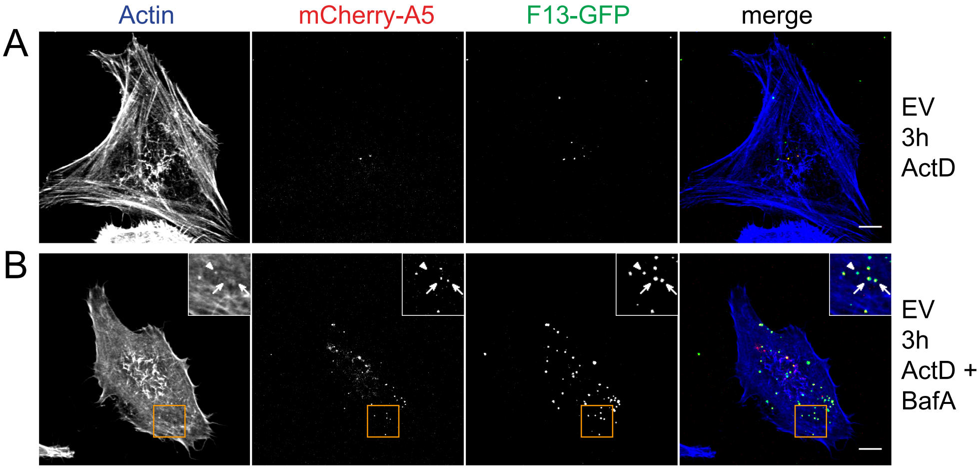

Figure 2.14 EV accumulation in the presence of BafA. HeLa cells were infected with IHD-J mCherry-A5 F13-GFP EVs (MOI 25) in the presence of 5 µg/mL ActD and 25 nM BafA where indicated. Particles were bound to pretreated cells on ice and incubated in full DMEM with drugs at 37 °C for 3 h. Samples were fixed and stained for actin. Images were recorded by confocal microscopy and representative maximum projections of Z-stacks are shown. Arrows in the insets of B highlight EVs, the arrowhead marks a free EV membrane. Scale bars = 10 µm.

EVs, whose underlying MV-like particles underwent fusion. Viral cores containing mCherry-A5 that were released into the cytosol could not be reliably detected with our confocal microscopy setup. When bound EV particles were stained under non-permeabilizing conditions, we found that the majority of EV particles that had accumulated in the presence of BafA was internalized (Figure 2.15).

If disruption of intact EVs is inhibited in the presence of BafA, it reasons that no MV-like particles would be exposed and therefore no viral cores could be released into the host cell cytosol by fusion. To analyse core release, we used IHD-J EGFP-A5 EVs and exploited that VACV cores accumulate in the presence of ActD [178]. Using this approach, we detected and quantified the percentage of free viral cores within the cytoplasm 3 h post infection. To differentiate between viral cores released by fusion and viral particles in endocytic vesicles or bound to the cell (EVs, released MV-like particles, or MVs), virions were stained for the presence of the MV membrane protein L1 (Figure 2.16 A–C and Figure 2.17). In addition, EVs were treated with 7D11 prior to infection, preventing any core release from disrupted EVs or contaminating MVs. Untreated MVs and MVs neutralized with 7D11 were used as controls. In the absence of BafA, 36 % of the total cores in cells infected with intact EVs were released into the cytosol. In the presence of

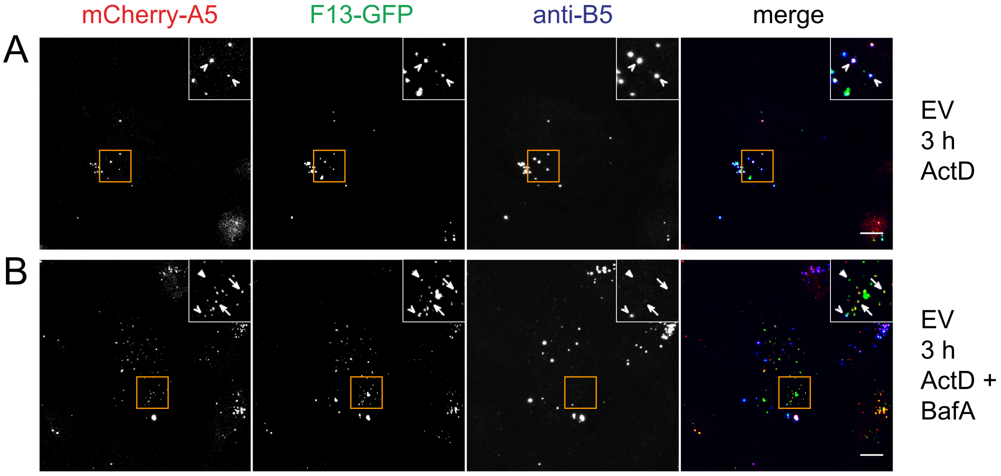

Figure 2.15 Intracellular accumulation of EVs in presence of BafA. HeLa cells were infected with IHD-J mCherry-A5 F13-GFP EVs (MOI 25) in the presence of 5 µg/mL ActD without (A) or with (B) 25 nM BafA. Particles were bound to pretreated cells on ice for 1 h, washed with PBS, and incubated in full medium with drugs for 3 h. Bound EV particles were stained with VMC-20 (anti-B5) under non-permeabilizing conditions. Images were recorded by confocal microscopy and representative maximum projections of Z-stacks are shown. Arrows in the inset of B highlight internalized EV particles not accessible to VMC-20 staining. A bound EV (open arrowhead), and a free membrane (closed arrowhead) are visualized as well. Scale bars = 10 µm.

BafA, the percentage of free cores was reduced to 4 %, indicating that BafA prevented release of EV-derived viral cores into the cytosol. MV core release was only moderately affected by BafA treatment, whereas MV neutralization with 7D11 almost completely abolished the release of cores.

Taken together, the results suggested that acidification of endocytic vacuoles was required for a step of EV entry after endocytic uptake and before release of viral cores. Since fusion of MVs was not inhibited by the concentration of BafA used, the acid-dependent step of EV entry is most likely the disruption of the EV membrane within endocytic compartments. This is further supported by the fact that artificial disruption of the EV membrane could bypass the need for low pH in endocytic vesicles and by the observation that EVs accumulated within BafA-treated cells.

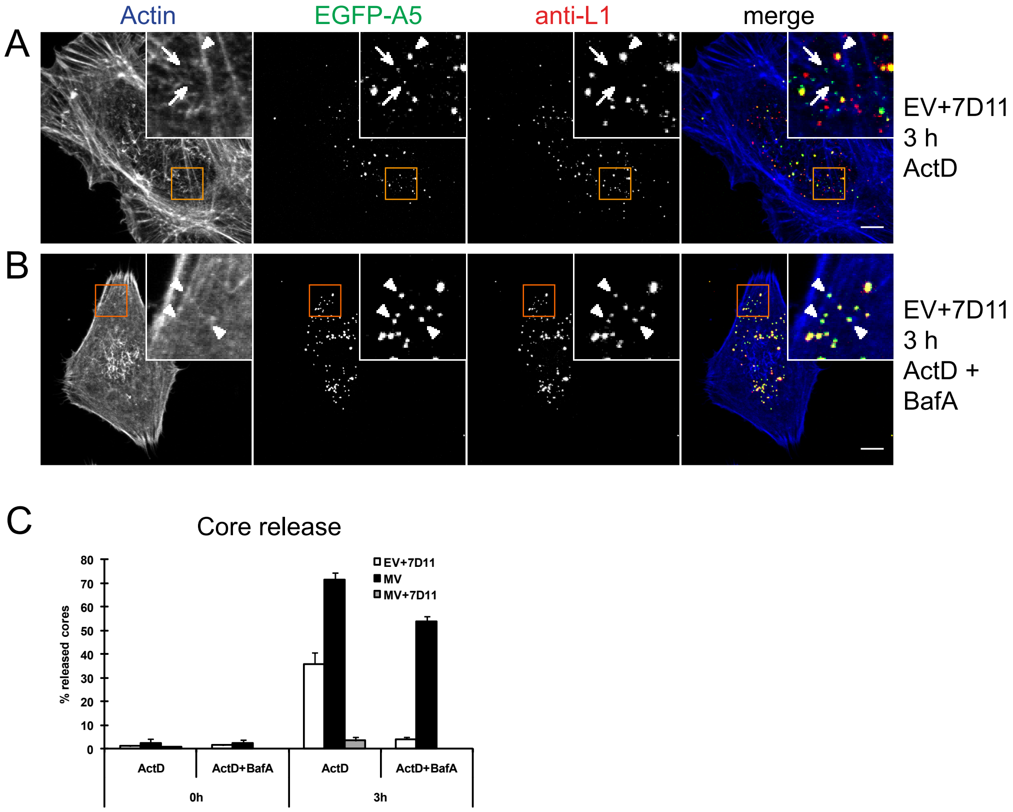

Figure 2.16 Core release in the presence of BafA. HeLa cells were infected with 7D11-treated IHD-J EGFP-A5 EVs (MOI 8 after 7D11 incubation) in the presence of 5 µg/mL ActD and 25 nM BafA where indicated. Particles were bound to pretreated cells on ice and incubated in full DMEM with drugs at 37 °C for 3 h. Samples were fixed and stained for L1 (Mab 7D11) and actin. (A)-(B) Images were recorded by confocal microscopy and representative maximum projections of Z-stacks are shown. Arrows in the insets of A and B highlight released viral cores, arrowheads point at viral particles that were stained for the MV membrane marker L1. Scale bars = 10 µm. (C) The percentage of released cores after infection with 7D11-treated EVs, MVs, and 7D11-treated MVs in the presence of the indicated drugs was quantified in three independent experiments. Controls with bound virus (0 h) were included. Core release from 7D11-neutralized MVs was only quantified in the presence of ActD. Mean values ± SEM are shown.

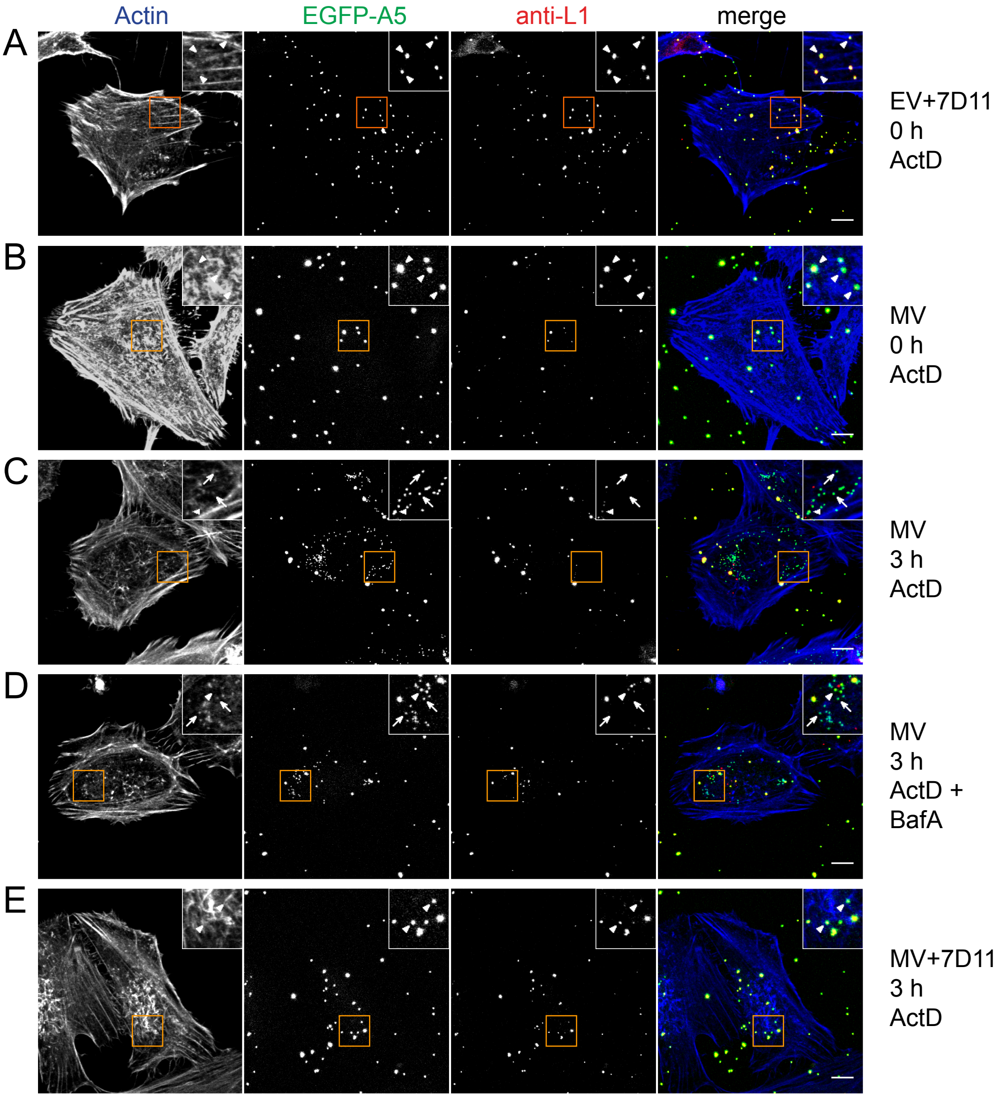

Figure 2.17 Exemplary images of core release assay. Additional exemplary images of core release assay quantification in Figure 2.16C. HeLa cells were infected with IHD-J EGFP-A5 7D11-treated EVs (MOI 8 after 7D11 incubation) (A), MVs (MOI 45) (B–D), or 7D11-treated MVs (equivalent to MOI 45 before neutralization) (E) in the presence of 5 µg/mL ActD and 25 nM BafA where indicated. Particles were bound to pretreated cells on ice for 1 h, washed with PBS, and fixed after binding (A–B) or after incubation in full medium with drugs for 3 h (C–E). L1 (Mab 7D11) and actin were stained and images were recorded by confocal microscopy. Representative maximum projections of Z-stacks are shown. Arrows in insets highlight released viral cores, closed arrowheads mark viral particles stained for the MV membrane marker L1. Scale bars = 10 µm.

2.4 Discussion

With this series of experiments, we aimed at characterizing the entry pathway of VACV EVs. We could show that EVs were rapidly internalized by endocytosis, and that the mechanism was virus-induced, macropinocytic, and essential for infection by intact EVs. We found that loss of the outer EV membrane occurred after endocytic internalization, and concluded that acidification of endocytic compartments was required for this step of EV entry. Presumably, as shown in the schematic view of the entry program in Figure 2.18, the inner membrane with the EFC was exposed after EV membrane rupture. It could then undergo fusion with the limiting membrane of the macropinosome, resulting in core release into the cytosol.

Judging by the insensitivity to MAb 7D11, only a relatively small fraction (10–40 %) of EVs released from VACV-infected RK13 cells and other cell types (data not shown) contained an intact outer membrane. Although previous studies have reported higher proportions of intact EVs (65–75 %) [107, 252, 128, 17], it is evident that many of the EVs released from cells possess outer membranes that are not fully sealed [102]. Although we could

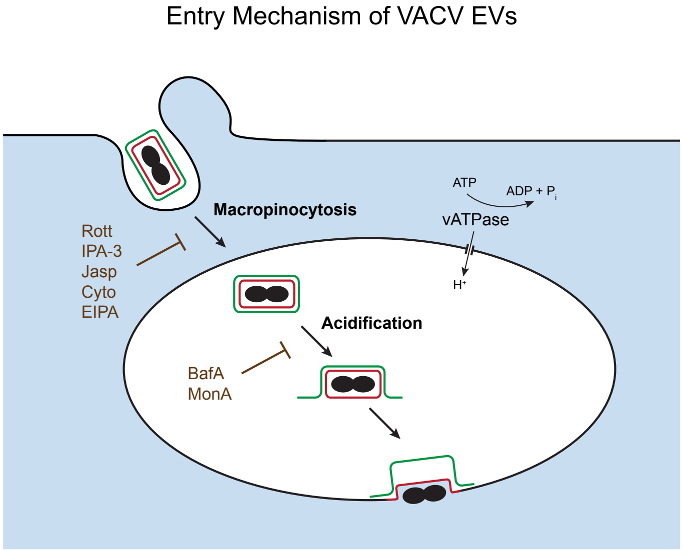

Figure 2.18 Mechanism of VACV EV entry. VACV EVs induce fluid phase uptake by macropinocytosis and are internalized with the bulk fluid. The pH in macropinosomes decreases in the course of their maturation, which triggers disruption of the outer EV membrane. Exposed EFCs in the membrane of MV-like particles catalyse or regulate fusion with limiting endocytic membranes and thereby release virus cores with the genome into the cytosol allowing for successful replication.

occasionally detect free outer membranes in our preparations, the ruptured EV membranes typically remained associated with the particles. Rupture of the EV membranes did not affect the virus infectivity, but it made them susceptible to antibodies against MV antigens.

Using fluorescence and electron microscopy, we could show that EVs were internalized into HeLa cells prior to loss of their outer membrane. In the fluorescence microscopy experiments, we used recombinant viruses in which the core and the EV membrane were visualized by different fluorescent proteins. By EM, we could identify intra-vacuolar virus particles with two membranes resolved, and with immunolabeling of GFP fused to the outer membrane protein F13. The internalization of EVs could also be confirmed by flow cytometry.

The mechanism of endocytosis used by EVs to enter cells was studied using a set of pharmacological inhibitors known to block endocytic processes [149]. It was found that EV infection was dependent on EGFR, PKC, sm-MLCK, PAK1, actin dynamics, and sodium proton exchangers. It was not affected by staurosporin, genistein, and wortmannin, three kinase inhibitors known to inhibit various endocytic mechanisms. Taken together, the inhibitor profile strongly suggested that infection by intact EVs involved macropinocytosis [149]. We could furthermore show that internalization of EVs was blocked by inhibitors of PAK1, actin dynamics, and sodium proton exchangers, and observed EVs in intracellular vesicles positive for the fluid phase marker dextran. Macropinocytic uptake was confirmed by experiments using WR Δ A34R, a mutant virus producing almost exclusively intact EVs. It was found to induce an MV-independent elevation in fluid phase uptake and induced PM ruffling in the form of blebs.

A role for macropinocytosis was consistent with a recent report showing that MV and EV internalization, as well as early gene expression, in monocyte-derived DCs depends on macropinocytosis [199]. However, the authors only visualized uptake of viral cores and did not follow the fate of EV membranes. Furthermore, DCs unlike most other cell types maintain ongoing, constitutive macropinocytosis without the requirement for external triggers [169, 170, 197]. This is part of their function as immune cells responsible for antigen capture and presentation. In other cell types, including the HeLa cells used here, macropinocytosis is a transient, ligand-triggered process [149]. Thus, our data showed a role for macropinocytosis in cell lines that do not undergo continuous, constitutive macropinocytosis. For productive infection of HeLa cells, EVs apparently induced the complete program of macropinocytosis starting with signal transduction, PM blebbing, and increased fluid uptake.

That MVs are also internalized by macropinocytosis has been recently shown with a variety of virus strains and cell types [148, 99, 126, 151, 160]. This is perhaps not surprising considering that EVs and MVs might be excluded from most other endocytic pathways in non-phagocytic cells due to their size. However, the mechanism of macropinocytosis induction was likely to be different for the two particle types as they do not contain common viral proteins on the surface and there is no evidence for common cellular components. In contrast to MV infection, EV infection was not inhibited by the PS-binding protein ANX5. Evidently, EVs did not share the apoptotic mimicry mechanism employed by MVs [148]. The requirement for macropinocytosis is, however, shared with a number of virus families including herpes- and filoviruses for which the mechanism of triggering is not clear [48, 6, 188, 115, 165, 196]. Macropinocytosis as a cellular mechanism is a potential drug target for new antiviral agents.

The effect of BafA and MonA showed that EV-induced infection of HeLa cells required organelle acidification. While internalization was not inhibited by BafA, the drug prevented the release of viral cores from intact EVs. That disruption of the outer EV membrane barrier within endocytic vesicles was the affected step, was supported by several observations. First, we confirmed previous reports that the EV membrane is sensitive to low pH *in vitro* [107, 252]. Second, we observed that artificial disruption of the EV membrane partially rescued infection in the presence of BafA. Third, we found that infection with EV suspensions in the absence of MAb 7D11 (containing 60–90 % disrupted EVs) was significantly less sensitive to BafA or MonA (data not shown). Fourth, EVs with both membranes accumulated intracellularly in the presence of BafA. Fifth, release of viral cores from MVs was not inhibited by the utilized BafA concentrations, suggesting fusion was not affected. MV-like particles wrapped in the EV membrane differ from MVs in that they lack A26 [246]. MVs of VACV strains lacking A26 were capable of fusing at neutral pH in conditions in which MV infection was sensitive to BafA [35], strengthening the conclusion that fusion of MV-like particles is insensitive to BafA. Although low pH seemed essential for EV disruption, we cannot exclude the possibility that the interaction with glycosaminoglycan (GAG)-chains contributes to disruption as previously suggested [128]. However, when the murine cell line L and its GAG-deficient derivative sog9 [12] were infected with IHD-J or WR EVs, infection levels in both cell lines were similar, suggesting that GAGs were not required for efficient EV infection. Inhibition of EV infection by BafA was similar in L and sog9 cells (data not shown).

The mutant WR Δ A34R is interesting because the outer membrane of its EVs is not as susceptible to disruption by GAG-chains [128] and low pH (Figure 2.13 B) as that of wild-type virus. EVs of this virus lack the EV membrane protein A34 and incorporate reduced amounts of two other EV membrane proteins, B5 and A33 [64, 181]. Acidic residues in the membrane-proximal stalk region of B5 are required for GAG-triggered EV disruption [193], and it is possible that both GAG- and low pH-mediated EV rupture share a mechanism that depends on B5 and A34. That WR Δ A34R EVs are infectious despite their resistance to low pH-mediated disruption implies that loss of the outer membrane can be triggered by other mechanisms. Nevertheless, infection remained sensitive to acidification inhibitors, suggesting a need for WR Δ A34R EVs to pass through acidified endocytic compartments for productive infection.

The immune system of poxvirus infected organisms is challenged by two distinct infectious entities, EVs and MVs, that expose no common epitopes. The outer EV membrane serves as a protective shield under which an MV-like particle can hide during virus spread through body fluids. Consistent with such a role, the EV membrane contains complement control proteins [252], and EVs are more difficult to neutralize with antibodies than MVs [129]. The key viral proteins involved in membrane fusion remain hidden and protected until needed. The cue for disruption of the outer EV membrane is the low pH, which the virus is likely to encounter for the first time in the macropinosome. Our results thus indicate that the protective outer membrane of an incoming EV is shed at the latest possible time point, i.e. when the virus has been internalized and is no longer accessible to extracellular factors.

2.5 Material and methods

2.5.1 Cell lines

BSC-40 (African green monkey) and HeLa (human) cells were cultivated in DMEM (Gibco BRL) supplemented with 10 % heat-inactivated FCS, glutamax, and penicillin-streptomycin; for BSC-40 cells non-essential amino acids and sodium pyruvate were added as well; RK13 (rabbit) cells were cultivated in MEM (Gibco BRL) supplemented with 10 % heat-inactivated FCS, glutamax, non-essential amino acids, penicillin-streptomycin, and sodium pyruvate.

2.5.2 Viruses

Recombinant Vaccinia viruses were generated based on VACV strain Western Reserve (WR), VACV WR Δ A34R (a kind gift of Bernard Moss, NIH, Bethesda, MD, USA) [268], and VACV strain International Health Department J (IHD-J) as previously described [148]. Briefly, GFP-expressing strains were generated using vectors based on the plasmid pJS4 [33]. Strains encoding EGFP-A5 or mCherry-A5 in the endogenous locus were constructed using vectors based on pBluescript II KS (Fermentas, St. Leon-Rot, Germany) bearing the EGFP or mCherry coding sequence flanked by the respective VACV WR genomic regions. VACV strains expressing F13-GFP were a kind gift of Rafael Blasco (INIA, Madrid, Spain) [77]. To build strains encoding both mCherry-A5 and F13-GFP, BSC-40 cells were co-infected with mCherry-A5 and F13-GFP viruses; dual-colored recombinants of the parental viruses were selected through four rounds of plaque purification on BSC-40 cells.

MV particles were produced in BSC-40 cells and purified from cytoplasmic lysates as described elsewhere [148]. EV particles were produced in RK13 cells and collected from the supernatant. Confluent tissue culture flasks were infected with the respective MVs in serum-free medium at an MOI of 1 for 1 h. Cells were washed with PBS and overlayed with full medium. 24 h post infection, supernatants were collected and loose cells sedimented by two low speed centrifugation steps (400 g, 10 min, 4 °C). EV-containing supernatants were either used directly or concentrated by sedimentation (40 min, 38,000 g, 4 °C) and re-suspended in full or serum-free medium.

2.5.3 Antibodies

Hybridoma cells to produce the mouse MAb 7D11 (anti-L1) [268] were kindly provided by Bernard Moss with permission of Alan Schmaljohn (University of Maryland, Baltimore, MA, USA). MAbs were purified from hybridoma supernatants by BioGenes (Berlin, Germany). MAb VMC-20 (anti-B5) from ascites fluid was a kind gift of Roselyn J. Eisenberg and Gary H. Cohen (University of Pennsylvania, Philadelphia, PA, USA) [4]. Rabbit polyclonal anti-GFP was purchased from Rockland (Gilbertsville, PA, USA). Fluorophore-coupled goat anti-mouse secondary antibodies were obtained from Invitrogen (Carlsbad, CA, USA).

2.5.4 Drugs and reagents

Actinomycin D, bafilomycin A1, calphostin C, cytochalasin D, chlorpromazine, ethylisopropyl amiloride (EIPA), 3-indolepropionic acid (IPA-3), genistein, ML-7, monensin A, rottlerin, staurosporine, and wortmannin were obtained from Sigma-Aldrich; jasplakinolide was purchased from Enzo Life Sciences (Farmingdale, NY, USA) and Iressa from LC laboratories (Woburn, MA, USA); AF 594-coupled phalloidin (Invitrogen) was used for actin staining, Draq 5 (Biostatus, Shepshed, UK) for DNA staining.

2.5.5 EV plaque assay

To assay the fraction of intact infectious EVs, virus samples were incubated with or without 5 µg/mL MAb 7D11 at 37 °C for 1.5 h. Serial dilutions were prepared and 50 µL of each added to confluent BSC-40 cells in 6-wells covered with 1 mL DMEM. After 1 h at 37 °C, cells were washed with 1 mL PBS and overlayed with 2 mL full DMEM (WR) or full DMEM with 1.5 % carboxymethyl cellulose (IHD-J). Cells were stained after 48 h to 72 h (0.1 % crystal violet, 2 % formaldehyde in $dd\mathrm{H_2O}$).

2.5.6 Microscopic analysis of EV particles

The integrity of EVs on the particle level was analysed using confocal microscopy. EV particles of strain IHD-J mCherry-A5 F13-GFP from clarified supernatants were incubated with 5 µg/mL MAb 7D11 at 37 °C for 1 h and bound to cover slips. Samples were fixed with formaldehyde and stained with AF 647 goat anti-mouse. Z-stacks were recorded using a Zeiss LSM510 Meta confocal system. Particles were detected using the ImageJ particle detector & tracker plug-in [204] on Z projections (radius = 3, cutoff = 0, percentile 0.07 [green]/0.1 [blue]/0.05 [red]) and coordinates compared with a custom-written Matlab program (distance cut-off $\rangle$ 3 pixels [540 nm]).

2.5.7 Confocal microscopy internalization experiment

To assay the internalization of EVs, IHD-J EV particles (3x concentrated supernatants) were bound to HeLa cells on cover slips for 1 h on ice. Cells were either stained directly or incubated in full medium at 37 °C for 30 min. Cells were cooled down, washed, and incubated with VMC20 (1:10,000 in PBS/1 % BSA) on ice for 2 h. Cells were fixed and stained with AF 647 goat anti-mouse and AF 594 phalloidin (where indicated). Control samples were fixed and permeabilized before staining. Z-stacks were recorded using a Zeiss LSM510 Meta confocal system.

2.5.8 Electron microscopy internalization experiment

To visualize internalized EVs, IHD-J F13-GFP EV particles (60x concentrated supernatants) were bound to HeLa cells on ice for 1 h. Cells were incubated in full medium at 37 °C for 30 min, and fixed in 4 % formaldehyde and

0.1 % glutaraldehyde in 1x PHEM buffer [208] for 90 min. Cryo-sectioning and immuno labelling was performed as described elsewhere [235, 220]. In brief, ultra-thin sections (50-70 nm) from gelatin-embedded and frozen cell pellets were obtained using a FC7/UC7-ultramicrotome (Leica, Vienna, Austria). Immunogold labelling was carried out on thawed sections with anti-GFP antibodies (1:200) and 10 nm protein A-gold (UMC Utrecht University, Utrecht, The Netherlands) (1:50); a mixture of uranyl acetate and methyl cellulose was used for embedding and negative staining. Sections were examined with a CM10 Philips transmission electron microscope with an Olympus "Veleta" 2k x 2k side-mounted TEM CCD camera.

2.5.9 Flow cytometry internalization assay

Subconfluent 12-wells of HeLa cells were used for flow cytometry-based internalization assays. Cells were pretreated with inhibitors for 15–60 min in full DMEM; EVs (IHD-J F13-GFP, 0.25 mL 35 x concentrated supernatants) or MVs (IHD-J EGFP-A5, $7.5 \cdot 10^7$ pfu in 0.25 mL) in serum-free medium were bound to cells on ice for 1 h. Cells were washed and incubated with full medium (+ inhibitors) at 37 or 0 °C for 30 min. Cells were washed with PBS and incubated with 0.25 % Trypsin/EDTA at 37 °C for 10 min to detach cells and remove bound virus. Alternatively, cells were detached with 1 mM EDTA/PBS at 0 C for 30 min. Cells were re-suspended and washed in 7 % FCS in PBS, fixed and analysed using a Becton Dickinson (BD) FACSCalibur flow cytometer and the FlowJo software package.

2.5.10 Flow cytometry infection assay

Confluent 12-wells of HeLa cells were infected for flow cytometry-based infection assays. Pretreatment with inhibitors was performed for 15–60 min in full MEM (as used for RK13 cells and present in EV supernatants). MVs ($2 \cdot 10^6$ pfu in 0.5 mL) and EVs (0.5 mL EV supernatant or concentrate) were prepared in full MEM (+ inhibitors). Disrupted EVs and contaminating MVs in the EV samples were neutralized with 5 µg/mL 7D11 for 1 h at 37 °C and added to cells. After 30 min at 37 °C, cells were washed and overlayed with 1 mL full MEM (+ inhibitors). 4 h post infection, cells were prepared for flow cytometry. Cells were analysed using a BD FACSCalibur flow cytometer and the BD CellQuest Pro software or the FlowJo software package.

2.5.11 Fluid phase uptake assay

Virus-induced fluid phase uptake was quantified as described previously [147]. Sub-confluent HeLa cells in 24-well plates were serum-starved in 0.2 % BSA/ DMEM for 4 hour. WR wt MVs or WR Δ A34R EVs in 0.2 % BSA/RPMI were then bound to the cells in the cold for 90 min. Cells were washed and pulsed for 10 min at 37 °C with 0.5 mg/mL 10 kDa dextran AF 488 (Invitrogen) in RPMI/BSA. Cells were washed with BSA/RPMI, PBS (2x), 100 mM NaOAc (pH 5.5)/50 mM NaCl, and PBS. Cells were detached with 0.25 % trypsin (25 min on ice, 1 min at RT), resuspeded with 7 % FCS in PBS and fixed in 4 % formaldehyde over night at 4 °C. Fluorescence of cells was quantified using a BD FACSCalibur flow cytometer and the FlowJo software package.

2.5.12 Blebbing assay

To quantify the induction of blebbing, HeLa cells were grown on cover slips to 50 % confluency. MV or EV suspensions (0.5 mL) of VACV WR Δ A34R EGFP-A5 in 2 % BSA/PBS were added to cells at RT for 1 h. Cells were washed and incubated with full medium at 37 °C for 40 min. Samples were fixed with 4 % formaldehyde at RT, and DNA and actin stained with Draq 5 and AF 594 phalloidin. Microscopy images were recorded using an Olympus Cellˆ R imaging station with DIC setup. Total and blebbing cells were counted manually ($n_{total} \sim 250$ cells/condition and experiment).

2.5.13 Annexin V binding

Exposed PS on virion membranes was masked with ANX5 to test the requirement of PS on infection. A modified version of the manufacturer's protocol (Vybrant Apoptosis Assay kit # 2; Molecular Probes) was used for labelling. In brief, sedimented virions were washed twice with ANX5-binding buffer (10 mM Hepes, 140 mM NaCl, 2.5 mM $CaCl_2$, pH 7.4), resuspended in 200 µL ANX5-binding buffer and split into two samples. Samples were left untreated or treated with 20 µL AF 647 ANX5 for 1 h at RT. Virions were washed twice with ANX5-binding buffer, re-suspended in DMEM and used for infection experiments.

2.5.14 EV disruption

To disrupt EV particles *in vitro*, 20 µL EVs (clarified supernatant of infected RK13 cells) were mixed with 180 µL 10 mM Na-citrate (pH 5.0), incubated at

37 °C for 5 min and neutralized with 100 µL 1 M Hepes pH 7.4. For controls, Hepes was added to virus samples premixed with low pH buffer. Integrity of EVs was quantified by plaque assay as described above. To rescue infection by low pH treatment, 7D11-treated EV particles were bound to drug-treated HeLa cells on ice for 1 h in the presence of drugs. Cells were incubated for 5 min with full DMEM containing 30 mM MES (pH 4.5) or full DMEM (pH 7.4) at 37 °C. Cells were washed twice and treated as described in the flow cytometry infection assay. SigmaPlot (Systat software) was used to compare sample groups by t-test.

2.5.15 Core release assay

To detect and quantify viral cores, HeLa cells on cover slips were pre-treated with inhibitors in full DMEM for 30 min. IHD-J EGFP-A5 EVs (0.25 mL 4x concentrated EV supernatant) or MVs ($1.3 \cdot 10^7$ pfu in 0.25 mL) in 2 % BSA/PBS were pretreated with or without 5 µg/mL 7D11 for 1 h at 37 °C. Virions were bound to cells on ice for 1 h in the presence of drugs. Cells were washed with PBS and incubated in full medium with drugs for 3 hours. Cells were fixed with formaldehyde, and stained with 7D11 (540 ng/mL) / AF 594 goat anti-mouse and AF 647 phalloidin. Z-stacks were recorded using a Zeiss LSM510 Meta confocal system. Green fluorescent cores were detected with the spot detection function of Imaris (Bitplane) using the quality parameter. Detected spots with a mean green intensity <20 were omitted and spots with a mean red fluorescent intensity <50 were classified as released cores ($n_{\text{total}} \sim 750$ cores in 10 cells/condition and experiment).

2.6 Acknowledgements

We thank Veronika Graml for help with image analysis, Stefan Kalin for help with dextran uptake experiments, and the Light Microscopy Center (LMC), ETH Zrich, for microscopy support. We are grateful to Lucia Reh, Andrea Rothballer, and Yohei Yamauchi for critical reading of the manuscript.

This work was in part funded by grants from EMBO, ETH Zurich, and the Swiss National Foundation (InfectX, Sinergia). FIS was supported by a Boehringer Ingelheim Ph.D. fellowship.

Chapter 3

RNAi screening reveals proteasome- and Cullin3-dependent stages in vaccinia virus infection

The results of this section have been published in:

*CellReports (2012), **2**, 1–12 (doi:10.1016/j.celrep.2012.09.003)*

RNAi screening reveals proteasome- and Cullin3-dependent stages in vaccinia virus infection

Jason Mercer[1a], Berend Snijder[2a], Raphael Sacher, Christine Burkard[3], Christopher Karl Ernst Bleck[4], Henning Stahlberg[4], Lucas Pelkmans[2*], and Ari Helenius[1†]

[1] ETH Zurich, Institute of Biochemistry, Schafmattstr. 18, 8093 Zurich, Switzerland

[2] University of Zurich, Institute of Molecular Life Sciences, Winterthurerstr. 190, 8057 Zurich, Switzerland

[3] Utrecht University, Department Infectious Diseases & Immunology, Yalelaan 1, 3584 Utrecht, Netherlands

[4] University Basel, Center for Cellular Imaging and NanoAnalytics (C-CINA), Structural Biology and Biophysics, Biozentrum, Mattenstrasse 26, 4058 Basel, Switzerland

[a] Contributed equally

[†] Corresponding author: ari.helenius@bc.biol.ethz.ch

[*] Corresponding author: Screening and Bioinformatics, lucas.pelkmans@imls.uzh.ch

Experiments shown in Figure 3.2 G and Supplementary Figure 3.9 and 3.10 were performed by Christopher K. E. Bleck.

3.1 Summary

A two-step, automated, high-throughput RNAi silencing screen was used to identify host cell factors required during vaccinia virus infection. Validation and analysis of clustered hits revealed previously unknown processes during virus entry including a new mechanism for genome uncoating. Viral core proteins were found to be ubiquitinated already during virus assembly. After entering the cytosol of an uninfected cell, the viral DNA was released from the core through the activity of the cell's proteasomes. Next, a Cullin3-based ubiquitin ligase-mediated round of ubiquitination and proteasome action was needed to initiate viral DNA replication. In addition to identifying novel cell functions required for poxvirus infection, these studies highlight the capacity of large-scale RNAi screens to direct detailed cell biological investigation of virus-host cell interaction.

3.2 Introduction

Poxviruses are enveloped DNA viruses characterized by their large size, intricate structure, and a complex cytoplasmic replication cycle [71]. Vaccinia virus (VACV), the prototypic poxvirus used in this study, served as a vaccine during the eradication of smallpox, one of the most devastating diseases of the 20th century [71]. The potential deployment of the smallpox virus as a biological weapon, risks associated with resumed vaccination, and recent monkey pox outbreaks warrant continued research towards new anti-poxvirus agents [58, 88].

The VACV life cycle begins with macropinocytic internalization of virus into host cells [99, 148]. This is followed by low pH dependent membrane fusion to release the viral core into the cytosol [239]. Post-penetration steps include loss of core-associated lateral bodies, core expansion, and transcription of early viral genes within the expanded core [51, 117, 161, 178]. Early mRNAs generate about 100 different viral proteins, including unidentified factors required for DNA uncoating [112, 138]. During the subsequent uncoating process, cores disappear as visible structures, the viral DNA is released and replicated, intermediate and late genes are expressed, and cytosolic virus factories formed. While many of the cellular factors and functions required for initial entry have been described [99, 127, 148, 211, 239], the cellular factors that participate in viral genome uncoating remain largely undefined. In the last few years, large-scale RNAi screening has become a powerful tool for the analysis of pathogen-host interactions. This approach has been previously applied to a variety of pathogens (reviewed in [37]). For VACV, a Drosophila kinome screen was used to identify and describe a role for AMPK during infection [160].

Our goal was to elucidate the host factors in tissue culture cells needed in the VACV life cycle. Using a large-scale RNAi screen we have defined critical cellular processes that the virus exploits during infection. By focusing on the identified protein clusters involved in ubiquitin-mediated proteasome degradation, we have uncovered roles for proteasomes, ubiquitination, and a Cullin3-based ubiquitin ligase in uncoating of viral genomes and their subsequent replication. Ultimately, this information could facilitate the development of novel antiviral agents that would target the host rather than the virus directly.

3.3 Results

3.3.1 RNAi screening identifies 188 cellular factors required for VACV infection

We used an automated, high-content, high-throughput RNA interference (RNAi) screen in human tissue culture cells (HeLa) to identify host cell factors and processes required during the VACV life cycle. Using the mature virus form of a recombinant VACV that expresses EGFP under a synthetic early/late viral promoter (VACV-EGFP) [148], we could readily distinguish infected from non-infected cells. Automated fluorescence microscopy and image analysis was employed to score for cell factors required during the replication cycle up to and including translation of late viral genes.

To avoid some of the pit-falls encountered in previous virus infection screens [37, 156], we chose to screen a set of 7,000 genes selected for their potential to be inhibited by small compounds (the 7,000 drug-able genome library; Qiagen). Although covering only one-third of human genes, these represent a well-studied and well-annotated cross-section of the full genome; and for these factors, reagents are more readily available for follow-up studies.

In addition, we improved image analysis, hit visualization, and hit validation.

To increase reliability, we introduced a fully automated computational pipeline for high-content image analysis [27, 224]. Over 200 quantitative features were extracted from each of 624 million individual cells from 1.45 million images [27]. Using these features as a basis, several iterations of supervised machine learning were applied to identify virus infection, mitosis, apoptosis, and technical phenotypes [189, 224] (Supplementary Information for details). Cell number and density (population context) effects were normalized to improve both reproducibility of screening results in different cell lines and consistency of phenotypes obtained by different siRNAs targeting the same genes [225].

The RNAi screen was carried out in two steps as detailed in Figure 3.1 A and in materials and methods. Three non-overlapping siRNAs against each gene were used in a primary screen, and three additional siRNAs in a secondary follow-up screen. Both screens were repeated independently three times. The primary screen using the 7000 drug-able genome led to the identification of 276 genes in which two or three of the three siRNAs reduced VACV infection relative to controls (Le. for the majority the median over the triplicates of at least two siRNAs had a median absolute deviation less than -1.5 over the whole screen).

The secondary screen, directed against the genes identified as hits in the primary screen, was performed using siRNAs from a different vendor (Ambion). It confirmed 68 % of the hits from the primary screen with a correlation coefficient of 0.34 between the validated RNAi phenotypes of the two screens ($P = 2.8 \cdot 10^{-6}$). A stringent, control-based analysis of non-targeting control siRNAs gave a false positive rate of 0.06 % in the secondary screen giving further confidence in the confirmed host-factors.

The final hit list had 188 genes representing a broad range of cell functions. Among them, several proteins have been previously implicated in VACV infection: EGFR, RAC1, PAK1, laminin (LAMAl and 2), the proteasome, Tsgl01, profilin, and RIPK3 [40, 42, 66, 93, 132, 136, 148, 151, 202, 233, 256]. Others, such as ribosomal proteins, were expected as hits for any virus. However, the majority had no prior connection to VACV infection.

To extract information regarding critical processes in the infection cycle, the list was submitted to rigorous bioinformatic analysis. For this, we developed an algorithm that combined functional-and interaction-based information (Supplementary Information; Network Visualization). This algorithm is applicable for the visualization and analysis of any gene list. The hits were first assigned to "functional annotation clusters" representing sets of proteins that share common annotations within public databases (DAVID [100]). As shown in Figure 3.5, the genes were enriched within 13 clusters and several

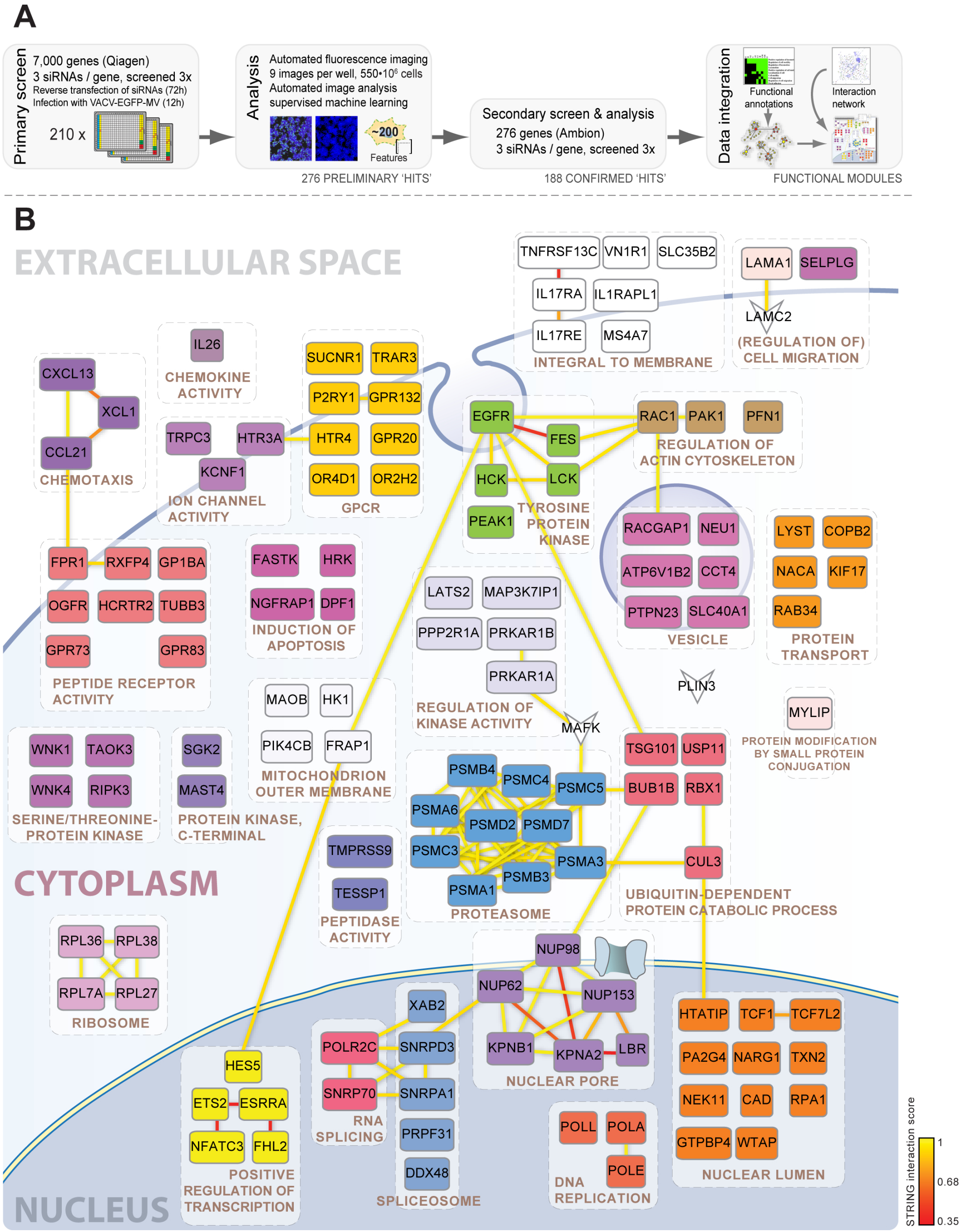

Figure 3.1 (A) Outline of screening and bioinformatic procedures. (B) Host factors in larger functional clusters that interact or share functional annotations are depicted. Individual genes were assigned to the highest enriched functional annotation cluster in which they were present (Figure 3.1 B). Functional clusters identified by DAVID with simplified annotations are pictured as white boxes with dashed outlines. Yellow lines between genes of different clusters indicate high-confidence (>0.9) STRING interactions, while those between genes within the same functional cluster include lower confidence (>0.35) STRING interactions. Selected genes not found within a functional annotation cluster are indicated as inverted arrowheads. Functional gene clusters are pictured in their approximate cellular location.

highly connected, functional annotation networks.

The function-based information was combined with data on physical interactions between individual host factors (STRING [231]). The result of the combined analysis is shown for 126 of the 188 host factors in Figure 3.1 B. Automatic annotation was used to visualize the interaction networks (yellow to red lines) both within and between functional annotation clusters (grey dashed boxes). Without going into detail, it was evident that although replication and assembly of progeny virus occurs in the cytoplasm of host cells, VACV depends on cytoplasmic, as well as, nuclear functions. The cytoplasmic functions included membrane trafficking, signalling, proteolysis, and ion transport. Factors in the tyrosine kinase and actin clusters have already been shown to be necessary for phosphatidylserine-mediated macropinocytosis of the virus during entry [148, 150].

3.3.2 Breakdown requires proteasome activity but is independent of new ubiquitination

The value of a screen depends ultimately on whether it leads to concrete new insights and novel mechanisms. In the follow-up, we focused on two prominent clusters; the proteasome and ubiquitination (Figure 3.1 B). siRNA-mediated depletion of proteasome subunits caused a nearly complete block in infection (Figure 3.2 A). For confirmation, we determined the virus yield in the presence of MG132, a proteasome inhibitor, and UBEI-41, an inhibitor of the cellular E1 ubiquitin conjugating enzyme UBA1. Both decreased viral yield by -3 logs, similar to cycloheximide (CHX), a protein synthesis inhibitor (Figure 3.1 B). When infection with VACV strains that express EGFP specifically from an early (E-EGFP-VACV), or a late (L-EGFP-VACV) promoter was analysed by flow cytometry using, we found that the inhibitors blocked late, but not early viral gene expression (Figure 3.2 C).

This suggested that the virus life-cycle prior to early gene expression, such as virus binding and endocytosis, were not impacted by these inhibitors. To confirm this, we tested whether the effects of MG132 and UBEI-41 could be circumvented by forcing fusion of virions at the plasma membrane with low pH. This treatment results in deposition of viral cores into the cytoplasm, effectively by-passing the need for endocytosis [148]. Consistent with a post-penetration block, the inhibitors could not be by-passed upon low pH treatment (Figure 3.2 D). Similar results regarding viral yield, gene expression, and inhibition after by-pass were observed with the more specific proteasome inhibitor, Velcade (Figure 3.6).

Having ruled out a role for the proteasome and UBA1 in virus endocytosis and penetration, we addressed genome uncoating. The efficient release of viral DNA from internalized cores is of interest because poxvirus particles and cores are extremely stable when exposed to desiccation, denaturants, proteases, extremes of temperature, etc. [68, 137, 140].

Using a virus in which the core protein AS was tagged with EGFP [148], and by immuno-fluorescence staining of the viral membrane protein Ll [210], we followed the fate of individual viruses and cores by fluorescence microscopy. HeLa cells were incubated at a multiplicity of infection (MOl) of 10 for 4 h, a time sufficient for virions to enter and undergo genome uncoating. External virions that still contained the viral membrane were yellow, and internalized, released viral cores devoid of membrane were green. When the cores in control cells were quantified Figure 3.7, few were observed (25-50 per cell; green) (Figure 3.2 E; UNTR). However, in the presence of CHX, which prevents core breakdown and genome uncoating [113], intact cytoplasmic cores numbered 275-320 per cell (Figure 3.2 E; CHX). The same was observed when the proteasome was inhibited with MG132 (250-300/cell) (Figure 3.2 E; MG132). UBEI-41 had virtually no impact on core breakdown (50-60 cores/cell) (Figure 3.2 E; UBEI-41). This suggested that protein synthesis and the proteasome were needed for uncoating, but UBA1 was not.

3.3.3 VACV core proteins are packaged in a K48- ubiquitinated state to mediate proteasome dependent genome uncoating

Using a similar fluorescence-based assay, Satheshkumar and co-workers have in a previous study reported that inhibition of proteasome activity has a minor impact on core breakdown [202]. They concluded that proteasomes were required for the subsequent viral DNA replication step. For clarification, we investigated the state of cytoplasmic cores after entry in the presence of MG 132 using electron microscopy.

The images confirmed that viral cores remained intact (Figure 3.2 F, MG 132; Figure 3.8). While core expansion occurred Figure 3.10, it was evident that the genome (the electron dense material within the cores) was not released (3.2 F; blow-up). Electron microscopy also showed that while UBEI-41 did not inhibit core breakdown, it prevented formation of viral DNA replication factories (Figure 3.2 F; UBEI-41; Figure 3.8). This was consistent with previous reports that ubiquitination is needed for DNA replication [202, 233]. Taken together, the results suggested somewhat paradoxically that proteasomes were needed for breakdown of the core whereas ubiquitination, which normally serves to prepare substrates for degradation, was required for a subsequent step, one preceding DNA replication.

To monitor release of incoming viral DNA as a consequence of core breakdown, we used immunofluorescence staining for the viral protein I3L that is bound to the viral DNA [260]. That antibodies directed against this protein can be used to detect uncoated parental VACV DNA in the absence of viral replication has been demonstrated [63, 260]. While unable to access the antigen in intact cores (Figure 3.10), antibodies to I3L stained cytoplasmic viral DNA after release from incoming cores (Figure 3.3 A). Later in infection, it also stained the I3L complexed with viral DNA in the large perinuclear virus factories.

When control cells were infected for 4 h at a MOl of 10, and the viral DNA visualized by anti-I3L, replication factories and cytoplasmic 13 staining were seen (Figure 3.3 A; UNTR). With CHX present to prevent early gene expression and genome release, only 5 % of cells had I3L-positive spots in the cytoplasm. In the presence of cytosine arabinoside (AraC), an inhibitor of viral DNA replication, 78 % of cells contained cytoplasmic I3L spots indicating that incoming viral DNA had been released, but not replicated. Cells infected in the presence of MG132 were positive for diffuse cytoplasmic I3L

Figure 3.2 ***(following page)*** Proteasome but not E1-activating enzyme function is required for VACV genome uncoating. (A) RNAi mediated silencing of proteasome subunits PSMAl and PSMB3 impair VACV infection (RII average representative images from the screen are displayed). (B) Proteasome (MG132) and E1-activating enzyme (UBEI-41) inhibitors block VACV production (MOI 1; 24 hour p.i.; 10 μM AraC, 10 μg/mL CHX, 25 μM MG132, and 50 μM UBEI-41 used throughout). (C) MG132 and UBEI-41 allow for early but not late VACV gene expression. Cells were infected with VACV (MOI 1) expressing EGFP from either an early (E-EGFP-VACV), or a late (L-EGFP VACV) promoter. Infections were performed in the presence of the indicated inhibitors. Cells were harvested 6 hour p.i. and analysed for the number of early or late EGFP expressing cells, respectively. Cells infected in the presence of CHX or AraC were used as controls. (D) MG132 and UBEI-41 inhibit VACV infection after internalization. VACV-EGFP MVs (MOI 1) were bound to cells for 1 hour in the presence of inhibitors. Cells were then washed, treated with pH 7.4 or pH 5.0 media for 5 min, washed, and media containing the inhibitors added back. Cells were analysed by flow cytometry for EGFP at 6 hour p.i. (E) VACV core degradation is proteasome, but not E1 activating enzyme dependent. Cells were infected with WR-EGFP-A5 (MOI 10) in the presence of CHX, MG132, or UBEI-41. At 4 hour p.i. cells were fixed and external virions identified by immunofluorescence against the viral membrane protein L1R. Experiments were performed in triplicate and the average number of cores per cell under each condition displayed as mean ± SEM (right)(see Figure 3.5). (F) EM shows that MG132 and UBEI-41 inhibit distinct stages of the VACV life cycle. Cells treated as in F (MOI 10; 4 hour p.i.) were analysed by EM. Blow-up of virion (MG132) indicates that the electron dense viral genome is still within the core. All experiments have been performed in triplicate and displayed as the mean ± STDV (B-D) or representative images displayed (F-G).

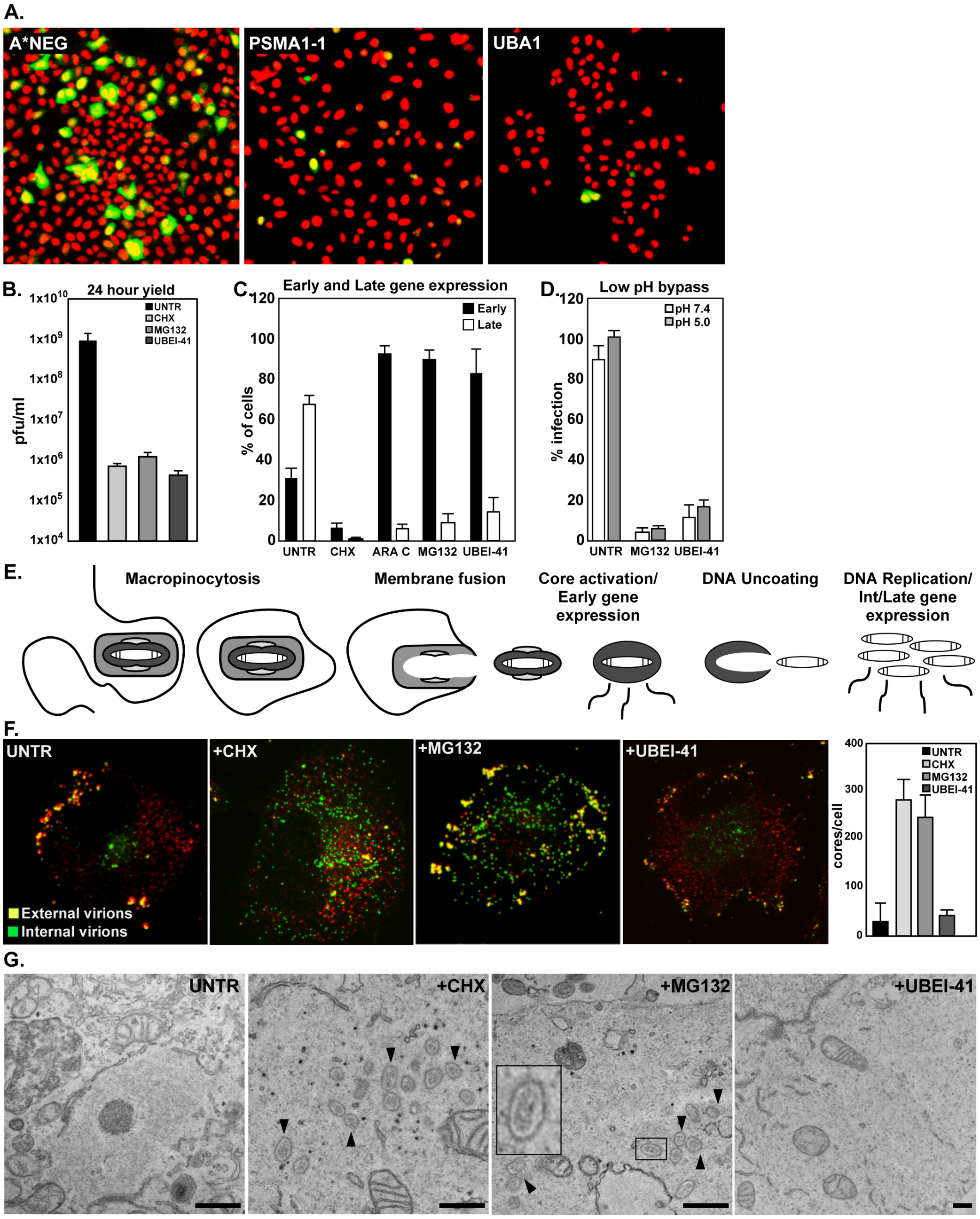
A.
A*NEG
PSMA1-1
UBA1
B.
24 hour yield
pfu/ml
1x10^10
1x10^9
1x10^8
1x10^7
1x10^6
1x10^5
1x10^4
■UNTR
□CHX
■MG132
■UBEI-41
C.
Early and Late gene expression
% of cells
■ Early
□ Late
120
100
80
60
40
20
0
UNTR
CHX
ARA C
MG132
UBEI-41
D.
Low pH bypass
% infection
□pH 7.4
■pH 5.0
UNTR
MG132
UBEI-41
E.
Macropinocytosis
Membrane fusion
Core activation/ Early gene expression
DNA Uncoating
DNA Replication/ Int/Late gene expression
F.
UNTR
+CHX
+MG132
+UBEI-41
External virions
Internal virions
cores/cell
400
300
200
100
0
■UNTR
□CHX
■MG132
■UBEI-41
G.
UNTR
+CHX
+MG132
+UBEI-41

staining, but did not contain I3L-positive viral DNA spots. This showed that even though expression of I3L (an early protein) had occurred, viral genomes had not been released (Figure 3.3 A). In contrast, UBEI-41-treated cells displayed diffuse cytoplasmic I3L staining and I3L-positive spots as seen in AraC-treated cells, confirming that viral genomes were released but not replicated. Collectively, these results showed that the proteasome and UBA1 acted in distinct steps in the early infection cycle; proteasomes in core breakdown and DNA release, and UBA1 (and thus ubiquitination) in replication of released viral DNA.

That core degradation was not dependent on UBA1 suggested that ubiquitin must have been added to core proteins prior to virus entry. Proteomic analysis of isolated VACV virions have indicated that ubiquitin accounts for 1-3 mole percent of total protein [43]. However, the location of this ubiquitin within the viral particle, and the potential role of this host protein in the virus life cycle has not been investigated.

Immunoblot analysis on highly purified VACV virions confirmed that they contained a striking amount of ubiquitin (Figure 3.3 B; left). The molecular weight of the detected bands indicated that these were ubiquitin-conjugated proteins, and not free ubiquitin. To assess the location of the ubiquitin-conjugated proteins, virions were separated into membrane and core fractions [154]. Immunoblot analysis on these fractions indicated and the vast majority of the ubiquitinated factors were components of the viral core (Figure 3.3 B; right). Using lysine-48- and lysine-63-linked poly-ubiquitin specific antibodies, we showed that only lysine-48-linked ubiquitinated proteins were present (Figure 3.3 C). Since lysine-48-linked ubiquitin chains mark proteins for proteasomal degradation [45, 124], it was evident that this was the mechanism that triggered proteasome-mediated genome uncoating.

Since ubiquitination of core proteins must occur during virion production in infected cells, we asked whether infectious virus could be produced if ubiquitination was inhibited late in infection. Addition of either AraC at 6 hour had little effect on late viral gene expression (Figure 3.3 D, white), and only marginally reduced the 24 hour virus yield (Figure 3.3 E; white). As late genes are expressed from newly replicated genomes, this indicates that by 6 hour p.i. viral DNA replication and late gene expression is sufficient for significant virus production. When UBEI-41 was added at 6 hour p.i., again there was no impact on late viral gene expression (Figure 3.3 D, grey). However, unlike AraC, that had little effect on virus yield, addition of UBEI-41 after 6 hour prevented the production of infectious virus (Figure 3.3 E; grey). We were, in fact, unable to isolate virus particles from infected cells treated with UBEI-41 from 6 hour p.i. (Figure 3.8). This indicated that there are at least two steps in the VACV infectious cycle that require ubiquitination:

not only viral DNA replication after genome uncoating but also assembly of progeny virus.

3.3.4 A Cullin-3 ubiquitin ligase complex is required for VACV genome replication

While responsible for genome uncoating (Figure 3.2 and 3.3), it remained unclear whether the proteasome was also required for a second step, namely to initiate genome replication as previously described [202, 233]. After confirming that both MG132 and UBEI-41 prevented VACV replication site formation (Figure 3.4 A), we used an AraC release approach to test for effects on replication. Cells were infected in the presence of AraC for 6 hour to allow uncoating but stop replication of incoming genomes. AraC was then washed out or replaced with either UBEI-41 or MG132. Infection was allowed to proceed for an additional 6 hour after which cells were analysed for viral

---

Figure 3.3 ***(following page)*** (A) MG132 prevents VACV genome release and UBEI-41 blocks viral DNA replication. Cells were infected (MOI 10) in the absence of inhibitors (UNTR), or in the presence of MG132 or UBEI-41. Cells were fixed 4 hour p.i. and immunoflouresence against the viral I3 DNA binding protein performed. Cells treated with CHX, which prevents genome release, or AraC, which allows for release of parental genomes but not their replication served as controls for the assay. The number of cells positive for parental DNA staining under each condition is displayed as the mean ± STDV (right). (B) VACV core proteins are packaged in a polyubiquitinated state. Immunoblots directed against total (mono and poly) ubiquitin were performed on 1.0, 2.5, and 5.0 μg of purified VACV MVs (left), or on 2.5 μg of whole (W) VACV MVs, or MVs separated into core (C), and membrane (M) fractions (right). As a control for detection of ubiquitin, 100 μg of cell lysate (Cells) was used. Experiments were performed in triplicate and representative blots shown. (C) Viral core proteins are positive for K-48-, but not K63-linked ubiquitin chains. Immunoblots directed against K-48 or K63-specific ubiquitin chains were performed on whole (W), core (C), and membrane (M) fractions of VACV MVs. 100 μg of cell lysate was used as a control for each antibody (Cells). (D) Late addition of MG132 or UBEI-41 does not impede late viral gene expression. Cells were infected (MOI 1) with VACV-EGFP-LATE. Either 10 μM AraC or 50 μM UBEI-41 were added at the indicated times. Infection was allowed to proceed for a total of 12 hour before cells were harvested and analysed by flow cytometry for EGFP expression. Values are displayed as the percentage of cells expressing late genes relative to untreated infected control cells at 12 hour p.i. (E) Inhibition of E1-ligase function at 6 hour p.i. impedes production of infectious virus. Cells were infected with VACV MVs (MOI 1) and AraC or UBEI-41 added at either the time of infection 0 hour (0) or after 6 hour (6). Cells were harvested 24 hour p.i. and progeny virus was purified by banding Figure 3.12 followed by titration for plaque forming units/mL. (A-C) Experiments were performed in triplicate and representative images shown. (D and E) Experiments were performed in triplicate and displayed as the mean ± STDV.

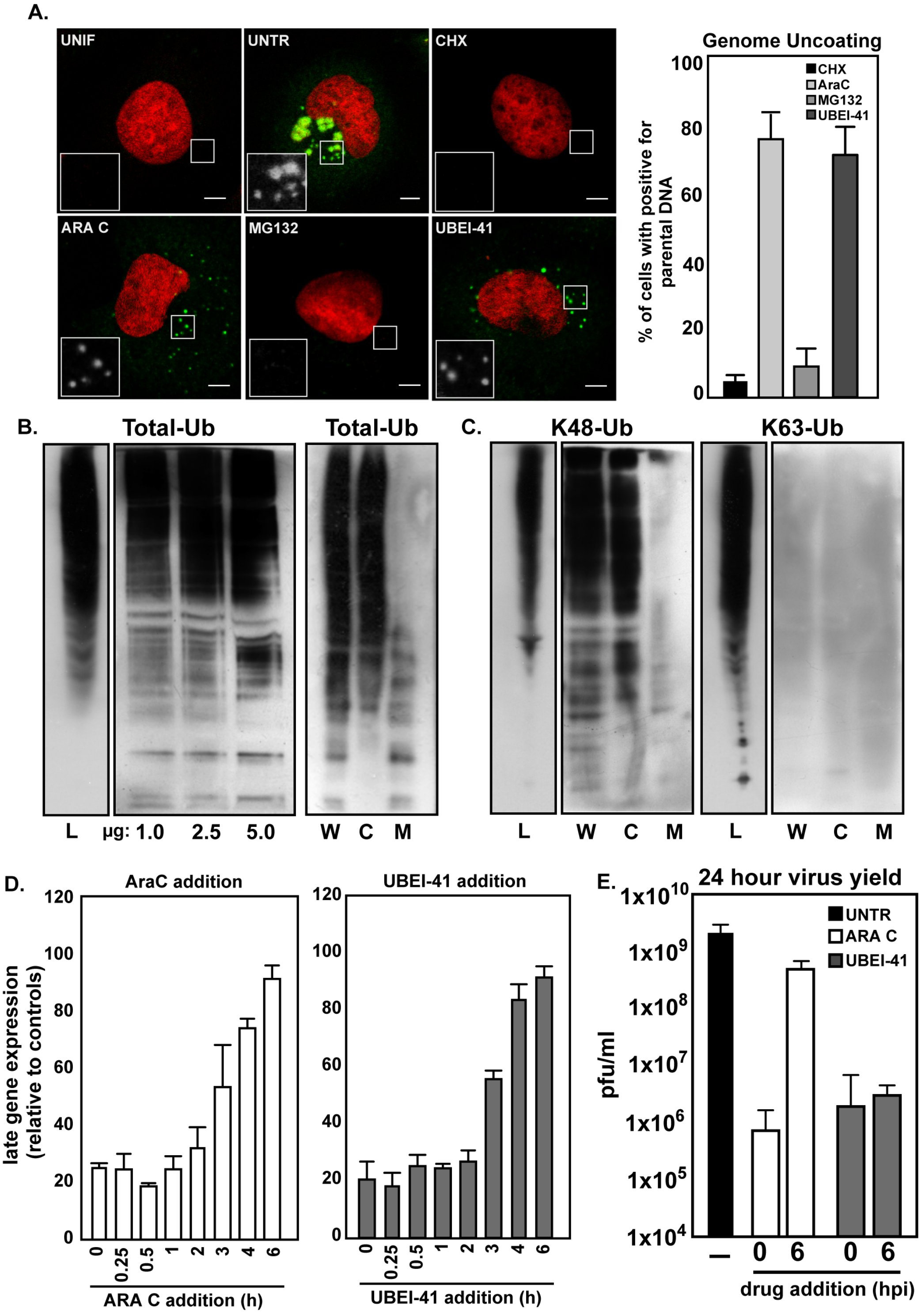
A.
UNIF
UNTR
CHX
ARA C
MG132
UBEI-41
Genome Uncoating
% of cells with positive for parental DNA
0
20
40
60
80
100
CHX
AraC
MG132
UBEI-41
B.
Total-Ub
Total-Ub
L
µg: 1.0
2.5
5.0
W
C
M
C.
K48-Ub
K63-Ub
L
W
C
M
L
W
C
M
D.
AraC addition
UBEI-41 addition
late gene expression (relative to controls)
0
20
40
60
80
100
120
0
0.25
0.5
1
2
3
4
6
ARA C addition (h)
UBEI-41 addition (h)
E.
24 hour virus yield
pfu/ml
1x10^4
1x10^5
1x10^6
1x10^7
1x10^8
1x10^9
1x10^10
UNTR
ARA C
UBEI-41
–
0
6
0
6
drug addition (hpi)

replication sites (Figure 3.4 B). In control cells without a second inhibitor (No Inh.), replication site formation was normal. However, in the presence of UBEI-41 or MG132, the formation of viral replication sites did not occur. Apparently, the initiation of DNA replication required both a ubiquitination step and proteasome-mediated degradation.

Reasoning that a cellular ubiquitin ligase was likely to be involved, we turned to the hits in the RNAi screen. The ubiquitin functional annotation cluster (Figure 3.1 B) contained two components of the BCR E3 ubiquitin-ligase complex; Cullin3 (Cul3) and RING-box protein 1 (Rbx1). Images from the screen indicated that depletion of these factors completely blocked infection (Figure 3.4 C). A requirement for Cul3 and Rbxl was validated with three independent siRNAs each. Depletion of either factor decreased the 24 hour viral yield by 2 logs. Silencing of Cullin-l (Cull), a component of the SCF E3 ubiquitin-ligase complex that was not a hit in the screen, had no impact (Figure 3.4 C and D, left). The knock-down efficiency of these siRNAs was confirmed by western blot (Figure 3.4 D; right). Subsequent experiments were performed using the siRNA with the strongest knock-down efficiency (Cul3-1, Rbx1-3, and Cul1-2). Depletion of Cul3 or Rbx1 was found to significantly decreased late, but not early gene expression (Figure 3.4 E) mirroring the effect of AraC and confirming a defect in DNA replication. In line with this, Cul3 and Rbx1 knock-down inhibited the formation of cytoplasmic DNA replication factories (Figure 3.4 F). We concluded that UBA1, a Cul3 ubiquitin ligase, and the proteasome were required to initiate the replication of uncoated VACV DNA.

Figure 3.4 ***(following page)*** (A) MG132 and UBEI-41 block VACV DNA replication site formation. Cells were infected with VACV MVs (MOI 1) in the presence of 10 μM AraC, 25 μM MG132, or 50 μM UBEI-41. Cells were fixed and stained for DNA at 4 hour p.i., Representative images (left); Mean ± STDV of triplicate experiments (right). (B) MG132 and UBEI-41 block VACV DNA replication after uncoating. Cells were infected with VACV MVs (MOI 1) in the presence of 10 μM AraC. At 6 hour p.i. cells were washed and released from AraC (No Inh.), or shifted into 25 μM MG132 or 50 μM UBEI-41. Cells were fixed at 12 hour p.i. and assessed for the presence of cytoplasmic DNA replication sites. (C) RNAi against Cul3 or Rbx1, but not Cul1, impairs VACV infection (Average RII and representative images from screen shown). (D) Silencing of Cul3 or Rbx1, but not Cul1, reduces virus production. Cells were reverse transfected with 20 nM of three independent siRNAs directed against either Cul3, Rbx1, or Cul1. After 72 hour cells were infected with VACV MVs (MOI 1). 24 hour later cells were harvest and lysates tittered for plaque forming units/mL (left). Immunoblot analysis of Cul3, Rbx1, and Cull after siRNA mediated silencing with 20 nM siRNA for 72 hour (right; representative blots shown). (E) Silencing of Cul3 and Rbx1, but not Cul1, reduces late but not early viral gene expression. Cells were subjected to siRNA mediated silencing as in (D) followed by infection with VACV (MOI 1) expressing EGFP specifically from an early, or a late promoter. Cells were harvested 6 hour p.i. and analysed for the number of cells expressing early and late EGFP, respectively. Cells infected in the presence of CHX or AraC were used as controls. (F) Cul3 and Rbxl are required for VACV DNA replication site formation. Cells in which Cul3, Rbx1, or Cull had been silenced (20 nM siRNA; 72 hour) were infected with VACV MVs (MOI 1). At 4 hour p.i. cells were fixed, stained with Draq5, and analysed for the presence of viral DNA replication sites. (A, B, D-F) Experiments were performed in triplicate and displayed as mean ± STDV. (G) Model of VACV core ubiquitination, core degradation/genome uncoating, and genome replication. During assembly of VACV MVs, viral core proteins are ubiquitinated in a K-48 linked fashion. Upon infection of naive cells, fusion of viral and cellular membranes releases the ubiquitinated viral core into the cytoplasm. A first round of cellular proteasome action directs the degradation of the ubiquitinated core and concomitant genome release. A Cul3-based ubiquitin ligase and second round of proteasome action serves to initiate replication of the released viral genomes. Ubiquitination events: New (red); Non-accessible (yellow); Accessible (green); proteasomes (grey bullets); cullin-based ubiquitin ligase complex (grey crescents).

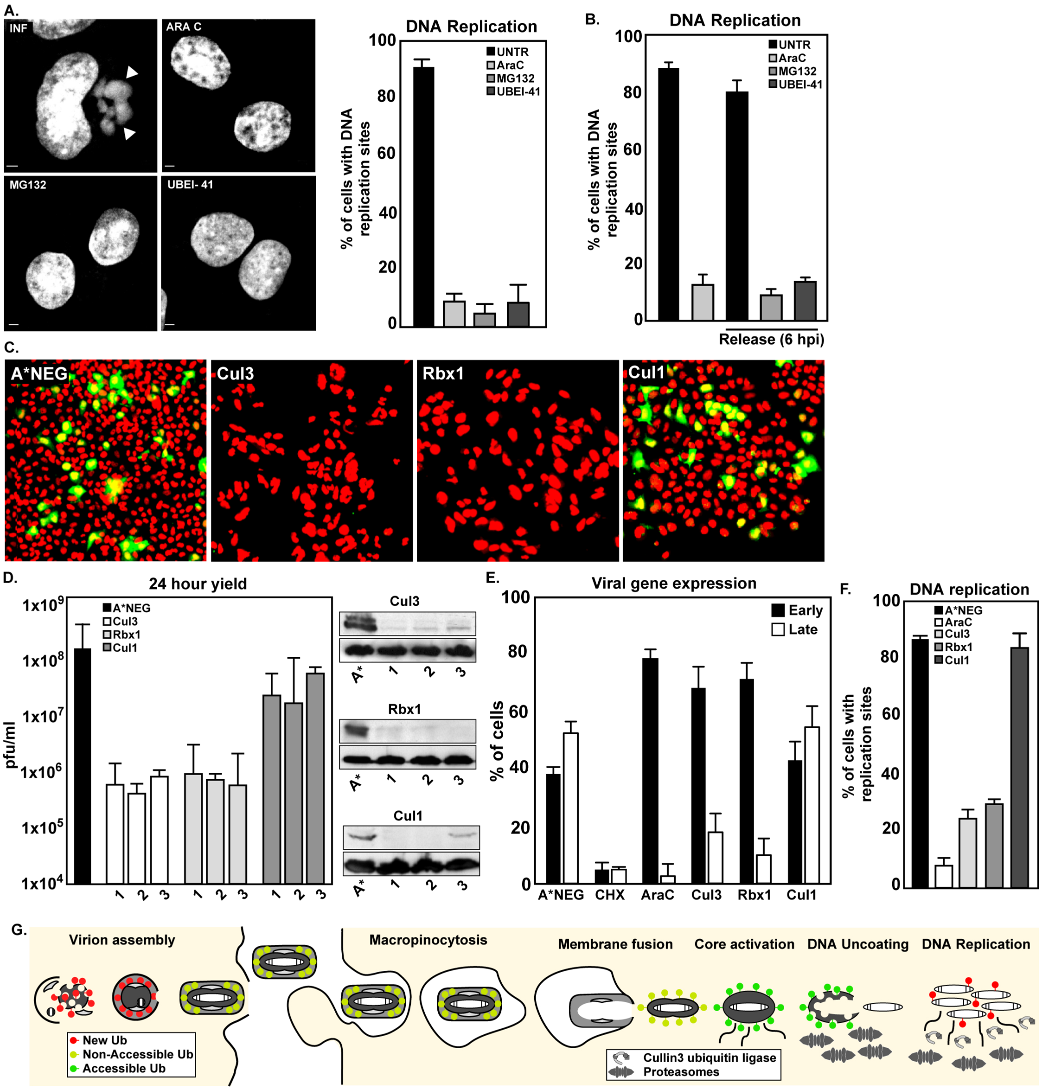
A.
INF
ARA C
MG132
UBEI- 41
DNA Replication
% of cells with DNA replication sites
100
80
60
40
20
0
UNTR
AraC
MG132
UBEI-41
B.
DNA Replication
% of cells with DNA replication sites
Release (6 hpi)
C.
A*NEG
Cul3
Rbx1
Cul1
D.
24 hour yield
pfu/ml
$1x10^9$
$1x10^8$
$1x10^7$
$1x10^6$
$1x10^5$
$1x10^4$
A*NEG
Cul3
Rbx1
Cul1
1 2 3 1 2 3 1 2 3
Cul3
Rbx1
Cul1
A* 1 2 3
E.
Viral gene expression
% of cells
Early
Late
A*NEG
CHX
AraC
Cul3
Rbx1
Cul1
F.
DNA replication
% of cells with replication sites
A*NEG
AraC
Cul3
Rbx1
Cul1
G.
Virion assembly
Macropinocytosis
Membrane fusion
Core activation
DNA Uncoating
DNA Replication
New Ub
Non-Accessible Ub
Accessible Ub
Cullin3 ubiquitin ligase
Proteasomes

3.4 Discussion

In summary, our results demonstrated that large-scale RNAi screening can, despite inherent problems and pitfalls (off-target effects, insufficient knockdown, cell population context effects, incomplete genome annotation, etc.) [37, 156] serve as a valuable tool in the study of pathogen/host interactions. The positive outcome relied in this case on a robust image-based assay, on supervised classification of cellular phenotypes, a separation of indirect and direct effects of siRNAs, and on improved bioinformatics analysis to identify gene clusters [225].

This allowed us to identify among the 188 hits several clusters in which multiple hits occurred in the same pathway or complex. Regarding the validity of the final hit list, we are encouraged by how many of the hits corresponded to factors identified earlier as essential genes in VACV infection. Follow-up studies with the clusters as a starting point revealed a unique role for ubiquitination, the proteasome, and Cul3 in virus assembly, uncoating, and DNA replication (Figure 3.4 G). These studies showed that the list is a valuable starting point for further functional studies.

Our results indicated that ubiquitination comes into play as an essential process already during the assembly of VACV particles in virus factories located in the cytoplasm of producer cells. Core proteins undergo extensive K48-linked polyubiquitination. This is consistent with the accumulation of ubiquitin observed in poxvirus replication sites and the detection of ubiquitin within purified VACV particles [43, 167]. The polyubiquitination is probably an essential step for virus assembly because inhibition of the E1 ligase prevented the purification of viral particles. VACV encodes one ubiquitin ligase, p28, which localizes to VACV replication sites [167].

However as this protein is not required for virus production in tissue culture, it is unlikely to be the ligase responsible for the ubiquitination of viral core proteins. Future work is needed to identify the core components that are ubiquitinated as well as the ubiquitin ligase(s) responsible. During egress from the viral factory, the viral membrane may protect the ubiquitinated core proteins from the degradation machinery. It is also evident that the ubiquitin tags remain inaccessible to proteasomes until cores are “activated” after entry into the cytosol of the next host cell.

After macropinocytic internalization of VACV into a new host cell, and low pH dependent membrane fusion, the poly-ubiquitinated core is released into the cytosol, where it immediately undergoes activation marked by major expansion in size, a step that does not require early gene expression [51, 108, 178]. The expanded cores serve as the site for early gene transcription [113, 138]. That they are not yet substrates for proteasome-mediated uncoating suggests that the ubiquitin chains are not accessible. For degradation of the core and uncoating of the DNA, the early genes have to be expressed. One or more of the early proteins are likely responsible for making the ubiquitinated core proteins accessible as substrates for the proteasome. The core particle is destroyed, and some of the core components such as the AS protein are degraded. As a result of the proteolysis, the viral DNA genome is released and core itself is no longer a recognizable structure in the cytosol. That UBA1 activity is not required, indicates that the ubiquitin present in the core is sufficient to mediate genome uncoating. Although proteasome function has been implicated in the regulation of viral trafficking, replication, egress, and immune evasion (reviewed in [13]), a direct role for proteasomes in the uncoating of other viruses or viral capsids has not to our knowledge been observed before. It was previously reported that viral DNA replication requires ubiquitination and proteasome activity [201, 233].

Our results extend these findings to show that replication of the viral DNA depends on Cul3 and Rbx1, two components of an important, multifunctional E3-ligase family [184]. VACV encodes at least four Cul3 substrate adapters, A55R, C2L, C5L, and F3L [15, 75, 185] and reviewed in [14]. Although each of these is required for VACV virulence, they are not essential for replication in tissue culture. This indicates that they are not the adapter proteins used by Cul3 to facilitate VACV DNA replication. While the substrates are not yet identified, one possibility involves the remaining DNA associated proteins. The proteasome thus plays a central role in at least two steps in the replication cycle of VACV. Collectively, RNAi screening and these findings are likely to provide a starting point for detailed cell and molecular biology analysis of poxvirus-host cell interactions, and they may facilitate the development of novel anti-poxvirus agents that target the host cell rather than viral factors.

3.5 Acknowledgements

We thank T. Steiger and O. Byrde for data storage and cluster computing, Pauli Ramo for statistical and image analysis, Karin Mench for technical assistance, Jacomine Krijnse-Locker for anti-I3L. J.M is supported by an SNF Ambizione (PZOOP3_ 131988), L.P by the University of Zurich, the SNSF, the CINA SystemsX.ch, RTD project InfectX, and the European Union, C.K.E.B by the SNF Sinergia CRSII3_ 125110 the SystemsX.ch RTD project C-CINA, and A.H by ETHZ, InfectX, and the ERe. The full set of images and analysis results are browsable and downloadable from www.infectome.org.

3.6 Supplementary Figures

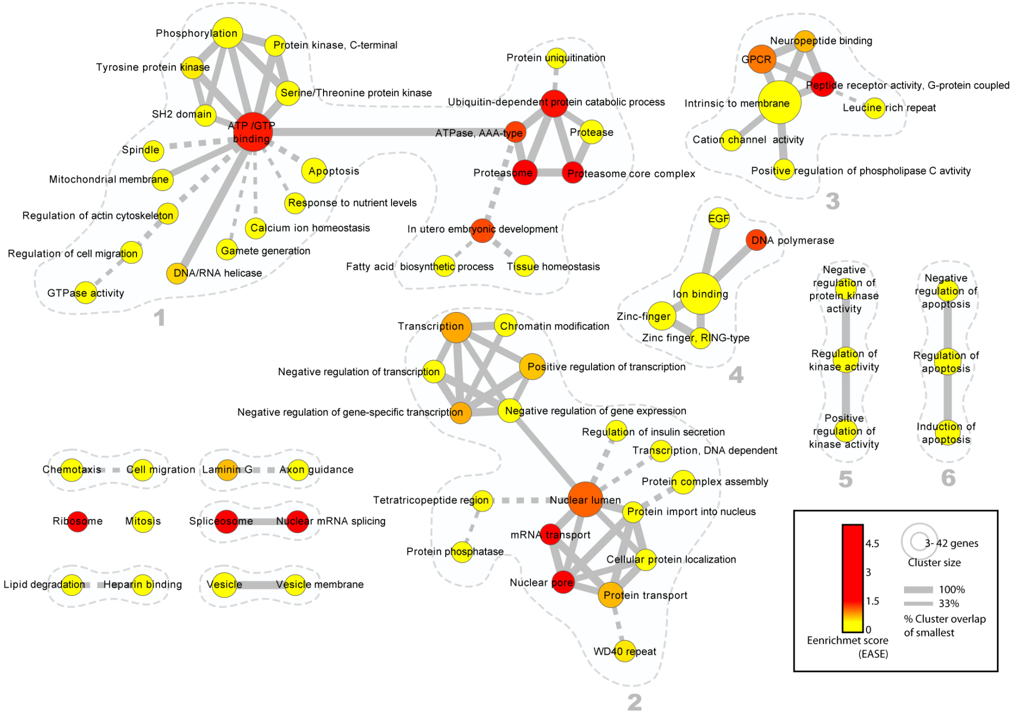

[h]

Figure 3.5 Supplementary Figure; Network view of 73 functional annotation clusters identified by DAVID (version 6.7) within the 188 host factors required for VACV infection. Network nodes represent individual functional annotation clusters. Node sizes reflect the number of factors in each cluster (see legend). Node color represents the enrichment relative to the total genes screened (see legend and supplementary information). Lines between the functional clusters indicate shared genes. The line thickness defines the percentage (33-10 %) of genes in the smaller cluster that are shared with the larger cluster. Solid lines represent all edges of at least 75 % similarity, while dashed lines represent the single strongest edge of 33 % or higher for otherwise unconnected clusters. Individual networks are outlined in dashed grey lines. The largest network (1) consists of 98 genes, occurring 233 times in 25 functional annotation clusters, and is centred around both ATP/GTP binding genes and proteasomal genes. The second largest network (2); consists of 93 genes, occurring 191 times in 18 functional annotation clusters and contains transcriptional regulators and nuclear lumen annotated genes involved in mRNA and protein transport. Smaller networks include: (3) Membrane intrinsic genes including cation channels and G-protein coupled receptors; (4) Ion binding genes with (Ring-type) zinc-finger domains, EGF binding domains, and DNA polymerases; (5) positive and negative regulators of kinase activity and; (6) apoptosis. Highly enriched clusters not in larger networks included the spliceosome, nuclear mRNA splicing, and the ribosome. Less enriched functional clusters included chemotaxis, cell-migration, mitosis, axon-guidance, laminin G, lipid degradation, heparin binding, and vesicle (membrane) annotated genes.

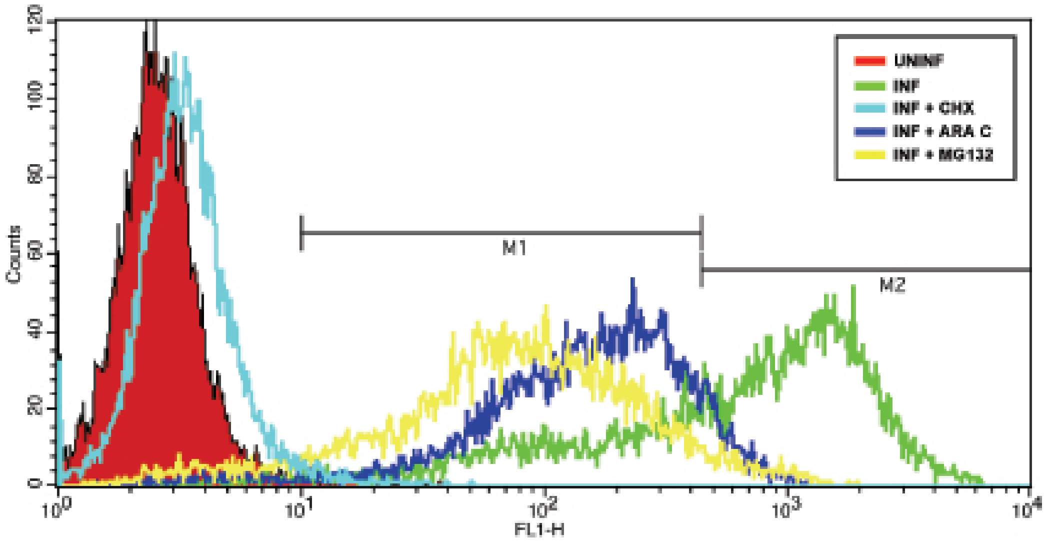

Figure 3.6 Supplementary Figure; Flow cytometry analysis assay for MV early and late gene expression. Confluent monolayers of HeLa cells were infected with WR E/L EGFP at an MOI of 1. Cells were harvested for flow cytometry at 6 hour p.i. A typical plot of cell number versus EGFP fluorescence (log scale) is shown. For each sample, 10,000 viable cells were counted in a flow fluorocytometer (FACSCalibur BD Biosciences) using emission filter 520-550 nm for green fluorescence. To gate for early versus late gene expressing cells, infections in the presences of CHX (light blue), which prevents early and late gene expression, or AraC (dark blue), which allows for early but prevents late gene expression were performed with each experiment. These cell populations were used to set gates for early (M1) and late (M2) gene expressing cell populations. As an example, the effect of MG132 (yellow), which prevents late but not early gene expression is shown.

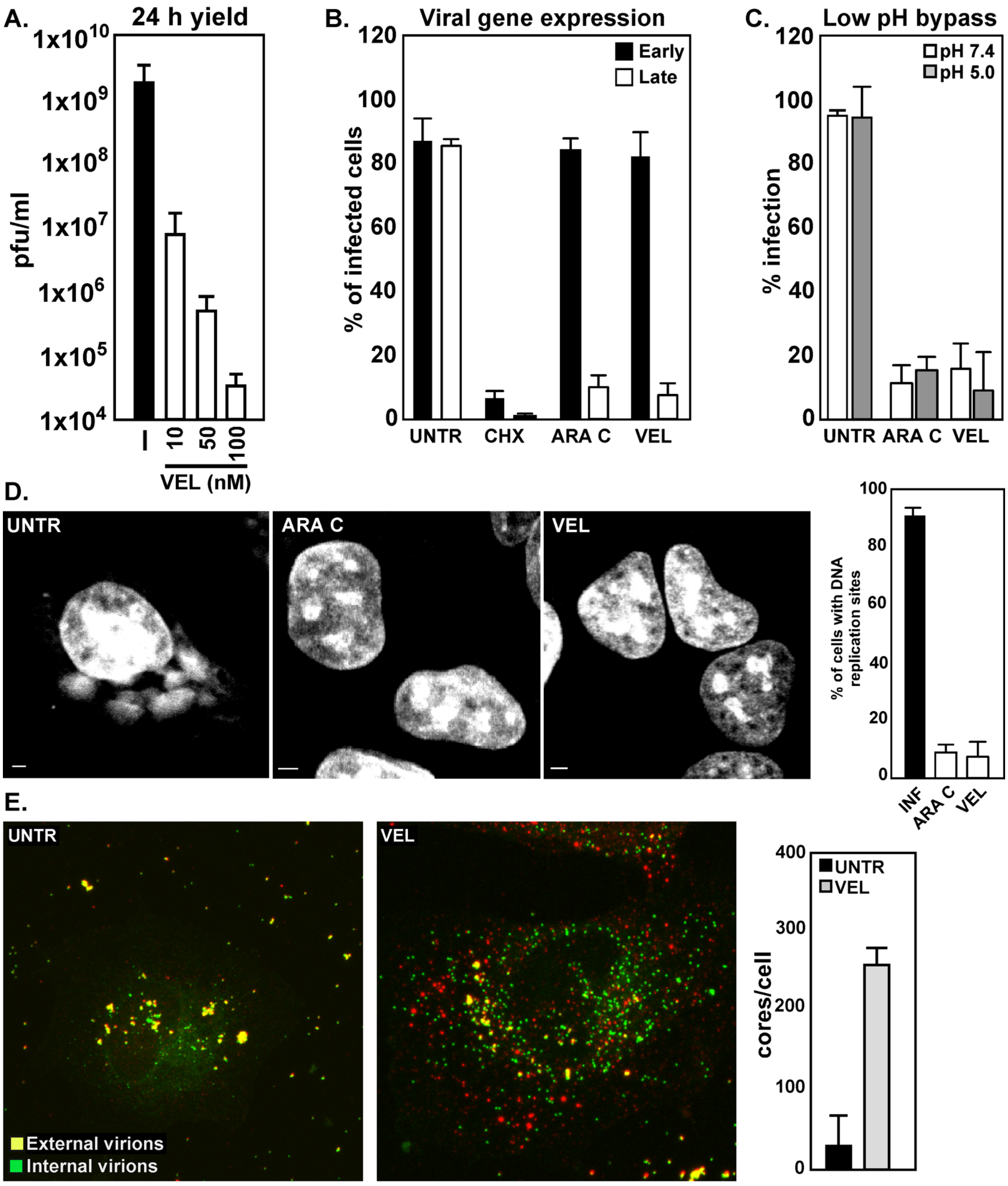

Figure 3.7 Supplementary Figure; Proteasome inhibition by Velcade blocks VACV production. Proteasome inhibitor (Velcade) blocks VACV production (MOI 1; 24 hour p.i.; 10-100 nM Velcade). (B) Velcade has no impact on early, but inhibits late VACV gene expression (MOI 1; 6 hour p.i.). Cells infected in the presence of CHX or AraC served as controls for gating early and late gene expressing cells (see Figure 3.6). (C) Velcade inhibits VACV infection after internalization. VACV-EGFP (MOI 1) was bound to cells for 1 hour in the presence of 100 nM Velcade. Cells were washed, treated with pH 7.4 or pH 5.0 media for 5 min, after which media containing 100 nM Velcade was added back. Cells were analysed by flow cytometry for EGFP at 6 hour p.i. (D) Velcade blocks VACV DNA replication site formation. Cells were infected with VACV MVs (MOI 1) in the presence of 10 μM AraC or 100 nM Velcade. Cells were fixed and stained for DNA at 4 hour p.i. Representative images (left); Mean ± STDV of triplicate experiments (right).

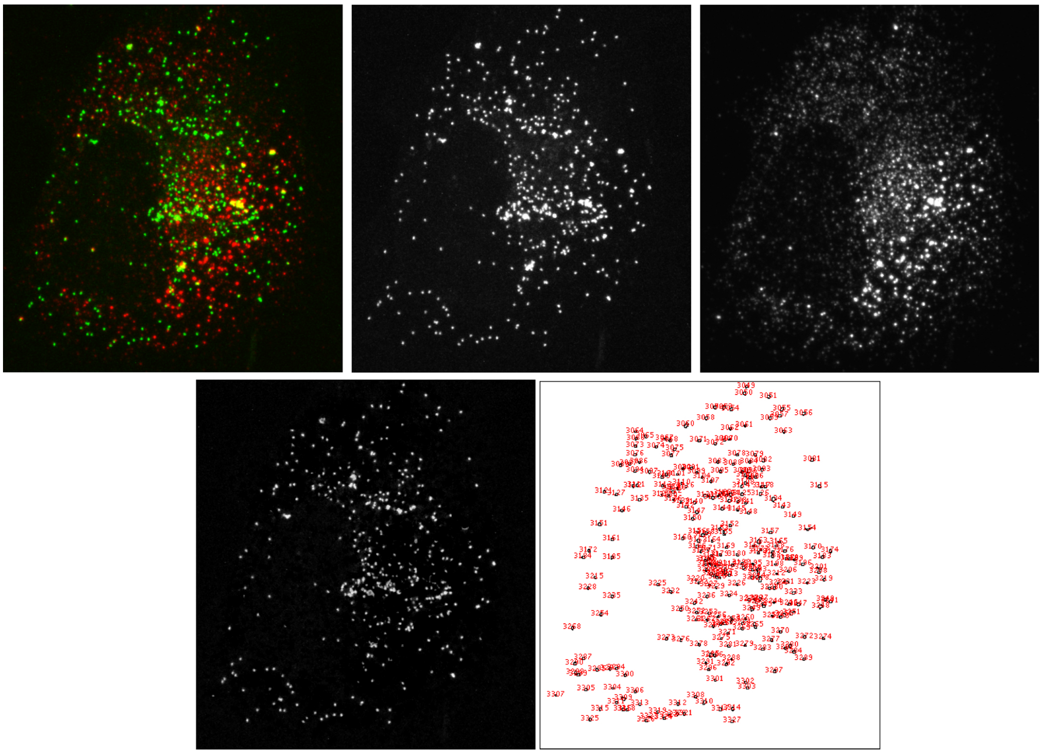

Figure 3.8 Supplementary Figure; Quantification of internalized cores. Ten confocal Z sections were collected for each cell and displayed as a maximum projection. In the merged image virus cores are (green), the virus membrane (red), and intact virions (yellow). To quantify the stabilized intracellular cores (total cores), the virus membrane signal (membrane), was subtracted from core images. Thus, both the red signal and overlapping red and green signals were removed from the core channel leaving only intracellular cores (cores with no membrane). These images were inverted and subjected to auto thresholding. Cores were then quantified with the image J particle analysis plug-in with settings (size pixel 0.05-5; circularity 0.0-1.0) which assured that only individual cores were counted with 94 % accuracy. 20 cells per condition from 3 independent experiments were analysed.

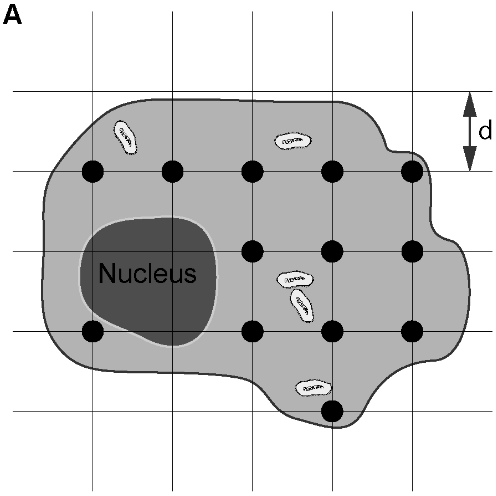

Sample calculation

Number of cores: $Q = 5$
Number of cytosolic points: $P = 13$
Distance between test lines: $d = 2\ \mu m$

$$\text{Number of cores/area} = Q/(P \times d^2) = 5/(13 \times 2^2\ \mu m^2) = 0.096\ \text{cores}\ \mu m^{-2}$$

-> 0.1 µm thick sections
=> 0.96 cores μm^{-3} (~1 core μm^{-3})

B

	UNTR	CHX	MG132	UBEI41
Average of observed cores	2.6	6.8	5.8	0.3
Average of cytosolic points	64.7	65.4	71.9	53.4
Average number of cores/volume [μm^{-3}]	0.13	0.32	0.36	0.02

Figure 3.9 Supplementary Figure; Quantification of internalized cores visualized by EM. (A) The number of stabilized cores in control cells and cells infected in the presence of cycloheximide (CHX), MG132, or UBEI-41 in micrographs of 0.1 μm thin epoxy sections were quantified by point counting. For each sample condition, 25 micrographs were acquired at a magnification of 5800x on a 2k x 2k camera (pixel size = 8.36 nm). A square lattice grid (2 cm grid spacing) was placed on printed micrographs to cover each micrograph completely. The number of cores per grid point in the cytosol were counted and analysed as published by [83]. (B) Cores are stabilized in the absence of proteasome but not UBA1 function. The average number of cores observed per cell and per unit volume in untreated, CHX, MG132 and UBEI-41 EM samples.

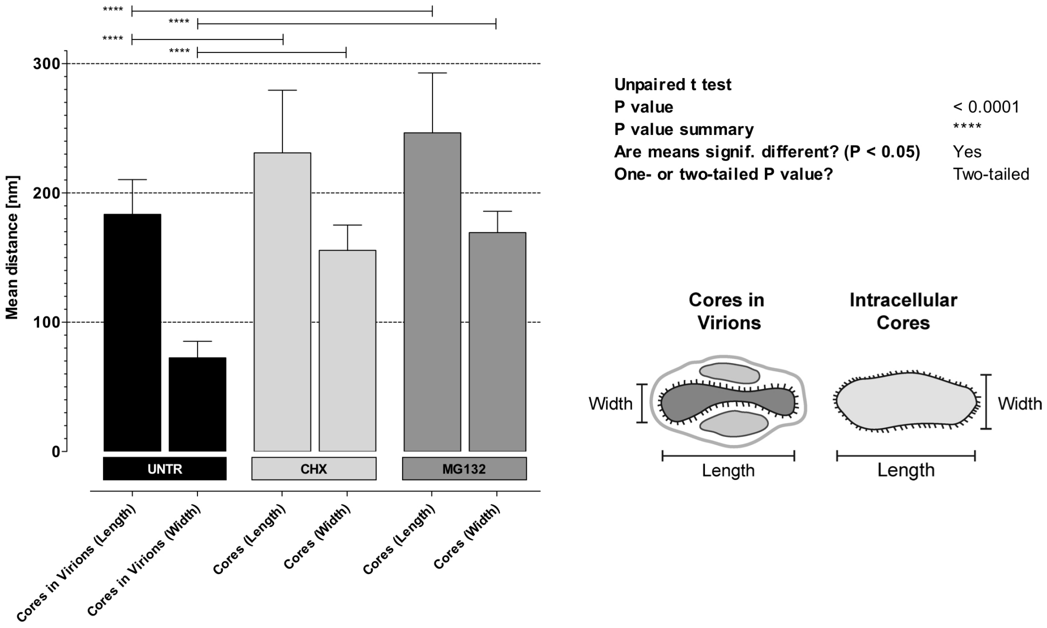

Unpaired t test	
P value	< 0.0001
P value summary	****
Are means signif. different? (P < 0.05)	Yes
One- or two-tailed P value?	Two-tailed

Figure 3.10 Supplementary Figure; Determination of core expansion. Intact external virions, cores within external virions, and internalized cytoplasmic cores were measured for both width and length. Representative EM micrographs of mock, cycloheximide (CHX), and MG132 treated infected cells were used for measurements. Under both conditions core expansion (activation) was determined to be unaffected. A minimum of 40 cytoplasmic cores and 80 intact virions from each condition were measured.

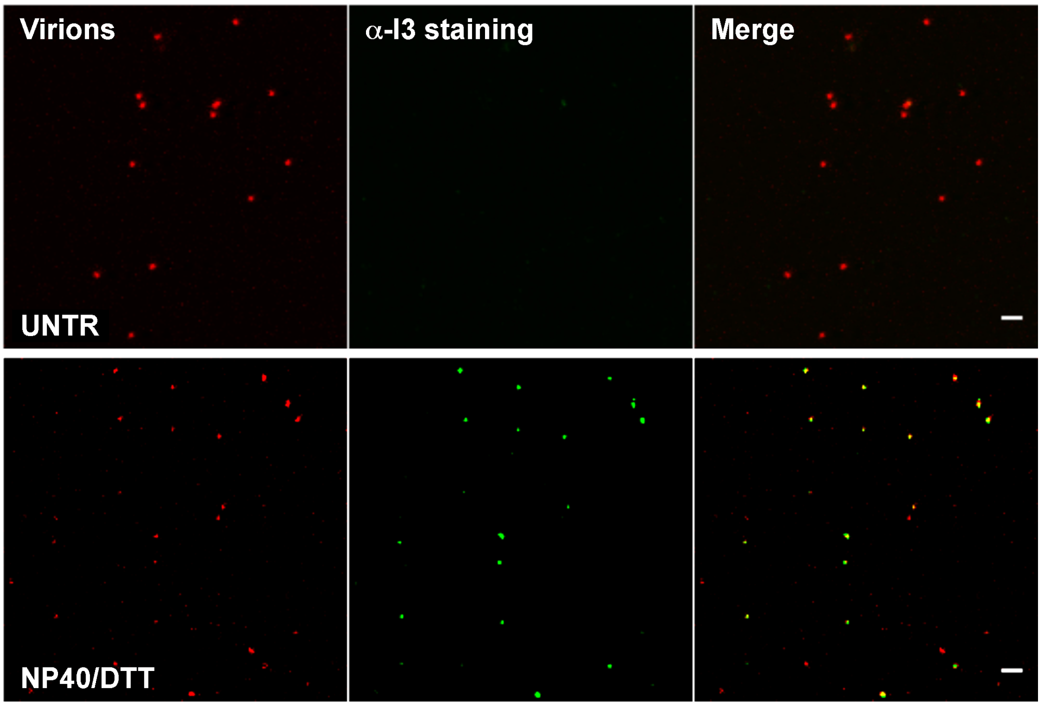

Figure 3.11 Supplementary Figure; The I3 protein is not accessible in intact VACV MVs. VACV MVs which package the A5 core protein as a mCherry fusion were left untreated (UNTR) or were treated with 1 % NP40/50 mM DTT to remove the viral membrane. These virions were bound to a cover-slip and stained with anti-I3L antibody, followed by secondary staining with a 488-coupled secondary antibody. The I3 protein could only be detected in samples that had been treated with NP40/DTT.

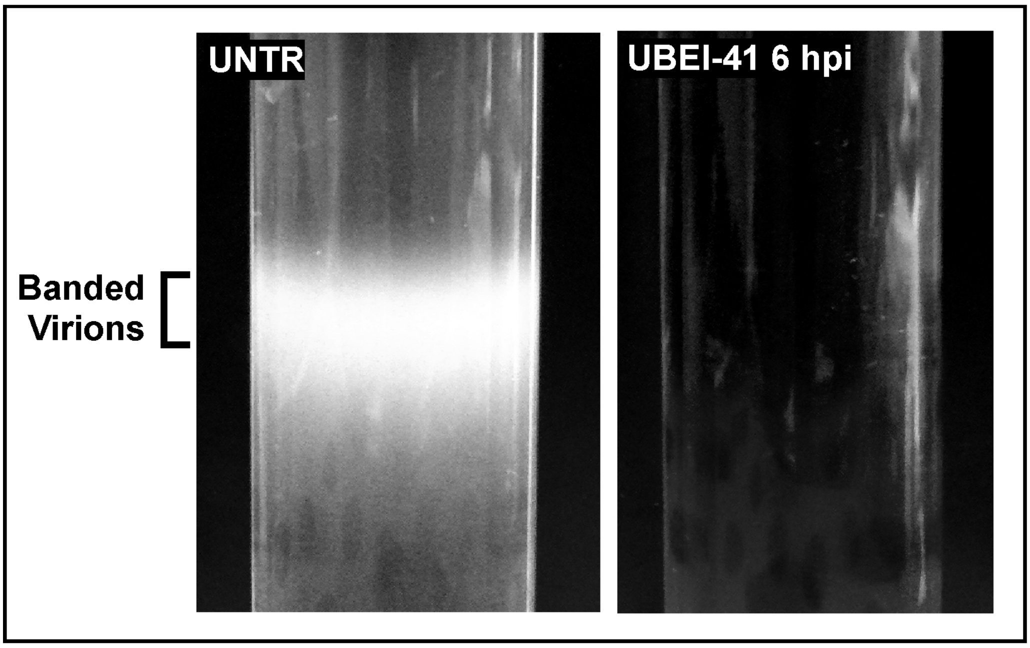

Figure 3.12 Supplementary Figure; VACV virions cannot be isolated in the presence of UBEI-41. HeLa cells were infected at an MOI of 1 with VACV-EGFP-A5. At 6 hour p.i. UBEI-41 (50 μM) was to one set of cells, a time when late gene expression was determined to be unaffected (Figure 3.3 D). Infections were allowed to proceed for a total of 24 hour before cells were harvested and progeny virions were collected and band purified over a 25-50 % sucrose gradient. Virions could not be obtained from samples treated with UBEI-41. Virions from untreated (UNTR) cells were purified in parallel for comparison (white band). One mL was collected from the same region of both gradients and tittered to determine the number of infectious particles produced. For the untreated sample $\sim 1 \cdot 10^9$ infectious particles were recovered. When the same region of the UBEI-41 treated gradient was measured by plaque titration $\sim 1 \cdot 10^6$ infectious particles were recovered.

Chapter 4

Vaccinia virus lateral bodies deliver immediate effector proteins into host cells

The results of this section will be submitted to a peer review journal, soon.

Christopher Karl Ernst Bleck[1†], Florian Ingo Schmidt[2†], Lucia Reh[2], Ari Helenius[2], Henning Stahlberg[1], and Jason Mercer[2*]

[1] University Basel, Center for Cellular Imaging and NanoAnalytics (C-CINA), Structural Biology and Biophysics, Biozentrum, Mattenstrasse 26, 4058 Basel, Switzerland

[2] ETH Zurich, Institute of Biochemistry, Schafmattstr. 18, 8093 Zurich, Switzerland

[†] Contributed equally

[*] Corresponding author: jason.mercer@bc.biol.ethz.ch

4.1 Abstract

Vaccinia virus, the model poxvirus, is a DNA virus with a complex structure. Infectious particles consist of the viral genome in a proteinaceous core, two lateral bodies of so far unknown function, and one or two viral membranes. During entry, both infectious forms of the virus release the viral core and the lateral bodies into the host cell cytosol by a fusion event. Using electron and fluorescence microscopy in combination with biochemical approaches, we defined the morphological and chemical changes that the core undergoes

after entry (activation). We identified F18 as a major structural protein of the lateral bodies, which are left back at the membrane after fusion. We found that the decomposition of lateral bodies by the host cell proteasome releases at least one immediate effector protein into the host cell, the dual specific viral phosphatase VH1. Only when the phosphatase is released from lateral bodies, VH1 catalyses the dephosphorylation of activated Stat1 and thus prevents the antiviral response of the type II interferon IFNγ. We thus identified a new viral delivery mechanism for immediate effector proteins that is very likely used to release additional, so far unknown, effector proteins.

4.2 Introduction

The ultimate goal of a virus particle is to transport the viral genome from one infected cell to the next. Within a viral particle, the viral DNA or RNA genome is typically organized in a proteinaceous core or capsid, which is surrounded by a lipid bilayer in enveloped viruses. While efficient packaging of the genome is obligatory for virus production, successful infection of a new host cell requires the disassembly of capsids or cores to release the viral genome. These antagonistic processes occur in the same host cells at different time points. Subtle changes in the viral particles or the host cell ensure that incoming viral cores or capsids are unstable and disassembly is energetically favourable. Instability may be generated by maturation steps of the viral particle, or by modification of the cellular environment of the host cells. The latter modifications may take place either in host cells producing progeny viruses or in newly infected cells [79].

Vaccinia virus (VACV) is the prototypic poxvirus and a close relative of variola virus, the causative agent of smallpox [53]. Both infectious forms of VACV, mature virions (MVs) and extracellular virions (EVs), contain the DNA genome packaged in a proteinaceous viral core. The viral core with two proteinaceous lateral bodies is enveloped by one or two viral membranes in MVs and EVs, respectively.

During morphogenesis, immature virions (IV, see Figure 1.3 and 1.4) surrounded by a single viral membrane are formed in the cytoplasmic viral factory. After membrane closure, the amorphous protein and DNA content of an IV undergoes dramatic rearrangements that involve the proteolytic cleavage of core proteins by the viral protease I7 and possibly G1 [24, 7, 8], as well as the formation of disulfide-bonds catalysed by the viral redox (see Figure 1.5) system involving E10, A2.5, and G4 [262, 217, 216]. Morphogenesis results in the formation of MVs and MV-like particles with a typical dumbbell-shaped core and two lateral bodies. The single membrane contains the viral entry/fusion complex (EFC), which catalyses or regulates fusion of the viral membrane with cellular membranes during entry [213]. A fraction of the matured viral particles, the MV-like particles, undergo further wrapping events that lead to the formation of EVs, which are surrounded by an additional membrane (see Figure 1.2 on page 4) [194].

Both MVs and EVs are internalised into host cells by virus-induced macropinocytosis [148, 210]. Acidification of macropinosomes triggers the necessary events to promote penetration of cellular membranes. In the case of MVs, low pH activates the EFC and directly induces fusion of the MV membrane with the limiting macropinosomal membrane [239]. After macropinocytosis of EVs, acidic pH triggers the disruption of the EV membrane, exposing the MV-like particle still surrounded by one membrane [210]. The EFC subsequently mediates fusion of the latter membrane with macropinosomal membranes. In both cases, the ultimate goal is the release of the viral core into the host cell cytosol [211].

Released cores undergo at least two distinct disassembly steps, activation and uncoating, that ultimately release the viral DNA genome from the core structure. During activation, viral cores undergo morphological changes and start the transcription of early viral genes. VACV cores within an MV or an EV are dumbbell shaped and are closely associated with the lateral bodies, which usually fill the indentations of the core. Viral cores released into the host cell cytoplasm exhibit an oval morphology and are no longer associated with lateral bodies [51]. The viral RNA polymerase and early transcription factors are pre-assembled on early promoters in the packaged genome and start to transcribe early genes immediately after core release [275]. While a relationship between morphological changes and the onset of transcription is imaginable, this has not been formally shown to date. The composition and function of lateral bodies after fusion remains elusive.

Released viral cores accumulate in the perinuclear region of the host cell and this localisation has been attributed to microtubule-dependent transport of VACV-induced cell contractions [30, 212]. Early viral mRNAs have been reported to move along microtubules as well, and accumulate in distinct sites of early gene translation [142].

In a second disassembly step, the genuine uncoating, viral DNA genomes are finally released in the cytosol [113]. This requires the expression of early viral proteins as well as the activity of host factors, e.g. the proteasome [112, 153] (see Chapter 3 on page 61).

Little is known about the exact timing or core activation, whether cellular and viral factors are required for this process, or whether the molecular changes are intrinsically laid down in the matured viral core. Indeed, not even the molecular components of the lateral bodies nor the exact architecture of the core wall have been clarified to date. Three of the major core proteins have been shown to exhibit intermolecular disulfide bonds, which are reduced in the course of infection [104, 135]. While the exact time point of reduction is unclear, reduction of core components has been linked to morphological changes of the latter [135]. Early gene transcription is known to require the import of NTPs, and – at least in the context of the viral core – depends on the presence or function of L3, VP8, H1, E6, E8, and F18, all of which do not contain any known enzymatic functions that contribute to transcription directly [269, 265, 134, 20, 118, 264].

In this study, we used fluorescence microscopy and electron microscopy in combination with biochemical approaches to study viral core activation and the function of lateral bodies after fusion. We found that expansion of viral cores occurs during or immediately after fusion and may not require any cellular factors. We identified a number of disulfide-bonded core proteins and found that some of them are reduced during activation. We identified F18 as a major lateral body component and found that lateral bodies are decomposed by the activity of the host cell proteasome. Only when this took place, effector proteins packaged into lateral bodies, like the dual-specific phosphatase VH1, were released and became catalytically active. We thus identified a pathway, with which poxviruses, similar to herpes viruses, deliver immediate effector proteins into the host cell cytosol prior to any viral gene expression.

4.3 Results

4.3.1 Cores rapidly undergo morphological changes during or after fusion

Morphological differences between VACV cores in MVs or EVs and cores released into the host cell cytosol have been observed repeatedly [51, 127]. However, viral cores are only transiently present in the host cell cytosol and disappear upon further uncoating. To accumulate viral cores, HeLa cells were infected with WR wt MVs for 3 h in the presence of actinomycin D (ActD), which prevents early viral gene transcription and thus uncoating. Both MVs in endocytic vesicles and free viral cores in the cytoplasm could be identified in epoxy-embedded and post-stained sections (see Figure 4.1 A). Cores in MVs exhibited a dumbbell shape, the indentations of which were filled with electron dense material that in some cases formed clearly visible lateral bodies (see Figure 4.1 C and Supplementary Figure 4.2 A). Cytosolic cores, in contrast, were oval, had an increased width, and lacked any visible lateral bodies or associated electron dense material (see Figure 4.1 A and Supplementary Figure 4.2).

To increase the number of cytosolic cores and synchronise core activation, we next bound MVs to HeLa cells in the cold and subsequently induced fusion by a short (5 min) pH 5 treatment. 30 min post fusion, we indeed observed large amounts of cytosolic cores close to the plasma membrane (see Figure 4.1 B). More importantly, activated cores exhibited the same morphological changes as activated cores in a normal infection, indicating that the release of viral cores at the plasma membrane permits proper activation (see Figure 4.1 B/C and Supplementary Figure 4.2).

Synchronization of MV fusion allowed us to address the timing of activation in more detail. When HeLa cells were fixed immediately after acid-induced fusion, we were able to visualise viral cores, which had just been released into the cytosol (see Figure 4.1 C). Remnants of the viral membrane and the lateral bodies were clearly visible as well. Released viral cores were already oval and wider, indicating that core activation had taken place during or immediately after fusion. Moreover, lateral bodies remained associated with the viral membranes that had merged with the plasma membrane and had not yet flattened into the plane of the plasma membrane.

Using classical thin section electron microscopy, characteristic changes of the core morphology could be observed right after acid-induced fusion at the plasma membrane (see Figure 4.1 C). Since the observed changes were comparable after fusion of MVs with macropinosomal membranes and after artificially induced MV fusion, it is likely that core expansion also happens during or right after fusion with the limiting membranes of a macropinosome.

To test whether the detectable changes could be an artifact of the sample preparation, which involved sample dehydration prior to embedding, we also analysed core morphology using a sample preparation protocol developed by Tokuyasu [235, 220]. This technique involves much milder sample fixation / preparation and cryo-sectioning from gelatin-embedded sample pellets. 30 min post fusion, both MVs and cytosolic cores could be detected by electron microscopy (see Figure 4.1 D-F and Supplementary Figure 4.2 C-E). Importantly, similar morphological features of released cores compared to cores within MV particles were detected.

A common method to prepare VACV cores *in vitro* is to treat purified MVs with mild detergents and reducing agents [65, 108]. We treated MVs with NP-40 and DTT and subjected the resulting *in vitro* cores to Tokuyasu preparation (see Figure 4.1 F), and compared them to unmodified MVs (see 4.1 E/F [top panels]). In agreement with the literature, *in vitro* cores lacked the viral membrane, but still contained lateral bodies [65]. The visibility of lateral bodies in MVs and *in vitro* cores, however, depended on the orien-

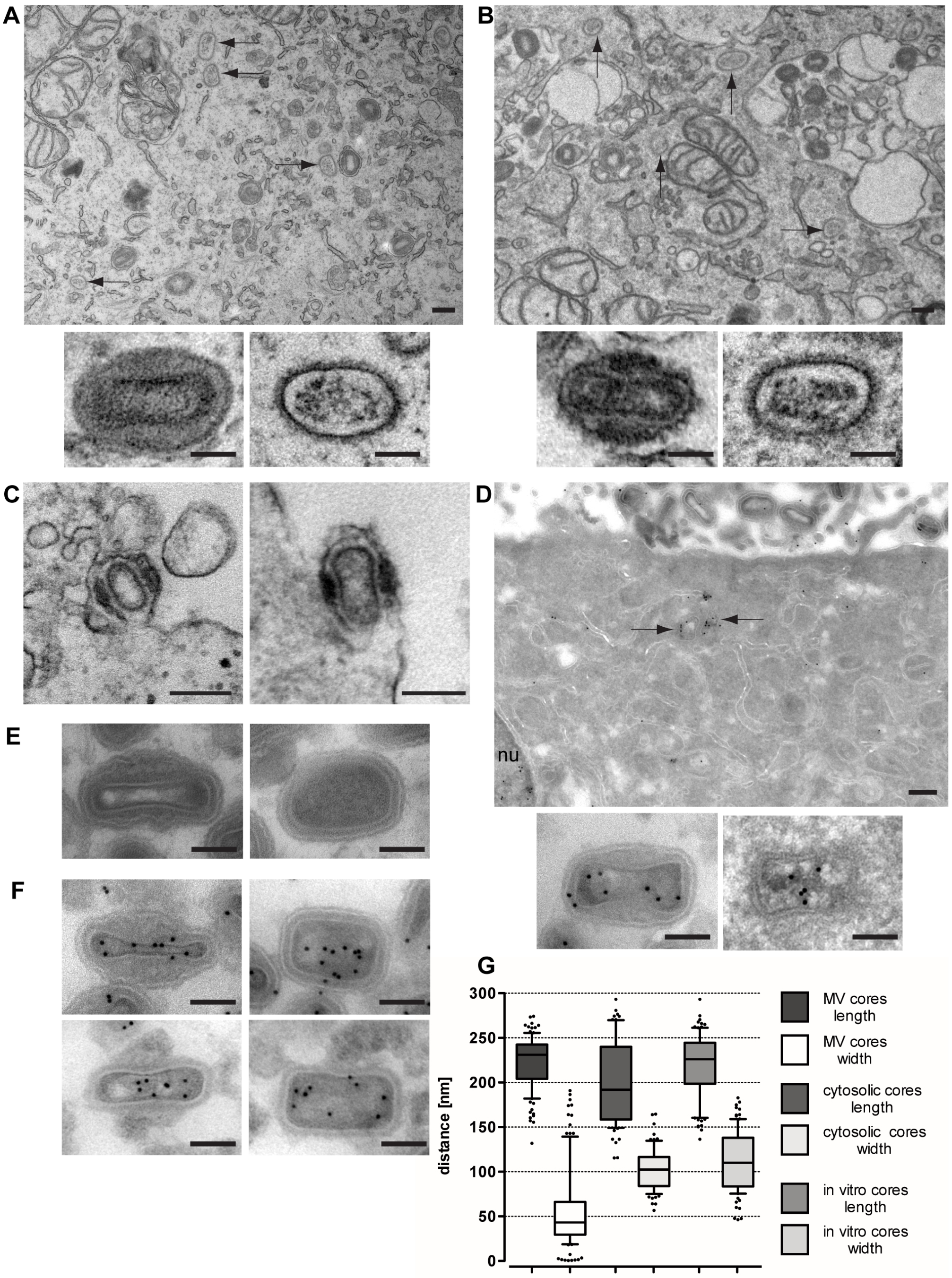

Figure 4.1 Morphological changes during VACV core activation. (A-D) WR wt MVs were bound to HeLa cells on ice (MOI 100) and cells were either incubated at 37 °C in the presence of 5 μg/mL ActD for 3 h (A), or treated with pH 5 medium for 5 min at 37 °C, followed by 30 min at 37 °C (B), or no further incubation (C/D). Samples were prepared following the protocols for epoxy-embedding (A-C) or sample preparation after Tokuyasu combined with anti-DNA immunogold-labelling (D/F). Typical images of thin sections are shown; scale bar = 100 nm; Nu: nucleus. Cytosolic cores are highlighted with black arrows. (F) Representative thin sections of MVs prepared by the Tokuyasu method (E) and immunogold-labelled with anti-DNA antibodies (F); scale bar = 100 nm. (G) Quantification of core length and width in MVs, cytosolic cores and *in vitro* cores as described in material and methods (N = 100). Boxes denote interquartile range, lines within boxes denote median, whiskers denote 10th and 90th percentiles, and round symbols denote outliers.

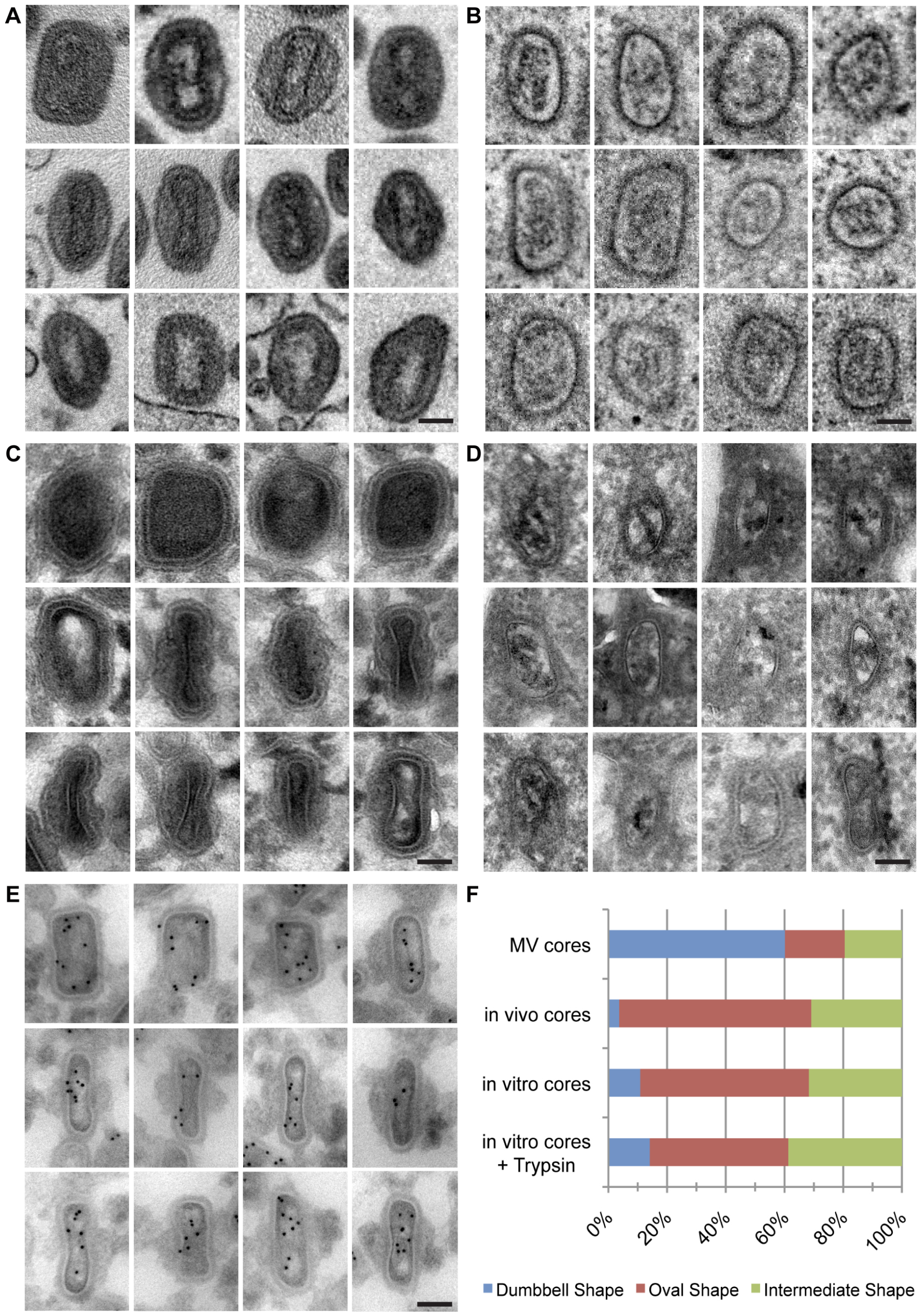

Figure 4.2 Supplementary Figure; Morphological changes during VACV core activation. (A-E) Representative thin projections of either epoxy-resin embedded MVs (A) and *in vitro* cores (B) or MVs (C) and *in vitro* cores (D) prepared by the Tokuyasu method and immunogold-labelled with anti-DNA antibodies (E); scale bar = 100 nm. (F) Bar diagram are shown percentage class values ("Dumbbell", "Oval" and "Intermediate" Shape) of MVs, *in vivo* and un- and treated *in vitro* cores.

tation of the sections and lateral bodies were even more pronounced after membrane removal (see Figure 4.1 F [bottom panels]). *In vitro* cores moreover, exhibited a more oval morphology that resembled cores found in the cytosol. To compare the morphological changes that cores underwent, we analysed cores in MVs, cores found in the cytosol during infection, and *in vitro*-generated cores. We measured the core widths in the centre of the core and also classified cores based on their shape as dumbbell, oval, or intermediate (see 4.1 G and Supplementary Figure 4.2 F). Cores within MVs had a mean width of 48 nm and 60 % of all cores were classified as dumbbell shaped. In contrast, cores found in the cytoplasm exhibited a mean width of 103 nm and 66 % of all cores were classified as oval. With a mean width of 113 nm and 57 % cores classified as oval *in vitro* cores more resemble free cores in the cytosol. This suggests that membrane removal, and perhaps reduction of viral proteins, may be sufficient to permit the observed morphology during activation.

We were thus able to verify changes in core morphology using a technique that preserved the hydration state of the samples. Moreover, we could describe the observed differences using objective measurements and classifications. Using these, we showed that cores generated *in vitro* exhibit features of activated cores.

4.3.2 F18 is absent in cytosolic cores

In order to understand core activation in more detail, we wondered which proteins are lost from viral cores during activation. The phosphoprotein F18 is one of the most abundant MV proteins and remains associated with *in vitro* cores [200, 116]. However, a previous study found that F18 is absent in cores released into the cytosol [178]. In order to monitor changes in protein composition during activation, we tried to generate a recombinant virus that encodes a fluorescent fusion protein of F18. While we were not able to modify the endogenous locus of F18R, we successfully generated a recombinant virus that encodes the fusion protein EGFP-F18 as an additional copy in the thymidin kinase locus under the control of the F18 promoter. EGFP-F18 was incorporated into MVs (see Figure 4.3 B and Supplementary Figure 4.4 A) and is present in cores generated *in vitro* (see Supplementary Figure 4.4 A), similar to an EGFP fusion of the *bona fide* core protein A5 (see Supplementary Figure 4.3 B).

To monitor the fate of EGFP-F18 during core activation, we infected HeLa cells with WR EGFP-F18 and WR EGFP-A5 MVs for 3 hours in the presence of ActD and stained MV membranes with antibodies against L1 (see Figure 4.3 A/B). In both samples, some MVs positive for L1 and EGFP-F18

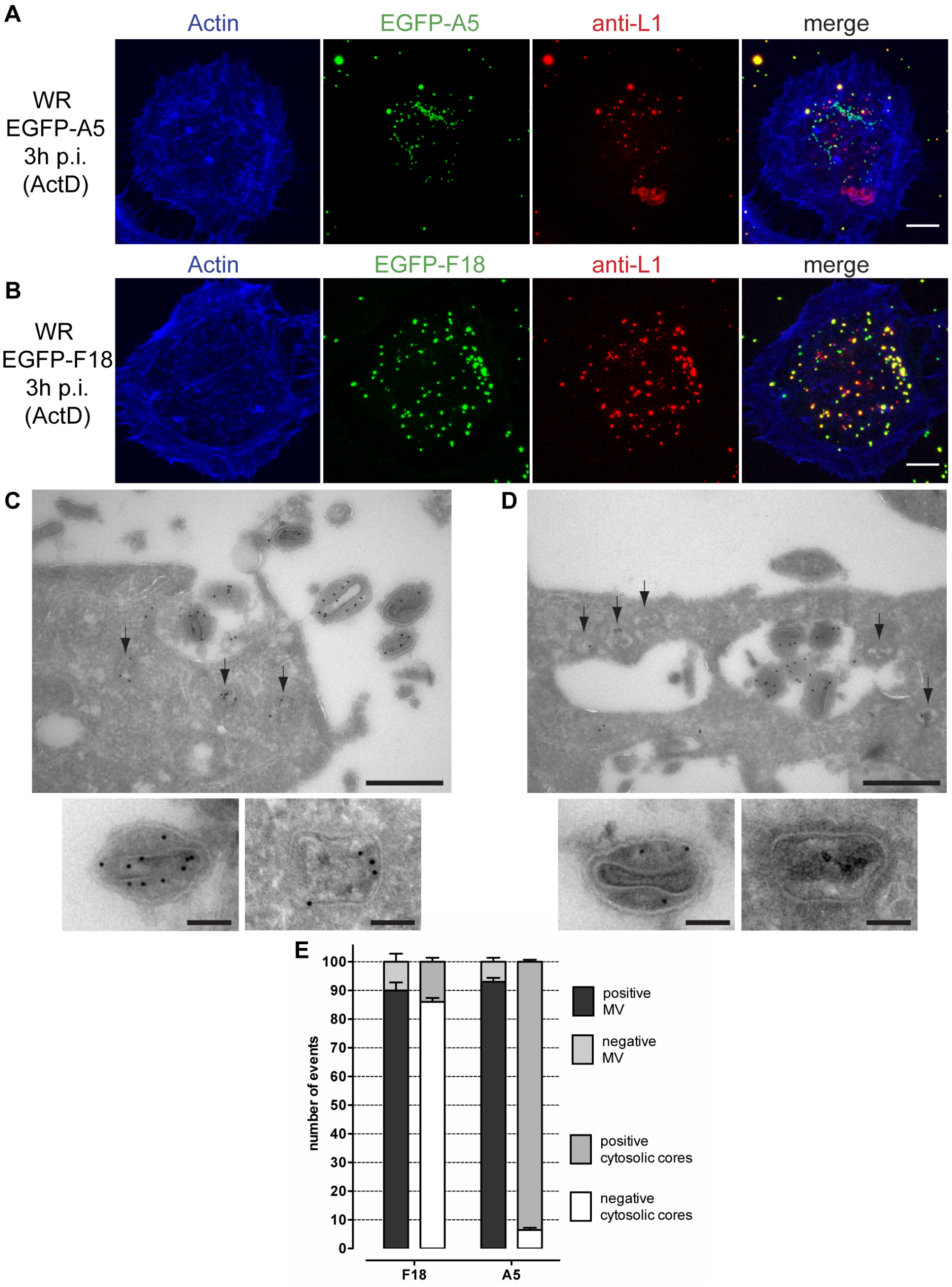

Figure 4.3 F18 is absent in cytosolic cores. WR EGFP-A5 (A) or WR EGFP-F18 (B) MVs were bound to HeLa cells for 1 h (MOI 10) and cells incubated at 37 °C for 3 h in the presence of 5 μg/mL ActD. Samples were stained for the MV membrane protein L1, representative maximum projections of Z-stacks are presented. Scale bar = 10 μm (A/B). (C/D) WR EGFP-F18 or EGFP-A5 MVs were bound to HeLa cells on ice (MOI 100) and cells treated with pH 5 medium for 5 min at 37 °C, followed by 30 min at 37 °C. Samples were prepared following the protocols for immunogold EM (Tokuyasu) combined with anti-GFP immunogold-labelling. (E) MVs and cores were counted and scored for immunogold-labelling of GFP fusion proteins. N = 100 for each criterion. scale bar = 10 μm (A/B), 500 nm (C/D), 100 nm (attached micrographs C/D), black arrows = *in vitro* cores (C/D).

or EGFP-A5 were detected bound to or internalised into infected cells. Viral cores accumulated in the presence of ActD were visible as green *punctae* negative for L1 in cells infected with WR EGFP-A5. However, hardly any green *punctae* negative for L1 were visible in cells infected with WR EGFP-F18. This suggests that EGFP-F18 may be absent from accumulated cytosolic cores.

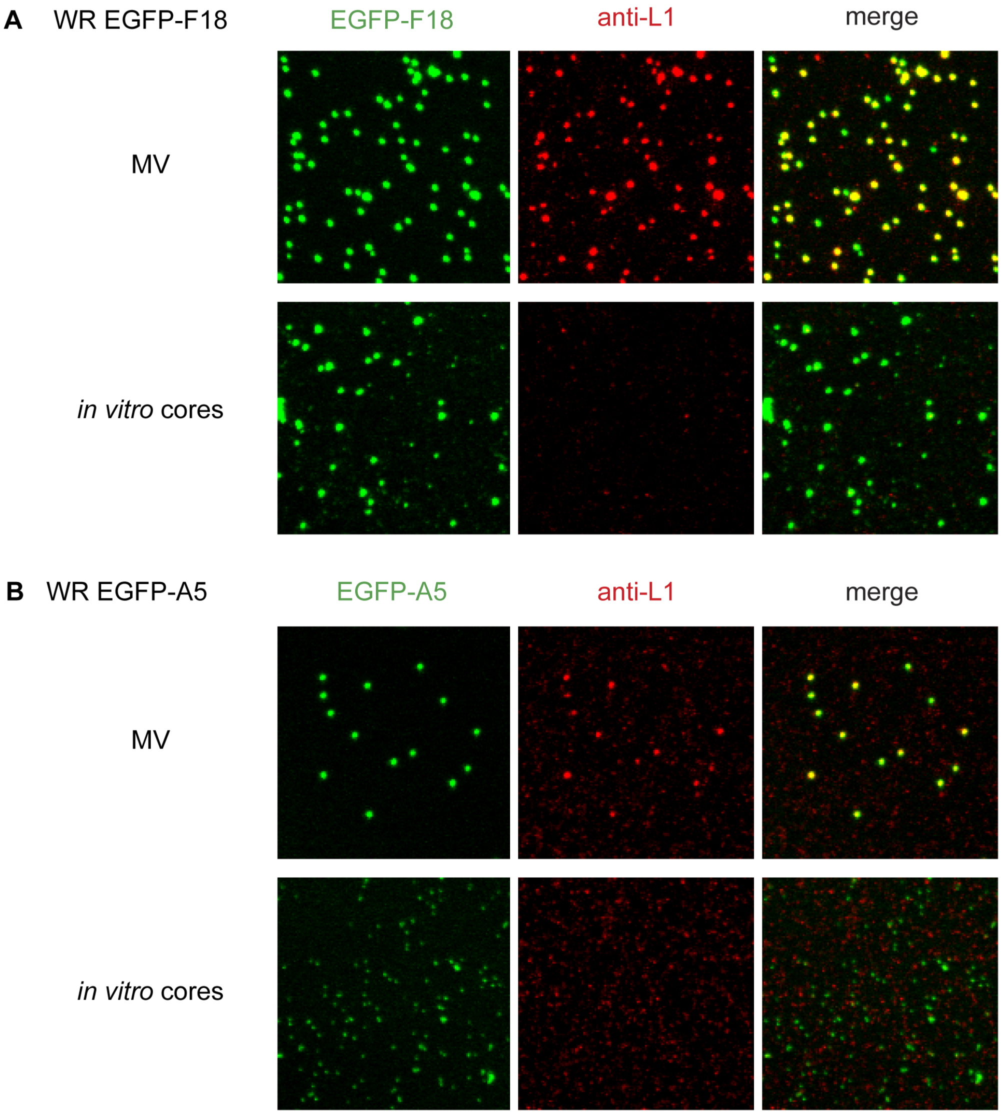

Figure 4.4 Supplementary Figure; Characterisation of WR EGFP-F18. WR EGFP-F18 (A) or WR EGFP-A5 (B) MVs or *in vitro* cores were bound to cover slips, fixed, and stained for the MV membrane protein L1. Representative image recorded by confocal microscopy are shown. Scale bar = 5 μm (A/B).

Since fluorescence microscopy does not allow the visualisation of unlabelled cores, we used electron microscopy to analyse cytosolic cores of WR EGFP-A5 and WR EGFP-F18 after acid-induced fusion (see Figure 4.3 C/D). The presence of EGFP in bound MVs and cytosolic cores was probed by immunogold-labelling with GFP antibodies. MVs of both recombinant virus strains were labelled with anti-GFP antibodies, confirming that both EGFP fusions were incorporated into particles. While the majority of all cytosolic cores of WR EGFP-A5 were positive for GFP (94 %), only 14 % of WR EGFP-F18 activated cores were labelled with GFP antibodies (see Figure 4.3 E). This indicates that EGFP-F18 was indeed absent from cytosolic cores. Similarly, WR wt MVs, but not cytosolic cores, could be efficiently labelled with anti-F18 antibodies (data not shown). This, and the fact that EGFP-F18 was highly enriched in MVs, confirmed that EGFP-F18 behaved similar to unmodified F18.

Taken together, our data indicated that F18 was lost from the viral particles after fusion. F18 could in principle be released from viral cores in the course of the activation process. Alternatively, it is possible that F18 – although described as *bona fide* core protein – was part of a viral structure that dissociates from the viral core after fusion.

4.3.3 F18 is a major lateral body component

F18 remained associated with *in vitro* cores, but not with viral cores found in the cytosol. We were intrigued by this finding because this paralleled the presence of a distinct subviral structure - the lateral body (LB). LBs were detected in MVs and *in vitro* cores, but remained associated with the cellular membrane upon fusion and were thus absent from cytosolic cores. We therefore hypothesised that F18 is indeed localised to the LBs and – due to its abundance (27,000 copies in an MV [116]) – may constitute a major component of the latter.

To analyse the subviral localisation of F18, we prepared Tokuyasu sections of MVs and *in vitro* cores, and immunogold-labelled F18 with anti-F18 antibodies (see Figure 4.5 A/B and Supplementary Figure 4.6 A/B). We quantified the localisation of gold particles and found that in mean 2.4 and 5.2 gold particles were visible in the position of the lateral body in MVs and *in vitro* cores, respectively (see Figure 4.5 E). However, a few gold particles were also found onto the core: a mean number of 0.8 and 1.0 gold particles were observed per core in MVs and *in vitro* cores, respectively. The partial localisation of gold labels onto the cores may be caused by the long distance between the actual epitope and the visible gold particle, which were linked by one IgG (ca. 10 nm) and protein A molecule. Only very few gold particles were found outside virus particles, confirming the specificity of F18 antibodies.

To verify the localisation of F18 to lateral bodies, we treated *in vitro* cores with limited amounts of trypsin - a method that had been previously used to remove lateral bodies (see Figure 4.5 C and Supplementary Figure 4.6 C) [65, 108]. Trypsin-treated *in vitro* cores were negative for F18 and did not contain intact lateral bodies, although remnants of the latter were visible on some cores. This suggests that F18 labelling was indeed dependent on the presence of full lateral bodies, supporting the hypothesis that F18 was localised to lateral bodies.

Treatment of MVs with SDS under non-denaturing conditions had previously been shown to yield so-called "ghosts"[108]. These structures lacked viral lipid membranes, but still contained the protein layer underlying the MV membrane, the lateral bodies, as well as parts of the core wall. Viral DNA and nucleoproteins were shown to be lost from these structures. When MVs were subjected to mild SDS treatment, we could detect the described "ghosts"(see Figure 4.5 D and Supplementary Figure 4.6 D), which could be immunogold-labelled with anti-F18. Although the localisation of gold particles could not be quantified using the same categories as in the previous samples, gold particles were predominantly found in what appeared to be the lateral bodies.

Taken together, F18 immunogold-labelling of sections of MVs and subviral structures supported the hypothesis that F18 localises to lateral bodies. The close proximity of lateral bodies and cores, however, did not allow an unambiguous labelling of lateral bodies entirely.

To study the fate and localisation of F18 and the viral core simultaneously, we next constructed a virus that incorporated EGFP-F18 as well as a fluorescent *bona fide* core protein. While it was not possible to combine EGFP-F18 with mCherry-A5, we were able to generate a virus which encodes EGFP-F18 and a fluorescent fusion of the DNA-binding core protein VP8, VP8-mCherry. VP8 is encoded by gene L4R and the translated precursor protein L4 is proteolytically cleaved during morphogenesis to yield VP8 (aa 33-251 of L4) [273]. Both fusion proteins were encoded as additional copies in the thymidine kinase locus under the control of their own endogenous promoters (see Figure 4.6 E for a scheme of the inserted cassette). Successful incorporation of both proteins into MVs was confirmed by fluorescence microscopy (see Figure 4.5 F/G) and immunoblot analysis (see Figure 4.6 F/G). Comparable levels of both F18 and EGFP-F18, as well as VP8 and VP8-mCherry, were incorporated into virions as shown by immunoblot analysis of purified MVs (see Figure 4.6 F/G). VP8-mCherry was proteolytically processed to the same degree as non-fluorescent VP8. EGFP-

WR wt - immunogold anti-F18

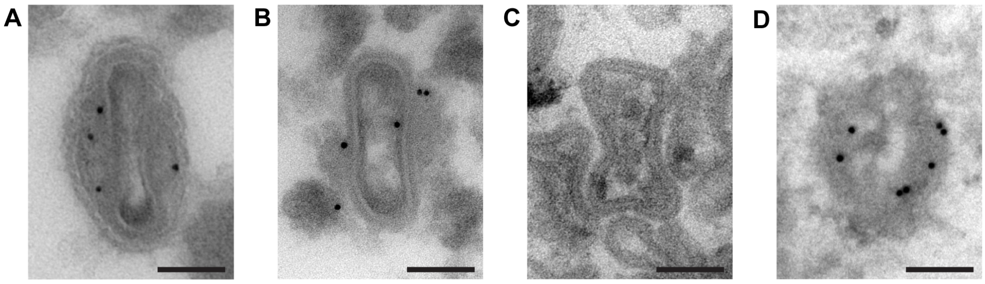

E

	core	lateral body	unclear
MV	0.8 ± 1.4	2.4 ± 1.8	0.1 ± 0.2
***in vitro* cores**	1.0 ± 1.0	5.2 ± 1.6	0.4 ± 0.5
***in vitro* cores + Trypsin**	0.1 ± 0.2	0.1 ± 0.3	n/a

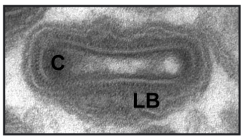

WR VP8-mCherry EGFP-F18 - confocal microscopy

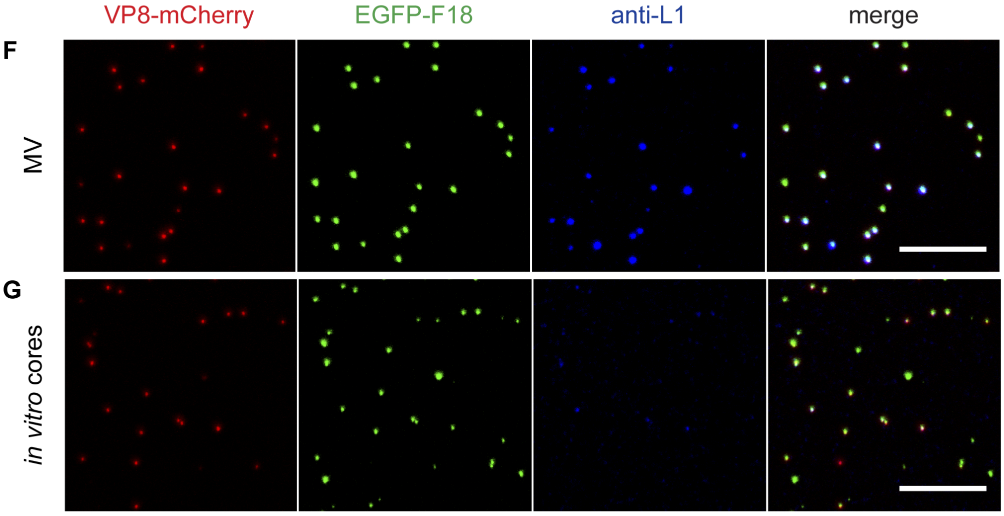

WR VP8-mCherry EGFP-F18 - structured illumination microscopy

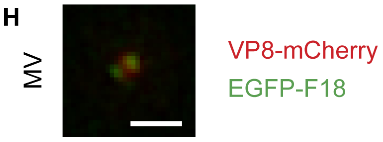

Figure 4.5 Visualisation of lateral bodies. (A-E) WR MVs were pelleted following the protocol for Tokuyasu combined with anti-F18 immunogold labelling. (A-D) representative micrographs of endogenous F18 distribution within WR wt MVs (A), *in vitro* cores (B), *in vitro* cores treated with trypsin (C), and MV treated with SDS (D); scale bar = 100 nm. The data in Table (E) represent counted gold particles in the respective subviral locations on thawed, immunogold labelled cryo sections; mean values ± standard deviation of the mean are shown. N = 50 virions, n/a = not applicable, C = core, LB = lateral bodies. (F-H) WR VP8-mCherry EGFP-F18 MVs (F/H) or *in vitro* cores (G) were bound to cover slips and fixed. Samples were either stained for the MV membrane protein L1 and analysed by confocal microscopy (F/G), or analysed by structured illumination microscopy without staining. Representative images are shown. Scale bar = 10 μm (F/G) or 500 nm (H).

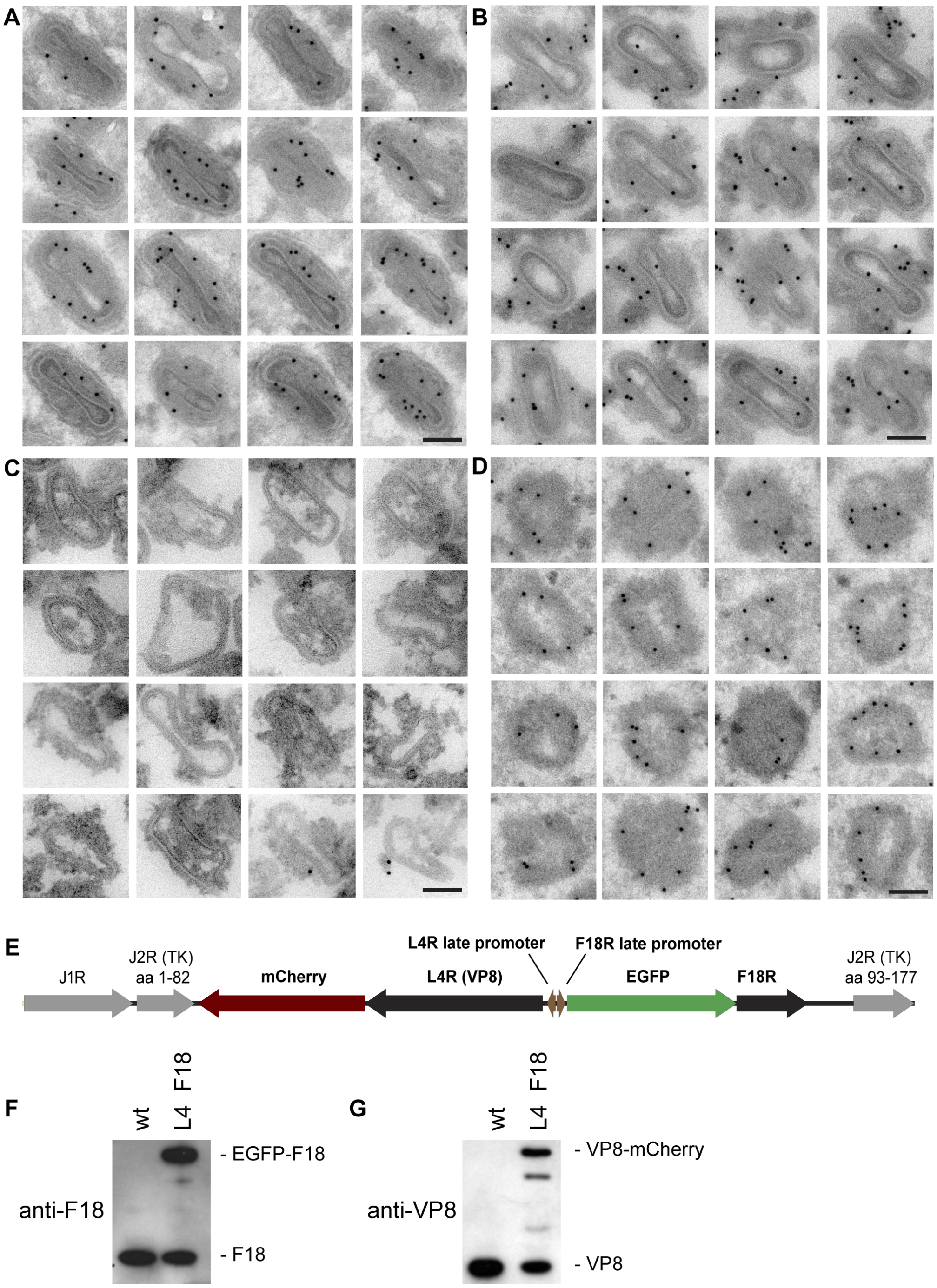

Figure 4.6 Supplementary Figure; Collection of virus particles immunogold labelled for endogenous F18. WR wt MVs (A), *in vitro* cores (B), *in vitro* cores treated with trypsin (C), MV particles treated with SDS (D); scale bar = 200 nm. (E) Overview of the insertion site of the VP8-mCherry and EGFP-F18 coding sequences in the tk locus. (F-G) Band-purified WR wt and WR VP8-mCherry EGFP-F18 MVs were denatured in sample buffer and proteins separated by SDS-PAGE. Presence of VP8 and VP8-mCherry (F) or F18 and EGFP-F18 (G) was tested with anti-VP8, or anti-F18 antibodies, respectively.

F18 and VP8-mCherry furthermore remained associated with *in vitro* cores, as expected for both core and LB components (see Figure 4.5 G).

To analyse the distribution of EGFP-F18 and VP8-mCherry within MV particles, we next analysed WR VP8-mCherry EGFP-F18 MVs by structured illumination microscopy (SIM) [86], a technique that allows improved resolution using conventional fluorescent proteins (see Figure 4.5 H). While VP8-mCherry was found in the centre of the particles, EGFP-F18 fluorescence was found more peripheral and – depending on the orientation – occurred as two distinct spots at both sides of the core. This distribution matched the expected pattern of VP8-mCherry in the core and EGFP-F18 in the lateral bodies.

We next used MVs of WR VP8-mCherry EGFP-F18 to infect HeLa cells and analysed samples by fluorescence microscopy. When MVs were bound to HeLa cells in the cold, virtually all VP8-mCherry-containing cores co-localised with EGFP-F18 as well as the MV membrane protein L1 (see Figure 4.7 A). When cells were infected for 3 h in the presence of ActD, some red fluorescent cores were positive for EGFP-F18 and L1, suggesting that the cores were part of intact MVs that had not yet undergone fusion (see Figure 4.6 B). The majority of red *punctae*, however, did not associate with L1 and EGFP-F18, confirming that the cores that accumulated after fusion were negative for EGFP-F18. This furthermore indicates that VP8-mCherry and EGFP-F18 act like the endogenous VP8 and F18, respectively.

In case EGFP-F18 is indeed localised to the lateral bodies as hypothesized, then the EGFP-F18 fluorescence would be expected to dissociate from the red fluorescent core as one distinct structure. Indeed, some *punctae* that were only green fluorescent were detected 3 h post infection. They were, however, outnumbered by the red fluorescent cores, suggesting that free lateral bodies were unstable. Similar green *punctae* were also observed 5 min post acid-induced fusion (data not shown). When F18 or EGFP-F18 in MVs was analysed by SDS-PAGE and immunoblot, we had repeatedly noticed a ladder of high molecular weight bands of F18 that were shifted by ca. 8 kDa, a pattern similar to proteins known to be conjugated to ubiquitin and oligoubiquitin-chains (see Figure 4.8 E). It was thus possible that ubiquitinated F18 was marked to be rapidly degraded by the proteasome. To test whether EGFP-F18 was degraded by the proteasome, we infected HeLa cells in the presence of the proteasome inhibitor MG132 3 h p.i. (see Figure 4.7 C) [195], VP8-mCherry containing cores as well as EGFP-F18 containing structures accumulated. This indicates that EGFP-F18 is indeed part of a distinct structure that is lost from the core upon fusion and that this structure is degraded or dissociated in a proteasome-dependent manner.

In conclusion, our experiments with WR VP8-mCherry EGFP-F18 con-

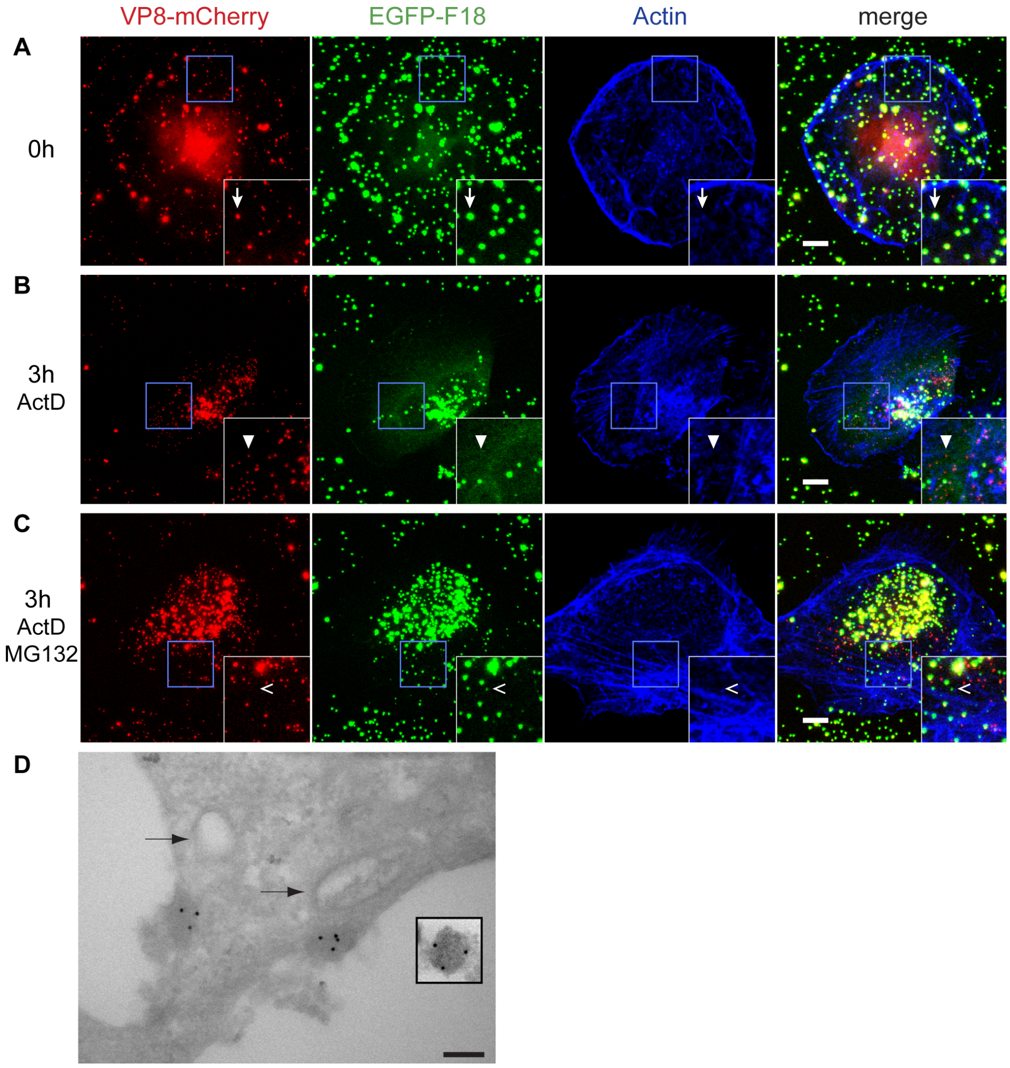

Figure 4.7 Visualisation of lateral bodies. WR VP8-mCherry EGFP-F18 MVs were bound to HeLa cells on ice (A-C: MOI 15, D: MOI 100). (A-C) Cells were either fixed directly (A), or incubated at 37 °C for 3 h in the presence of ActD (B), or ActD and MG132 (C). Samples were analysed by confocal microscopy and maximal projections of representative Z-stacks are presented. Examples of an MV (arrow), a cytosolic core (closed arrowhead), and a free lateral body (open arrowhead) are highlighted in the insets. Scale bar = 10 μm. (D) Cells were treated with pH 5 medium at 37 °C for 5 min, fixed and prepared for immunogold EM (Tokuyasu) combined with anti-F18 immunogold labelling. The micrograph shows viral cytosolic cores (black arrows) and the lateral bodies left behind after fusion. The inset shows a single lateral body found in an *in vitro* cores preparation, subjected to the same immunogold labelling and represent in the same scale. Scale bar = 100 nm.

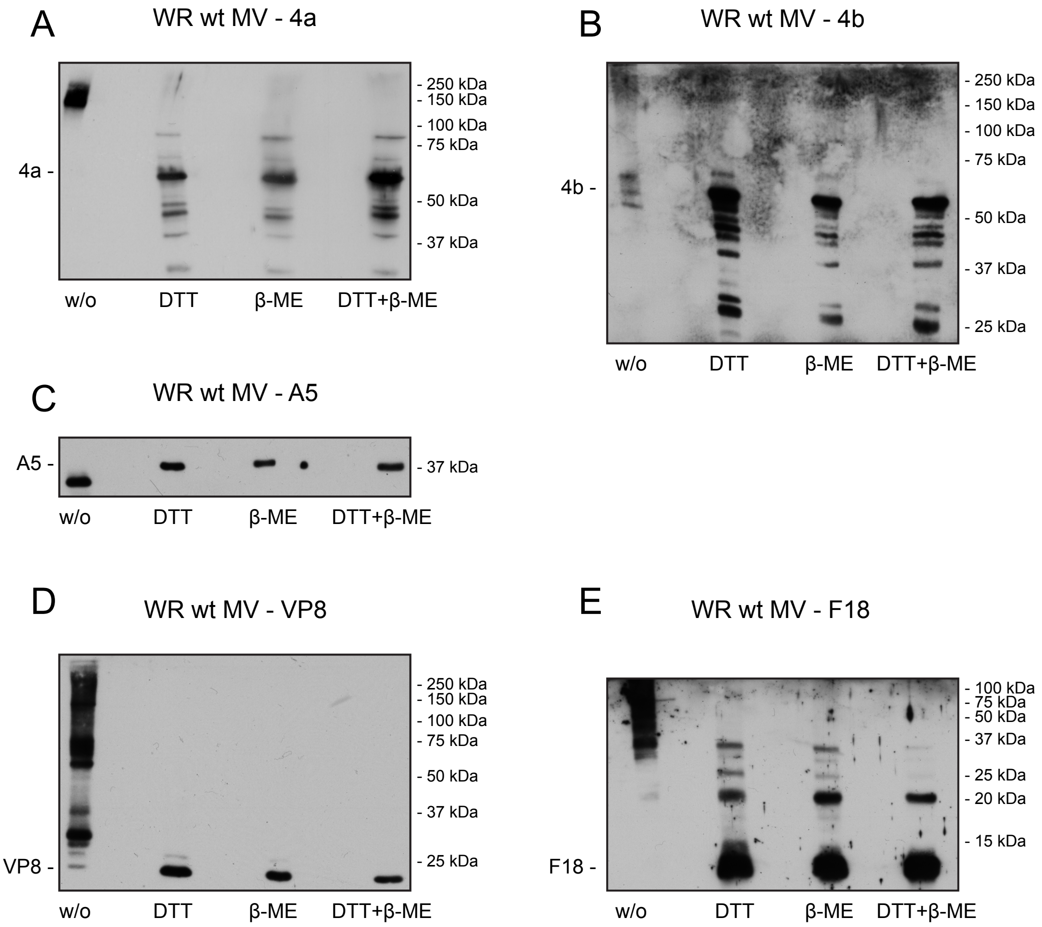

Figure 4.8 Verification of identified disulfide-bonded core proteins. WR wt MVs were alkylated with NEM and boiled in sample buffer w/o reducing agents, with 100 mM DTT, 5 % β-mercaptoethanol (β-ME), or both. Proteins were separated on 10 % (A–D) or 15 % (E) SDS-PAGE gels, transferred to nitrocellulose membranes and 4a (A), 4b (B), A5 (C), VP8 (D), and F18 (E) detected by Western blot. Positions of monomeric reduced proteins are indicated on the left.

firmed the localisation of F18 determined by EM and demonstrated that EGFP-F18-positive structures dissociated from the core as distinct objects, presumably lateral bodies.

Our initial morphological studies had shown that lateral bodies remained at the plasma membrane after acid-induced fusion. Since they were not very electron dense, LBs were difficult to identify in Tokuyasu samples. We therefore applied WR VP8-mCherry EGFP-F18 MVs and a correlative light and electron microscopy (CLEM, see Figure 4.9) setup to identify viral cores and lateral bodies at the plasma membrane in Tokuyasu sections. When this technique was combined with anti-F18 immunogold-labelling, we were able to identify viral cores and LBs 5 min after acid-induced fusion (see Figure 4.7 D and 4.9 E). More importantly, the distance between cores and LBs was great enough to unambiguously determine that F18-staining was only found in the LBs, but not in the cores. This proves that F18 is indeed localised to LBs, which are left behind upon fusion.

4.3.4 F18 degradation releases the LB protein H1 and thereby regulates H1 activity

F18 can be phosphorylated on serine residues 53 and 62 by cellular proline-directed kinases and can be dephosphorylated by the viral dual-specific phosphatase VH1 [134, 264]. In fact, F18 in virions is hyper-phosphorylated in the absence of VH1 [134]. MVs lacking VH1 exhibit defects in early gene expressions similar to MVs incorporating a mutant version of F18 that cannot be phosphorylated. While VH1 has only been shown to be present in *in vitro*

Figure 4.9 ***(following page)*** Appearing of single fusion events by correlative light and EM approach. WR wt MVs were bound to HeLa cells for 1 h on ice (MOI 100) treated with pH 5.0 medium for 5 min and fixed directly. Samples were subjected to correlative light and electron microscopy (CLEM). Ninety-nm thin cryo-serial sections were cut and transferred to a copper finder grid at RT. After several PBS washing steps, acquiring of fluorescence images was performed in a new designed light microscopy chamber for wet, thawed sections. Subsequently, immunogold-labelling of GFP was executed on identical thawed sections (D, insert and E) as previously described [235, 220]. (A/D) show the fluorescent signal in serial sections of cultured cells with adherent virions expressing EGFP-F18. The cartoon (top right) illustrates a simplified fusion event. (D) represents CLEM of fluorescent and transmission electron microscopy (TEM) and a higher magnification of a representative F18 immunogold-labelled virion in (D, insert). (C) shows a sequentially acquired and merged fluorescent image showing the separation of VP8-mCherry and EGFP-F18. (E) An enlarged TEM area of a single fusion event in which a lateral body was positive labelled for EGFP-F18 (black arrow). Scale bars are as follows: (A) = 100 μm, (D) = 5 μm and (D insert, E) = 200 nm. Attention: Figure is presented in a colour vision deficiency version.

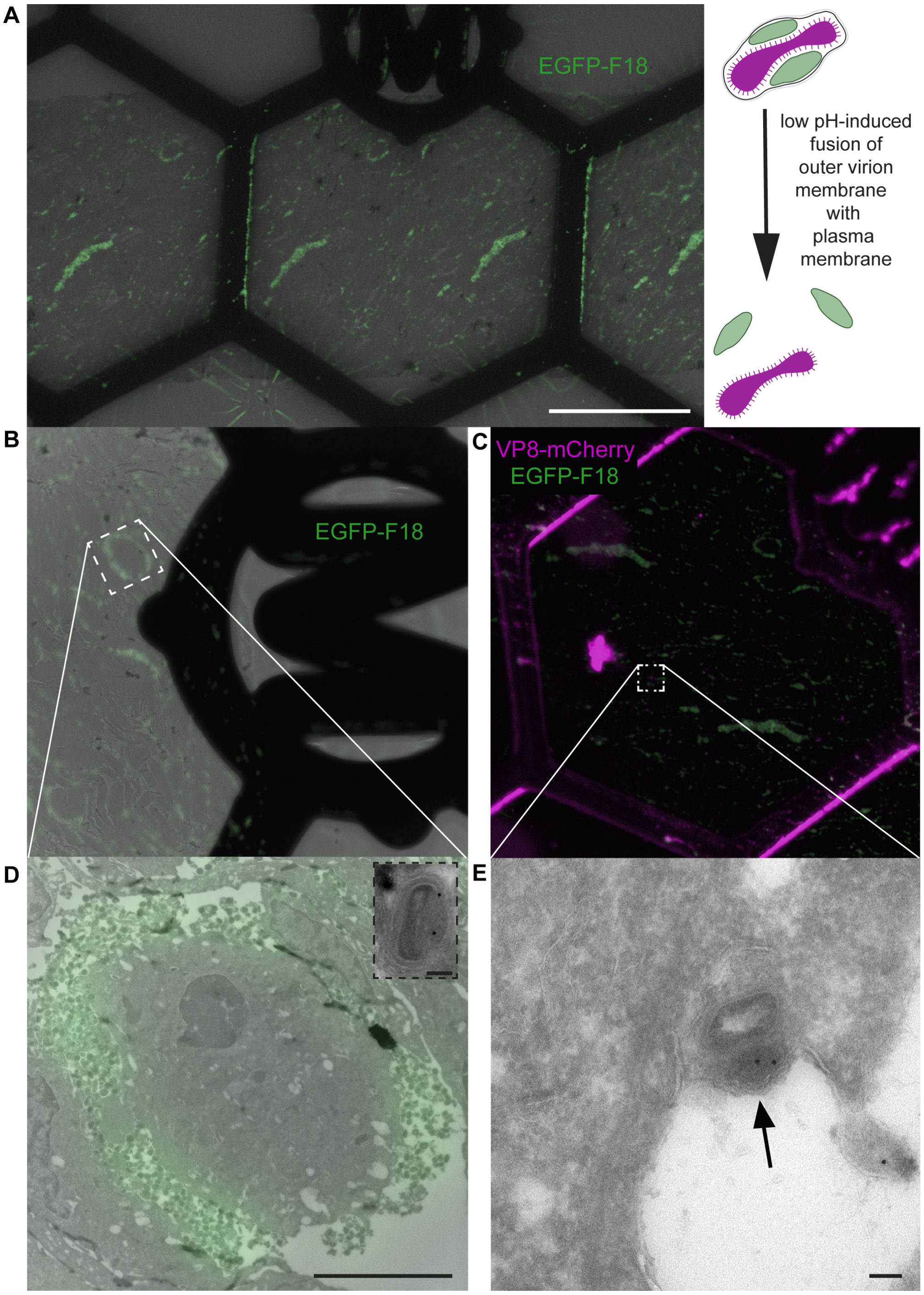
A
EGFP-F18
low pH-induced fusion of outer virion membrane with plasma membrane
B
EGFP-F18
C
VP8-mCherry
EGFP-F18
D
E

cores, their functional relationship suggests that F18 and VH1 may occur in close proximity in the virion. To test whether VH1 localises to LBs, we generated a virus expressing VH1-HA from the endogenous locus and analysed the distribution of VH1-HA by electron microscopy and immunogold-labelling with anti-HA antibodies.

When MVs of WR VH1-HA were artificially fused to HeLa cells, we were able to analyse both bound MVs and virus particles shortly after fusion (see Figure 4.10 A/B). Within a bound MV (see Figure 4.10 A), on average 4.1 gold particles were found in the position of the lateral bodies in between the core and the MV membrane. In contrast, only around 0.2 gold particles were found in the core. In addition, anti-HA immunogold-labelling was found in LBs left behind at the plasma membrane after acid-induced fusion, but hardly any staining was detected in released cores (see Figure 4.10 B). Taken together, the results of anti-HA immunogold-labelling indicate that VH1 almost exclusively localises to the lateral bodies.

Besides its essential role in the replication cycle, VH1 has an additional function that only becomes apparent in the presence of a cellular immune system. In uninfected cells, IFNγ stimulation leads to the recruitment and activation of janus kinases, which subsequently phosphorylate the antiviral transcription factor Stat1 on tyrosine 701 (p-Stat1) (see Figure 4.11 B). p-Stat1 dimerises and is imported into the nucleus, where it activates the transcription of GAS element-dependent genes. However, VH1 brought into the cell with the incoming virus catalyses the de-phosphorylation of p-Stat1 and thus prevents its nuclear import and Stat1-dependent gene expression [164] (see Figure 4.11 C). This way, VACV-infected cells suppress the expression of antiviral proteins immediately after entry, before early gene expression.

We wondered whether VH1 has to be released from LBs to become catalytically active and decided to use nuclear localisation of Stat1 in HeLa cells as a read-out for VH1 activity. While Stat1 is mostly found in the cytosol in untreated cells (see Figure 4.11 A), phosphorylated Stat1 dimers are transported into the nucleus upon IFNγ treatment, which can be visualised with anti-Stat1 immunofluorescence staining (see Figure 4.11 B). As described in the literature [87], VACV infection with WR wt prior to IFNγ-treatment prevented nuclear localisation of Stat1 (see Figure 4.11 D) and this effect was reverted when VH1 activity was inhibited with the broad phosphatase inhibitor orthovanadate (see Figure 4.11 F). In the presence of the proteasome inhibitor MG132, which leads to the stabilization of LBs, Stat1 was mainly found in the nucleus after WR wt infection and IFNγ-treatment (see Figure 4.11 E). This indicates that VH1 requires proteasome activity to inactivate dephosphorylated Stat1. Since VH1 is active in the absence of any cofactors [134], the proteasome is most likely required for the dissociation of

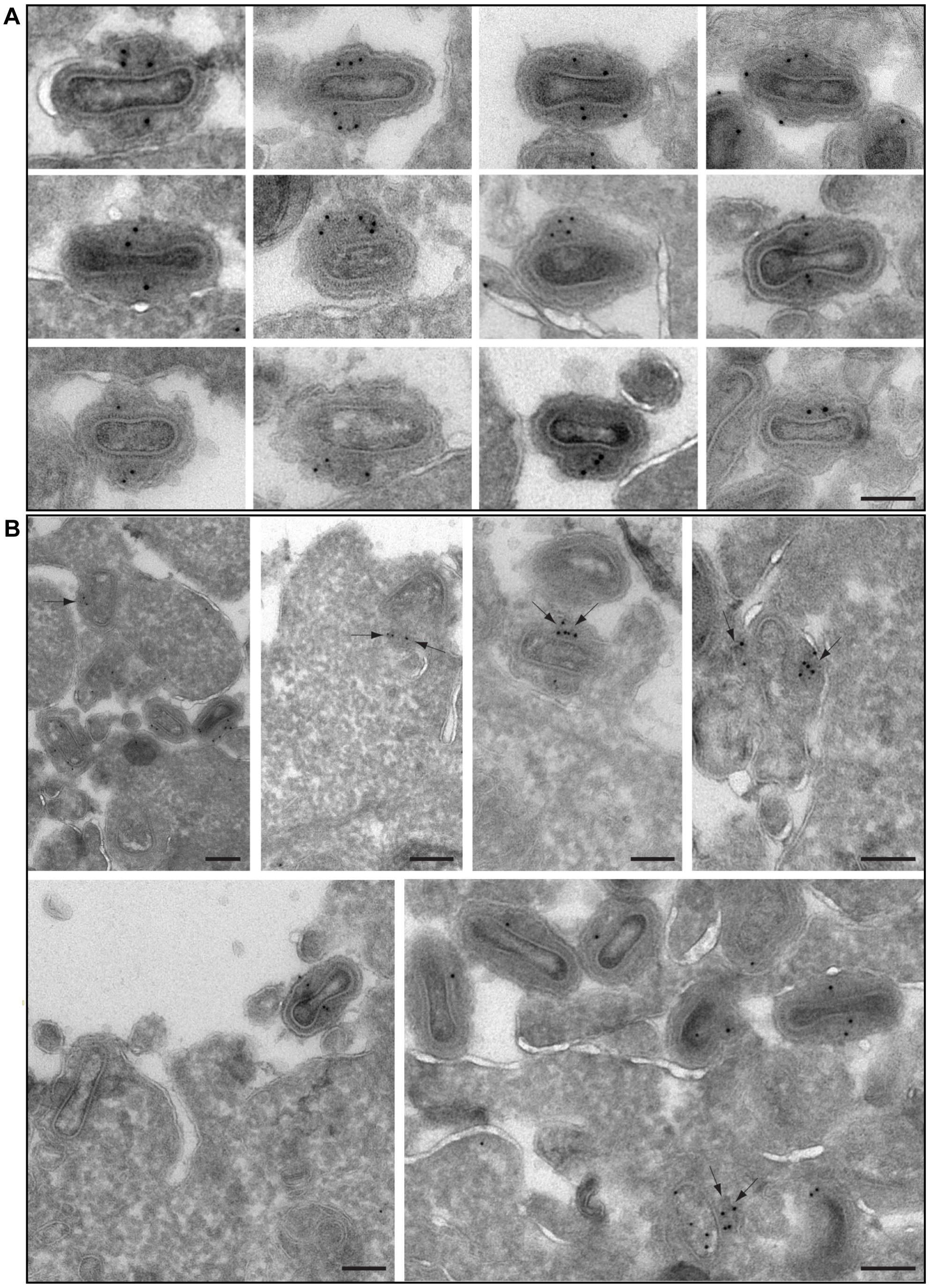

Figure 4.10 VH1 localizes to lateral bodies. WR VH1-HA MVs were bound to HeLa cells on ice (MOI 100) and fusion induced by a 5 min treatment with pH 5 medium at 37 °C. Samples were then fixed and prepared for immunogold EM (Tokuyasu) combined with anti-HA immunogold labelling. Representative thin projections of bound MVs (A) and a fusion event (B) are shown; black arrow: VH1 positive lateral bodies; scale bar = 100 nm.

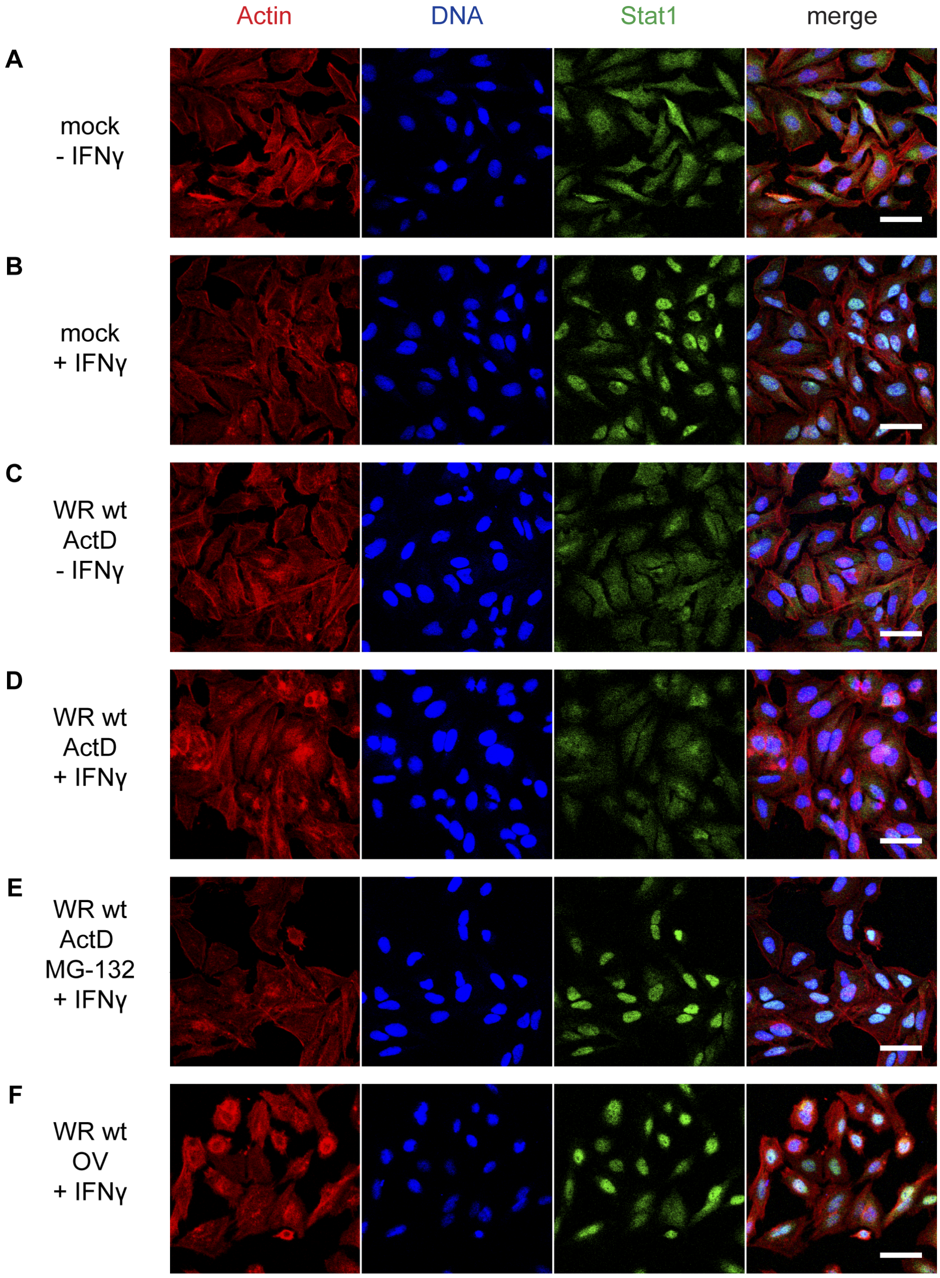

Figure 4.11 Dephosphorylation of P-Stat1 by VH1 requires proteasome activity. WR wt MVs were bound to HeLa cells on ice (MOI 20), followed by incubation at 37 °C for 1 h. Cells were subsequently fed with medium containing 1000 U/mL human IFNγ and incubated for an additional 1 h at 37 °C. The indicated drugs were present during binding and all later steps. Cells were fixed and stained for Stat1, actin, and DNA. Samples were analysed by confocal microscopy and representative images are shown. Scale bar = 50 μm.

LBs to release effector proteins. This way, F18 may act as a LB scaffolding protein that – through its ubiquitination – is destined for proteasomal degradation. Upon destruction, viral effectors like VH1 are released, which are immediately active to modify the host cell.

4.3.5 Viral core proteins are reduced during activation

Despite MV formation in the reducing environment of the cytosol, a number of VACV core proteins have been found to be involved in inter- and intramolecular disulfide bonds [104, 135]. MVs produced in the presence of DTT or treated with DTT *in vitro* have been shown to exhibit an oval shape resembling activated cores [135]; we made similar observations in MVs treated with DTT and NP-40 (*in vitro* cores). Two viral core proteins, 4a and VP8, have furthermore been shown to be reduced in a not further characterised step of infection [135].

To investigate whether core activation involves the reduction of viral core proteins, we first set out to identify disulfide-bonded core proteins in an unbiased biochemical approach. We applied redox 2D SDS PAGE [228] as well as a combination of sucrose gradient and reducing SDS PAGE to specifically identify disulfide-bonded proteins based on their different electro-mobility or sedimentation coefficient before and after reduction (see Figure 4.12 and Table 4.1). We identified 13 disulfide-bonded VACV proteins, of which 6 were MV membrane proteins that were not further considered. The core proteins VP8, A5, 4a, 4b, and the RNA polymerase subunits RPO132 and RPO147, as well as F18 were identified. VP8, 4a, 4b, and F18 were packaged into MVs as high-molecular weight complexes. The latter migrated slowly in non-reducing SDS-PAGE or did not even enter the gel, but migrated as monomers upon reduction (see Figure 4.12). A5 exhibited intra-molecular disulfide bonds that rendered denatured A5 more condensed, leading to a faster migration in non-reducing SDS-PAGE. High molecular-weight complexes of RPO132 and RPO147 were only confirmed in infected cells using transiently transfected expression vectors for HA-tagged proteins.

To monitor the redox state of disulfide-bonded proteins during infection, we next bound WR wt MVs to HeLa cells in the cold and incubated cells at 37 °C for 3 h in the presence or absence of ActD. As controls, cells were kept on ice, or MVs were incubated with monoclonal anti-L1 antibody 7D11 prior to binding, which blocks MV fusion. Cells were harvested and proteins were analysed by non-reducing or reducing SDS PAGE and immunoblot with antibodies against F18, 4b, and VP8 (see Figure 4.8 on page 103). The majority of all three proteins ran as monomers after reduction. Under non-reducing conditions, low molecular weight bands of F18 and 4b were detected

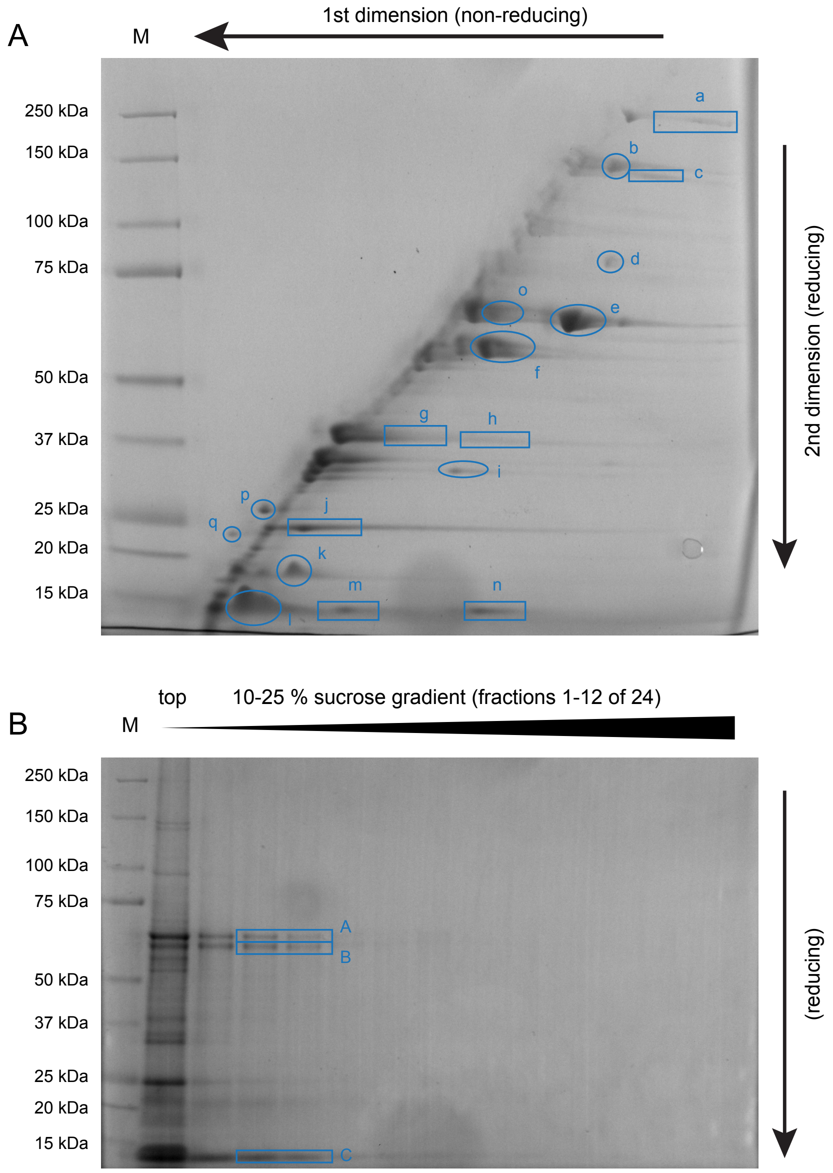

Figure 4.12 Identification of disulfide-bonded VACV proteins. Disulfide-bonded VACV proteins were identified by redox 2D SDS-PAGE (A) or sucrose velocity gradients of denatured proteins in combination with reducing one-dimensional SDS-PAGE (B). Proteins were stained with colloidal Coomassie and the highlighted protein spots or band identified by mass spectrometry (see Table 4.1 on page 112). M = molecular weight standard.

3 h post infection in the absence or presence of ActD, suggesting that proteins were in the reduced state when samples were prepared. No low molecular weight bands of F18 and 4b were detected when MVs were only bound or fusion was inhibited with neutralising antibodies. The low molecular weight band of F18, which occurred after infection, ran slower than monomeric, unmodified F18 and was found to be shifted by ca. 8 kDa. It ran at the same height as one of the minor bands of F18 found in reduced samples. The redox state of VP8 did not change during infection.

To identify disulfide-bonded VACV proteins by redox 2D SDS-PAGE, MV protein samples boiled in sample buffer were separated by SDS-PAGE under non-reducing conditions in the first dimension, and subsequently separated by reducing SDS-PAGE in the second dimension (see Figure 4.12 A). All proteins that did not contain any disulfide bonds exhibited the same electrophoretic mobility in both conditions and thus occurred as a diagonal in the 2D gel. All proteins present in complexes linked by intermolecular disulfide bonds ran slower under non-reducing conditions and faster after reduction and thus were expected to occur below the diagonal in the 2D gel. Proteins with intra-molecular disulfide bonds have a more compact structure and thus ran faster under non-reducing conditions and slower after reduction. They were therefore expected to be found above the diagonal. Many spots below the diagonal were revealed by colloidal Coomassie staining and in most cases proteins rather ran as a smear in the first (non-reducing) dimension. This may be caused by the reduced solubilisation of protein complexes before reduction or by the presence of the same proteins in high molecular weight complexes of different size. Two protein spots were identified above the diagonal. The respective spots or bands were cut out and the proteins within identified by mass spectrometry (see Table 4.1 on page 112). We identified 5 core proteins as present in intermolecular disulfide bonds: the RNA polymerase subunits RNA pol 147 and RNA pol 132, 4a, A5, and VP8. Furthermore, 4 MV membrane proteins were found to contain intermolecular disulfide bonds: A25, A26, D8, and A27. L1 and possibly F9, of which only one peptide was identified, were found to contain intra-molecular disulfide bonds.

While large proteins or protein complexes have a reduced electrophoretic mobility and thus may not even enter a polyacrylamid gel, they have a larger sedimentation coefficient and thus move faster in sucrose gradients during velocity runs. To identify viral proteins in bigger disulfide-bonded complexes, MVs boiled in sample buffer were therefore first separated on a 10–25 % sucrose gradient. The gradient was fractionated, proteins reduced, and separated by SDS-PAGE. Three prominent bands were observed throughout the sucrose gradient after silver staining and in the upper five fractions after

Sample	Protein	Peptides	Gene	MW [kDa]	Cysteins
a	Myosin-9	5	MYH9	227	21
b	RNA pol 147 subunit	32	J6R	147	19
c	RNA pol 132 subunit	19	A24R	133	20
d	A25	23	A25L	84	23
e/o	4a (aa 1-614 of A10)	45/39	A10L	62	7
f	A26	12	A26L	58	6
g/h	A5	23/16	A4L	31	4
i	D8	8	D8L	35	1
j	VP8 (aa 33-251 of L4)	25	L4R	28	2
k	lost				
l/m/n	A27	2/14/14	A27L	13	2
p	L1	12	L1R	27	6
q	F9	1	F9L	24	7
A	4a (aa 1-614 of A10)	7	A10L	62	7
B	4b (aa 62-643 of A3)	7	A3L	66	7
C	F18	2	F17R	11	5

Table 4.1 Identification of disulfide-bonded proteins by mass spectrometry (proteins identified in experiments in Figure 4.12). Protein names, number of peptides identified with >95 % confidence, gene name, theoretical molecular weight (MW), and number of cystein residues of each identified protein are present. Sample k was lost during sample preparation.

Coomassie staining (see Figure 4.12 B). This suggested that the respective proteins were present in high molecular weight complexes with high – but inhomogeneous – sedimentation coefficients, and that the respective complexes were disassembled after reduction. When MV protein samples were reduced first and then ran on parallel gradients, almost all proteins were found in the top fraction and few in the second fractions (data not shown). The identified bands were cut out and determined by mass spectrometry as the core proteins 4a, 4b, and F18 (see Table 4.1 on page 112).

In order to verify that the identified core proteins indeed formed high molecular weight complexes via intermolecular disulfide bonds, polyclonal antibodies against F18, VP8, 4b, and 4a were used to detect the respective core proteins by Western blot. MVs were boiled in sample buffer without reducing agents, with DTT, with β-mercaptoethanol, or with DTT and β-mercaptoethanol and separated by SDS-PAGE (see Figure 4.8).

Using two different biochemical assays, we found that six core proteins and F18 contain disulfide-bonds. Our infection experiments (data not shown) suggest that F18 and 4b are reduced during infection and that this happens after fusion, but before uncoating, i.e. most likely during core activation.

In summary, the core proteins F18, VP8, 4b, 4a, RNA pol 132, and RNA pol 147 as well as the MV membrane proteins A27, D8, A26, and A25 were found to be present in disulfide-bonded high molecular weight complexes. It is likely that this approach did not identify all disulfide-bonded proteins, since only abundant structural proteins could be detected by Coomassie staining.

4.3.6 Changes in core morphology may not require host factors

Our initial morphological studies had shown that the core morphology changes immediately after or during fusion. Generation of *in vitro* cores with detergents and reducing agents led to a core morphology resembling activated cores, and at least two core proteins were found to be reduced during core activation. It was thus possible that core activation occurs when viral cores are released into the reducing environment of the cytosol. However, it remained unclear if the reduction of core proteins is directly linked to changes in core morphology, and if host factors are involved in core activation at all.

We thus intended to study core activation after fusion with artificial liposomes – a minimalistic system in the absence of any host factors and reducing agents. For this, we first needed to test whether fusion of VACV MVs with artificial vesicles lacking proteins or glycosaminoglycans can be induced by low pH. To be able to monitor hemifusion, we labelled VACV MVs with self-quenching quantities of the fluorescent lipid dye octadecyl rhodamine B (R18), which would be de-quenched upon fusion [90]. When these virions were bound to HeLa S3 suspension cells in the cold, hemifusion and presumably full fusion could be efficiently induced by a pH 5 buffer at 37 °C, as apparent by the rapid increase of R18 fluorescence in the sample cuvette (data not shown).

We next generated large unilamellar vesicles (LUVs) with an average diameter of ca. 170 nm composed of lipids commonly found in the plasma membrane: the phosphatidylcholine DOPC, the phosphatidylethanolamine DOPE, sphingomyelin, and cholesterol in the ratios 8:2:1:9 [277]. When LUVs and R18-labelled MVs were mixed and the pH was lowered to 5 at 37 °C, rapid R18 de-quenching was observed, suggesting that MVs can undergo hemifusion with LUVs in the absence of any fusion receptor (data not shown).

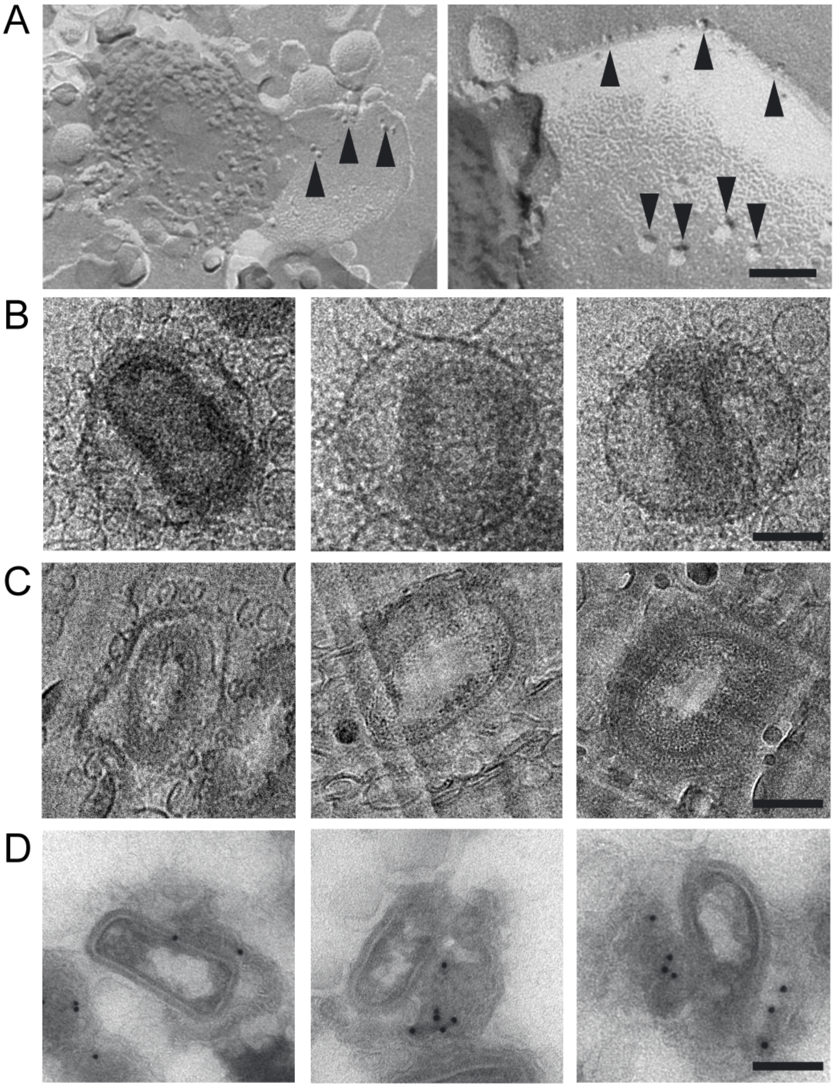

Figure 4.13 Morphological changes of cores during fusion with LUV. (A-D) WR wt MVs were bound to 200 nm LUVs and fusion induced by pH 5 treatment for 10 min at 37 °C. Samples were prepared using (A) tensile freeze fracture EM technique, (B) cryo-transmission electron microscopy technique, (C) cryo-electron microscopy vitreous sections, (D) Tokuyasu method combined with labelling of endogenous F18. Selected fusion events are shown. Of note, clear fusion events could only be detected in few cases. This is possibly due to low fusion efficiency, as well as a too small increase in vesicle volume during fusion; black arrowheads = transmembrane proteins of viral origin, scale bar = 200 nm (A-D).

To investigate the products of MV-LUV fusion, we incubated LUVs and

MVs for 10 min at pH 5, fixed virions with glutaraldehyde and subsequently analysed the samples by electron microscopy. To verify that fusion events occurred, we employed tensile freeze fracture electron microscopy and found that transmembrane proteins of viral origin were indeed deposited in LUV membranes (see Figure 4.13 A). We next used cryo-transmission electron microscopy (CTEM) after plunge freezing in liquid ethane (see Figure 4.13 B), cryo-electron microscopy of vitrified sections (CEMOVIS) [2] after high pressure freezing (see Figure 4.13 C), as well as Tokuyasu sectioning combined with anti-F18 immunogold-labelling to analyse the resulting samples (see Figure 4.13 D). Since LUVs had a significantly smaller diameter and surface area than MVs, we did not expect to be able to visualise the fusion of one MV with a single LUV. Instead, fusion of the same virus particle with multiple LUVs would be required to see a significant increase in the surface area and thus the diameter of the fusion product. While many vesicles were found attached to MVs, very few cores within a large vesicles – as expected after fusion of one MV with multiple LUVs – were detected. The intra-vesicular cores appeared oval and wider than cores in MVs. However, the number of events was too low to quantify core width and shape and to compare it to values obtained for MVs and cytosolic cores (see Figure 4.1 on page 92 and Supplementary Figure 4.2 D on page 93). LBs were only visible in samples prepared after Tokuyasu and even fewer sections (see Figure 4.13 D). Where visible, however, LBs seemed to be dissociated from cores and anti-F18 immunogold-labelling confirmed the localisation of F18 to LBs.

Taken together, fusion experiments of MVs with LUVs suggested that morphological changes of the core after fusion happened in the absence of host factors and are thus an intrinsic property of mature cores. Although hemifusion seemed to be induced by low pH treatment, it remains unclear, how efficient full fusion of MVs with LUVs is in the absence of any receptors or tethering factors. This is in part due to the fact that not all fusion events can be visualised by EM because a single fusion does not increase the volume of the fusion product significantly enough for unequivocal detection.

4.4 Discussion

The entry of both infectious forms of VACV, MVs and EVs, results in the release of virus cores into the host cell cytosol. Viral cores subsequently undergo an activation step that allows the packaged transcription machinery to start early gene expression and prepare the cell for further uncoating and virus replication. In an attempt to describe and understand core activation in structural and molecular detail, we found that VACV cores undergo morphological changes immediately after fusion, a step that possibly does not involve any cellular factors. At the same time, two proteinaceous lateral bodies of previously unknown composition and function, are left behind where the viral and the cellular membrane have fused. We identified the viral protein F18 as one of the major lateral body proteins and found that at least one effector protein, the dual-specific phosphatase VH1, is brought into newly infected cells in lateral bodies. Only when lateral bodies and presumably their scaffold protein F18 are degraded by the host cell proteasome, effector proteins are released and become active. Poxvirus lateral bodies may therefore be a transport vessel for effector proteins that become active upon host cell-mediated release, but before viral gene expression.

Using different electron microscopy techniques, we could follow the structural changes upon fusion of an MV with cellular membranes in detail. While LBs remain associated with the membrane upon fusion, cores are released into the host cell cytosol. LBs probably remain bound to viral membrane proteins deposited in the cellular membrane in the fusion process. In contrast, when membranes are released from MVs using NP-40 and DTT, LBs remain attached to the core. This suggests that LBs may directly bind to both the core and the viral membrane or the membrane associated protein layer. Interactions may be rearranged during fusion and core activation. Alternatively, binding to components of the viral membrane may be stronger than binding to the core.

F18 is one of the most abundant proteins in an MV and was previously described as a core or even DNA-binding protein [108]. Our analysis showed that F18 is present in MVs, in *in vitro* cores still containing the lateral bodies, as well as in lateral bodies found at the plasma membrane after acid-induced fusion. However, F18 was absent from cores released into the cytosol, and from *in vitro* cores incubated with trypsin to partially remove the lateral bodies. Furthermore the fusion protein EGFP-F18 correctly localised to LBs and was shown in discrete spots next to VP8-mCherry-containing cores in MVs using structured illumination microscopy. Previous studies had shown F18 throughout immature virions (IVs), and at the rim of the core of MVs [240]. These findings are consistent with a recruitment of F18 to immature virions, followed by partitioning into the lateral bodies during morphogenesis. Indeed, VACV exhibits severe morphogenesis defects in the absence of F18, and only few aberrant MVs lacking visible lateral bodies are formed [264]. In a seminal study by Ichihashi and colleagues, protein 13.8K and four other proteins had already been interpreted as LB components based on electron microscopy and SDS-PAGE [65]. While the other four proteins cannot be identified using the given information, it seems likely that the basic protein 13.8K indeed was F18, although it was identified as A27 in a later study of the same group [232].

The fate of lateral bodies after release from the core could be followed by fluorescence microscopy and free lateral bodies were stabilised in the presence of the proteasome inhibitor MG-132. Indeed, the band-pattern of F18 on Western Blots suggests that at least a fraction of F18 is ubiquitinated and it is tempting to speculate that the protein is in this way primed for proteasomal degradation.

An additional LB component that we identified in the course of this study is the dual-specific phosphatase VH1, of which around 200 molecules are packaged into an MV [134]. VH1 is presumably essential for the viral life cycle, as no deletion virus could be generated [134]. Known substrates of VH1 include the viral proteins F18, A14, and A17, as well as the cellular protein Stat1 and possibly Stat2 [134, 164, 240, 57, 123]. In the absence of VH1 during morphogenesis, the incorporated viral proteins F18, A14, and A17 are hyperphosphorylated and early transcription is impaired. Interestingly, MVs incorporating F18 mutants that cannot be phosphorylated exhibit normal morphology, but also have defects in early transcription. It remains unclear, whether VH1 activity is required during MV formation, or after viral entry. It was speculated that some defects in early transcription in the absence of VH1 could be partially rescued by background levels of VH1 released from other virions [134]. This would support a role for VH1 after entry. *In trans* complementation, however, was only inferred indirectly and was not shown in the context of an infected cell.

Dephosphorylation of Stat1 by VH1 is most likely an additional immunomodulatory function of VH1, which is not required for virus replication in tissue culture in the absence of IFNγ-secreting cells. Nevertheless, since phosphorylation of Stat1 and subsequent nuclear import can be artificially induced by IFNγ stimulation, p-Stat1 is a suitable model substrate to analyse VH1 activity. Our experiments showed that VH1 requires functional proteasomes to become active and dephosphorylate p-Stat1. Since LBs are stabilised under the same conditions, and since recombinant VH1 can dephosphorylate phosphorylated F18 and A14 in the absence of any cofactors [134], it is most likely that packaging of VH1 in lateral bodies renders the protein inactive. Only proteasome-dependent disassembly or degradation of LBs releases active VH1. Indeed, previous experiments had already shown that packaged VH1 must be regulated: WR wt MVs contain phosphorylated F18 despite the presence of VH1, suggesting VH1 in the virus is inactive or cannot access its substrates. Recombinantly expressed VH1, however, can dephosphorylate F18 within *in vitro* cores [134]. It cannot be ruled out that the observed reduction of F18 intermolecular disulfide bonds contributes to the disassembly of LBs. Similarly, it is possible that VH1 regulates LB disassembly by dephosphorylating F18. The VH1 inhibitor orthovanadate, however, did not lead to the accumulation of lateral bodies (data not shown).

Taken together, our data on F18 and VH1 describe a pathway that allows the delivery of host modulatory proteins into the host cell by the viral LBs. Viral effector proteins are released from LBs by the activity of the host cell proteasome and function without the need for any viral gene expression. In some aspects, the poxvirus LBs thus resemble the tegument of herpes viruses. The disassembly step catalysed by the host cell proteasome adds a level of regulation whose advantages remain to be fully understood. This strategy may allow the virus to package inactive viral effectors that are deleterious in the producer cell or the virion itself. Alternatively, host cell-mediated LB disassembly may ensure the correct timing for effector proteins. It is very likely that VH1 is not the only viral effector delivered to host cells by the LB pathway. Similarly, we cannot rule out that F18 itself has a direct function in host cells, although it is most likely degraded rapidly. Curiously, a basic 11 kDa phosphoprotein present in disulfide-bonded high molecular weight complexes was purified from MVs by Person-Fernandez *et al.* in 1986 [183]. This protein resembles F18 in its physical properties and was described to bind to ribosomes and inhibit protein translation. Conditions that led to the release of this protein from cores, though, did not lead to the separation of LBs and cores (data not shown).

It would be of outstanding interest to identify further components of LBs and study their function immediately after infection. The identification of packaging signals would furthermore allow artificial targeting of effector proteins into recombinant poxvirus strains used as vaccines or oncolytic agents. In some settings, it may be advantageous to deliver a protein of interest into cells before or in the absence of any viral gene expression. Interestingly, when the first 42 amino acids of F18 were fused to the reporter protein β-galactosidase, the respective fusion protein was incorporated and catalytically active in newly infected cells in the absence of viral gene expression [98].

During core activation, viral cores undergo the necessary changes to begin early gene transcription. In line with the previous literature, we have shown that a number of structural changes of the viral core occur immediately after fusion. Cores become oval, wider, and less electron dense. These changes in the core can be partly mimicked during *in vitro* core generation with mild detergents and reducing agents. Limited structural data after fusion of MVs with liposomes suggests that the observed morphological changes are indeed an intrinsic property of the mature core and occur independently of any host factors. The observed changes are probably already laid down in the structure of the core during maturation, and may just need membrane removal for completion. A direct link between changes in core morphology and early gene expression, however, has not been established. In conditions that do not allow early gene transcription despite the presence of all required viral factors, e.g. after fusion of MVs lacking VH1 or L3, or MVs containing ts mutants of E6 and E8, normal changes in core morphology were observed (data not shown) [190, 134, 20, 118]. Using biochemical approaches, we found that the viral core wall protein 4b is reduced during activation. It remains at this point unclear, whether this contributes to changes in core morphology or transcriptional activity. In principle, it is conceivable that early transcription starts when viral components involved in NTP import or mRNA export are activated upon milieu changes in the cytosol.

Alternatively, the catalytic activity of the viral RNA polymerase itself may be subject of regulation. It is possible that the disulfide-bonded RNA polymerase subunits RPO132 and RPO147 are redox-regulated and become active upon reduction in the host cell cytosol, but this was not tested further.

A complete understanding of the core changes that allow early gene transcription may require more detailed knowledge on core architecture and core formation during morphogenesis. Structural changes during this process render the core unstable and prone to activation upon arrival of the cytosol of new host cells.

In summary, our study describes the early stages of poxvirus uncoating in more detail. Furthermore, we have identified F18 as a structural and VH1 as an effector component of VACV LBs and for the first time impute a function to these enigmatic viral structures. We suggest that LBs act as delivery containers for viral effector proteins that become active upon proteasome-dependent LB disassembly, and thus much earlier than early viral proteins. Decipherment of the molecular components and functions of LB components will not only contribute to a deeper understanding of the early stages of the viral life cycle, but also help to understand how poxviruses modulate the immune system. Protein delivery via LBs may also open attractive possibilities to improve poxvirus-based vaccines or oncolytic viruses, and even allow delivery of proteins into cells that do not permit early gene expression.

4.5 Material and methods

4.5.1 Cell lines

BSC-40 (African green monkey) and HeLa (human) cells were cultivated in DMEM (Gibco BRL) supplemented with 10 % heat-inactivated FCS, glutamax, and penicillin-streptomycin; for BSC-40 cells non-essential amino acids and sodium pyruvate were added as well; RK13 (rabbit) cells were cultivated in MEM (Gibco BRL) supplemented with 10 % heat-inactivated FCS, glutamax, non-essential amino acids, penicillin-streptomycin, and sodium pyruvate.

4.5.2 Viruses

Recombinant Vaccinia viruses were generated based on VACV strain Western Reserve (WR) by transfecting infected cells with plasmids containing genomic viral sequences as described elsewhere [148]. WR EGFP-A5 was described previously [210]. To generate WR EGFP-F18 and WR VP8-mCherry EGFP-F18, the endogenous promoter as well as the coding sequence of the fusion protein were inserted into the tk locus using vectors based on pJS4 [33] (see Appendix Figure A.1 on page 139). An intermediate virus, WR neoR GYR-PKR, which encodes neomycin phosphotransferase (neoR) and a fusion protein of the gyrase dimerisation domain and the protein kinase R (PKR) catalytic domain [247] under a viral promoter in the tk locus, was constructed to facilitate insertion into this site. Adapting a strategy described by White *et al.* [263], coumermycin A1 was used to negatively select parental viruses and greatly increased the fraction of recombinant virus, which was detected based on the fluorescence of plaques. To generate WR VH1-HA, a vector based on pBluescript II KS (Fermentas, St. Leon-Rot, Germany) was built, which contains the coding sequences for GFP-neoR and GYR-PKR under the control of viral promoters, as well as the HA coding sequence flanked by genomic viral DNA sequences. The latter defined the insertion of HA at the C-terminus of VH1; the overlap of the J6 and the VH1 coding sequence was resolved by duplicating the overlapping four nucleotides. Intermediate viruses containing the full plasmid inserted into the genome were selected by plaque purification in the presence of 2.8 mg/mL G418. Full recombined viruses lacking the G418 and coumermycin A1 selection cassettes were plaque purified in the absence of G418 and the presence of 100 ng/mL coumermycin A1. Recombinants bearing the HA coding sequence were identified by plaque PCR.

MV particles were produced in BSC-40 cells and purified from cytoplasmic lysates as described elsewhere [148].

To label viral membranes with octadecyl rhodamine B chloride (R18), sedimented MVs from cytosolic extracts were incubated with R18 at a final concentration of 22.5 μM for 2 h at room temperature. MVs were subsequently sedimented at 38,000 g for 40 min and purified through a 25-40 % sucrose gradient as for purification of unlabelled MVs.

4.5.3 Preparation of *in vitro* cores and other subviral particles

In vitro cores were generated by incubating MVs with 1 % NP-40 and 50 mM DTT in 10 mM Tris (pH 9.0) for 30 min at 37 °C. Cores were subsequently sedimented for 1 h at 16,000 g and 4 °C in a tabletop centrifuge and re-suspended in 1 mM Tris (pH 9.0). To partially remove lateral bodies, the *in vitro* core pellet was re-suspended in PBS and treated with 20 μg/mL trypsin at 37 °C for 15 min. The trypsin digest was stopped with 200 μg/mL aprotinin on ice and virions processed for electron microscopy. To produce VACV "ghosts", MVs were treated with 1 % SDS in 50 mM Tris, pH 7.4, at 37 °C for 30 min; sub-viral particles were sedimented and processed for electron microscopy.

4.5.4 Antibodies

Hybridoma cells to produce the mouse anti-L1 (MAb 7D11) [269] were kindly provided by Bernard Moss with permission of Alan Schmaljohn (University of Maryland, Baltimore, MA, USA). MAbs were purified from hybridoma supernatants by BioGenes (Berlin, Germany). Rabbit anti-F18 [134] was obtained from Paula Traktman (Medical College of Wisconsin, Milwaukee, WI, USA), rabbit anti-4a, anti-4b, and anti-VP8 [254] were kind gifts of Dennis Hruby (Oregon State University, Corvallis, OR, USA). Rabbit anti-A5 [49] was kindly provided by Mariano Esteban (Centro Nacional de BiotecnologÃa, Madrid, Spain). Rabbit poly-clonal anti-GFP was purchased from Rockland (Gilbertsville, PA, USA), mouse anti-DNA (MAb AC-30-10) from Progen Biotechnik (Heidelberg, Germany) [206], mouse anti-HA.11 (Clone 16B12) from Covance Inc., mouse anti-Stat1 (Mab HPA000982) from Sigma Aldrich, and rabbit anti-P-Stat1 (Tyr701) (#9171) from Cell Signaling Technology. Rabbit polyclonal anti-mouse immuno-globulins were obtained from Dako-Cytomation (Glostrup, Denmark), fluorophore-coupled goat anti-mouse secondary antibodies from Invitrogen (Carlsbad, CA, USA), and HRP-coupled goat secondary antibodies from Bio-Rad (Hercules, CA, USA).

4.5.5 Drugs and reagents

Actinomycin D, aprotinin, cytosine arabinoside (AraC), coumermycin A1, MG-132, and sodium orthovanadate (Na_3VO_4) were obtained from Sigma-Aldrich; G418, fluorophore-coupled phalloidin, and octadecyl rhodamine B chloride (R18) were purchased from Invitrogen; human recombinant interferon γ was bought from eBioscience (San Diego, CA, USA); DOPC, DOPE, sphingomyelin, and cholesterol were obtained from Avanti Polar Lipids (Alabaster, AL, USA). Draq 5 (Biostatus, Shepshed, UK) was used for DNA staining.

4.5.6 Identification of disulfide-bonded viral proteins

To identify disulfide-bonded proteins by redox 2D SDS-PAGE, samples alkylated with 20 mM NEM were heated in LDS sample buffer (2 % LDS, 0.51 % EDTA, 10 % glycerol, 0.22 mM SERVA Blue G250, 0.175 mM phenol red, 247 mM Tris [pH 8.5]) for 10 min at 70 °C. Proteins were run on a 4-12 % NuPAGE® Bis-Tris gel (Invitrogen) using MOPS electrophoresis buffer. The whole lane was cut out and the gel piece heated in LDS buffer with 250 mM DTT for 20 min at 70 °C. After a washing step with LDS buffer, proteins in the gel were alkylated in LDS buffer with 100 mM NEM for 10 min at RT and the gel piece washed in LDS buffer again. The gel piece was placed horizontally on a 4-12 % NuPAGE® Bis-Tris gel with a 2D well and proteins separated in the second dimension using MOPS electrophoresis buffer. The gel was fixed in 50 % MeOH, 7 % acetic acid, and stained with colloidal Coomassie. Protein spots were cut out with a razor blade and proteins identified by the Functional Genomics Center Zurich using in-gel trypsin digestion and LC/ESI/MS/MS.

To identify disulfide-bonded proteins using sucrose velocity gradients, samples alkylated with 20 mM NEM were heated in LDS sample buffer, diluted and run though a 10-25 % sucrose gradient in 10 mM Tris (pH 9.0), 0.1 % SDS (SW41 rotor, 28,000 g, 45 min, RT). 500 μL fractions were collected and proteins precipitated with trichloro acetic acid. After a washing step with 80 % ice cold acetone, precipitated proteins were dissolved in 2 x LDS buffer with 200 mM DTT, heated for 10 min at 70 °C and separated on 4-12 % NuPAGE® Bis-Tris gels using MOPS buffer. Gels were fixed and stained as above and proteins in chosen bands identified by mass spectrometry.

4.5.7 Immunoblot

Samples to be analysed by immunoblot were boiled in SDS sample buffer (2 % SDS, 10 % glycerol, 0.1 % bromophenol blue, 50 mM Tris [pH 6.8], 100 mM DTT) for 5 min at 95 °C. To analyse the redox state of viral proteins, samples were alkylated with 20 mM NEM prior to denaturation and boiled in SDS sample buffer with or without DTT. Subsequently, proteins were separated on 10 or 15 % discontinuous SDS-PAGE gels and transferred to nitrocellulose membranes. Proteins were detected using rabbit anti-4b, anti-4a, anti-A5, anti-VP8, or anti-F18 (all 1:1,000) and goat anti-rabbit HRP (1:5,000) with the ECL Plus Western Blotting Detection Reagent (GE Healthcare).

4.5.8 Infection experiments

For infection experiments, the indicated amount of MVs were bound to HeLa cells in the cold for 1 h. Cells were subsequently incubated in full medium at 37 °C for the denoted time and processed for immunofluorescence microscopy or different electron microscopy methods. When infection experiments were performed in the presence of drugs, drugs were present during binding and incubation. In some cases, artificial fusion with the plasma membrane was induced after binding by a 5 min treatment with full DMEM containing 30 mM MES, pH 5.0, at 37 °C.

4.5.9 Immunofluorescence microscopy

To stain proteins for immunofluorescence microscopy, cells were fixed with 4 % formaldehyde (FA) and permeabilized in permeabilisation buffer (PS) (0.05 % saponin, 1 % BSA, 0.05 % NaN_3 in PBS) for 20 min. Samples were incubated with primary antibodies in PS (anti-L1 0.54 μg/mL; anti-Stat1 1 μg/mL) for 2 h, washed with PBS, and subsequently incubated with fluorophore-coupled goat secondary antibodies (1:1,000) for 1 h. Where indicated, filamentous actin was stained with fluorophore-coupled phalloidin (1:100), and DNA with Draq5 (1:1,000). Samples were washed with PBS and H_2O and mounted with Immu-Mount (Thermo Fisher Scientific).

4.5.10 Sample processing for epoxy embedding EM

Infected cells were fixed in 2.5 % glutaraldehyde (GA) (50 mM sodium cacodylate pH 7.2, 50 mM KCl, 2.5 mM $CaCl_2$, 2.5 mM $MgCl_2$) for 90 min at room temperature [19]. After several rinses in pre-warmed buffer (50 mM sodium cacodylate pH 7.2, 50 mM KCl, 2.5 mM $CaCl_2$, 2.5 mM $MgCl_2$), the specimens were postfixed in fresh prepared reduced osmium tetroxide (1.5 % KFeCN, 2 % OsO_4, 50 mM sodium cacodylate pH 7.2, 50 mM KCl, 2.5 mM $CaCl_2$, 2.5 mM $MgCl_2$) for 1 h on ice [144], subsequently rinsed in water on ice. Afterwards cells were again fixed in 2 % osmium tetroxide (50 mM sodium cacodylate pH 7.2, 50 mM KCl, 2.5 mM $CaCl_2$, 2.5 mM $MgCl_2$) for 30 min on ice, rinsed in ddH_2O, and stained overnight at 4 °C in aqueous 0.5 % uranyl acetate. The specimens were then dehydrated in graded ethanol series and propylene oxide, followed by embedding in Epon 812 (Serva, Heidelberg, Germany).

Ultrathin sections (50-60 nm) from cell monolayers were obtained using an Leica EM FC7 ultramicrotome (Leica, Vienna, Austria) and counter stained with aqueous uranyl acetate and lead citrate [191], if required for increased contrast. Sections were examined with a CM10 Philips transmission electron microscope at 80 kV with an Olympus Veleta 2k x 2k side-mounted TEM CCD camera.

4.5.11 Sample processing for immunogold EM

Samples were fixed by adding an equal volume of a 2x fixative (8 % FA, 0.2 % GA in PHEM, pH 6.9) [207] to the culture medium. After 5-10 min this mixture was removed and replaced with 1x fixative (4 % FA, 0.1 % GA in PHEM, pH 6.9) for 90-120 min at RT. Cells were scraped and sedimented (300 g). *In vitro* samples were pelleted by centrifugation at 10,500 g.
The pellets were washed by centrifugation and re-suspending and incubated in PBS-glycine for 10 min at RT. Samples were then re-suspended carefully in 10 % gelatin/PBS, incubated for 10 min at 37 °C, pelleted by centrifugation and immediately placed on ice until the gelatin was hardened. The pellet was cut into 1 mm^3 pieces. Gelatin-embedded samples were infiltrated with 2.3 M sucrose [235] and kept at 4 °C over night on a rotating wheel, mounted onto sample pins and plunge frozen by hand in liquid nitrogen.

50-60 nm cryo-sections were obtained with diamond knives (Diatome Ltd., Bienne, Switzerland) in a Leica EM FC7/UC7-ultramicrotome (Leica, Vienna, Austria), at -120 °C. Copper grids were coated with 1 % Formvar [67] and a thin carbon layer. Sections were thawed in a drop of “pick-up solution”(2 % methyl cellulose mixed with 2.3 M sucrose in a ratio of 1:2), transferred to coated copper grids and stored covered by the “pick-up solution”[80] at 4 °C.

For immunogold-labelling, 50-60 nm cryo-sections were thawed and incubated with primary antibodies against endogenous F18 (1:200), GFP (final concentration: 2.5 μg/mL), DNA (final concentration: 0.33 μg/mL), with the secondary poly-clonal antibody rabbit anti-mouse IgGs (final concentration: 0.5 μg/mL) and subsequently with 10 nm protein A gold (1:60, PAG, CMC, Utrecht, The Netherlands) as described in [82, 220] and stained/embedded in 4 % uranyl acetate / 2 % methyl cellulose mixture (ratio 1:9) [236].

4.5.12 Analysis of the core length and width

Analysis of the core length and width was performed as follows. Regions of interest (ROIs) were traced in ImageJ by exactly following the core outlines. All ROIs were processed in Matlab using Dynamo [31]. An adapted Dynamo algorithm performed the following steps. The core length was defined as the greatest distance between any two points on a single drawn ROI, which determine the main axis. This axis is then divided in three segments. Then, the maximal and minimal widths perpendicular to the main axis in those segments were measured, inducing a rough classification. Three classes were defined as “oval”(maximum in central segment is larger than both maxima in the lateral segments), “dumbbell”(maximum in central segment is smaller than maxima in both lateral segments) and “intermediate”shape (all other cases, see Figure 4.2 F).

Values for average length and width are shown in Figure 4.1 G. The minimal width was determined with in the 2nd third segment of each core length. Boxes denote interquartile range, lines within boxes denote median, whiskers denote 10th and 90th percentiles, and round symbols denote outliers. The box plot was created using GraphPad Prism version 5.0d for Mac OS X, GraphPad Software, San Diego, CA, USA, www.graphpad.com.

4.5.13 Analysis of Stat1 localisation

To analyse Stat1 localisation as a readout for VH1 activity, WR wt MVs (MOI 25) were bound to HeLa cells on cover slip at 4 °C for 1h in the presence of the indicated drugs. Cells were incubated at 37 °C for one hour with drugs, and subsequently fed with fresh medium containing drugs and 1000 U/mL IFNγ. After 1 h at 37 °C, cells were fixed, and processed for immunofluorescence staining with anti-Stat1 as described above.

4.5.14 Fusion assay – large unilamellar vesicles

To prepare large unilamellar vesicles (LUVs), 5 mg lipids dissolved in chloroform/methanol (DOPC, DOPE, sphingomyelin, and cholesterol in a molar ratio of 8:2:1:9) were mixed and dried under an Argon stream. Lipids were further dried in a speed vacuum concentrator over night and then hydrated for two hours at RT in 1 mL PBS. LUVs were prepared by extrusion through a polycarbonate filter with 200 nm pore size using an Avanti Mini-Extruder (21 strokes). WR wt MVs (109 pfu) were added to the LUV suspension and incubated for 1 h at 4 °C. The pH was lowered to 5.0 by adding 105 μL 1 M MES and the mixture was incubated at 37 °C for 10 min. The reaction mixture was diluted with 4 mL 2x PHEM, and both virions and LUVs sedimented by ultra-centrifugation (SW55, 38,000 g, 4 °C, 30 min). Samples were subsequently processed for electron microscopy as described below.

4.5.15 Sample processing for tensile freeze fracture replica

A droplet of 2 μL sample was placed on the cleaned copper holder and manually plunged into liquid propane [1]. The frozen sample was fractured at -125 °C in a vacuum of about 10^{-5} Pa with a liquid nitrogen-cooled knife in a Balzers 400 freeze-etching device. The fractured sample was replicated with a 1-1.5 nm deposit of platinum-carbon, and coated with a 20 nm carbon film. The Pt/C replica was cleaned with 2 % SDS, washed with $dd\mathrm{H_2O}$, transferred onto copper EM grid and observed with a Philips CM10 EM (see above).

4.5.16 Sample processing for cryo-electron microscopy of vitreous sections (CEMOVIS)

For CEMOVIS, samples were prefixed with 0.5 % GA in 1x PHEM buffer [207] for 15 min and supplemented with an equal volume of 40 % dextran/PBS [10] (average molecular mass 40 kDa; Sigma-Aldrich, Buchs, Switzerland). They were then introduced into copper tubes and vitrified with an EMPACT 2 high-pressure freezer (Leica, Vienna, Austria) [230]. Afterwards, tubes were mounted in the tube holder of an Leica EM FC7/UC7 cryo-ultramicrotome (Leica, Vienna, Austria) and trimmed to a pyramidal shape, as previously described [3].

40-50 nm feed cryo-sections were cut with a 45° diamond knife (Diatome, Biel, Switzerland) under standard cutting conditions [279]. They were collected on Quantifoil® (Micro Tools GmbH, Jena, Germany) holey carbon films (copper 200 mesh grids, R3.5/1) or Quantifoil® with hexagonal geometry (slot grids) with the help of Leica EM CRION device and stored in liquid nitrogen.

4.5.17 Sample processing for plunge freezing

Samples were prepared by adsorbing 3 μL of the virion fused liposome suspension onto Quantifoil® R3.5/1 holey carbon film mounted on 200 mesh copper grids (Quantifoil® Micro Tools GmbH, Jena, Germany). Prior to adsorption, the grid was rendered hydrophilic by glow discharge in a reduced atmosphere of air for 15 sec. The specimen was applied and after 30 sec incubation on the surface, the grid was blotted and quick-frozen in liquid ethane using a robotic plunge freezer Vitrobot (FEI Company, Eindhoven, The Netherlands).

4.5.18 Cryo-Transmission Electron Microscopy (Cryo-TEM) imaging

For cryo-TEM imaging (CEMOVIS or plunge freezing) grids were either transferred to a Gatan 626 cryo-holder (Gatan, Pleasanton, CA, USA) kept below -170 °C and inserted into a FEI CM200FEG or – using the fully automated FEI AutoLoader™ unit – into a Titan Krios™ cryo-electron microscope (FEI, Eindhoven, Netherlands), both equipped with a field emission gun. The accelerating voltages were 200 and 300 kV, respectively. Specimens were irradiated with a low electron dose (< 20 e$^-$/Å^2). Electron diffraction was used to check whether the frozen water embedding the sample was vitreous or crystalline. Crystalline sections were discarded. Micrographs were recorded with a TemCam-F416 (4k x 4k, 16 μpixel, CMOS camera, Tietz Video and Image Processing Systems, Gauting, Germany) or Ultrascan 4000 (4k x 4k, CCD mounted in front of GIF) from Gatan Company (Gatan Company, Pleasanton, CA, USA) at different magnifications. No image processing was performed.

4.5.19 Flow cytometry infection assay

Confluent 12-wells of HeLa cells were infected for flow cytometry-based infection assays. Pretreatment with inhibitors was performed for 15-60 min in DMEM. MVs ($2{\cdot}10^6$ pfu in 0.5 mL) were prepared in DMEM (+ inhibitors). After 30 min at 37 °C, cells were washed and overlayed with 1 mL full MEM (+ inhibitors). 4 h post infection, cells were prepared for flow cytometry. Cells were analysed using a BD FACSCalibur flow cytometer and the BD CellQuest Pro software or the FlowJo software package.

4.6 Acknowledgements

This work was in part funded by grants from EMBO, ETH Zurich, and the Swiss National Foundation (InfectX, Sinergia). CKEB was supported by the CINA, SystemX and SNF Sinergia Projects (CRSII3_125110/1). We thank Daniel Castaño-Diez for introducing Dynamo software, Mohamed Chami and Kenneth N. Goldie for help and advice with freeze fracture replica and plunge freezing experiments, respectively. We are grateful to Kenneth N. Goldie for critical reading of the manuscript.

Chapter 5

Conclusion and Outlook

5.1 Host cell entry of vaccinia virus EVs

Like all viruses, poxvirus MVs (matured virus) and EVs (enveloped virus) are metabolically inactive transport carriers of the viral genome and accessory enzymes. They are completely dependent on the cellular machinery to gain access to their site of replication, the cytosol. A summary of the entry processes of MVs and EVs is presented in Figure 5.1 (see page 130).

MV infection presumably represents the event that initiates primary infection of a host organism with a poxvirus. Depending on the poxvirus, primary infection may happen after inhalation of MV-containing material or after exposure of skin lesions to MVs [53]. By exposing phosphatidylserine (PS), MVs stimulate macropinocytosis in their host cells and are subsequently internalised with the bulk fluid. Acidification of macropinosomes possibly inactivates fusion inhibitory proteins in the MV membrane, which subsequently allow the entry fusion complex (EFC) to mediate fusion of the viral membrane with cellular membranes [239, 148, 152, 35]. It is possible that other mechanisms can regulate virus fusion or inactivation of fusion inhibitors because not all vaccinia virus (VACV) strains and not all other poxviruses undergo acid-induced fusion [150, 256].

Cell-associated and released EVs are thought to spread VACV infection within a host. While entry of cell-associated EVs on actin tails into adjacent cells has not yet been studied, this thesis focussed on the infection of host cells by free EVs. Infection of epithelial cells by free EVs presumably happens when infected cells release EVs into body fluids, which then infect new tissues within the organism. Since it is unlikely that medical intervention can prevent primary infection, spread of infection through body fluids is the step in a poxvirus infection that would need to be controlled to treat a dis-

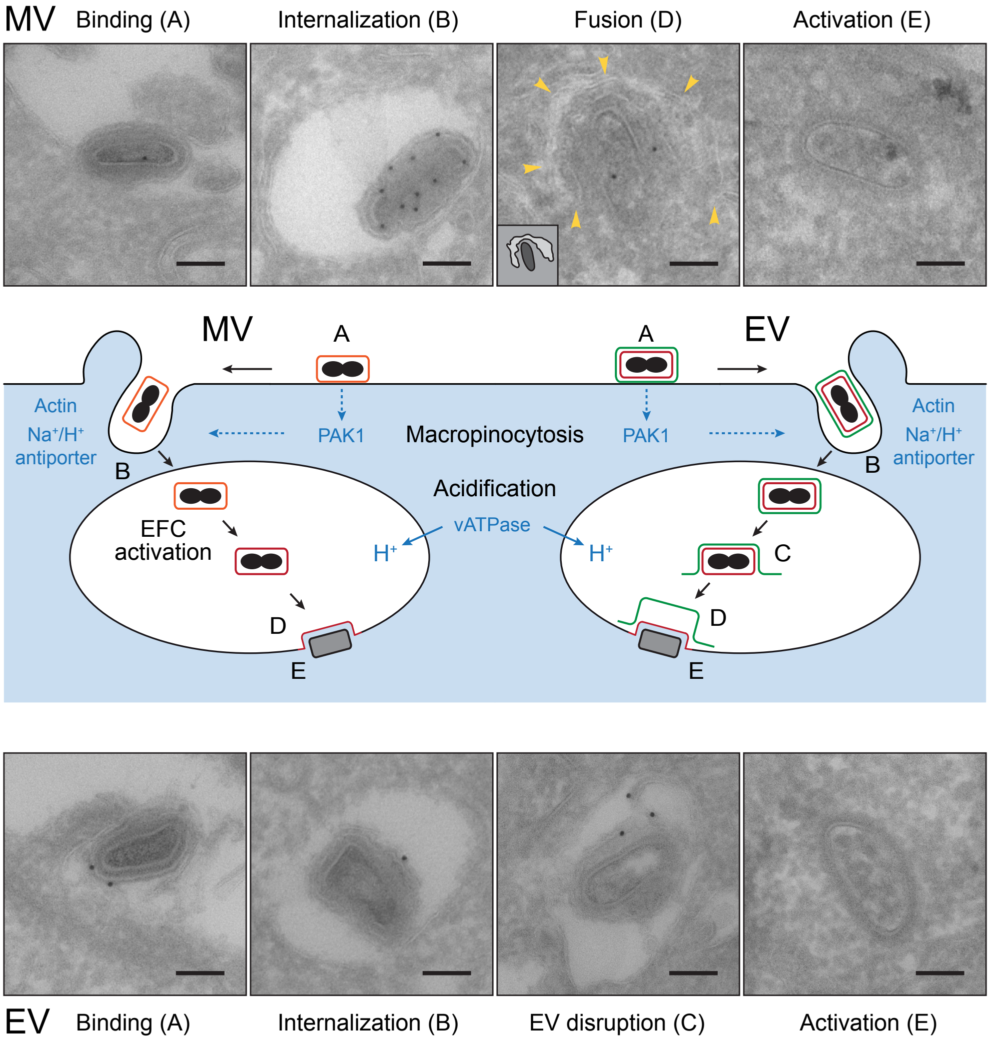

Figure 5.1 Visualisation of VACV pathway for MVs and EVs. VACV MVs and EVs enter host cells in a stepwise process that includes binding (A), internalisation (B) by macropinocytosis, as well as EFC activation and fusion (D) in the case of MVs, or EV membrane disruption (C), and fusion (D) in the case of EVs. Released cores are activated (E) and subsequently start early gene expression. Representative electron micrographs are shown for MVs (top) and EVs (bottom), EGFP-A5 is immuno-gold labelled in the case of MVs and F13-GFP in the case of EVs; scale bars = 100 nm. In top row image (D), a schematic of membranes and viral cores is inset. Critical cellular components are shown in blue, arrows with solid lines represent physical movement, arrows with dashed lines depict signalling events [211].

ease caused by poxviruses. We found that EVs – like MVs – actively trigger macropinocytosis to be internalised into host cells with both their membranes. However, they possibly induce macropinocytosis through a different mechanism than MVs. EV membranes are disrupted upon acidification of macropinosomes and thus exposes an MV-like particle that contains the EFC in the membrane. Since EVs lack the described fusion inhibitory complexes [246], the EFC may already be in an active state and subsequently mediate fusion. This would release the viral core into the host cell cytoplasm and allow for successful infection.

Fusion proteins of many viruses are sensitive to neutralising antibodies. While RNA viruses with a high mutation rate can evade the humoral immune response to some extent by mutation, this is not possible for DNA viruses that exhibit a low mutation rate. One strategy to protect fusion proteins from the humoral immune system is to adopt the active conformation only upon certain cues at the desired site of fusion. However, this still renders fusion proteins sensitive to neutralising antibodies that prevent the required conformational changes or block fusion sterically. Another strategy is to prevent exposure of viral fusion proteins to the humoral immune response. This may be accomplished by cell-to-cell spread that does not involve release of viral particles [203], or by intracellular long-distance transport, e.g. along axons as in the case of several neurotropic viruses [203]. Poxviruses have evolved another strategy: They produce infectious particles surrounded by two membranes. The second membrane of EVs shields critical components of the inner membrane from the humoral immune response and, by the incorporation of host complement control genes [251, 252], is even well protected against non-specifc destruction by the host complement system. A mechanism of EV entry that involves endocytosis of intact EVs is thus consistent with such a protective role of the EV membrane. EV membranes are only lost inside the macropinosomes of host cells, i.e. when the underlying MV-like particles are no longer accessible to the humoral immune system of the host.

It is at present unclear how VACV EVs trigger macropinocytosis. While both MV and EV infection requires the activity of EGFR, EV infection was not sensitive to the PS-binding protein annexin V, which blocks MV infections. This suggests that EVs trigger macropinocytosis through a different mechanism than MVs. Even though EV and WV membranes were reported to contain significant amounts of PS [226], this lipid is preferentially found in the cytosolic leaflet of cellular membranes and would therefore be expected to be in the inner leaflet of EV membranes. Theoretically, we cannot rule out that PS exposed in EV membranes was already bound by PS-binding proteins present in the serum, such as Gas6, and could therefore not be blocked

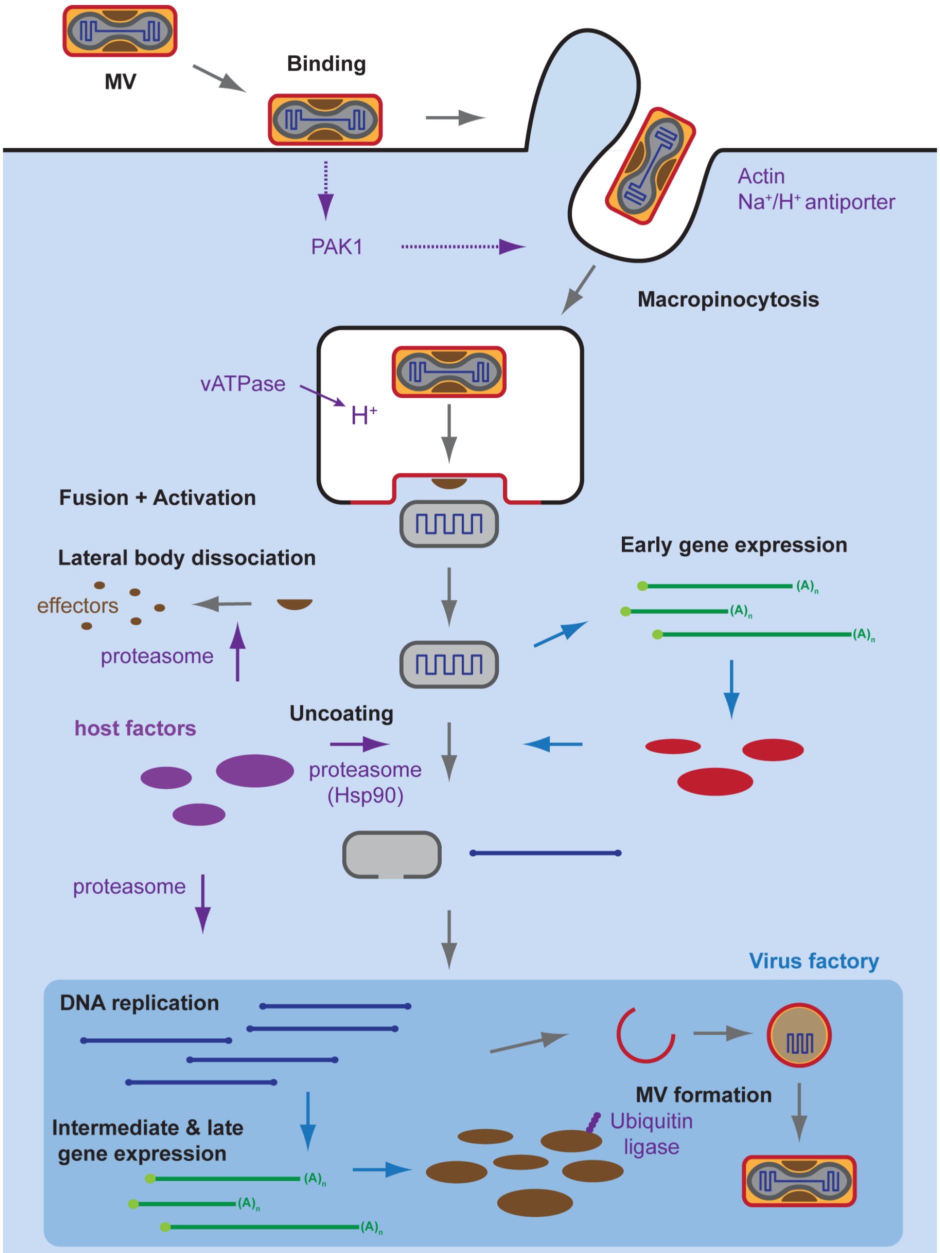

Figure 5.2 Entry pathway of VACV MVs and early/late replication steps. Purple = cellular components involved in the endocytic processes.

by annexin V. Since macropinocytosis is a signalling-induced process, it is possible that clustering of receptors triggers the respective signalling events. EVs have been shown to use different attachment factors than MVs [250] and those factors may be candidates for the triggering mechanism. However, they have not been identified yet and therefore cannot be tested.

The fate of newly formed macropinosomes, their maturation, and their cross-talk with the classical endosomal system is poorly characterised. Viruses have been used to define many endocytic pathway and allowed researchers to follow the fate of virions as traceable cargo [143]. While our EV infection experiments confirm that macropinosomes can be acidified by vATPases, VACV MVs rather than EVs should be used to further characterise the fate of macropinosomal cargo because they are easier to obtain and due to their stability comprise the more homogeneous and more defined macropinocytic cargo.

The molecular mechanism of EV disruption is not understood and needs further investigation. Rupture of continuous biological membranes is a process that is energetically highly unfavourable and is e.g. involved in endosomal escape of non-enveloped viruses [242], or in the proposed mechanism of action of some antimicrobial peptides [174]. A similar process was proposed to play a role in VACV crescent formation [41]. However, no molecular basis for the triggered rupture of membranes by proteins that are embedded in the membrane itself has been described. Intriguingly, electron micrographs suggest that disrupted membranes form an intact bilayer sheet that remains associated with the underlying particle [128]. This is in line with our observation that F13-GFP, which is inserted into the EV membrane via its palmitate moiety [84], and the transmembrane protein B5 remain associated with the underlying particle upon rupture. The employed mechanism therefore does not involve membrane solubilisation or a complete destabilisation of membranes, but rather a regulated process that opens the closed EV membrane and results in a membrane sheet.

EV disruption by low pH or by anionic polysaccharides may involve similar mechanisms because both require the EV protein A34. However, it cannot be ruled out that the only function of A34 is to recruit sufficient amounts of B5 to the EV membrane, which has also been shown to be required for EV disruption by GAGs [128]. Interestingly, EV neutralising antibodies directed against B5 were shown to block EV infection and comet tail formation in monolayers [4]. The latter process has been attributed to the formation of satellite plaques by EVs released into the medium by producer cells. Roberts *et al.* proposed that acidic residues in the membrane-proximal stalk of B5 are required for artificial EV disruption by anionic polysaccharides, although they do not show the successful incorporation of the generated B5 mutants into EVs [193]. The authors further demonstrated that the interaction between B5 and A34 was sensitive to large poly-anions or poly-cations. They speculated that the disruption of this interaction would release the negatively charged stalk region of B5 close to the membrane, which could destabilise membranes by electrostatic repulsion of negatively charged lipid head-groups.

Since many modifications of EV proteins result in reduced amounts of EVs and their analysis is rather complex, a reductionist approach to study EV disruption may be helpful. If EV membrane proteins such as B5 or A34 could be reconstituted in liposome membranes after heterologeous expression or purification from EV membranes, the protein requirements for membrane disruption upon different triggers could be studied.

We speculated that fusion of MV-like particles exposed after EV membrane disruption may not require additional hints since the fusion inhibitory proteins A25 and A26 are missing in EVs. However, it remains to be determined whether fusion of MV-like particles is regulated. Interestingly, infection of mostly disrupted EVs in the absence of MV-neutralising antibodies was still sensitive to inhibitors of macropinocytosis, but was not blocked by bafilomycin A1 (BafA, see Figure 5.2). This suggests that disrupted EVs were still endocytosed by macropinocytosis and did not fuse with the plasma membrane. However, it remains unclear whether the insensitivity towards bafilomycin A1 suggests acid-independent fusion, since MV infection in our hands was only mildly affected by bafilomycin A1, while we at the same time determined a clear pH optimum of 5.0 for fusion in our fusion assay.

While this thesis contributed to the understanding of the cellular entry pathway of VACV EVs, mechanistic details on the involved processes, i.e. macropinocytosis, acid mediated EV disruption, and fusion of MV-like particles, still demand further clarification. It remains to be seen to what extent our findings on the entry of free EVs hold true for cell-associated EVs that are projected to adjacent cells on the tip of actin tails. Furthermore EV as well as MV entry into polarised cells or cells embedded into a tissue need to be studied to fully understand the role of MVs and EVs *in vivo*.

Roughly summarised, there is a quite clear understanding how MVs and EVs using macropinocytosis to enter a host cell by non-specific uptake of fluids. However all further maturation and traffic steps of macropinocytosis as well as the connection with early / late endosomes are still unclear and must be examined in the future. In this context, VACV will be a powerful tool.

5.2 RNAi screening in VACV infection

The ubiquitin-proteasome protein degradation system is involved in many essential cellular processes including cell cycle regulation, cell differentiation, and the unfolded protein response [146]. Ubiquitylation is further a widely used post-translational protein modification that regulates many biological processes, including immune responses. The role of ubiquitin in immune regulation was originally uncovered. Recent studies have revealed crucial roles of ubiquitylation in many aspects of the immune system, including innate and adaptive immunity and antimicrobial autophagy. In addition, rising evidence indicates that (i) microbial pathogens exploit the ubiquitin pathway to evade the host immune system [111] and (ii) viruses use various strategies to hijack the ubiquitination pathway and target cellular proteins for degradation (or disruption of function) in order to evade cellular innate antiviral response [36]. It should be also noted however that the cellular autophagy machinery is not required for vaccinia virus replication and maturation [278].

As previously reported, inhibition of the ubiquitin-proteasome system prevents vaccinia virus DNA replication and expression of intermediate and late genes [201].

In our present study, our results strongly indicated that ubiquitination comes into play as an essential process already during the assembly of VACV particles in virus factories located in the cytoplasm of host cells. Core proteins undergo extensive K48-linked polyubiquitination. This is consistent with the accumulation of ubiquitin observed in poxvirus replication sites and the detection of ubiquitin within purified VACV particles. The polyubiquitination is probably an essential step for virus assembly.

5.3 Core activation

Most enveloped viruses that organise their genome in a capsid or core structure have to solve the same problem: assembly in producer cells and uncoating in newly infected cells occurs in the same cellular compartment. In most cases, viral cores undergo an irreversible maturation step at some point between initial assembly and uncoating that renders viral capsids or cores unstable and favours uncoating in newly infected cells. In rare cases, the compartment of capsid assembly itself may have different properties than the equivalent compartment during uncoating [79].

VACV MV and EV entry pathways converge when the VACV cores are deposited in the host cell cytosol by fusion. Immediately after fusion, cores undergo morphological changes described as activation. Those go along with the removal of lateral bodies, possibly reduction of disulfide-bonded core proteins, and onset of early gene expression. Therefore, a defined program of immediate early steps is already berthed in the core structure and does not require early gene expression. In other words, VACV cores and lateral bodies wrapped into the MV or MV-like membrane are metastable. A number of maturation steps that occur after membrane closure in immature virions (IV) (see Figure 1.3) have primed the resulting MV (or EV) for these processes. Maturation of MVs or MV-like particles results in the reorganisation of the packaged viral proteins, which transforms an IV filled with amorphous proteinaceous material and a DNA nucleoid into an MV with defined structures: a core that contains DNA-protein complexes surrounded by the core wall as well as two lateral bodies. On a molecular level, structural proteins are processed by two viral proteases and disulfide bonds are formed in core and membrane proteins. In addition, several viral proteins are phosphorylated during assembly or maturation and some of the incorporated viral proteins are post-translationally modified by ubiquitination.

A detailed knowledge of virus assembly and maturation would be required to fully understand the molecular mechanisms that underlay core activation. However, we found that cellular factors or the cytosolic environment are required for core activation and dissociation of lateral bodies from the incoming core. We established an *in vitro* system that includes acid-induced fusion of MVs with liposomes. This system may help to define the exact requirements for the observed processes.

Treatment of MVs with detergents and reduction of solvent-accessible disulfide bonds is not enough to dissociate lateral bodies from cores. However, lateral bodies could be removed from cores by a short treatment of *in vitro* cores with proteases such as trypsin or proteinase K [65, 108, 125]. Whether dissociation of lateral bodies from cores after fusion requires proteolytic processes or other cellular activities or components will be tested.

While it is imaginable that changes in the core structure are required to support early gene expression and prepare the core for uncoating, it is less clear what removal of lateral bodies does to the core or to the host cell. Lateral bodies could be a simple structural component of MVs or EVs, or they could negatively regulate activities in the viral core until the cytosol of the host cell is reached. In both cases, removal of the lateral bodies after penetration would be enough. Alternatively, lateral bodies could contain effector proteins that are released into the host cell cytosol. These factors could modify the host cell in an extent that supports infection, similar to tegument proteins of herpes viruses, which are fully formed and active and control viral entry, gene expression, and immune evasion [26, 25].

We have observed a number of changes that VACV cores undergo when they are released into the host cell cytosol by fusion. We are able to describe the early stages of poxvirus uncoating in more detail. Furthermore, we have identified F18 as a structural and dual-specific phosphatase VH1 as an effector component of VACV LBs and for the first time assign a function to these elusive viral structures.

Hence, we propose that LBs act as delivery containers for viral effector proteins that become active upon proteasome-dependent LB disassembly, and thus much earlier than early viral proteins. Decipherment of the molecular components and functions of LB factors will not only contribute to a deeper understanding of the early stages of the viral life cycle, but also help to understand how poxviruses modulate the immune system. Protein delivery via LBs may also open attractive possibilities to improve poxvirus-based vaccines or oncolytic viruses, and even allow delivery of proteins into cells that do not allow early gene expression.

5.4 Virus uncoating process

We found, that 6 core proteins F18, VP8, 4b, 4a, RNA pol 132, and RNA pol 147 were identified and confirmed to contain inter-molecular disulfide bonds. While proteins of similar molecular weight had been shown to occur in disulfide-bonded protein complexes before [108, 108], only VP8 and 4a had been identified and assigned to the respective gene [135].

Although not in our close thoughts, 4 viral MV membrane proteins, A27, D8, A26, and A25, were identified to contain intermolecular disulfide bonds. Intermolecular disulfide bonds in A26 [94], A27 [94], and D8 [135] have already been described and similarly, intramolecular disulfide bonds in L1 [216] and F9 [216] are known from literature.

At least two of the disulfide-bonded core proteins, F18 and 4b, were shown to be reduced after fusion and in the absence of viral gene expression. Another core protein that formed intermolecular disulfide bonds to other core proteins, VP8, however, did not become reduced. VP8 has been observed to be released from viral cores with the viral DNA during uncoating [178] and thus may be buried within the core and be impenetrable to solvent or oxidoreductases.

The finding that *in vitro* cores generated in 50 mM DTT and 1 % NP-40 still exhibit characteristics of cores in MVs (dumbbell shape, associated with lateral bodies) suggests that reduction of solvent-accessible core disulfide bonds alone is not sufficient for core activation and loss of lateral bodies. However, it remains to be determined to what extent core disulfide bonds indeed are reduced during this treatment. While disulfide bonds can be reduced when MV samples are boiled in sample buffer containing SDS and DTT, it is unclear if disulfide bonds are accessible to the reducing agents under non-denaturing conditions. Reduction of core proteins may also require the rearrangement of core components by other means, or the activity of cellular or viral oxidoreductases.

Worthy of note, the viral core protein A14 has been shown to form disulfide-bonded dimers in the lumenal domain of the virus [154] and was proposed to be one major component of the basal protein layer below the MV membrane by Ichihashi [104]. The basal protein layer has to be disrupted or dissolved in the line of core release and it may therefore be of interest to follow the redox state of this protein during entry as well.

To understand the role of disulfide-bonded core proteins and their reduction, it has to be more specifically analysed whether reduction coincides with morphological changes or transcriptional activity. Furthermore, it would be crucial to test whether reduction of core proteins requires cellular or viral proteins, or the reducing environment of the cytosol. More extensive fusion experiments of MVs with liposomes may take forward to follow core protein reduction under more controlled conditions.

Appendix A

Appendix

A.1 Plasmid

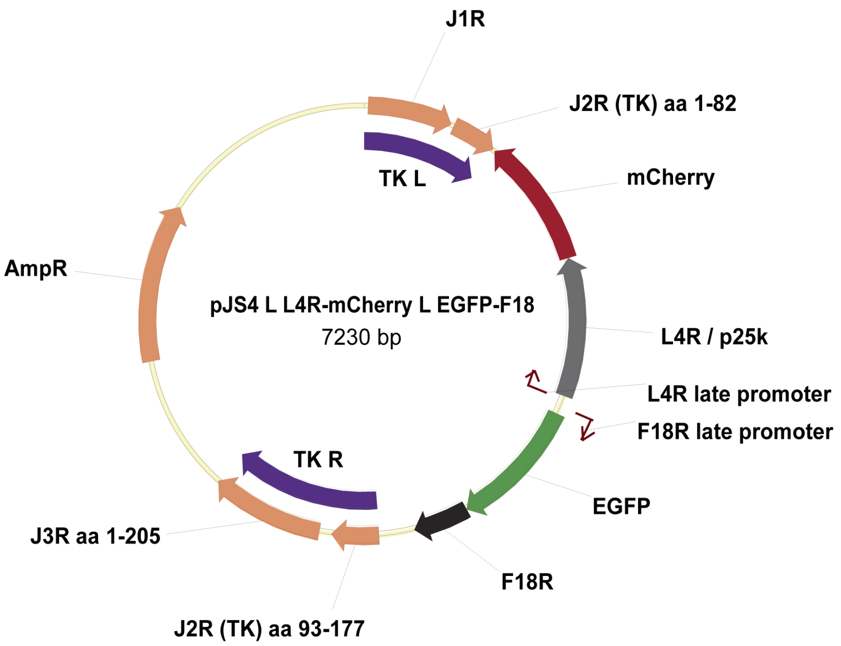

Figure A.1 Plasmid used to generate recombinant VACV strains by a combination of positive selection. L4R (VP8) here is under the control of a synthetic early / late vaccinia virus promoter, F18 is under the control of the late promoter. The purple areas (TK L and TK R) define the regions of the plasmid that are the homologue to the vaccinia virus genome and determine the insertion site. The genes in this range [J1, J2, and J3 (partially)] are also shown. J2, thymidine kinase is destroyed during the insertion, but not required for replication in cell culture. The coding sequences for the fluorescent fusions of F18 and VP8 are thus inserted in addition to the endogenous genes. F18 and EGFP-F18, as well as VP8 and VP8-mCherry, are therefore expressed simultaneously.

A.2 Hallway

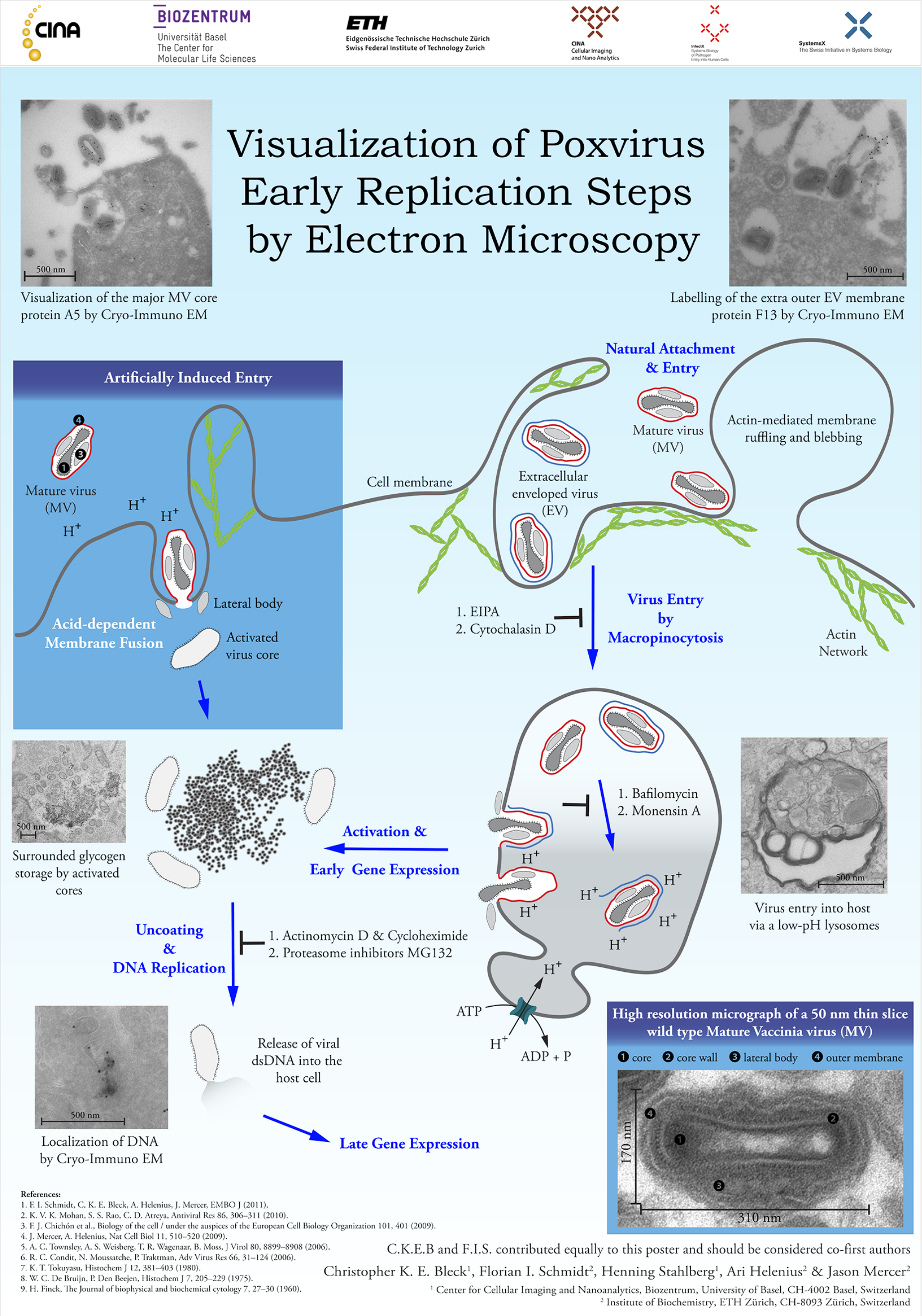

Visualization of Poxvirus Early Replication Steps by Electron Microscopy

Visualization of the major MV core protein A5 by Cryo-Immuno EM

Labelling of the extra outer EV membrane protein F13 by Cryo-Immuno EM

Artificially Induced Entry

Surrounded glycogen storage by activated cores

Virus entry into host via a low-pH lysosomes

Localization of DNA by Cryo-Immuno EM

High resolution micrograph of a 50 nm thin slice wild type Mature Vaccinia virus (MV)

❶ core ❷ core wall ❸ lateral body ❹ outer membrane

References:
1. F. I. Schmidt, C. K. E. Bleck, A. Helenius, J. Mercer, EMBO J (2011).
2. K. V. K. Mohan, S. S. Rao, C. D. Atreya, Antiviral Res 86, 306–311 (2010).
3. F. J. Chichón et al., Biology of the cell / under the auspices of the European Cell Biology Organization 101, 401 (2009).
4. J. Mercer, A. Helenius, Nat Cell Biol 11, 510–520 (2009).
5. A. C. Townsley, A. S. Weisberg, T. R. Wagenaar, B. Moss, J Virol 80, 8899–8908 (2006).
6. R. C. Condit, N. Moussatche, P. Traktman, Adv Virus Res 66, 31–124 (2006).
7. K. T. Tokuyasu, Histochem J 12, 381–403 (1980).
8. W. C. De Bruijn, P. Den Beejen, Histochem J 7, 205–229 (1975).
9. H. Finck, The Journal of biophysical and biochemical cytology 7, 27–30 (1960).

C.K.E.B and F.I.S. contributed equally to this poster and should be considered co-first authors

Christopher K. E. Bleck[1], Florian I. Schmidt[2], Henning Stahlberg[1], Ari Helenius[2] & Jason Mercer[2]
[1] Center for Cellular Imaging and Nanoanalytics, Biozentrum, University of Basel, CH-4002 Basel, Switzerland
[2] Institute of Biochemistry, ETH Zürich, CH-8093 Zürich, Switzerland

Figure A.2 Hallway Poster at C-CINA. Visualization of *Vaccinia virus* pathway.

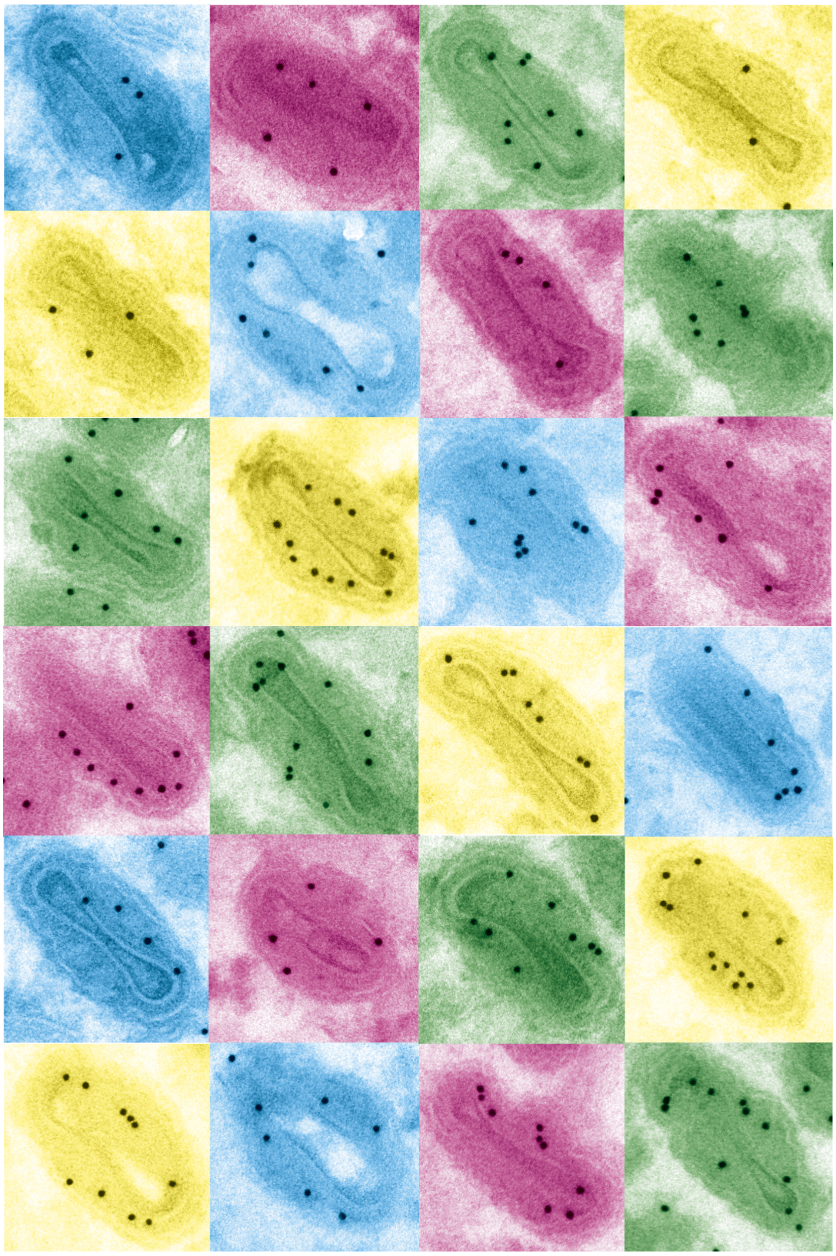

Figure A.3 CINA Hallway Poster, Arts & Science; A Homage to Andy Warhol; Immunogold-labelling of viral F18-protein on ultra-thin cryo sections (*Vaccinia virus*).

List of Figures

Bibliography

[1] L. P. Aggerbeck and T. Gulik-Krzywicki. Studies of lipoproteins by freeze-fracture and etching electron microscopy. *Methods in enzymology*, 128:457–472, 1986.

[2] A. Al-Amoudi, J.-J. Chang, A. Leforestier, A. McDowall, L. M. Salamin, L. P. O. Norlén, K. Richter, N. S. Blanc, D. Studer, and J. Dubochet. Cryo-electron microscopy of vitreous sections. *The EMBO journal*, 23(18):3583–3588, Sept. 2004.

[3] A. Al-Amoudi, D. Studer, and J. Dubochet. Cutting artefacts and cutting process in vitreous sections for cryo-electron microscopy. *Journal of structural biology*, 150(1):109–121, Apr. 2005.

[4] L. Aldaz-Carroll, J. C. Whitbeck, M. Ponce de Leon, H. Lou, L. K. Pannell, J. Lebowitz, C. Fogg, C. L. White, B. Moss, G. H. Cohen, and R. J. Eisenberg. Physical and immunological characterization of a recombinant secreted form of the membrane protein encoded by the Vaccinia Virus L1R gene. *Virology*, 341(1):59–71, Oct. 2005.

[5] B. Y. Amegadzie, J. R. Sisler, and B. Moss. Frame-shift mutations within the Vaccinia Virus a-type inclusion protein gene. *Virology*, 186(2):777–782, 1992.

[6] B. Amstutz, M. Gastaldelli, S. Kälin, N. Imelli, K. Boucke, E. Wandeler, J. Mercer, S. Hemmi, and U. F. Greber. Subversion of CtBP1-controlled macropinocytosis by human adenovirus serotype 3. *The EMBO journal*, 27(7):956–969, Apr. 2008.

[7] C. Ansarah-Sobrinho and B. Moss. Role of the I7 protein in proteolytic processing of Vaccinia Virus membrane and core components. *The Journal of Virology*, 78(12):6335–6343, June 2004.

[8] C. Ansarah-Sobrinho and B. Moss. Vaccinia Virus G1 protein, a predicted metalloprotease, is essential for morphogenesis of infectious viri-

ons but not for cleavage of major core proteins. *The Journal of Virology*, 78(13):6855–6863, July 2004.

[9] Y. Arakawa, J. V. Cordeiro, S. Schleich, T. P. Newsome, and M. Way. The release of Vaccinia Virus from infected cells requires RhoA-mDia modulation of cortical actin. *Cell host & microbe*, 1(3):227–240, May 2007.

[10] M. J. Ashwood-Smith and C. Warby. Studies on the molecular weight and cryoprotective properties of polyvinylpyrrolidone and dextran with bacteria and erythrocytes. *Cryobiology*, 8(5):453–464, Oct. 1971.

[11] M. W. Bahar, S. C. Graham, R. A.-J. Chen, S. Cooray, G. L. Smith, D. I. Stuart, and J. M. Grimes. How Vaccinia Virus has evolved to subvert the host immune response. *Journal of structural biology*, 175(2):127–134, Aug. 2011.

[12] B. W. Banfield, Y. Leduc, L. Esford, K. Schubert, and F. Tufaro. Sequential isolation of proteoglycan synthesis mutants by using herpes simplex virus as a selective agent: evidence for a proteoglycan-independent virus entry pathway. *The Journal of Virology*, 69(6):3290–3298, June 1995.

[13] L. Banks, D. Pim, and M. Thomas. Viruses and the 26S proteasome: hacking into destruction. *Trends in biochemical sciences*, 28(8):452–459, Aug. 2003.

[14] M. Barry, N. van Buuren, K. Burles, K. Mottet, Q. Wang, and A. Teale. Poxvirus exploitation of the ubiquitin-proteasome system. *Viruses*, 2(10):2356–2380, Oct. 2010.

[15] P. M. Beard. Vaccinia Virus kelch protein A55 is a 64 kDa intracellular factor that affects virus-induced cytopathic effect and the outcome of infection in a murine intradermal model. *The Journal of general virology*, 87(6):1521–1529, July 2006.

[16] Z. Bengali, A. C. Townsley, and B. Moss. Vaccinia Virus strain differences in cell attachment and entry. *Virology*, 389(1-2):132–140, June 2009.

[17] M. R.-E.-I. Benhnia, M. M. McCausland, J. Moyron, J. Laudenslager, S. Granger, S. Rickert, L. Koriazova, R. Kubo, S. Kato, and S. Crotty. Vaccinia Virus extracellular enveloped virion neutralization in vitro

and protection in vivo depend on complement. *Journal of virology*, 83(3):1201–1215, Feb. 2009.

[18] H. Bisht, A. S. Weisberg, and B. Moss. Vaccinia Virus l1 protein is required for cell entry and membrane fusion. *Journal of virology*, 82(17):8687–8694, Sept. 2008.

[19] C. Bleck, A. Merz, M. G. Gutierrez, P. Walther, J. Dubochet, B. Zuber, and G. Griffiths. Comparison of different methods for thin section EM analysis of Mycobacterium smegmatis. *Journal of microscopy*, 237(1):23–38, Jan. 2010.

[20] O. Boyd, A. L. Strahl, C. Rodeffer, R. C. Condit, and N. Moussatché. Temperature-sensitive mutant in the Vaccinia Virus E6 protein produce virions that are transcriptionally inactive. *Virology*, 399(2):221–230, Apr. 2010.

[21] O. Boyd, P. C. Turner, R. W. Moyer, R. C. Condit, and N. Moussatche. The E6 protein from Vaccinia Virus is required for the formation of immature virions. *Virology*, 399(2):201–211, Apr. 2010.

[22] E. Brown, T. G. Senkevich, and B. Moss. Vaccinia Virus F9 virion membrane protein is required for entry but not virus assembly, in contrast to the related L1 protein. *The Journal of Virology*, 80(19):9455–9464, Oct. 2006.

[23] M. R. Bubb, A. M. Senderowicz, E. A. Sausville, K. L. Duncan, and E. D. Korn. Jasplakinolide, a cytotoxic natural product, induces actin polymerization and competitively inhibits the binding of phalloidin to F-actin. *The Journal of biological chemistry*, 269(21):14869–14871, May 1994.

[24] C. M. Byrd, T. C. Bolken, and D. E. Hruby. Molecular dissection of the Vaccinia Virus I7L core protein proteinase. *The Journal of Virology*, 77(20):11279–11283, Oct. 2003.

[25] G. Campadelli-Fiume, L. Menotti, E. Avitabile, and T. Gianni. Viral and cellular contributions to herpes simplex virus entry into the cell. *Current opinion in virology*, 2(1):28–36, Feb. 2012.

[26] G. Cardone, J. B. Heymann, N. Cheng, B. L. Trus, and A. C. Steven. Procapsid assembly, maturation, nuclear exit: dynamic steps in the production of infectious herpesvirions. *Advances in experimental medicine and biology*, 726:423–439, 2012.

[27] A. E. Carpenter, T. R. Jones, M. R. Lamprecht, C. Clarke, I. H. Kang, O. Friman, D. A. Guertin, J. H. Chang, R. A. Lindquist, J. Moffat, P. Golland, and D. M. Sabatini. CellProfiler: image analysis software for identifying and quantifying cell phenotypes. *Genome biology*, 7(10):R100, 2006.

[28] D. S. Carroll, G. L. Emerson, Y. Li, S. Sammons, V. Olson, M. Frace, Y. Nakazawa, C. P. Czerny, M. Tryland, J. Kolodziejek, N. Nowotny, M. Olsen-Rasmussen, M. Khristova, D. Govil, K. Karem, I. K. Damon, and H. Meyer. Chasing Jenner's vaccine: revisiting cowpox virus classification. *PLoS ONE*, 6(8):e23086, 2011.

[29] G. C. Carter, M. Law, M. Hollinshead, and G. L. Smith. Entry of the Vaccinia Virus intracellular mature virion and its interactions with glycosaminoglycans. *The Journal of general virology*, 86(Pt 5):1279–1290, May 2005.

[30] G. C. Carter, G. Rodger, B. J. Murphy, M. Law, O. Krauss, M. Hollinshead, and G. L. Smith. Vaccinia Virus cores are transported on microtubules. *The Journal of general virology*, 84(Pt 9):2443–2458, Sept. 2003.

[31] D. Castaño-Diez, M. Kudryashev, M. Arheit, and H. Stahlberg. Dynamo: A flexible, user-friendly development tool for subtomogram averaging of cryo-EM data in high-performance computing environments. *Journal of structural biology*, Jan. 2012.

[32] A. Chahroudi, R. Chavan, N. Kozyr, N. Koyzr, E. K. Waller, G. Silvestri, and M. B. Feinberg. Vaccinia Virus tropism for primary hematolymphoid cells is determined by restricted expression of a unique virus receptor. *The Journal of Virology*, 79(16):10397–10407, Aug. 2005.

[33] S. Chakrabarti, J. R. Sisler, and B. Moss. Compact, synthetic, Vaccinia Virus early/late promoter for protein expression. Technical report, National Institute of Allergy and Infectious Diseases, National Institutes of Health, Bethesda, MD 20892-0445, USA., Dec. 1997.

[34] A. Chang and D. H. Metz. Further investigations on the mode of entry of Vaccinia Virus into cells. *The Journal of general virology*, 32(2):275–282, Aug. 1976.

[35] S.-J. Chang, Y.-X. Chang, R. Izmailyan, Y.-L. Tang, and W. Chang. Vaccinia Virus A25 and A26 proteins are fusion suppressors for mature

virions and determine strain-specific virus entry pathways into HeLa, CHO-K1, and L cells. *Journal of virology*, 84(17):8422–8432, Sept. 2010.

[36] M. Chen and D. Gerlier. Viral hijacking of cellular ubiquitination pathways as an anti-innate immunity strategy. *Viral immunology*, 19(3):349–362, 2006.

[37] S. Cherry. What have RNAi screens taught us about viral-host interactions? *Current opinion in microbiology*, 12(4):446–452, Aug. 2009.

[38] F. J. Chichón, M. J. Rodríguez, C. Risco, A. Fraile-Ramos, J. J. Fernández, M. Estéban, and J. L. Carrascosa. Membrane remodelling during Vaccinia Virus morphogenesis. *Biology of the cell / under the auspices of the European Cell Biology Organization*, 101(7):401, July 2009.

[39] P.-L. Chiu, M. D. Pagel, J. Evans, H.-T. Chou, X. Zeng, B. Gipson, H. Stahlberg, and C. M. Nimigean. The structure of the prokaryotic cyclic nucleotide-modulated potassium channel MloK1 at 16 A resolution. *Structure (London, England : 1993)*, 15(9):1053–1064, Sept. 2007.

[40] W.-L. Chiu, C.-L. Lin, M.-H. Yang, D.-L. M. Tzou, and W. Chang. Vaccinia Virus 4c (A26L) protein on intracellular mature virus binds to the extracellular cellular matrix laminin. *The Journal of Virology*, 81(5):2149–2157, 2007.

[41] P. Chlanda, M. A. Carbajal, M. Cyrklaff, G. Griffiths, and J. Krijnse Locker. Membrane rupture generates single open membrane sheets during Vaccinia Virus assembly. *Cell host & microbe*, 6(1):81–90, July 2009.

[42] Y. S. Cho, S. Challa, D. Moquin, R. Genga, T. D. Ray, M. Guildford, and F. K.-M. Chan. Phosphorylation-driven assembly of the RIP1-RIP3 complex regulates programmed necrosis and virus-induced inflammation. *Cell*, 137(6):1112–1123, July 2009.

[43] C.-S. Chung, C.-H. Chen, M.-Y. Ho, C.-Y. Huang, C.-L. Liao, and W. Chang. Vaccinia Virus proteome: identification of proteins in Vaccinia Virus intracellular mature virion particles. *The Journal of Virology*, 80(5):2127–2140, Mar. 2006.

[44] C. S. Chung, J. C. Hsiao, Y. S. Chang, and W. Chang. A27L protein mediates Vaccinia Virus interaction with cell surface heparan sulfate. *The Journal of Virology*, 72(2):1577–1585, Feb. 1998.

[45] M. J. Clague and S. Urbé. Ubiquitin: same molecule, different degradation pathways. *Cell*, 143(5):682–685, Nov. 2010.

[46] R. C. Condit, N. Moussatche, and P. Traktman. In a nutshell: structure and assembly of the vaccinia virion. *Advances in virus research*, 66:31–124, 2006.

[47] J. A. Cooper. Effects of cytochalasin and phalloidin on actin. *The Journal of cell biology*, 105(4):1473–1478, Oct. 1987.

[48] C. B. Coyne, K. S. Kim, and J. M. Bergelson. Poliovirus entry into human brain microvascular cells requires receptor-induced activation of SHP-2. *The EMBO journal*, 26(17):4016–4028, Sept. 2007.

[49] S. Cudmore, R. Blasco, R. Vincentelli, M. Esteban, B. Sodeik, G. Griffiths, and J. Krijnse Locker. A Vaccinia Virus core protein, p39, is membrane associated. *The Journal of Virology*, 70(10):6909–6921, Oct. 1996.

[50] M. Cyrklaff, C. Risco, J. J. Fernández, M. V. Jiménez, M. Estéban, W. Baumeister, and J. L. Carrascosa. Cryo-electron tomography of Vaccinia Virus. *Proceedings of the National Academy of Sciences of the United States of America*, 102(8):2772–2777, Feb. 2005.

[51] S. Dales. The uptake and development of Vaccinia Virus in strain L cells followed with labeled viral deoxyribonucleic acid. *The Journal of cell biology*, 18:51–72, July 1963.

[52] E.-M. Damm, L. Pelkmans, J. Kartenbeck, A. Mezzacasa, T. Kurzchalia, and A. Helenius. Clathrin- and caveolin-1-independent endocytosis: entry of simian virus 40 into cells devoid of caveolae. *The Journal of cell biology*, 168(3):477–488, Jan. 2005.

[53] I. K. Damon. *Poxviruses*, volume 2 of *Fields Virology*. Wolters Kluwer Health/Lippincott Williams & Wilkins, Philadelphia, 5th edition, Jan. 2007.

[54] S. P. Davies, H. Reddy, M. Caivano, and P. Cohen. Specificity and mechanism of action of some commonly used protein kinase inhibitors. *The Biochemical journal*, 351(Pt 1):95–105, Oct. 2000.

[55] E. de Vries, D. M. Tscherne, M. J. Wienholts, V. Cobos-Jiménez, F. Scholte, A. García-Sastre, P. J. M. Rottier, and C. A. M. de Haan. Dissection of the influenza A virus endocytic routes reveals macropinocytosis as an alternative entry pathway. *PLoS pathogens*, 7(3):e1001329, Mar. 2011.

[56] S. W. Deacon, A. Beeser, J. A. Fukui, U. E. E. Rennefahrt, C. Myers, J. Chernoff, and J. R. Peterson. An isoform-selective, small-molecule inhibitor targets the autoregulatory mechanism of p21-activated kinase. *Chemistry & biology*, 15(4):322–331, Apr. 2008.

[57] M. Derrien, A. Punjabi, M. Khanna, O. Grubisha, and P. Traktman. Tyrosine phosphorylation of A17 during Vaccinia Virus infection: involvement of the H1 phosphatase and the F10 kinase. *Journal of virology*, 73(9):7287–7296, Sept. 1999.

[58] D. B. Di Giulio and P. B. Eckburg. Human monkeypox: an emerging zoonosis. *The Lancet infectious diseases*, 4(1):15–25, Feb. 2004.

[59] V. Doceul, M. Hollinshead, L. van der Linden, and G. L. Smith. Repulsion of superinfecting virions: a mechanism for rapid virus spread. *Science (New York, NY)*, 327(5967):873–876, Feb. 2010.

[60] M. P. Dodding, T. P. Newsome, L. M. Collinson, C. Edwards, and M. Way. An E2-F12 complex is required for intracellular enveloped virus morphogenesis during vaccinia infection. *Cellular microbiology*, 11(5):808–824, May 2009.

[61] M. P. Dodding and M. Way. Coupling viruses to dynein and kinesin-1. *The EMBO journal*, 30(17):3527–3539, Aug. 2011.

[62] G. J. Doherty and H. T. McMahon. Mechanisms of endocytosis. *Annual review of biochemistry*, 78:857–902, 2009.

[63] A. Domi and G. Beaud. The punctate sites of accumulation of Vaccinia Virus early proteins are precursors of sites of viral DNA synthesis. *The Journal of general virology*, 81(Pt 5):1231–1235, June 2000.

[64] A. K. Earley, W. M. Chan, and B. M. Ward. The Vaccinia Virus B5 protein requires A34 for efficient intracellular trafficking from the endoplasmic reticulum to the site of wrapping and incorporation into progeny virions. *Journal of virology*, 82(5):2161–2169, Mar. 2008.

[65] K. B. Easterbrook. Controlled degradation of vaccinia virions in vitro: an electron microscopic study. *Journal of ultrastructure research*, 14(5):484–496, Mar. 1966.

[66] D. A. Eppstein, Y. V. Marsh, A. B. Schreiber, S. R. Newman, G. J. Todaro, and J. J. Nestor. Epidermal growth factor receptor occupancy inhibits Vaccinia Virus infection. *Nature*, 318(6047):663–665, Feb. 1985.

[67] M. A. Epstein. A technique for transferring cells prepared on Formvar coated slides to electron microscope specimen grids. *Journal. Royal Microscopical Society (Great Britain)*, 75(2):100–102, Jan. 1956.

[68] S. Essbauer, H. Meyer, M. Porsch-Ozcürümez, and M. Pfeffer. Long-lasting stability of Vaccinia Virus (orthopoxvirus) in food and environmental samples. *Zoonoses and public health*, 54(3-4):118–124, 2007.

[69] V. A. Fadok, D. L. Bratton, A. Konowal, P. W. Freed, J. Y. Westcott, and P. M. Henson. Macrophages that have ingested apoptotic cells in vitro inhibit proinflammatory cytokine production through autocrine/paracrine mechanisms involving TGF-beta, PGE2, and PAF. *The Journal of clinical investigation*, 101(4):890–898, Feb. 1998.

[70] F. Fenner. The biological characters of several strains of vaccinia, cowpox and rabbitpox viruses. *Virology*, 5(3):502–529, June 1958.

[71] B. Fields, D. M. Knipe, and P. Howley. *Fields Virology*. Knipe, Fields Virology. Wolters Kluwer Health/Lippincott Williams & Wilkins, 2007.

[72] R. S. Flannagan, V. Jaumouillé, and S. Grinstein. The cell biology of phagocytosis. *Annual review of pathology*, 7:61–98, 2012.

[73] C. H. Foo, H. Lou, J. C. Whitbeck, M. Ponce de Leon, D. Atanasiu, R. J. Eisenberg, and G. H. Cohen. Vaccinia Virus L1 binds to cell surfaces and blocks virus entry independently of glycosaminoglycans. *Virology*, 385(2):368–382, Mar. 2009.

[74] F. Frischknecht, V. Moreau, S. Röttger, S. Gonfloni, I. Reckmann, G. Superti-Furga, and M. Way. Actin-based motility of Vaccinia Virus mimics receptor tyrosine kinase signalling. *Nature*, 401(6756):926–929, Oct. 1999.

[75] G. C. Froggatt, G. L. Smith, and P. M. Beard. Vaccinia Virus gene F3L encodes an intracellular protein that affects the innate immune

response. *The Journal of general virology*, 88(Pt 7):1917–1921, July 2007.

[76] Y. Gao, J. Xing, M. Streuli, T. L. Leto, and Y. Zheng. Trp(56) of rac1 specifies interaction with a subset of guanine nucleotide exchange factors. *The Journal of biological chemistry*, 276(50):47530–47541, Dec. 2001.

[77] M. M. Geada, I. Galindo, M. M. Lorenzo, B. Perdiguero, and R. Blasco. Movements of Vaccinia Virus intracellular enveloped virions with GFP tagged to the F13L envelope protein. *The Journal of general virology*, 82(Pt 11):2747–2760, Nov. 2001.

[78] T. S. Gomez and D. D. Billadeau. A FAM21-containing WASH complex regulates retromer-dependent sorting. *Developmental cell*, 17(5):699–711, Nov. 2009.

[79] U. F. Greber, I. Singh, and A. Helenius. Mechanisms of virus uncoating. *Trends in microbiology*, 2(2):52–56, Feb. 1994.

[80] J. M. Griffith and G. Posthuma. A reliable and convenient method to store ultrathin thawed cryosections prior to immunolabeling. *The journal of histochemistry and cytochemistry : official journal of the Histochemistry Society*, 50(1):57–62, Dec. 2002.

[81] G. Griffiths, R. Back, and M. Marsh. A quantitative analysis of the endocytic pathway in baby hamster kidney cells. *The Journal of cell biology*, 109(6 Pt 1):2703–2720, Nov. 1989.

[82] G. Griffiths, B. Burke, and J. M. Lucocq. *Fine Structure Immunocytochemistry.* Dec. 1993.

[83] G. Griffiths and H. Hoppeler. Quantitation in immunocytochemistry: correlation of immunogold labeling to absolute number of membrane antigens. *The journal of histochemistry and cytochemistry : official journal of the Histochemistry Society*, 34(11):1389–1398, Nov. 1986.

[84] D. W. Grosenbach, D. O. Ulaeto, and D. E. Hruby. Palmitylation of the Vaccinia Virus 37-kDa major envelope antigen. Identification of a conserved acceptor motif and biological relevance. *The Journal of biological chemistry*, 272(3):1956–1964, Jan. 1997.

[85] M. Gschwendt, H. J. Müller, K. Kielbassa, R. Zang, W. Kittstein, G. Rincke, and F. Marks. Rottlerin, a novel protein kinase inhibitor.

Biochemical and biophysical research communications, 199(1):93–98, Feb. 1994.

[86] M. G. Gustafsson. Surpassing the lateral resolution limit by a factor of two using structured illumination microscopy. *Journal of microscopy*, 198(Pt 2):82–87, May 2000.

[87] D. J. Hakes, K. J. Martell, W. G. Zhao, R. F. Massung, J. J. Esposito, and J. E. Dixon. A protein phosphatase related to the Vaccinia Virus VH1 is encoded in the genomes of several orthopoxviruses and a baculovirus. *Proceedings of the National Academy of Sciences of the United States of America*, 90(9):4017–4021, Apr. 2005.

[88] S. C. Harrison, B. Alberts, E. Ehrenfeld, L. Enquist, H. Fineberg, S. L. McKnight, B. Moss, M. O'Donnell, H. Ploegh, S. L. Schmid, K. P. Walter, and J. Theriot. Discovery of antivirals against smallpox. *Proceedings of the National Academy of Sciences of the United States of America*, 101(31):11178–11192, Aug. 2004.

[89] J. E. Heuser. Deep-etch EM reveals that the early poxvirus envelope is a single membrane bilayer stabilized by a geodetic "honeycomb" surface coat. *The Journal of cell biology*, 169(2):269–283, Apr. 2005.

[90] D. Hoekstra, T. de Boer, K. Klappe, and J. Wilschut. Fluorescence method for measuring the kinetics of fusion between biological membranes. *Biochemistry*, 23(24):5675–5681, Nov. 1984.

[91] P. R. Hoffmann, A. M. deCathelineau, C. A. Ogden, Y. Leverrier, D. L. Bratton, D. L. Daleke, A. J. Ridley, V. A. Fadok, and P. M. Henson. Phosphatidylserine (PS) induces PS receptor-mediated macropinocytosis and promotes clearance of apoptotic cells. *The Journal of cell biology*, 155(4):649–659, Nov. 2001.

[92] M. Hollinshead, A. Vanderplasschen, G. L. Smith, and D. J. Vaux. Vaccinia Virus intracellular mature virions contain only one lipid membrane. *The Journal of Virology*, 73(2):1503–1517, Feb. 1999.

[93] K. M. Honeychurch, G. Yang, R. Jordan, and D. E. Hruby. The Vaccinia Virus F13L YPPL motif is required for efficient release of extracellular enveloped virus. *The Journal of Virology*, 81(13):7310–7315, July 2007.

[94] A. R. Howard, T. G. Senkevich, and B. Moss. Vaccinia Virus A26 and A27 proteins form a stable complex tethered to mature virions by

association with the A17 transmembrane protein. *Journal of virology*, 82(24):12384–12391, 2008.

[95] A. R. Howard, A. S. Weisberg, and B. Moss. Congregation of orthopoxvirus virions in cytoplasmic A-type inclusions is mediated by interactions of a bridging protein (A26p) with a matrix protein (ATIp) and a virion membrane-associated protein (A27p). *Journal of virology*, 84(15):7592–7602, Aug. 2010.

[96] J. C. Hsiao, C. S. Chung, and W. Chang. Cell surface proteoglycans are necessary for A27L protein-mediated cell fusion: identification of the N-terminal region of A27L protein as the glycosaminoglycan-binding domain. *The Journal of Virology*, 72(10):8374–8379, Oct. 1998.

[97] J. C. Hsiao, C. S. Chung, and W. Chang. Vaccinia Virus envelope D8L protein binds to cell surface chondroitin sulfate and mediates the adsorption of intracellular mature virions to cells. *The Journal of Virology*, 73(10):8750–8761, Oct. 1999.

[98] C. Huang, W. A. Samsonoff, and A. Grzelecki. Vaccinia Virus recombinants expressing an 11-kilodalton beta-galactosidase fusion protein incorporate active beta-galactosidase in virus particles. *Journal of virology*, 62(10):3855, Oct. 1988.

[99] C.-Y. Huang, T.-Y. Lu, C.-H. Bair, Y.-S. Chang, J.-K. Jwo, and W. Chang. A novel cellular protein, VPEF, facilitates Vaccinia Virus penetration into HeLa cells through fluid phase endocytosis. *Journal of virology*, 82(16):7988–7999, Aug. 2008.

[100] D. W. Huang, B. T. Sherman, and R. A. Lempicki. Systematic and integrative analysis of large gene lists using DAVID bioinformatics resources. *Nature protocols*, 4(1):44–57, 2009.

[101] J. Huotari and A. Helenius. Endosome maturation. *The EMBO journal*, 30(17):3481–3500, 2011.

[102] M. Husain, A. S. Weisberg, and B. Moss. Resistance of a Vaccinia Virus A34R deletion mutant to spontaneous rupture of the outer membrane of progeny virions on the surface of infected cells. *Virology*, 366(2):424–432, Sept. 2007.

[103] J.-K. Hyun, C. Accurso, M. Hijnen, P. Schult, A. Pettikiriarachchi, A. K. Mitra, and F. Coulibaly. Membrane remodeling by the double-barrel scaffolding protein of poxvirus. *PLoS pathogens*, 7(9):e1002239, Sept. 2011.

[104] Y. Ichihashi. Unit Complex of vaccinia polypeptides linked by disulfide bridges. *Virology*, 113(1):277–284, Aug. 1981.

[105] Y. Ichihashi and S. Dales. Biogenesis of poxviruses: Interrelationship between hemagglutinin production and polykaryocytosis. *Virology*, 46(3):533–543, Dec. 1971.

[106] Y. Ichihashi and M. Oie. The activation of Vaccinia Virus infectivity by the transfer of phosphatidylserine from the plasma membrane. *Virology*, 130(2):306–317, Oct. 1983.

[107] Y. Ichihashi and M. Oie. Neutralizing epitope on penetration protein of Vaccinia Virus. *Virology*, 220(2):491–494, June 1996.

[108] Y. Ichihashi, M. Oie, and T. Tsuruhara. Location of DNA-binding proteins and disulfide-linked proteins in Vaccinia Virus structural elements. *Journal of virology*, 50(3):929–938, June 1984.

[109] L. M. Iyer, S. Balaji, E. V. Koonin, and L. Aravind. Evolutionary genomics of nucleo-cytoplasmic large DNA viruses. *Virus research*, 117(1):156–184, Apr. 2006.

[110] R. A. Izmailyan, C.-Y. Huang, S. Mohammad, S. N. Isaacs, and W. Chang. The envelope G3L protein is essential for entry of Vaccinia Virus into host cells. *The Journal of Virology*, 80(17):8402–8410, Sept. 2006.

[111] X. Jiang and Z. J. Chen. The role of ubiquitylation in immune defence and pathogen evasion. *Nature reviews Immunology*, 12(1):35–48, Jan. 2012.

[112] W. K. Joklik. The interacellular uncoating of poxvirus DNA. II. The molecular basis of the uncoating process. *Journal of molecular biology*, 8:277–288, Mar. 1964.

[113] W. K. Joklik. The intracellular uncoating of poxvirus DNA. I. The fate of radioactively-labeled rabbitpox virus. *Journal of molecular biology*, 8:263–276, Mar. 1964.

[114] W. K. Joklik and Y. Becker. The replication and coating of Vaccinia DNA. *Journal of molecular biology*, 10:452–474, Dec. 1964.

[115] S. Kälin, B. Amstutz, M. Gastaldelli, N. Wolfrum, K. Boucke, M. Havenga, F. DiGennaro, N. Liska, S. Hemmi, and U. F. Greber.

Macropinocytotic uptake and infection of human epithelial cells with species B2 adenovirus type 35. *Journal of virology*, 84(10):5336–5350, May 2010.

[116] S. Y. Kao and W. R. Bauer. Biosynthesis and phosphorylation of Vaccinia Virus structural protein VP11. *Virology*, 159(2):399–407, Aug. 1987.

[117] J. Kates and J. Beeson. Ribonucleic acid synthesis in Vaccinia Virus. I. The mechanism of synthesis and release of RNA in vaccinia cores. *Journal of molecular biology*, 50(1):1–18, June 1970.

[118] S. E. M. Kato, R. C. Condit, and N. Moussatché. The Vaccinia Virus E8R gene product is required for formation of transcriptionally active virions. *Virology*, 367(2):398–412, Oct. 2007.

[119] G. C. Katsafanas and B. Moss. Colocalization of Transcription and Translation within Cytoplasmic Poxvirus Factories Coordinates Viral Expression and Subjugates Host Functions. *Cell host & microbe*, 2(4):221–228, Oct. 2007.

[120] M. C. Kerr and R. D. Teasdale. Defining macropinocytosis. *Traffic (Copenhagen, Denmark)*, 10(4):364–371, Apr. 2009.

[121] E. Kobayashi, H. Nakano, M. Morimoto, and T. Tamaoki. Calphostin C (UCN-1028C), a novel microbial compound, is a highly potent and specific inhibitor of protein kinase C. *Biochemical and biophysical research communications*, 159(2):548–553, Mar. 1989.

[122] M. Koivusalo, C. Welch, H. Hayashi, C. C. Scott, M. Kim, T. Alexander, N. Touret, K. M. Hahn, and S. Grinstein. Amiloride inhibits macropinocytosis by lowering submembranous pH and preventing Rac1 and Cdc42 signaling. *The Journal of cell biology*, 188(4):547–563, Feb. 2010.

[123] A. C. Koksal and G. Cingolani. Dimerization of Vaccinia Virus VH1 is essential for dephosphorylation of STAT1 at Tyrosine 701. *Journal of Biological Chemistry*, 286(16):14373–14382, Apr. 2011.

[124] D. Komander. The emerging complexity of protein ubiquitination. *Biochemical Society transactions*, 37(Pt 5):937–953, Oct. 2009.

[125] Y. Kuznetsov, P. D. Gershon, and A. McPherson. Atomic force microscopy investigation of Vaccinia Virus structure. *Journal of virology*, 82(15):7551–7566, Aug. 2008.

[126] J. P. Laliberte and B. Moss. Appraising the apoptotic mimicry model and the role of phospholipids for poxvirus entry. *Proceedings of the National Academy of Sciences of the United States of America*, 106(41):17517–17521, Oct. 2009.

[127] J. P. Laliberte, A. S. Weisberg, and B. Moss. The membrane fusion step of Vaccinia Virus entry is cooperatively mediated by multiple viral proteins and host cell components. *PLoS pathogens*, 7(12):e1002446, Dec. 2011.

[128] M. Law, G. C. Carter, K. L. Roberts, M. Hollinshead, and G. L. Smith. Ligand-induced and nonfusogenic dissolution of a viral membrane. *Proceedings of the National Academy of Sciences of the United States of America*, 103(15):5989–5994, Apr. 2006.

[129] M. Law and G. L. Smith. Antibody neutralization of the extracellular enveloped form of Vaccinia Virus. *Virology*, 280(1):132–142, Feb. 2001.

[130] J. A. Leite, B. P. Drumond, G. S. Trindade, Z. I. P. Lobato, F. G. da Fonseca, dos Santos Marieta, J. R. C. Madureira, M. I. M. C. Guedes, J. M. S. Ferreira, C. A. Bonjardim, P. C. P. Ferreira, and E. G. Kroon. Passatempo virus, a Vaccinia Virus strain, Brazil. *Emerging infectious diseases*, 11(12):1935, Dec. 2005.

[131] R. S. Levine, A. T. Peterson, K. L. Yorita, D. Carroll, I. K. Damon, and M. G. Reynolds. Ecological niche and geographic distribution of human monkeypox in Africa. *PLoS ONE*, 2(1):e176, 2007.

[132] Y. Li, S. Grenklo, T. Higgins, and R. Karlsson. The profilin:actin complex localizes to sites of dynamic actin polymerization at the leading edge of migrating cells and pathogen-induced actin tails. *European journal of cell biology*, 87(11):893–904, Nov. 2008.

[133] C. L. Lin, C. S. Chung, H. G. Heine, and W. Chang. Vaccinia Virus envelope H3L protein binds to cell surface heparan sulfate and is important for intracellular mature virion morphogenesis and virus infection in vitro and in vivo. *The Journal of Virology*, 74(7):3353–3365, Apr. 2000.

[134] K. Liu, B. Lemon, and P. Traktman. The dual-specificity phosphatase encoded by Vaccinia Virus, VH1, is essential for viral transcription in vivo and in vitro. *The Journal of Virology*, 69(12):7823–7834, Dec. 1995.

[135] J. K. Locker and G. Griffiths. An unconventional role for cytoplasmic disulfide bonds in Vaccinia Virus proteins. *The Journal of cell biology*, 144(2):267–279, Jan. 1999.

[136] J. K. Locker, A. Kuehn, S. Schleich, G. Rutter, H. Hohenberg, R. Wepf, and G. Griffiths. Entry of the two infectious forms of Vaccinia Virus at the plasma membane is signaling-dependent for the IMV but not the EEV. *Molecular biology of the cell*, 11(7):2497–2511, July 2000.

[137] F. O. MACCALLUM and J. R. MCDONALD. Effect of temperatures of up to 45 degrees C on survival of variola virus in human material in relation to laboratory diagnosis. *Bulletin of the World Health Organization*, 16(2):441–443, 1957.

[138] W. E. Magee and O. V. Miller. Initiation of Vaccinia Virus infection in actinomycin D-pretreated cells. *The Journal of Virology*, 2(7):678–685, July 1968.

[139] M. Makishima, Y. Honma, M. Hozumi, K. Sampi, M. Hattori, K. Umezawa, and K. Motoyoshi. Effects of inhibitors of protein tyrosine kinase activity and/or phosphatidylinositol turnover on differentiation of some human myelomonocytic leukemia cells. *Leukemia research*, 15(8):701–708, 1991.

[140] A. J. Malkin, A. McPherson, and P. D. Gershon. Structure of intracellular mature Vaccinia Virus visualized by in situ atomic force microscopy. *The Journal of Virology*, 77(11):6332–6340, July 2003.

[141] M. Mallardo, E. Leithe, S. Schleich, N. Roos, L. Doglio, and J. Krijnse Locker. Relationship between Vaccinia Virus intracellular cores, early mRNAs, and DNA replication sites. *The Journal of Virology*, 76(10):5167–5183, May 2002.

[142] M. Mallardo, S. Schleich, and J. Krijnse Locker. Microtubule-dependent organization of Vaccinia Virus core-derived early mRNAs into distinct cytoplasmic structures. *Molecular biology of the cell*, 12(12):3875–3891, Dec. 2001.

[143] M. Marsh and A. Helenius. Virus entry: open sesame. *Cell*, 124(4):729–740, Feb. 2006.

[144] K. McDonald. Osmium ferricyanide fixation improves microfilament preservation and membrane visualization in a variety of animal cell types. *Journal of ultrastructure research*, 86(2):107–118, Jan. 1984.

[145] G. McFadden. Poxvirus tropism. *Nature reviews Microbiology*, 3(3):201–213, Mar. 2005.

[146] J. R. McLean, D. Chaix, M. D. Ohi, and K. L. Gould. State of the APC/C: organization, function, and structure. *Critical reviews in biochemistry and molecular biology*, 46(2):118–136, Apr. 2011.

[147] O. Meier, K. Boucke, S. V. Hammer, S. Keller, R. P. Stidwill, S. Hemmi, and U. F. Greber. Adenovirus triggers macropinocytosis and endosomal leakage together with its clathrin-mediated uptake. *The Journal of cell biology*, 158(6):1119–1131, Sept. 2002.

[148] J. Mercer and A. Helenius. Vaccinia Virus uses macropinocytosis and apoptotic mimicry to enter host cells. *Science (New York, NY)*, 320(5875):531–535, Apr. 2008.

[149] J. Mercer and A. Helenius. Virus entry by macropinocytosis. *Nature cell biology*, 11(5):510–520, May 2009.

[150] J. Mercer and A. Helenius. Apoptotic mimicry: phosphatidylserine-mediated macropinocytosis of Vaccinia Virus. *Annals of the New York Academy of Sciences*, 1209:49–55, Oct. 2010.

[151] J. Mercer, S. Knébel, F. I. Schmidt, J. Crouse, C. Burkard, and A. Helenius. Vaccinia Virus strains use distinct forms of macropinocytosis for host-cell entry. *Proceedings of the National Academy of Sciences of the United States of America*, May 2010.

[152] J. Mercer, M. Schelhaas, and A. Helenius. Virus entry by endocytosis. *Annual review of biochemistry*, Mar. 2010.

[153] J. Mercer, B. Snijder, R. Sacher, C. Burkard, C. Bleck, H. Stahlberg, L. Pelkmans, and A. Helenius. RNAi Screening Reveals Proteasome- and Cullin3-Dependent Stages in Vaccinia Virus Infection. *CellReports*, pages 1–12, Oct. 2012.

[154] J. Mercer and P. Traktman. Investigation of structural and functional motifs within the Vaccinia Virus A14 phosphoprotein, an essential component of the virion membrane. *The Journal of Virology*, 77(16):8857–8871, Aug. 2003.

[155] W. Mitsuhashi, H. Kawakita, R. Murakami, Y. Takemoto, T. Saiki, K. Miyamoto, and S. Wada. Spindles of an entomopoxvirus facilitate its infection of the host insect by disrupting the peritrophic membrane. *The Journal of Virology*, 81(8):4235–4243, Apr. 2007.

[156] S. Mohr, C. Bakal, and N. Perrimon. Genomic screening with RNAi: results and challenges. *Annual review of biochemistry*, 79:37–64, 2010.

[157] V. Moreau, F. Frischknecht, I. Reckmann, R. Vincentelli, G. Rabut, D. Stewart, and M. Way. A complex of N-WASP and WIP integrates signalling cascades that lead to actin polymerization. *Nature cell biology*, 2(7):441–448, July 2000.

[158] G. W. Morgan, M. Hollinshead, B. J. Ferguson, B. J. Murphy, D. C. J. Carpentier, and G. L. Smith. Vaccinia Protein F12 Has Structural Similarity to Kinesin Light Chain and Contains a Motor Binding Motif Required for Virion Export. *PLoS pathogens*, 6(2):e1000785, Feb. 2010.

[159] K. Morizono, Y. Xie, T. Olafsen, B. Lee, A. Dasgupta, A. M. Wu, and I. S. Y. Chen. The soluble serum protein Gas6 bridges virion envelope phosphatidylserine to the TAM receptor tyrosine kinase Axl to mediate viral entry. *Cell host & microbe*, 9(4):286–298, Apr. 2011.

[160] T. S. Moser, R. G. Jones, C. B. Thompson, C. B. Coyne, and S. Cherry. A kinome RNAi screen identified AMPK as promoting poxvirus entry through the control of actin dynamics. *PLoS pathogens*, 6(6):e1000954, 2010.

[161] B. Moss. Regulation of Vaccinia Virus transcription. *Annual review of biochemistry*, 59:661–688, 1990.

[162] B. Moss. Poxvirus entry and membrane fusion. *Virology*, 344(1):48–54, Jan. 2006.

[163] B. Moss. Poxviridae: The viruses and their replication. In B. Fields, D. M. Knipe, and P. Howley, editors, *Fields Virology*, pages 2905–2947. Wolters Kluwer Health/Lippincott Williams & Wilkins, Philadelphia, Jan. 2007.

[164] P. Najarro, P. Traktman, and J. A. Lewis. Vaccinia Virus blocks gamma Interferon signal transduction: Viral VH1 phosphatase reverses Stat1 activation. *The Journal of Virology*, 75(7):3185–3196, Apr. 2001.

[165] A. Nanbo, M. Imai, S. Watanabe, T. Noda, K. Takahashi, G. Neumann, P. Halfmann, and Y. Kawaoka. Ebolavirus is internalized into host cells via macropinocytosis in a viral glycoprotein-dependent manner. *PLoS pathogens*, 6(9):e1001121, 2010.

[166] G. E. Nelson, J. R. Sisler, D. Chandran, and B. Moss. Vaccinia Virus entry/fusion complex subunit A28 is a target of neutralizing and protective antibodies. *Virology*, 380(2):394–401, Oct. 2008.

[167] B. T. H. Nerenberg, J. Taylor, E. Bartee, K. Gouveia, M. Barry, and K. Früh. The poxviral RING protein p28 is a ubiquitin ligase that targets ubiquitin to viral replication factories. *The Journal of Virology*, 79(1):597–601, Feb. 2005.

[168] R. J. Nichols, E. Stanitsa, B. Unger, and P. Traktman. The Vaccinia Virus gene I2L encodes a membrane protein with an essential role in virion entry. *Journal of virology*, 82(20):10247–10261, Oct. 2008.

[169] C. C. Norbury. Drinking a lot is good for dendritic cells. *Immunology*, 117(4):443–451, Apr. 2006.

[170] C. C. Norbury, B. J. Chambers, A. R. Prescott, H. G. Ljunggren, and C. Watts. Constitutive macropinocytosis allows TAP-dependent major histocompatibility complex class I presentation of exogenous soluble antigen by bone marrow-derived dendritic cells. *European journal of immunology*, 27(1):280–288, Jan. 1997.

[171] S. Ojeda, A. Domi, and B. Moss. Vaccinia Virus G9 protein is an essential component of the poxvirus entry-fusion complex. *The Journal of Virology*, 80(19):9822–9830, Oct. 2006.

[172] S. Ojeda, T. G. Senkevich, and B. Moss. Entry of Vaccinia Virus and cell-cell fusion require a highly conserved cysteine-rich membrane protein encoded by the A16L gene. *Journal of virology*, 80(1):51–61, 2006.

[173] Z. Orynbayeva, S. Kolusheva, N. Groysman, N. Gavrielov, L. Lobel, and R. Jelinek. Vaccinia Virus interactions with the cell membrane studied by new chromatic vesicle and cell sensor assays. *The Journal of Virology*, 81(3):1140–1147, Feb. 2007.

[174] R. Pálffy, R. Gardlík, M. Behuliak, L. Kadasi, J. Turna, and P. Celec. On the physiology and pathophysiology of antimicrobial peptides. *Molecular medicine (Cambridge, Mass.)*, 15(1-2):51–59, Jan. 2009.

[175] L. Payne. Polypeptide composition of extracellular enveloped Vaccinia Virus. *The Journal of Virology*, 27(1):28–37, July 1978.

[176] L. G. Payne. Identification of the vaccinia hemagglutinin polypeptide from a cell system yielding large amounts of extracellular enveloped virus. *The Journal of Virology*, 31(1):147–155, July 1979.

[177] L. G. Payne. Significance of extracellular enveloped virus in the in vitro and in vivo dissemination of vaccinia. *The Journal of general virology*, 50(1):89–100, Sept. 1980.

[178] K. Pedersen, E. J. Snijder, S. Schleich, N. Roos, G. Griffiths, and J. K. Locker. Characterization of Vaccinia Virus intracellular cores: implications for viral uncoating and core structure. *Journal of virology*, 74(8):3525–3536, Apr. 2000.

[179] C. B. Pedley and R. J. Cooper. The assay, purification and properties of Vaccinia Virus-induced uncoating protein. *The Journal of general virology*, 68 (Pt 4):1021–1028, Apr. 1987.

[180] L. Pelkmans and A. Helenius. Endocytosis via caveolae. *Traffic (Copenhagen, Denmark)*, 3(5):311–320, May 2002.

[181] B. Perdiguero, M. M. Lorenzo, and R. Blasco. Vaccinia Virus A34 glycoprotein determines the protein composition of the extracellular virus envelope. *Journal of virology*, 82(5):2150–2160, Mar. 2008.

[182] J. Perino, C. H. Foo, D. Spehner, G. H. Cohen, R. J. Eisenberg, J.-M. Crance, and A.-L. Favier. Role of sulfatide in Vaccinia Virus infection. *Biology of the cell / under the auspices of the European Cell Biology Organization*, 103(7):319–331, July 2011.

[183] A. Person-Fernandez and G. Beaud. Purification and characterization of a protein synthesis inhibitor associated with Vaccinia Virus. *The Journal of biological chemistry*, 261(18):8283–8289, June 1986.

[184] M. D. Petroski and R. J. Deshaies. Function and regulation of cullin-RING ubiquitin ligases. *Nature reviews Molecular cell biology*, 6(1):9–20, Feb. 2005.

[185] M. Pires de Miranda, P. C. Reading, D. C. Tscharke, B. J. Murphy, and G. L. Smith. The Vaccinia Virus kelch-like protein C2L affects calcium-independent adhesion to the extracellular matrix and inflammation in a murine intradermal model. *The Journal of general virology*, 84(Pt 9):2459–2471, Sept. 2003.

[186] G. Powis, R. Bonjouklian, M. M. Berggren, A. Gallegos, R. Abraham, C. Ashendel, L. Zalkow, W. F. Matter, J. Dodge, and G. Grindey. Wortmannin, a potent and selective inhibitor of phosphatidylinositol-3-kinase. *Cancer research*, 54(9):2419–2423, May 1994.

[187] J. R. S. B. M. R Blasco. Dissociation of progeny Vaccinia Virus from the cell membrane is regulated by a viral envelope glycoprotein: effect of a point mutation in the lectin homology domain of the A34R gene. *Journal of virology*, 67(6):3319, June 1993.

[188] H. Raghu, N. Sharma-Walia, M. V. Veettil, S. Sadagopan, and B. Chandran. Kaposi's sarcoma-associated herpesvirus utilizes an actin polymerization-dependent macropinocytic pathway to enter human dermal microvascular endothelial and human umbilical vein endothelial cells. *Journal of virology*, 83(10):4895–4911, May 2009.

[189] P. Rämö, R. Sacher, B. Snijder, B. Begemann, and L. Pelkmans. CellClassifier: supervised learning of cellular phenotypes. *Bioinformatics (Oxford, England)*, 25(22):3028–3030, Nov. 2009.

[190] W. Resch and B. Moss. The conserved poxvirus L3 virion protein is required for transcription of Vaccinia Virus early genes. *The Journal of Virology*, 79(23):14719–14729, Dec. 2005.

[191] E. Reynolds. The use of lead citrate at high pH as an electron-opaque stain in electron microscopy. *The Journal of cell biology*, 17:208–212, Mar. 1963.

[192] J. Rietdorf, A. Ploubidou, I. Reckmann, A. Holmström, F. Frischknecht, M. Zettl, T. Zimmermann, and M. Way. Kinesin-dependent movement on microtubules precedes actin-based motility of Vaccinia Virus. *Nature cell biology*, 3(11):992–1000, Nov. 2001.

[193] K. L. Roberts, A. Breiman, G. C. Carter, H. A. Ewles, M. Hollinshead, M. Law, and G. L. Smith. Acidic residues in the membrane-proximal stalk region of Vaccinia Virus protein B5 are required for glycosaminoglycan-mediated disruption of the extracellular enveloped virus outer membrane. *The Journal of general virology*, 90(Pt 7):1582–1591, July 2009.

[194] K. L. Roberts and G. L. Smith. Vaccinia Virus morphogenesis and dissemination. *Trends in microbiology*, 16(10):472–479, Oct. 2008.

[195] K. L. Rock, C. Gramm, L. Rothstein, K. Clark, R. Stein, L. Dick, D. Hwang, and A. L. Goldberg. Inhibitors of the proteasome block the degradation of most cell proteins and the generation of peptides presented on MHC class I molecules. *Cell*, 78(5):761–771, Sept. 1994.

[196] M. F. Saeed, A. A. Kolokoltsov, T. Albrecht, and R. A. Davey. Cellular entry of ebola virus involves uptake by a macropinocytosis-like mechanism and subsequent trafficking through early and late endosomes. *PLoS pathogens*, 6(9):e1001110, 2010.

[197] F. Sallusto, M. Cella, C. Danieli, and A. Lanzavecchia. Dendritic cells use macropinocytosis and the mannose receptor to concentrate macromolecules in the major histocompatibility complex class II compartment: downregulation by cytokines and bacterial products. *The Journal of experimental medicine*, 182(2):389–400, Aug. 1995.

[198] C. M. Sanderson, M. Hollinshead, and G. L. Smith. The Vaccinia Virus A27L protein is needed for the microtubule-dependent transport of intracellular mature virus particles. *The Journal of general virology*, 81(Pt 1):47–58, Jan. 2000.

[199] K. J. Sandgren, J. Wilkinson, M. Miranda-Saksena, G. M. McInerney, K. Byth-Wilson, P. J. Robinson, and A. L. Cunningham. A differential role for macropinocytosis in mediating entry of the two forms of Vaccinia Virus into dendritic cells. *PLoS pathogens*, 6(4):e1000866, Apr. 2010.

[200] I. Sarov and W. K. Joklik. Studies on the nature and location of the capsid polypeptides of vaccinia virions. *Virology*, 50(2):579–592, Nov. 1972.

[201] P. S. Satheshkumar, L. C. Anton, P. Sanz, and B. Moss. Inhibition of the ubiquitin-proteasome system prevents Vaccinia Virus DNA replication and expression of intermediate and late genes. *Journal of virology*, 83(6):2469–2479, Mar. 2009.

[202] P. S. Satheshkumar and B. Moss. Characterization of a newly identified 35-amino-acid component of the Vaccinia Virus entry/fusion complex conserved in all chordopoxviruses. *Journal of virology*, 83(24):12822–12832, Dec. 2009.

[203] Q. Sattentau. Avoiding the void: cell-to-cell spread of human viruses. *Nature reviews Microbiology*, 6(11):815–826, Nov. 2008.

[204] I. F. Sbalzarini and P. Koumoutsakos. Feature point tracking and trajectory analysis for video imaging in cell biology. *Journal of structural biology*, 151(2):182–195, Aug. 2005.

[205] N. Scaplehorn, A. Holmström, V. Moreau, F. Frischknecht, I. Reckmann, and M. Way. Grb2 and Nck act cooperatively to promote actin-based motility of Vaccinia Virus. *Current biology : CB*, 12(9):740–745, Apr. 2002.

[206] U. Scheer, K. Messner, R. Hazan, I. Raska, P. Hansmann, H. Falk, E. Spiess, and W. W. Franke. High sensitivity immunolocalization of double and single-stranded DNA by a monoclonal antibody. *European journal of cell biology*, 43(3):358–371, June 1987.

[207] M. Schliwa, U. Euteneuer, J. C. Bulinski, and J. G. Izant. Calcium lability of cytoplasmic microtubules and its modulation by microtubule-associated proteins. *Proceedings of the National Academy of Sciences of the United States of America*, 78(2):1037–1041, Jan. 1981.

[208] M. Schliwa and J. van Blerkom. Structural interaction of cytoskeletal components. *The Journal of cell biology*, 90(1):222–235, July 1981.

[209] F. I. Schmidt. *Host cell entry of Vaccinia Virus extracellular virions.* PhD thesis, ETH Zurich, Jan. 2011.

[210] F. I. Schmidt, C. Bleck, A. Helenius, and J. Mercer. Vaccinia extracellular virions enter cells by macropinocytosis and acid-activated membrane rupture. *The EMBO journal*, July 2011.

[211] F. I. Schmidt, C. Bleck, and J. Mercer. Poxvirus host cell entry. *Current opinion in virology*, Dec. 2011.

[212] B. Schramm, C. A. M. de Haan, J. Young, L. Doglio, S. Schleich, C. Reese, A. V. Popov, W. Steffen, T. Schroer, and J. K. Locker. Vaccinia-virus-induced cellular contractility facilitates the subcellular localization of the viral replication sites. *Traffic (Copenhagen, Denmark)*, 7(10):1352–1367, Oct. 2006.

[213] T. G. Senkevich, S. Ojeda, A. Townsley, G. E. Nelson, and B. Moss. Poxvirus multiprotein entry-fusion complex. *Proceedings of the National Academy of Sciences of the United States of America*, 102(51):18572–18577, Dec. 2005.

[214] T. G. Senkevich, B. M. Ward, and B. Moss. Vaccinia Virus A28L gene encodes an essential protein component of the virion membrane with intramolecular disulfide bonds formed by the viral cytoplasmic redox pathway. *Journal of virology*, 78(5):2348–2356, Mar. 2004.

[215] T. G. Senkevich, B. M. Ward, and B. Moss. Vaccinia Virus entry into cells is dependent on a virion surface protein encoded by the A28L gene. *The Journal of Virology*, 78(5):2357–2366, Mar. 2004.

[216] T. G. Senkevich, C. L. White, E. V. Koonin, and B. Moss. Complete pathway for protein disulfide bond formation encoded by poxviruses. *Proceedings of the National Academy of Sciences of the United States of America*, 99(10):6667–6672, May 2002.

[217] T. G. Senkevich, C. L. White, A. Weisberg, J. A. Granek, E. J. Wolffe, E. V. Koonin, and B. Moss. Expression of the Vaccinia Virus A2.5L redox protein is required for virion morphogenesis. *Virology*, 300(2):296–303, Sept. 2002.

[218] D. J. Shedlock, M. A. Bailey, P. M. Popernack, J. M. Cunningham, D. R. Burton, and N. J. Sullivan. Antibody-mediated neutralization of Ebola virus can occur by two distinct mechanisms. *Virology*, 401(2):228–235, June 2010.

[219] S. Shuman and B. Moss. Bromouridine triphosphate inhibits transcription termination and mRNA release by vaccinia virions. *The Journal of biological chemistry*, 264(35):21356–21360, Dec. 1989.

[220] J. W. Slot and H. J. Geuze. Cryosectioning and immunolabeling. *Nature protocols*, 2(10):2480–2491, Dec. 2007.

[221] G. L. Smith and M. Law. The exit of Vaccinia Virus from infected cells. *Virus research*, 106(2):189–197, Dec. 2004.

[222] G. L. Smith, B. J. Murphy, and M. Law. Vaccinia Virus motility. *Annual review of microbiology*, 57:323–342, 2003.

[223] G. L. Smith, A. Vanderplasschen, and M. Law. The formation and function of extracellular enveloped Vaccinia Virus. *The Journal of general virology*, 83(Pt 12):2915–2931, Dec. 2002.

[224] B. Snijder, R. Sacher, P. Rämö, E.-M. Damm, P. Liberali, and L. Pelkmans. Population context determines cell-to-cell variability in endocytosis and virus infection. *Nature*, 461(7263):520–523, Sept. 2009.

[225] B. Snijder, R. Sacher, P. Rämö, P. Liberali, K. Mench, N. Wolfrum, L. Burleigh, C. C. Scott, M. H. Verheije, J. Mercer, S. Moese, T. Heger, K. Theusner, A. Jurgeit, D. Lamparter, G. Balistreri, M. Schelhaas, C. A. M. de Haan, V. Marjomäki, T. Hyypiä, P. J. M. Rottier, B. Sodeik, M. Marsh, J. Gruenberg, A. Amara, U. Greber, A. Helenius, and L. Pelkmans. Single-cell analysis of population context advances RNAi screening at multiple levels. *Molecular systems biology*, 8:579, 2012.

[226] B. Sodeik, R. W. Doms, M. Ericsson, G. Hiller, C. E. Machamer, W. van t Hof, G. van Meer, B. Moss, and G. Griffiths. Assembly of Vaccinia Virus: role of the intermediate compartment between the endoplasmic reticulum and the Golgi stacks. *The Journal of cell biology*, 121(3):521–541, May 1993.

[227] S. P. Soltoff. Rottlerin is a mitochondrial uncoupler that decreases cellular ATP levels and indirectly blocks protein kinase Cdelta tyrosine phosphorylation. *The Journal of biological chemistry*, 276(41):37986–37992, Oct. 2001.

[228] A. Sommer and R. R. Traut. Diagonal polyacrylamide-dodecyl sulfate gel electrophoresis for the identification of ribosomal proteins crosslinked with methyl-4-mercaptobutyrimidate. *Proceedings of the National Academy of Sciences of the United States of America*, 71(10):3946–3950, Oct. 1974.

[229] A. F. Straight, A. Cheung, J. Limouze, I. Chen, N. J. Westwood, J. R. Sellers, and T. J. Mitchison. Dissecting temporal and spatial control of cytokinesis with a myosin II Inhibitor. *Science (New York, NY)*, 299(5613):1743–1747, Mar. 2003.

[230] D. Studer, W. Graber, A. Al-Amoudi, and P. Eggli. A new approach for cryofixation by high-pressure freezing. *Journal of microscopy*, 203(Pt 3):285–294, Aug. 2001.

[231] D. Szklarczyk, A. Franceschini, M. Kuhn, M. Simonovic, A. Roth, P. Minguez, T. Doerks, M. Stark, J. Muller, P. Bork, L. J. Jensen, and C. von Mering. The STRING database in 2011: functional interaction networks of proteins, globally integrated and scored. *Nucleic acids research*, 39(Database issue):D561–8, Feb. 2011.

[232] T. Takahashi, M. Oie, and Y. Ichihashi. N-terminal amino acid sequences of Vaccinia Virus structural proteins. *Virology*, 202(2):844–852, Aug. 1994.

[233] A. Teale, S. Campbell, N. Van Buuren, W. C. Magee, K. Watmough, B. Couturier, R. Shipclark, and M. Barry. Orthopoxviruses require a functional ubiquitin-proteasome system for productive replication. *Journal of virology*, 83(5):2099–2108, Apr. 2009.

[234] D. M. Tillman, K. Izeradjene, K. S. Szucs, L. Douglas, and J. A. Houghton. Rottlerin sensitizes colon carcinoma cells to tumor necrosis factor-related apoptosis-inducing ligand-induced apoptosis via uncoupling of the mitochondria independent of protein kinase C. *Cancer research*, 63(16):5118–5125, Aug. 2003.

[235] K. T. Tokuyasu. A technique for ultracryotomy of cell suspensions and tissues. *The Journal of cell biology*, 57(2):551–565, Apr. 1973.

[236] K. T. Tokuyasu. Immunochemistry on ultrathin frozen sections. *The Histochemical journal*, 12(4):381–403, June 1980.

[237] A. C. Townsley and B. Moss. Two distinct low-pH steps promote entry of Vaccinia Virus. *The Journal of Virology*, 81(16):8613–8620, Aug. 2007.

[238] A. C. Townsley, T. G. Senkevich, and B. Moss. The product of the Vaccinia Virus L5R gene is a fourth membrane protein encoded by all poxviruses that is required for cell entry and cell-cell fusion. *The Journal of Virology*, 79(17):10988–10998, Sept. 2005.

[239] A. C. Townsley, A. S. Weisberg, T. R. Wagenaar, and B. Moss. Vaccinia Virus entry into cells via a low-pH-dependent endosomal pathway. *The Journal of Virology*, 80(18):8899–8908, Sept. 2006.

[240] P. Traktman, K. Liu, J. DeMasi, R. Rollins, S. Jesty, and B. Unger. Elucidating the essential role of the A14 phosphoprotein in Vaccinia Virus morphogenesis: construction and characterization of a tetracycline-inducible recombinant. *The Journal of Virology*, 74(8):3682–3695, Apr. 2000.

[241] G. S. Trindade, G. L. Emerson, D. S. Carroll, E. G. Kroon, and I. K. Damon. Brazilian Vaccinia Viruses and their origins. *Emerging infectious diseases*, 13(7):965–972, July 2007.

[242] B. Tsai. Penetration of nonenveloped viruses into the cytoplasm. *Annual review of cell and developmental biology*, 23:23–43, 2007.

[243] P. C. Turner and R. W. Moyer. An orthopoxvirus serpinlike gene controls the ability of infected cells to fuse. *The Journal of Virology*, 66(4):2076–2085, Apr. 1992.

[244] P. C. Turner and R. W. Moyer. The cowpox virus fusion regulator proteins SPI-3 and hemagglutinin interact in infected and uninfected cells. *Virology*, 347(1):88–99, Mar. 2006.

[245] P. C. Turner and R. W. Moyer. The Vaccinia Virus fusion inhibitor proteins SPI-3 (K2) and HA (A56) expressed by infected cells reduce the entry of superinfecting virus. *Virology*, 380(2):226–233, Oct. 2008.

[246] D. Ulaeto, D. Grosenbach, and D. E. Hruby. The Vaccinia Virus 4c and A-type inclusion proteins are specific markers for the intracellular mature virus particle. *The Journal of Virology*, 70(6):3372–3377, July 1996.

[247] T. L. Ung, C. Cao, J. Lu, K. Ozato, and T. E. Dever. Heterologous dimerization domains functionally substitute for the double-stranded RNA binding domains of the kinase PKR. *The EMBO journal*, 20(14):3728–3737, July 2001.

[248] C. Upton, S. Slack, A. L. Hunter, A. Ehlers, and R. L. Roper. Poxvirus orthologous clusters: toward defining the minimum essential poxvirus genome. *The Journal of Virology*, 77(13):7590–7600, July 2003.

[249] G. van Meer, D. R. Voelker, and G. W. Feigenson. Membrane lipids: where they are and how they behave. *Nature reviews Molecular cell biology*, 9(2):112–124, Feb. 2008.

[250] A. Vanderplasschen, M. Hollinshead, and G. L. Smith. Antibodies against Vaccinia Virus do not neutralize extracellular enveloped virus but prevent virus release from infected cells and comet formation. *The Journal of general virology*, 78 (Pt 8):2041–2048, Aug. 1997.

[251] A. Vanderplasschen, M. Hollinshead, and G. L. Smith. Intracellular and extracellular vaccinia virions enter cells by different mechanisms. *The Journal of general virology*, 79 (Pt 4):877–887, Apr. 1998.

[252] A. Vanderplasschen, E. Mathew, M. Hollinshead, R. B. Sim, and G. L. Smith. Extracellular enveloped Vaccinia Virus is resistant to complement because of incorporation of host complement control proteins into its envelope. *Proceedings of the National Academy of Sciences of the United States of America*, 95(13):7544–7549, June 1998.

[253] A. Vanderplasschen and G. L. Smith. A novel virus binding assay using confocal microscopy: demonstration that the intracellular and extracellular vaccinia virions bind to different cellular receptors. *The Journal of Virology*, 71(5):4032–4041, June 1997.

[254] J. K. Vanslyke and D. E. Hruby. Immunolocalization of Vaccinia Virus structural proteins during virion formation. *Virology*, 198(2):624–635, Feb. 1994.

[255] P. Vigne, C. Frelin, E. J. Cragoe, and M. Lazdunski. Ethylisopropylamiloride: a new and highly potent derivative of amiloride for the inhibition of the Na+/H+ exchange system in various cell types. *Biochemical and biophysical research communications*, 116(1):86–90, Oct. 1983.

[256] N. Y. Villa, E. Bartee, M. R. Mohamed, M. M. Rahman, J. W. Barrett, and G. McFadden. Myxoma and Vaccinia Viruses exploit different mechanisms to enter and infect human cancer cells. *Virology*, 401(2):266–279, June 2010.

[257] T. R. Wagenaar and B. Moss. Expression of the A56 and K2 proteins is sufficient to inhibit Vaccinia Virus entry and cell fusion. *Journal of virology*, 83(4):1546–1554, Feb. 2009.

[258] T. R. Wagenaar, S. Ojeda, and B. Moss. Vaccinia Virus A56/K2 fusion regulatory protein interacts with the A16 and G9 subunits of the entry fusion complex. *Journal of virology*, 82(11):5153–5160, June 2008.

[259] I. Weisswange, T. P. Newsome, S. Schleich, and M. Way. The rate of N-WASP exchange limits the extent of ARP2/3-complex-dependent actin-based motility. *Nature*, 458(7234):87–91, Mar. 2009.

[260] S. Welsch, L. Doglio, S. Schleich, and J. Krijnse Locker. The Vaccinia Virus I3L gene product is localized to a complex endoplasmic reticulum-associated structure that contains the viral parental DNA. *Journal of virology*, 77(10):6014–6028, Apr. 2003.

[261] J. C. Whitbeck, C. H. Foo, M. Ponce de Leon, R. J. Eisenberg, and G. H. Cohen. Vaccinia Virus exhibits cell-type-dependent entry characteristics. *Virology*, 385(2):383–391, Mar. 2009.

[262] C. L. White, A. S. Weisberg, and B. Moss. A glutaredoxin, encoded by the G4L gene of Vaccinia Virus, is essential for virion morphogenesis. *The Journal of Virology*, 74(19):9175–9183, Oct. 2000.

[263] S. D. White, K. Conwell, J. O. Langland, and B. L. Jacobs. Use of a negative selectable marker for rapid selection of recombinant Vaccinia Virus. *BioTechniques*, 50(5):303–309, May 2011.

[264] N. T. Wickramasekera and P. Traktman. Structure/Function analysis of the Vaccinia Virus F18 phosphoprotein, an abundant core component required for virion maturation and infectivity. *Journal of virology*, 84(13):6846–6860, July 2010.

[265] D. Wilcock and G. L. Smith. Vaccinia virions lacking core protein VP8 are deficient in early transcription. *The Journal of Virology*, 70(2):934–943, Feb. 1996.

[266] J. D. Williamson, R. W. Reith, L. J. Jeffrey, J. R. Arrand, and M. Mackett. Biological characterization of recombinant Vaccinia Viruses in mice infected by the respiratory route. *The Journal of general virology*, 71 (Pt 11):2761–2767, Nov. 1990.

[267] C. L. Wolfe and B. Moss. Interaction between the G3 and L5 proteins of the Vaccinia Virus entry-fusion complex. *Virology*, 412(2):278–283, Apr. 2011.

[268] E. J. Wolffe, E. Katz, A. Weisberg, and B. Moss. The A34R glycoprotein gene is required for induction of specialized actin-containing microvilli and efficient cell-to-cell transmission of Vaccinia Virus. *The Journal of Virology*, 71(5):3904–3915, May 1997.

[269] E. J. Wolffe, S. Vijaya, and B. Moss. A myristylated membrane protein encoded by the Vaccinia Virus L1R open reading frame is the target of potent neutralizing monoclonal antibodies. *Virology*, 211(1):53–63, Aug. 1995.

[270] J. R. Woodburn. The epidermal growth factor receptor and its inhibition in cancer therapy. *Pharmacology & therapeutics*, 82(2-3):241–250, May 1999.

[271] S. Yadav, M. Hosamani, V. Balamurugan, V. Bhanuprakash, and R. K. Singh. Partial genetic characterization of viruses isolated from pox-like infection in cattle and buffaloes: evidence of buffalo pox virus circulation in Indian cows. *Archives of virology*, 155(2):255–261, Feb. 2010.

[272] J.-C. Yang and C.-T. Chien. A new approach for the prevention and treatment of Helicobacter pylori infection via upregulation of autophagy and downregulation of apoptosis. *Autophagy*, 5(3):413–414, Apr. 2009.

[273] W. P. Yang, S. Y. Kao, and W. R. Bauer. Biosynthesis and post-translational cleavage of Vaccinia Virus structural protein VP8. *Virology*, 167(2):585–590, Dec. 1988.

[274] Z. Yang, D. P. Bruno, C. A. Martens, S. F. Porcella, and B. Moss. Simultaneous high-resolution analysis of Vaccinia Virus and host cell transcriptomes by deep RNA sequencing. *Proceedings of the National Academy of Sciences of the United States of America*, 107(25):11513–11518, June 2010.

[275] Z. Yang and B. Moss. Interaction of the Vaccinia Virus RNA polymerase-associated 94-kilodalton protein with the early transcription factor. *Journal of virology*, 83(23):12018–12026, Dec. 2009.

[276] Z. Yang, S. E. Reynolds, C. A. Martens, D. P. Bruno, S. F. Porcella, and B. Moss. Expression profiling of the intermediate and late stages of poxvirus replication. *The Journal of Virology*, pages JVI.05446–11v1, July 2011.

[277] E. Zaitseva, S.-T. Yang, K. Melikov, S. Pourmal, and L. V. Chernomordik. Dengue virus ensures its fusion in late endosomes using compartment-specific lipids. *PLoS pathogens*, 6(10):e1001131, 2010.

[278] H. Zhang, C. E. Monken, Y. Zhang, J. Lenard, N. Mizushima, E. C. Lattime, and S. Jin. Cellular autophagy machinery is not required for Vaccinia Virus replication and maturation. *Autophagy*, 2(2):91–95, Mar. 2006.

[279] B. Zuber, M. Haenni, T. Ribeiro, K. Minnig, F. Lopes, P. Moreillon, and J. Dubochet. Granular layer in the periplasmic space of gram-positive bacteria and fine structures of Enterococcus gallinarum and Streptococcus gordonii septa revealed by cryo-electron microscopy of vitreous sections. *Journal of bacteriology*, 188(18):6652–6660, Aug. 2006.

[280] H. T. Zwartouw. The chemical composition of Vaccinia Virus. *Journal of general microbiology*, 34:115–123, Feb. 1964.

List of Acronyms

Å	Ångström (10^{-10} m)
AraC	cytosine arabinoside
ANX5	annexin V
ATI	A-type inclusion
BafA	bafilomycin A1
BSA	bovine serum albumin
bona fide	genuine
c	centi (10^{-2})
CalC	calphostin C
CCD	charge-coupled device
CEMOVIS	cryo-electron microscopy of vitrified sections
Chlo	chlorpromazine
CHX	cycloheximide
CLEM	correlative light and electron microscopy
CME	clathrin-mediated endocytosis
CPXV	cowpox virus
Cyto	cytochalasin D
CMOS	complementary metal oxide semiconductor
dd	double distilled
D	dimension
Da	dalton
de novo	“from the beginning”
DIKC	differential interference contrast
DMEM	Dulbecco’s Modified Eagle Medium
DOPC	phosphatidylcholine
DOPE	phosphatidylethanolamine
dsDNA	double-stranded deoxyribonucleic acid
DTT	dithiothreitol
e^-	negatively charged electron
EGTA	ethyleneglycoltetraacetic acid
EDTA	ethylenediaminetetraacetic acid

EE	early endosome
EFC	entry/fusion complex
EGFP	enhanced green fluorescent protein
EGFR	epidermal growth factor receptor
EIPA	5-(N-ethyl-N-isopropyl) amiloride
EM	electron microscopy
et al.	*et alia* (“and others”)
EV	enveloped virion
°C	grad Celsius
FEG	emission electron gun
g	gravitational
GAG	glycosaminglycan
Geni	genistein
GFP	green fluorescent protein
GIF	Gatan, Inc. post-column imaging filter
h	hour(s)
HA	haemagglutinin
HeLa	Henrietta Lacks (uterine cell line, named for deceased patient)
IHD-J	International Health Department-J
in vitro	“in glass”
in vivo	“within the living”
Ires	Iressa
IFN	interferon
IgG	immunoglobulin G
IV	immature virion
IVN	immature virion with nucleoid
Jasp	jasplakinolide
k	kilo (10^3)
L	litre
LB	lateral bodies
LE	late endosome
LDS	lithium dodecyl sulfate
LUV	large unilamellar vesicles
μ	micron (10^{-6})
m	milli (10^{-3})
Mab	monoclonal antibody
MDDC	monocyte-derived dendritic cell
ME	maturing endosome
MG132	N-(benzyloxycarbonyl)leucinylleucinylleucinal
min	minute(s)
MOCV	molluscum contagiosum virus

MOI	multiplicity of infection
MonA	monensin A
MOPS	3-(N-morpholino)propanesulfonic acid
MPXV	monkeypos virus
MV	molecular weight
mRNA	messenger RNA
MV	mature virion
n/a	not applicable
n	nano (10^{-9})
N	number
NEM	n-ethyl maleimide
Nu	nucleus
NuPAGE®	Neutral-pH Gel Buffer System
NTP	nucleoside triphosphate
OV	orthovanadate
PAK1	p21-activated kinase 1
PBS	phosphate buffered saline
pH	power of hydrogen
p.i.	post infection
PKC	protein kinase C
PS	phosphatidylserine
punctae	minute rounded dots
R18	octadecyl rhodamine B
redox	reduction-oxidation
Rott	rottlerin
RT	room temperature
SD	standard deviation
SDS	sodium dodecyl sulfate polyacrylamide
SDS-PAGE	sodium dodecyl sulfate polyacrylamide gel electrophoresis
sec	second(s)
SEM	standard error of the mean
SIM	structured illumination microscopy
smMLCK	smooth muscle myosin light chain kinase
Stau	staurosporine
SW	swinging bucket rotor
tk	thymidine kinase
Tris	2-Amino-2-hydroxymethyl-propane-1,3-diol
ts	temperature sensitive
U	unit
UBEI	ubiquitin E1 inhibitor
UNTR	untreated

VACV	vaccinia virus
VARV	variola virus
VH1	*Vaccinia* virus gene H1
Wort	wortmannin
VP8	viral protein 8 (aa 33-251 of L4, 25k)
WR	Western Reserve
WV	wrapped virion

Acknowledgements

I am grateful to you, Henning Stahlberg, for allowing me to do my PhD thesis in your lab, for advice, discussions, and freedom to pursue my own research interests.

Thank you Jason Mercer and Florian I. Schmidt for being great advisors.

I would like to thank Christoph Dehio for being in my thesis committee, accepting to be my co-referee.

Big thanks to all present and past Stahlberg lab and all Helenii members – I have learned so much from you.

Special thanks go to Kenneth N. Goldie, Bill Anderson, Mohamed Chami, Paul Baumgartner and Alexandra Graff, thank you for always being helpful and your kind words of advice.

Thanks to my grand aunt and grand uncle, Hildegard Völlmer von Moers-Messmer and Dr. Gerd von Moers-Messmer – I will always keep you in good memory.

Sincere thanks to my parents, Waltraud M. and Wolfgang E., and parents-in-law, Emiko and Katsumi, who despite financial challenges supported my family in various ways in this thesis.

Last but not least, I must thank my beautiful and lovely wife, Hinako, and my son, Yuito, for their support, patience and encouragements.

Curriculum vitae

Personal data

Name	Christopher Karl Ernst Bleck
Birth	June 17^{th} 1976 in Heidelberg, Germany
Citizenship	German
Languages	German (native), English, Spanish (basic), Japanese (basic)
Address	Oetlingerstr. 1 4057 Basel Switzerland
e-mail	christopher.bleck@unibas.ch, christopher.bleck@me.com

Current position

10/2009–11/2012	Ph.D. candidate in the laboratory of Prof. Dr. H. Stahlberg Center for Cellular Imaging and NanoAnalytics (C-CINA), Biozentrum, University of Basel, Basel, Switzerland

Education

10/2004–9/2007	Master of Science in Biology, Ruprecht-Karls University Heidelberg, Germany
10/2001–9/2004	Bachelor of Science in Biology, University of Konstanz, Germany
09/2001	Abitur, Carl-Engler-Schule, Karlsruhe, Germany

Research experience

01–09/2009	Electron Microscopist Research Technician in the laboratory of Prof. T. Yoshimori Research Institute for Microbial Diseases Osaka University, Osaka, Japan
09/2007–12/2008	Electron Microscopist Research Technician in the laboratory of Dr. G. Griffiths Cell Biology of Pathogens European Molecular Biology Laboratory, Heidelberg, Germany
10/2006–05/2007	Master's Thesis in the laboratory of Dr. G. Griffiths Cell Biology of Pathogens European Molecular Biology Laboratory, Heidelberg, Germany
11/2005–09/2006	Lab assistant in the laboratory of Dr. C. Antony Cell Biology and Biophysics European Molecular Biology Laboratory, Heidelberg, Germany
05/2005–11/2005	Lab assistant in the laboratory of Prof. R. Bartenschlager Department of Molecular Virology University Heidelberg, Heidelberg, Germany
04/1999–09/2004	Research Technician & Electron Microscopist (part time) in the laboratory of Prof. J. Kartenbeck Department of Cell Biology German Cancer Research Center, Heidelberg, Germany

Publications

1. Akat, K. *et al.*, 2008. Characterization of a novel type of adherens junction in meningiomas and the derived cell line HBL-52. Cell Tissue Res.
2. Akat, K. *et al.*, 2003. Molecular characterization of desmosomes in meningiomas and arachnoidal tissue. Acta neuropathologica
3. Anand, P.K. *et al.*, 2010. Exosomal Hsp70 induces a pro-inflammatory response to foreign particles including mycobacteria. PLoS ONE
4. Bleck, C.K.E. *et al.*, 2010. Comparison of different methods for thin section EM analysis of Mycobacterium smegmatis. Journal of microscopy
5. Fabrino, D.L. *et al.*, 2009. Porins facilitate nitric oxide-mediated killing of mycobacteria. Microbes and infection / Institut Pasteur
6. Fernandez-Arenas, E. *et al.*, 2009. Candida albicans actively modulates intracellular membrane trafficking in mouse macrophage phagosomes. Cellular microbiology
7. Jordao, L. *et al.*, 2008. On the killing of mycobacteria by macrophages. Cellular microbiology
8. Mercer, J. *et al.*, 2012. RNAi screening reveals proteasome- and Cullin3-dependent stages in vaccinia virus infection. CellReports
9. Schmidt, F.I. *et al.*, 2011. Vaccinia extracellular virions enter cells by macropinocytosis and acid-activated membrane rupture. The EMBO journal
10. Schmidt, F.I. *et al.*, 2011. Poxvirus host cell entry. Current opinion in virology.
11. Stoeber, M. *et al.*, 2012. Oligomers of the ATPase EHD2 confine caveolae to the plasma membrane through association with actin. The EMBO journal
12. Welsch, S. *et al.*, 2009. Composition and three-dimensional architecture of the dengue virus replication and assembly sites. Cell host & microbe
13. Zhuravleva, E. *et al.*, 2012. Acyl-CoA thioesterase Them5/Acot15 is involved in cardiolipin remodeling and fatty liver development. Molecular and cellular biology

November 13, 2012